Late Cycle Soot Oxidation in Diesel Engines

Gallo, Yann

2016

Document Version:
Publisher's PDF, also known as Version of record

Late Cycle Soot Oxidation in Diesel Engines

YANN GALLO | DIVISION OF COMBUSTION ENGINES
DEPARTMENT OF ENERGY SCIENCES | LUND UNIVERSITY | 2016

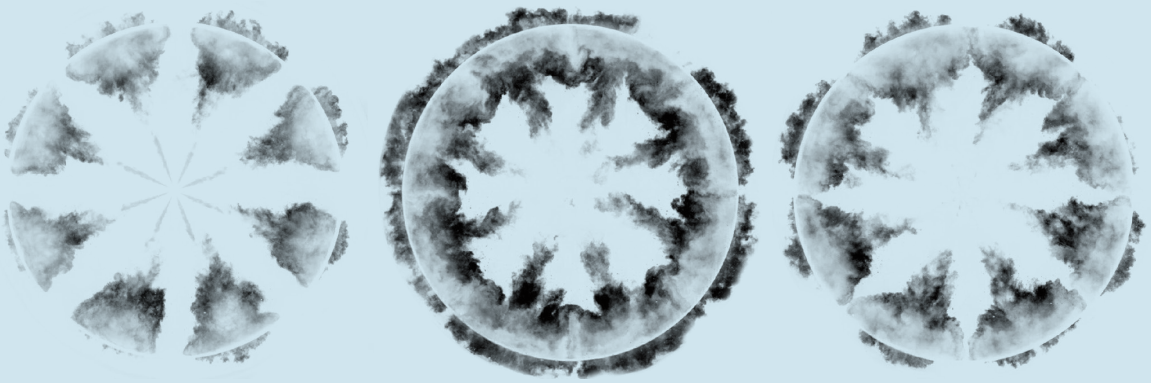

Late Cycle Soot Oxidation in Diesel Engines

Yann Gallo

DOCTORAL DISSERTATION
by due permission of the Faculty of Engineering, Lund University, Sweden.
To be defended at M-Huset, LTH, Ole Römers väg 1. Date December 2nd 2016.

Faculty opponent

Dr. Ezio Mancaruso

Organization	Document name: Doctoral Dissertation	
LUND UNIVERSITY Division of Energy Sciences Department of Combustion Engines P.O Box 118, SE-211 00 Lund, Sweden	Author: Yann Gallo Date of issue: 02/12/2016 Language: English	Number of pages: 189

Title and subtitle: Late Cycle Soot Oxidation in Diesel Engines

Abstract

Diesel engines are the most common engine technology used in transportation. Its widespread use comes from its inherent high efficiency and its relative low cost. It suffers from pollutant emission issues, however, that need detailed understanding of their origins to meet the strictest current and upcoming emission standards. The work presented in this thesis focuses on the study of the mechanism at the origin of soot particle emissions and gives indications on which parameters can effectively reduce them.

There are two competing in-cylinder processes, soot formation and soot oxidation, governing soot emissions from conventional combustion in diesel engines. To this day, it is still often believed that inhibiting the formation of soot reduces its emissions, despite several studies showing poor relationship between soot formation and emission in most conditions encountered in diesel engines. The results presented in this thesis aims at highlighting the importance of soot oxidation in the late cycle over the soot formation process. An effort was realized to identify the parameters governing its oxidation and how it results in lower emission levels. The study of those parameters has been realized through the use of in-cylinder sampling of gases and optical measurements.

The optical measurements were realized in a heavy-duty diesel engine using a Bowditch design with a specifically designed three-valve cylinder head. This cylinder head had an optical access located at the top of the combustion chamber, allowing the study of processes occurring in the late cycle, when the piston is moving down into the cylinder. The diagnostic chosen for this study is called laser extinction, a line of sight technique based on the absorption of light by the soot particles present in the flame. The data collected gave information on the evolution of the soot concentration and could be used to characterize the soot oxidation rate in the late cycle. The in-cylinder sampling measurements were realized in order to gather information on the soot particle characteristics.

The results showed a strong correlation between the soot oxidation rates and the emission levels, underlining the importance of improving the oxidation rate rather than the soot formation in order to reduce soot emissions. It was shown that increasing the mixing of gases in the cylinder by means of increased turbulences could lead to a negative impact on the soot oxidation rates that were passed on to the soot levels in the exhaust. A variation of temperature of gases showed little to no impact on the soot oxidation rates and did not seem to effectively impact the emission levels. An increase of the gas density in the cylinder of gases lead to improved oxidation rate that also reduced emission levels. Of the injection related parameters studied, the injection pressure and the injector hole size had a strong impact on the soot oxidation rates even long after the end of the injection process. The most important parameter identified that affected the soot oxidation rates was the oxygen concentration. This parameter was studied in detail and it showed that a reduction of oxygen concentration lead to a slower maturation of soot during the combustion. While this feature produced more reactive soot particles prone to be more easily oxidized, it was revealed to be concerning a limited amount of particles in the cylinder. Moreover, it was largely overruled by the reduction of OH produced in the flame. Using simulation tools, it was shown that lowering the oxygen concentration reduced the flame temperature, which in turn reduced the OH concentration. The reduction of OH correlated strongly with the reduction in oxidation rates observed in the optical measurements, to a greater extent than just the drop of oxygen concentration.

Key words: Soot oxidation, laser extinction, optical diagnostics, diesel engines, gas sampling, PM

ISSN: 0282-1990	ISBN: 978-91-7753-054-1 (print)
ISRN: LUTMDN/TMHP-16/1124-SE	ISBN: 978-91-7753-054-1 (pdf)

Late Cycle Soot Oxidation in Diesel Engines

Yann Gallo

LUND
UNIVERSITY

Faculty of Energy Sciences, Combustion Engines
ISBN 978-91-7753-054-1 (print)
ISBN 978-91-7753-055-8 (pdf)
ISSN 0282-1990
ISRN LUTMDN/TMHP-16/1124-SE

Printed in Sweden by E-Huset Tryckeriet, Lund University
Lund 2016

If you're reading this, it means that next time we meet could be called a doctor's appointment.

Abstract

Diesel engines are the most common engine technology used in transportation. Its widespread use comes from its inherent high efficiency and its relative low cost. It suffers from pollutant emission issues, however, that need detailed understanding of their origins to meet the strictest current and upcoming emission standards. The work presented in this thesis focuses on the study of the mechanism at the origin of soot particle emissions and gives indications on which parameters can effectively reduce them.

There are two competing in-cylinder processes, soot formation and soot oxidation, governing soot emissions from conventional combustion in diesel engines. To this day, it is still often believed that inhibiting the formation of soot reduces its emissions, despite several studies showing poor relationship between soot formation and emission in most conditions encountered in diesel engines. The results presented in this thesis aims at highlighting the importance of soot oxidation in the late cycle over the soot formation process. An effort was realized to identify the parameters governing its oxidation and how it results in lower emission levels. The study of those parameters has been realized through the use of in-cylinder sampling of gases and optical measurements.

The optical measurements were realized in a heavy-duty diesel engine using a Bowditch design with a specifically designed three-valve cylinder head. This cylinder head had an optical access located at the top of the combustion chamber, allowing the study of processes occurring in the late cycle, when the piston is moving down into the cylinder. The diagnostic chosen for this study is called laser extinction, a line of sight technique based on the absorption of light by the soot particles present in the flame. The data collected gave information on the evolution of the soot concentration and could be used to characterize the soot oxidation rate in the late cycle. The in-cylinder sampling measurements were realized in order to gather information on the soot particle characteristics.

The results showed a strong correlation between the soot oxidation rates and the emission levels, underlining the importance of improving the oxidation rate rather than the soot formation in order to reduce soot emissions. It was shown that increasing the mixing of gases in the cylinder by means of increased turbulences could lead to a negative impact on the soot oxidation rates that were passed on to the soot levels in the exhaust. A variation of temperature of gases showed little to

no impact on the soot oxidation rates and did not seem to effectively impact the emission levels. An increase of the gas density in the cylinder of gases lead to improved oxidation rate that also reduced emission levels. Of the injection related parameters studied, the injection pressure and the injector hole size had a strong impact on the soot oxidation rates even long after the end of the injection process. The most important parameter identified that affected the soot oxidation rates was the oxygen concentration. This parameter was studied in detail and it showed that a reduction of oxygen concentration lead to a slower maturation of soot during the combustion. While this feature produced more reactive soot particles prone to be more easily oxidized, it was revealed to be concerning a limited amount of particles in the cylinder. Moreover, it was largely overruled by the reduction of OH produced in the flame. Using simulation tools, it was shown that lowering the oxygen concentration reduced the flame temperature, which in turn reduced the OH concentration. The reduction of OH correlated strongly with the reduction in oxidation rates observed in the optical measurements, to a greater extent than just the drop of oxygen concentration.

Populärvetenskaplig Sammanfattning

Det finns över en miljard fordon i omlopp i världen. Trots ökningen av alternativ teknologi som hybrid och elektriska fordon, är motorfordon drivna på fossila bränslen fortfarande ett utbrett transportmedel i dagens samhälle. Oavsett om de används för transport av personer eller gods är de oftast det första valet för företag och privatpersoner på grund av deras låga priser, lättillgänglighet och effektivitet. Fossilt drivna motorfordon producerar dock utsläpp som har långsiktiga skadeeffekter på miljö och hälsa. För att reducera miljöpåverkan har EU infört en miljölagstiftning som innebär påtryckningar på biltillverkare för att minska dessa utsläpp. Denna lagstiftning definierar ett utsläppstak som måste vara uppfyllt för fordon som släpps ut på marknaden. Mot bakgrund av Euro 7, nästa generation av annalkande utsläppsnormer, är en förbättring av den nuvarande motortekniken nödvändig.

I detta sammanhang är dieselmotorn ett utmärkt val på grund av sin höga verkningsgrad. Den höga verkningsgraden leder till fordon med låg bränsleförbrukning, vilket ger en fördel gentemot andra tillgängliga motortekniker som inte uppnår detta i samma utsträckning. Nackdelen med dieseltekniken ligger i dess höga utsläpp av kväveoxider och sotpartiklar som är kända för sina negativa effekter på både miljö och hälsa. Dieselpartikelfilter och SCR-katalysatorer är två tillgängliga efterbehandlingssystem som kan hjälpa till med reduktionen av dessa två emissioner. Dessa system möjliggör ett effektivt sätt att hantera emissionerna för den nuvarande generationen av fordon i syfte att uppfylla gällande utsläppsnormer. Samtidigt gör dessa system att den totala motorverkningsgraden minskar genom att motståndet ökar på utgående luftflöde från motorn samt att komponentkostnaden för fordonet ökar. I ett mycket konkurrensutsatt område, som drivs av kundens begäran för billiga och effektiva fordon, krävs en bättre förståelse av mekanismerna bakom källan till dessa föroreningar. Att förstå grunderna i dessa mekanismer är ett viktigt ändamål för dagens fordonsforskning.

Det är i detta sammanhang som denna avhandling är skriven. Kväveoxider bildas under själva förbränningen i motorns cylindrar. En lösning att få ner utsläppen är således att sänka deras bildning under och efter förbränning av dieselbränsle. Även sotpartiklar bildas och oxideras inuti motorn under och efter förbränningen. Trots att studier har visat att minskning av sotbildningsprocessen inte nödvändigtvis resulterar i reducerade utsläpp, visar resultaten som presenteras i denna avhandling

att förbättrad oxidation av partiklarna resulterar i lägre sotutsläpp från motorn. En uttömmande studie av de olika parametrarna som påverkar sotoxidation, genom reglering eller motordesign, har förverkligats och resultaten visade att injektionsrelaterade parametrar har en väsentlig betydelse även lång tid efter slutet av bränsleinjektionen. En annan påverkande motorparameter som identifierades, var en ökning av gasdensiteten som uppnåddes genom att öka överladdningstrycket. Slutligen har även effekten av syrekoncentrationen i cylindern studerats detaljerat. En reduktion av syrekoncentrationen leder till bildningen av mer reaktivt sot som har en högre tendens att oxidera. Men denna påverkan var dock begränsad. Den huvudsakliga effekten av närvaro av syre var att flamtemperaturen ökade. En högre flamtemperatur gynnar produktionen av hydroxidradikaler som dominerar sotets oxidationsprocess.

Acknowledgement

Obtaining a PhD is a considerable personal achievement and one of the most prestigious academic diplomas one could work toward. I would not celebrate it without the support of many persons that I wish to take the time to thank.

My first *Merci!* Goes to my supervisor Öivind Andersson for his availability, support and patient guidance along all the years. I have learnt so many things under his supervision and I will forever be grateful.

My next acknowledgement goes to the other professors of our division Per Tunestål and Martin Tunér for the occasional advices as well as in the informal discussions in the fika room.

I would like to thank Bengt Johansson for welcoming me in his department and for always being enthusiastic to share his knowledge about internal combustion engines.

I am grateful for the help I got from other staff from the division, including the administrative, IT and technical staff, particularly Kjell Jonholm and Martin Carlsson for their precious help on the capricious Scania engine.

The work presented in this thesis has been realized in collaboration with other departments. I really appreciated the expertise brought by the division of Combustion Physics regarding optical diagnostics. It has been a pleasure working with Johan Simonsson and ZheMing Li on the extinction campaigns and many thanks to their respective supervisors Per-Erik Bengtsson and Mattias Richter for the discussions and their expertise. The sampling measurements were realized in collaboration with the department of Ergonomics & Aerosol Technology and it was a real breath of fresh air to actually pull the head out of the engine to look at the bigger picture regarding the impact of particles. Many thanks to Ville Malmborg and his supervisor Joakim Pagels for always being so eager to work with our division, I really appreciated the hard work and the dedication you put in our collaboration.

It was a pleasure to occasionally welcome visitors in our department. I am grateful to have had the chance to meet Noud Maes from the Technische Universiteit Eindhoven, Luigi Sequino from the Istituto Motori, Daniela de Lima, Carlos Mico Reche, Antonio Garcia from the Centro de Motores Termicos and Sanghoon Kook

from the University of New South Wales. Each of you has provided ad hoc support and I appreciated the discussions and moments we shared.

I cannot forget to mention my colleagues at the division of Combustion Engine. I want you to know that I am glad to have met you and I thank you wholeheartedly for the discussions and many laughs we have shared. Particular thanks to Sam for being you, Kenan for the good laughs about Labview, Maja for the discussions, Vikram for the good times, Ashish for his kindness…

It would be too long to mention everyone that counted dearly to me during those years. If I did not mention you here, I will do it in person.

List of Papers

This thesis is based on the following publications, referred to by their Roman numerals. The papers are appended to the thesis.

I. Gallo, Y., Simonsson, J., Lind, T., Bengtsson, P., et al., "A Study of In-Cylinder Soot Oxidation by Laser Extinction Measurements During an EGR-Sweep in an Optical Diesel Engine," SAE Technical Paper 2015-01-0800, doi:10.4271/2015-01-0800, 2015.

II. Gallo, Y., Li, Z., Richter, M., Andersson, Ö., "Parameters Influencing Soot Oxidation Rates in an Optical Diesel Engine," *SAE Int. J. Engines* 9(4):2016, doi:10.4271/2016-01-2183, 2016.

III. Gallo, Y., Malmborg, V., Simonsson, J., Svensson, E., Shen, M., et al., "Investigation of Late-Cycle Soot Oxidation Using Laser Extinction and In-Cylinder Gas Sampling at Varying Inlet Oxygen Concentrations in Diesel Engines," *Submitted to Fuel*, 2016.

IV. Li, Z., Gallo, Y., Richter, M., Lind, T., et al., "Comparison of Laser-Extinction and Natural Luminosity Measurements for Soot Probing in Diesel Optical Engines," SAE Technical Paper 2016-01-2159, doi:10.4271/2016-01-2159, 2016.

V. Shen, M., Malmborg, V., Gallo, Y., Waldheim, B., et al., "Analysis of Soot Particles in the Cylinder of a Heavy Duty Diesel Engine with High EGR," SAE Technical Paper 2015-24-2448, doi:10.4271/2015-24-2448, 2015.

VI. Malmborg, V., Eriksson, A., Shen, M., Nilsson P., et al., "Evolution of in-cylinder diesel soot and emission characteristics investigated with on-line aerosol mass spectrometry," *Submitted to Journal of Environmental Science & Technology*, 2016.

Other related work:

A. Sjoholm, J., Chartier, C., Kristensson, E., Berrocal, E., et al., " Quantitative in-cylinder fuel measurements in a heavy-duty diesel engine using Structured Laser Illumination Planar Imaging (SLIPI)," COMODIA 2012, MD2-3, 2012.

B. Lequien, G., Berrocal, E., Gallo, Y., Themudo e Mello, A. et al., "Effect of Jet-Jet Interactions on the Liquid Fuel Penetration in an Optical Heavy-Duty DI Diesel Engine," SAE Technical Paper 2013-01-1615, doi:10.4271/2013-01-1615, 2013.

Nomenclature

ATDC	After Top Dead Center
AOM	Acousto-Optic Modulator
BC	Black Carbon
CA50	Crank Angle at 50% completion of total heat released
CAD	Crank Angle Degree
CDC	Conventional Diesel Combustion
CFD	Computational Fluid Dynamics
CI	Compression Ignition
CO	Carbon monoxide
CO_2	Carbon dioxide
DBI	Diffused Back Illumination
DPF	Diesel Particulate Filter
EC	Elemental Carbon
EFTA	European Free Trade Association
EGR	Exhaust Gas Recirculation
EOI	End Of Injection
EU15	15 member states of Europe as of December 31st 2013
EVO	Exhaust Valve Opening
FILE	Forward Illumination Light Extinction
FSN	Filtered Smoke Number
GMD	Geometrical Mean Diameter
H_2O	Dihydrogen monoxide
HC	HydroCarbon

HCCI	Homogeneous Charge Compression Ignition
IPCC	Intergovernmental Panel on Climate Change
K	Kelvin
KL	Optical thickness
LEM	Laser Extinction Method
LII	Laser Induced Incandescence
LTC	Low Temperature Combustion
N_2	Nitrogen
NL	Natural Luminosity
NO_x	Nitrous Oxides
NSC	Nagle/Strickland-Constable (model)
O	Oxygen atom
O_2	Oxygen molecule
OH	Hydroxide
PAH	Polycyclic Aromatic Hydrocarbons
PM	Particulate Matter
PPC	Partially Premixed Combustion
rBC	Refractive Black Carbon
RPM	Revolutions Per Minute
SI	Spark Ignition
SMPS	Scanning Mobility Particle Sizer
SOI	Start Of Injection
SP-AMS	Soot Particle Aerosol Mass Spectrometer
TDC	Top Dead Center
TTL	Transistor-Transistor Logic
UHC	Unburnt HydroCarbon
UNICEF	United Nations Children's Fund
WHO	World Health Organization

Table of Contents

1 Introduction

1.1 Background

1.1.1 Importance of Diesel Engines

Combustion engines have been of paramount importance in the development of our society. Internal combustion engines have been instrumental for the growth of transportation and virtually shortened distances for people and goods [1]. In 1862, Alphonse Beau de Rochas, a French engineer first described the basic principle of the four-stroke engine. Over 150 years later the principle remains the same, though the technology has seen tremendous improvements in terms of efficiency, reliability and emissions [2]. Despite the emergence of modern alternative technologies (e.g. hybrid and electric powertrains), four-stroke gasoline and diesel engines still largely dominate the transportation market, with a slight dominance of diesel in Europe (EU15+EFTA) with 53% of new registered diesel passenger cars in 2015 [3].

A partial explanation for the dominance of diesel technology comes from one of the inherent properties of the engine's working principle. In 1892, Rudolf Diesel, its inventor, specifically designed the engine to extract as much power as possible per unit of fuel [1]. In other words, the diesel engine is by design more efficient than the gasoline engine. This feature leading to lower fuel consumption, combined with favorable taxation on diesel fuel in most European countries [4] leads customers to prefer diesel engines to gasoline engines.

1.1.2 Emissions

There are five legislated emissions from diesel engines: particulate matter (PM), nitrogen oxides (NO_x), unburned hydrocarbons (UHC), carbon monoxide (CO) and carbon dioxide (CO_2). They are strictly regulated by standards varying on the region and conditioning the market release of road vehicles. Under the current trends (Euro 6), diesel combustion occurs with sufficient excess air so UHC and CO emissions are typically low. However, the high gas temperatures due to high

compression ratios promote NO_x formation and emissions. Moreover, due to local fuel rich regions in the cylinder during the combustion, soot particles are emitted.

In diesel engines, soot emissions work in a trade-off with NO_x emissions. They are therefore treated in a tandem due to the fact that reducing emissions of one will often increase the emissions of the other [5]. A reduction of the temperature during combustion, by means of exhaust gas recirculation (EGR) for example, will limit the NO_x formation and reduce the emissions. However, in return, soot particle emissions will increase [6]. After the development and broad use of diesel particulate filters (DPF), the focus was initially put on reducing NO_x by lowering the combustion temperature. This resulted in increased soot exhaust levels that were more easily taken care of by the efficient after-treatment device. More recently, stricter NO_x regulations has lead to widespread use of NO_x aftertreatment in Europe. This typically means that EGR is reduced to increase the exhaust gas temperatures (which is beneficial for the operation of the exhaust aftertreatment system) and this leads to new trade-offs between soot and NO_x.

Newer concepts exist for low temperature combustion (LTC) such as homogeneous charge compression ignition (HCCI) or partially premixed combustion (PPC). They focus on reducing both NO_x and soot emissions thanks to higher premixing of the charge and lower oxygen content. However, they do suffer major drawbacks in terms of operation range, thus a better understanding of conventional diesel combustion (CDC) is required.

In most conditions found in diesel engines where CDC is used, large amounts of NO_x are formed early during the cycle, whereas soot is characterized by both strong formation *and* oxidation, according to processes that will be developed in detail in following chapters. Since soot formation correlates poorly with soot exhaust levels [7], the quality of the soot oxidation process seems to have a strong impact on soot emissions [8].

1.1.3 Soot Particles and Health

The terminology *particulate matter* (PM) is often used interchangeably in the combustion-engineering field with *soot*. The approximation is acceptable in the sense that engine-out PM mostly consists of combustion-generated soot particles. However, it is a shortcut that can lead to confusion when considered in inter-disciplinary research contexts. Though no clear official classification exists, a brief clarification of the various terminologies used to denominate particles in this thesis will be presented, following the principles presented in [9].

An aerosol is a suspension of liquid or solid particles in a gaseous medium. Both the particles and surrounding gases constitute the aerosol. For example, the black

smoke coming from unfiltered diesel exhaust is an aerosol, constituting soot particles, water vapor and other species.

Particulate matter is the generic term describing the particles contained in an aerosol. They can vary in shapes, sizes (1 nm-100 μm) and chemical composition. They are generally categorized depending on their sizes as coarse particles (larger than 2 μm), fine particles (0.1-2 μm) and ultrafine particles (less than 0.1 μm). Particles from engine emissions are usually falling in the two latter categories. In the engine community, PM is defined as anything that sticks on a filter in a gravimetric test. In such a test, the (diluted) exhausts are drawn through an efficient filter, which is weighed before and after the test. The difference in mass (due to both solid and liquid particles) is the PM mass.

A soot particle is an agglomerate of roughly spherical primary particles. It is black or blackish and often approximated as a blackbody. It originates from the combustion of hydrocarbons. This is the terminology of choice widely used in the automotive engineering field to refer to particles from combustion sources.

Black carbon (BC) is equivalent to soot but gets its own terminology from the optical property of the soot and the way it is measured. It is a light-absorbing carbonaceous particle originating from combustion sources. It is more commonly encountered in environmental contexts like aerosol physics, atmospheric chemistry or geophysical fields.

Refractory black carbon (rBC) is similar to black carbon. It holds its appellation for its thermal stability and represents the mass of carbon derived from incandescence-based measurement techniques.

Elemental carbon (EC) is preferably used when the measurement technique specifically targets the carbon content of particles and allows for characterizing the structure of the carbonaceous particle.

Soot particles have been associated with inflammatory response in airways, decreased lung function and are classified as carcinogenic [10,11]. The severity of the symptoms depends on the intensity, duration and timing of exposure to the particles. The size of the particle will affect their ability to penetrate the organism. Since particles are mostly airborne they usually penetrate the body through airways. Despite the lungs acting as natural filters, the finer particles will find their way to the bloodstream and are responsible for cardiovascular issues, while the larger ones adsorbed in the airways can cause irritations and breathing difficulties. In a report by UNICEF, the acute impact of air pollution from combustion-originated particles on children is put in the spotlight. The report states that approximately two billions children live in areas where the air pollution exceeds the quality standards set by the World Health Organization (WHO) and

their developing systems make them more sensitive to the adverse effect of particles [12].

Soot is also pointed out for its impact on the environment and its role in climate change. Its impact on global warming is evaluated through its radiative forcing, a metric representing the importance of the considered element affecting the balance between the incoming solar radiation and the outgoing infrared emissions. An element with positive radiative forcing will lead to an increase of the earth atmosphere. The positive radiative forcing due to particles from combustion origins is the second anthropogenic most important according to the Intergovernmental Panel on Climate Change (IPCC) fifth assessment report as published in 2013 [13].

1.2 Objective/Scope of the Thesis

The objective of the thesis is to address diesel combustion related issues with a strong focus on the soot oxidation process, particularly to highlight the importance of soot oxidation over soot formation for improving engine-out levels. An important focus was to investigate which are the relevant parameters, whether by design or control, that can affect the soot oxidation and what are their effect on the soot processes and chemical properties. A final objective is to emphasize the importance of OH in the flame and its role as main oxidizer.

The scope of this research is to study the late cycle oxidation of soot in a four-stroke heavy-duty diesel engine operating with conventional diesel combustion using optical diagnostic and in-cylinder sampling of gases.

1.3 Approach

In this thesis, the measurements have been realized using two main techniques. The first one is optical diagnostics, allowing the study of the combustion process in detail by monitoring the evolution of combustion species during the cycle. The second technique used is in-cylinder sampling, which allowed a closer look into the characteristics of the probed combustion species and complemented the optical measurements. The optical measurements were conducted in collaboration with the division of combustion physics at Lund University. The in-cylinder sampling measurements were realized in collaboration with the division of Ergonomics and Aerosol Technology at Lund University.

1.4 Thesis Contribution

The work presented in this thesis showcases novel insights regarding the importance of soot oxidation rate and negates any correlation between soot formation and soot exhaust level in conventional diesel combustion situations. The late cycle soot oxidation rates have been characterized thanks to the definition of a global metric that allowed comparison of all points of operation regardless of the formation impact. The effects of various parameters on the soot oxidation have been investigated. It has notably been shown that injection related parameters have a strong impact on the late cycle soot oxidation, even after the end of injection. Moreover and unexpectedly, swirl and engine speed seemed to have a negative impact on the soot oxidation rates. Finally, the influence of oxygen variation has shown the strongest impact on the soot oxidation rates and it has been observed using different techniques. The effect of this parameter has been studied in more detailed and has stressed the importance of OH as main oxidizer in the flame.

2 Soot Processes in Direct Injection Diesel Engines

2.1 Mixing-Controlled Combustion

The combustion process in a compression ignition (CI) engines is typically monitored by the heat release. It is extracted from the pressure trace following a procedure presented in a later subchapter of this thesis. A typical heat release rate from a conventional diesel combustion process is presented in Figure 2.1.

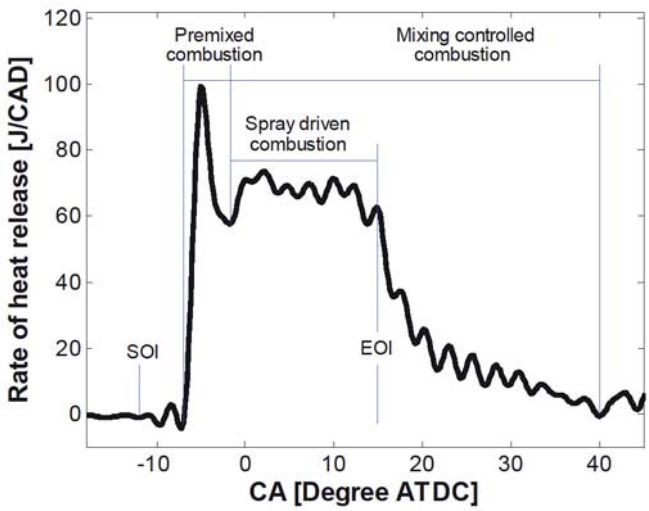

Figure 2.1 Typical rate of heat released in CI engine [14].

The curve is characterized by 4 phases. At the end of the compression stroke, when the fuel is injected, it mixes with the surrounding hot intake gases. The high temperature of the mixture leads to the vaporization and auto-ignition of the fuel vapor. The phase between the start of injection (SOI) and auto-ignition (usually

defined as the point where the heat release rate turns positive) is called the ignition delay and is due to both physical processes, such as evaporation and air entrainment, and to chemical processes such as fuel breakdown and auto-ignition chemistry [15].

Once the mixture ignites, the portion of the fuel that forms a combustible mixture burns rapidly. This provokes a steep increase of temperature and pressure, giving rise to the characteristic clattering sound of CI combustion. The high peak in the heat release rate is identified as the premixed combustion phase, and occurs around 5 CAD ATDC in Figure 2.1.

The following phase occurs when the combustible mixture has been consumed and the heat release rate drops after the peak. During this phase, the combustion is continuously happening as the fuel is injected, vaporized and ignited in the cylinder. The burn rate is now limited by the rate of mixing between fuel from the injected sprays and fresh gases from the cylinder. This part of the combustion, which takes place up to the end of injection (EOI), is therefore called the spray-driven mixing-controlled phase.

After the end of injection, no more fuel is injected but the remaining kinetic energy from the sprays dissipates into turbulence in the bulk gases, helping the remaining combustion species to mix and oxidize slowly following the drop of temperature caused by the expansion and the ending of the combustion. This fourth and last phase is referred to as the late cycle mixing-controlled combustion. Much diesel engine research has focused on the ignition process and the spray driven part of combustion. This is particularly the case for research in optical engines. As discussed below, these processes have a strong impact on the formation of soot, and they are also relatively simple to study in optical engines. The late cycle oxidation is not as well studied, although it typically comprises a substantial part of the heat release. A possible reason is that the combustion process is less structured after the EOI, meaning that it is more difficult to study optically. During expansion, the interesting processes also tend to take place deeper in the cylinder, which adds to the difficulty of studying them. It is important to note, however, that since soot and other combustion intermediates are oxidized during the late cycle, this phase can be expected to significantly influence the emissions.

The heat release only gives a global overview of the process, without spatial information. In 1997, combining laser-sheet measurement techniques, John Dec presented a conceptual model detailing the various processes taking place in various parts of a free spray [16]. The conceptual model is represented in Figure 2.2 and gives a simplified, yet valuable, representation of the flame. Three relevant areas of the flame are highlighted: the lift-off length (1), the premixed reaction zone (2) and the diffusion combustion zone (3).

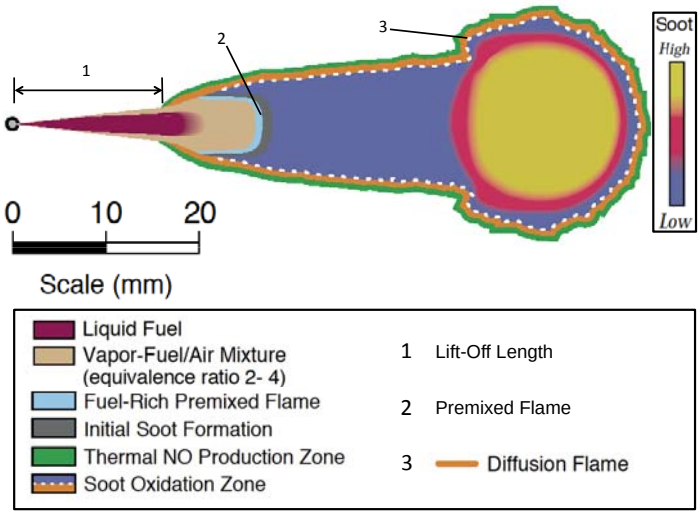

Figure 2.2 Diagram of the diesel jet during the quasi-steady diffusion flame. Conceptual model by Dec [16].

During the injection process, the flame typically stabilizes at a certain distance from the nozzle, called the quasi-steady lift-off length. The stabilization mechanism is not quite clear. The classical picture is that a balance is established between the velocities of the injected fuel downstream the spray and the speed of the flame front travelling upstream the spray. A more recent picture is that the flame stabilizes through a process related to auto-ignition [17]. The lift off length is important since it defines the distance over which air can be entrained into the jet to reduce the soot formation. Downstream of the lift off length, air entrained into the jet is consumed in the diffusion flame.

The second highlighted area is the premixed reaction zone. This part of the flame is normally fuel rich with an equivalence ratio (Φ) greater than 2 [16,18]. In this fuel rich region, the oxygen (O_2) entrained upstream of the lift-off length is completely consumed and partially burned hydrocarbons (HC) are formed. Among those partially burned hydrocarbons, short-branched ones including, between others, acetylene (C_2H_2), Ethylene (C_2H_4) and propynyls (C_3H_3) are basis for soot precursors. As seen in Figure 2.2, the fuel is completely vaporized before it reaches the premixed reaction zone.

The diffusion flame (third area in Figure 2.2) is the envelope of the jet, where products from the partial combustion mix and react with oxygen in the fresh gases surrounding the burning spray. It is a hot zone (>2500K) suitable for OH formation [2], which are favorable conditions for soot oxidation and NO_x formation.

2.2 Soot Formation General Aspects

As mentioned earlier soot precursors are formed in the premixed part of the flame, in a process called pyrolysis. This is the first of many steps that leads to full-grown soot particles. A schematic diagram of those steps is shown in Figure 2.3. The fuel pyrolysis takes place when the fuel reaches approximately 1600 K [16]. It is a process where hydrocarbon molecules alter their molecular structure in the presence of high temperature and low oxygen. The soot precursor species formed during the pyrolysis will start bonding with each other in a process called particle inception where they will form larger aromatic rings called polycyclic aromatic hydrocarbons (PAH). The PAHs will grow further by bonding with alkyl groups forming larger aromatic structures. The resulting particles from the inception are soot particle nuclei, hence the alternative naming of the process as "nucleation". These nuclei are relatively small and represent a minor part of the total soot mass. However, they play crucial role in the subsequent mass additions as they provide sites for surface growth.

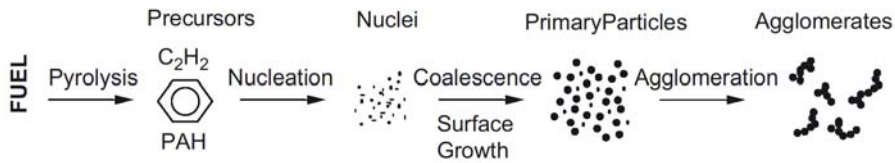

Figure 2.3 Soot particle formation process. Reproduced from [19].

As the particle travels further from the premixed zone, the nuclei's highly reactive surfaces bond more and more soot precursors, increasing the size of the nuclei up to primary soot particles. During this process, few new particles are formed while the mass of existing particles increases. This step is called the surface growth. The developing nuclei also coalesce (or coagulate), forming larger primary particles. This phenomenon keeps proceeding between the primary particles leading to formation of chain-like agglomerates of primary particles.

In summary, the soot particles originate from the soot precursors formed in the premixed flame. From this region, the precursors travel downstream the burning spray while undergoing the various chemical and physical reactions that lead to growth in size and agglomeration.

2.3 Soot Oxidation

A simplified view of soot oxidation is the reaction between a carbon molecule (C) and an oxygen atom (O) resulting in combustion products such as CO, CO_2. The soot oxidation and soot formation are competing processes, occurring in parallel as long as soot (any of the aforementioned forms of it contained in Figure 2.3), oxidizers and high temperature (>1300K [20]) are combined. Below this threshold temperature, the reaction kinetics are virtually frozen without the help of catalysts such as used in diesel particulate filter (DPF).

The oxidation of soot has traditionally been described as a reaction between the particles and molecular oxygen, as in the Nagle/Strickland-Constable (NSC) Model from 1962 [21]. The NSC model is based on the oxidation of soot particles by oxygen on two major sites (*A* and *B*) and is expressed by the equation

$$\frac{w}{12} = \left(\frac{k_A p_{O_2}}{1+k_z p_{O_2}}\right) x + k_b p_{O_2}(1-x) \qquad (2.1)$$

where *w* denotes the specific soot oxidation rate ($g.cm^{-2}.s^{-1}$) and *x* represents the fraction of the soot particle surface occupied by *A* sites given by the equation

$$x = \left(1 + \frac{k_T}{1+k_B p_{O_2}}\right)^{-1} \qquad (2.2)$$

where the values of the NSC constants k_A, k_B, k_Z and k_T can be found in the Table 2.1 and p_{O_2} is the partial pressure of oxygen. The sites A are more reactive than sites B, but as temperature increases, the rate *w* decreases because of the thermal rearrangement of the surface of the particle where more B sites will be present. Beyond a certain point, only B sites can be found on the surface and the rate becomes linearly proportional to the partial pressure of oxygen and increases again with temperature.

Table 2.1 Constants from the Nagle/Strickland-Constable model [22]

Rate constants	Units
$k_A = 20 \exp(-15100/T)$	$g/(cm^2.s.atm)$
$k_B = 4{,}46 \times 10^{-3} \exp(-7640/T)$	$g/(cm^2.s.atm)$
$k_T = 1{,}51 \times 10^5 \exp(-48800/T)$	$g/(cm^2.s)$
$k_Z = 21{,}3 \exp(2060/T)$	atm^{-1}

In 1969, Fenimore and Jones highlighted that OH had an important role in the oxidation of soot and, depending on the conditions, other oxidizing species like O,

H_2O, CO, CO_2, and NO_x as well [23]. A kinetic model for oxidation by OH was proposed in 1981 by Neoh et al. [24] and the same group pointed out a few years later that the agglomerates break during the oxidation under fuel lean condition as a consequence of internal burning by O_2 [25]. Under fuel rich conditions, they showed that OH was dominating and, being more reactive than O_2, mostly participated in superficial oxidation. The oxidation of soot by OH as described by Neoh et al. can be written as

$$w_{OH} = \gamma_{OH} \frac{3n_{OH}}{N_A} \left(\frac{8RT}{\pi M_{OH}}\right)^{1/2} \tag{2.3}$$

where, w_{OH} is the soot oxidation rate, n_{OH} and M_{OH} are the number density and the molar mass of OH respectively, R is the general gas constant and N_A is Avogadro's number. γ_{OH} is the collisional frequency between OH and the soot surface and is usually assigned a value of 0.13 [25].

In engines, the research focus has traditionally been put on the early and middle stages of the combustion because more than 90% of the soot formed and oxidized happens before the end of injection [2]. However the remaining parts explain most of the exhaust soot level source. An attempt at characterizing the soot burnout by Dec and Kelly-Zion in 2000 using laser diagnostics pointed out that reducing the availability of oxygen significantly affected the emission levels [26], already linking the importance of late cycle soot burnout with exhaust levels. In 2007, Huestis et al. studied with optical diagnostics both the in-cylinder soot processes and emissions for a variation of intake O_2. What they found out was that emissions paralleled the in-cylinder soot trend [27].

Despite the latest studies on the late cycle soot burnout, a few questions are left unanswered. First, which of the processes of soot oxidation and soot formation is the most important in terms of predicting emissions? Second, which are the parameters that we can affect, by control or design, that are the most relevant to optimize the soot burnout?

3 Experimental Tools

In-cylinder research techniques can be categorized according to the extent to which they interfere with the studied phenomenon. One category is called *intrusive* where the sampling device will physically affect the on-going processes such as measurement of temperature with thermocouples or gas sampling. On the opposite, *non-intrusive* techniques, also called *optical* for being based on light interaction, do not interfere with the processes under study or do so in a negligible way.

3.1 Optical Engine

In order to make optical measurements, the engine needs to be modified for optical access. It is realized by replacing metal parts of the engine with transparent material such as quartz or sapphire. A design developed in the 1960s by the General Motors engineer Fred Bowditch became widely spread in the engine research field [28]. It provides a wide range of optical accesses, albeit at the cost of limiting the load range in which it can be operated. A 3D sketch of such design can be seen in Figure 3.1. The right part of the figure shows the assembly of the engine block extension and disconnects the cylinderhead of the engine from the engine block. The piston extension is shown on the left of Figure 3.1. This extension sits on the original engine piston and serves the purpose of bringing the combustion chamber to a location where more optical accesses can be created. It is hollow for 2 main reasons: first, reducing the weight of the extension and, secondly, providing a location for a fixed 45° tilted mirror. A transparent piston made of quartz creates an optical access from the bottom of the combustion chamber, which can be used to observe the injection or combustion process during operation.

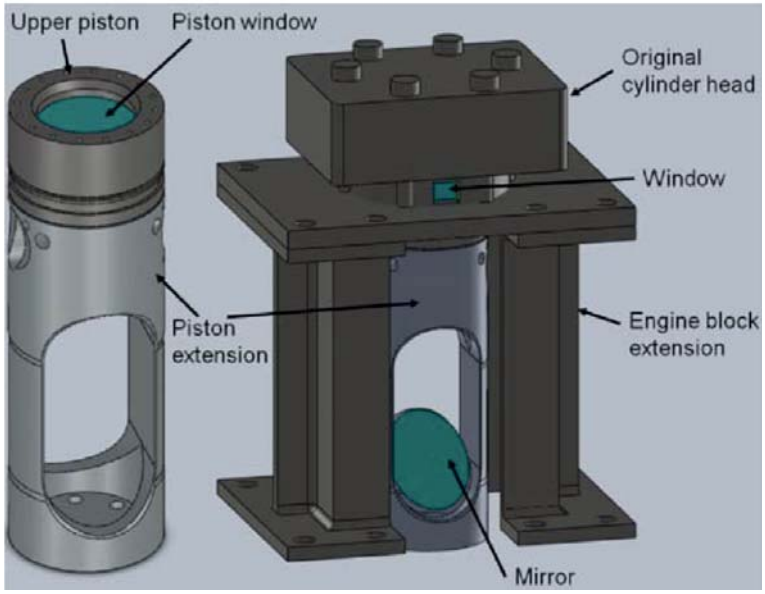

Figure 3.1 *3D sketch of the Bowditch design. The piston extension (on the left) is also shown mounted in the engine extension on the right. [29].*

Other forms of optical access such as windows or a full transparent liner can be used depending on the needs of the study and techniques, for example to allow a laser beam access to the combustion chamber. The rest of the original engine is left mostly unchanged below apart from extended fuel and electrical connections. By design, the upper optical piston is not lubricated during engine operation. A set of composite dry piston rings is then used to handle the guiding of the piston extension in the new cylinder.

The optical access created can be used for viewing the injection or combustion process and also create various paths for laser-based diagnostics.

The study of this thesis concerns the late cycle soot oxidation. Therefore, optical accesses during the late parts of the cycle are necessary. Except from the transparent piston, most of the optical accesses available on the Bowditch engine presented above are limited studies close to TDC. A first setup was developed to gain an extra optical access from the roof of the combustion chamber, which would allow a laser beam to pass vertically through the cylinder and probe processes occurring when the piston has moved far below the side-port windows. A 3D sketch of this setup can be found in Figure 3.2.

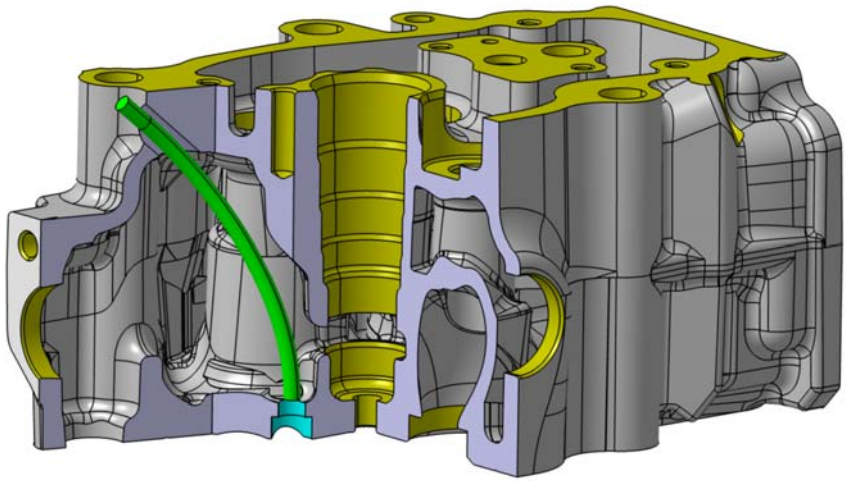

Figure 3.2 *3D sketch of the cylinder head used in the first setup. The green tube is the housing for an optical fiber. The blue socket is the location for a small quartz window.*

In this setup, an optical fiber was guided through the water jackets to the firedeck of the combustion chamber. The quartz window protecting the fiber was located between the two exhaust valves. The minimum bending radius is 100 mm to avoid losses of light in the fiber.

The idea was to guide a laser beam through the optical fiber. Despite the precautions taken in designing this cylinderhead and optical access, the losses of light in the fiber were too large. Moreover, the collimation of the light at the output was not good enough and the critical location of the output could not allow for a better re-collimation of the laser beam.

A new way to gain an optical access from the top of the combustion chamber was designed. In this new design shown in Figure 3.3, one of the exhaust valves was removed and the water jackets were re-machined in order to leave space for a cylindrical insert to be inserted into the cylinder head.

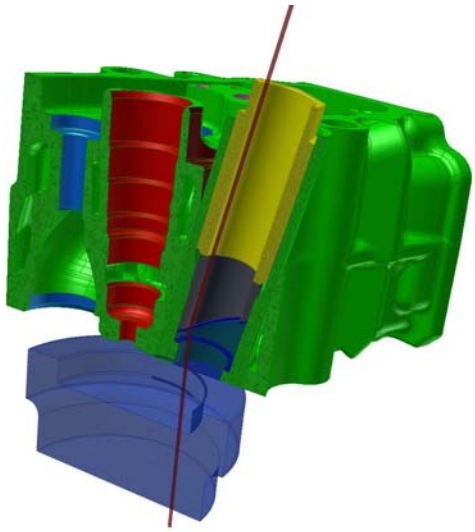

Figure3.3 *3D cut of the 3-valve cylinderhead design. The insert is represented in yellow; the red socket is the location of the injector.*

The quartz window was designed with a flat surface on the combustion chamber side and a tilted surface on its other The combination of angles ensured that the laser beam passed vertically through the cylinder, although it entered the cylinderhead at an angle. Despite its larger diameter compared to the previous design, the location of the access limited the laser path to a region close to the bowl wall. The piston used for the experiments was designed with a flat bowl to keep the straight path.

In terms of scavenging, removing one of the exhaust valves is less critical than removing an inlet valve. Furthermore, the engine is operated in skip-fire mode during the optical measurements, meaning that injection and combustion does not occur during every cycle, giving the burned gases a few cycles to be fully replaced with fresh ones. Moreover, the engine is operated relatively slowly (1200 rpm max), allowing for effective gas scavenging.

3.2 Optical Soot Diagnostics

There are various optical diagnostics used for the study of soot particles during the combustion. The most common one due to its simplicity is called natural luminosity (NL). It is based on the Planck radiation law and only requires an optical access through a single port and a light sensor. The Planck law describes the intensity of the light emitted by a blackbody, for instance a soot particle

$$I(\lambda, T) = \varepsilon_\lambda \frac{2\pi hc^2}{\lambda^5 (e^{\frac{hc}{\lambda KT}} - 1)} \tag{3.1}$$

where λ is the wavelength of the emission, T the temperature of the particle, h the Planck's constant, c the speed of light in a vacuum, K the Boltzmann constant and ε_λ is the monochromatic emissivity of the particle varying between zero and one, with a value of one in the case of a perfect blackbody.

As a result from this law, the radiation spectrum is broadband and extends beyond the visible region. Moreover, the total intensity from the blackbody can be calculated with Stefan-Boltzmann's

$$I = \sigma T^4 \tag{3.2}$$

where σ is the Stefan-Boltzmann constant. It highlights the strong temperature dependence of the total intensity emitted by a particle.

There are a few important issues for using this technique even to a semi-quantitative level. The soot particles drop quickly in temperature during the expansion, thus reducing strongly the signal emitted. Moreover, the concentration and sizes of soot particles is expected to reduce during the oxidation, thus making the drop of signal difficult to interpret. Emission from other combustion species called chemiluminescence will contribute to the background noise, albeit to a limited extent at typical flame temperatures where the NL from soot is intense. Finally, the technique is spatially limited in that the source of the signal emitted may come from a dense field (optical thickness) and may be lost by absorption by other particles along the way to the detector. A successful application of this technique can be seen in [30] thanks to a complex calibration and knowledge of the fuels compositions. However, the authors do not recommend the use of such technique in the late cycle where the intensity of the radiation drops too much due to the presence of non-emitting cooled particles.

The two-color pyrometry is also based on the previously described Planck radiation law. It is primarily a thermometric technique. In the two-color method, the concept of apparent temperature T_a is introduced. It is defined as the temperature a black body would be at while emitting the same amount of radiation

$$I_{b,\lambda}(T_a) = I_\lambda(T) \tag{3.3}$$

The emissivity of the particle introduced in equation (3.1) can be written

$$\varepsilon_\lambda = \frac{I_{b,\lambda}(T_a)}{I_{b,\lambda}(T)} \tag{3.4}$$

Combining (3.1), (3.4) and using the "new" Planck constant ($C = hc/K$) to simplify the writings, the monochromatic emissivity is given by

$$\varepsilon_\lambda = \frac{e^{C/\lambda T}-1}{e^{C/\lambda T_a}-1} \tag{3.5}$$

The emissivity can be described using the empirical correlation of Hottel and Broughton,

$$\varepsilon_\lambda = 1 - e^{(-KL/\lambda^\alpha)} \tag{3.6}$$

where KL describes the optical thickness with K the absorption coefficient and L the thickness of the probed medium and α is a coefficient generally chosen as $\alpha = 1{,}39$ according to the literature for wavelength chosen in the visible range [31].

A system can then be created from equations (3.5) and (3.6) to extract the value of T

$$\left[1 - \left(\frac{e^{(C/\lambda_1 T)}-1}{e^{(C/\lambda_1 T_{a1})}-1}\right)\right] = \left[1 - \left(\frac{e^{(C/\lambda_2 T)}-1}{e^{(C/\lambda_2 T_{a2})}-1}\right)\right] \tag{3.7}$$

The value of T found will give the optical thickness KL using the equation (3.5) and (3.6) written as

$$KL = -\lambda^\alpha ln\left[1 - \left(\frac{e^{(C/\lambda_2 T)}-1}{e^{(C/\lambda_2 T_a)}-1}\right)\right] \tag{3.8}$$

The technique uses a relatively simple background theory. However, it still faces a similar lack of signal as for the NL when it comes to cool soot particles in the late cycle. Moreover, variation of temperatures of particles in the field of view creates large variation in the evaluation of KL. The technique is nonetheless chosen and applied successfully for soot studies granted careful assumptions and calibration [32,33].

Another technique also based on the Planck radiation is called laser-induced incandescence (LII). For this technique, the soot particle is subjected to a short (10 ns) high-intensity laser pulse that will vaporize it by elevating its temperature above 4000 K. The intensity of the radiation is much higher than the one from of a flame (1500-2500 K) as expected from eq. (3.2). For a duration of approximately 100 ns after the pulse, the light emission due to thermal radiation is detected and recorded. The decay of the signal due to the cooling can be compared to a time-dependent model to evaluate the particle size and the total intensity of the signal is proportional to the soot volume fraction. These measurements can be applied in

2D by using a laser sheet. There are however drawbacks to the technique when used in sooting conditions. For example, the laser sheet can suffer extinction along its path, leading to underestimation of the soot concentration downstream the laser sheet. Another issue called signal trapping occurs when the signal is attenuated between the measurement plane and the detector due to the presence of soot particles, also leading to an underestimation of the soot concentration. Though time consuming, those effects can be compensated with three-dimensional studies [34,35]. For quantitative measurements the LII technique relies on an external calibration, for example by laser extinction in a controlled flame. The technique does not suffer from the loss of signal due to cooling soot during the late cycle. In the most common setup it is restricted to studies close to TDC, however, and relies on careful calibration. It has been implemented in engine studies such as [36].

3.3 Laser Extinction

The optical diagnostic of choice for this thesis was the laser extinction method (LEM). It is a quantitative technique with high time resolution. Its setup is simple and enables collection of large amounts of data for exhaustive studies. It has been applied for several decades in internal combustion engines [37-39]. It is a technique relying on the comparison of a reference intensity collected before going through the combustion medium and the measured intensity after attenuation by absorption in the flame.

The principle of this technique is based on the Beer-Lambert law

$$I = I_0 e^{-KL} \tag{3.9}$$

where I and I_0 are the transmitted and reference intensity respectively, K is the extinction coefficient and L is the length of the absorbing medium. In the present study, L corresponds to the vertical extent of the combustion chamber through which the laser is passing as shown on Figure 3.3. If the particles sizes are much smaller than the laser wavelength, the scattering can be neglected and the extinction coefficient K is roughly equal to the absorption coefficient K_{abs}. With this assumption, the extinction coefficient can be related to the soot volume fraction f_v by

$$K = \frac{f_v 6\pi E(m)}{\lambda} \tag{3.10}$$

where λ is the laser wavelength and $E(m)$ is the refractive index function, representing the imaginary part of $(m^2-1)/(m^2+2)$, in which m is the

complex refractive index of the soot particles. In the results of this thesis however, the soot concentration is presented as the optical thickness KL. This product is directly related to the average soot concentration in the beam path and is derived directly from the relative transmission measurements.

The technique presents various drawbacks and challenges. It is a line of sight technique, meaning that variations of absorption along the path are not distinguished. There are known workarounds that involves measurements at different angles, positions and using symmetry properties of the flame in the evaluation [40-42]. The technique also suffers from a very limited spatial resolution. In the studies presented in articles I and II, the extinction is measured along the thin beam path located at the edge of the combustion chamber. High-speed video imaging shows that the soot cloud becomes rather homogeneous during the expansion, so the assumption that the measurements are relevant everywhere in the cylinder was made. The collimated light of the laser could possibly be deviated away from its path due to beam steering. This phenomenon is caused by sharp differences in the temperature gradients during the combustion. The focus of the thesis concerns the late cycle oxidation of soot during which temperature gradients are less sharp and the beam steering has been demonstrated to be negligible. Finally, the choice of a long wavelength in this thesis, close to 700 nm, has two motivations. Firstly, it minimizes influence from polycyclic aromatic hydrocarbons, which are known to absorb radiation in both the ultraviolet and visible spectral regions [43-45]. Secondly, a longer wavelength also minimizes potential scattering contribution from the soot to the extinction measurements.

There is a possibility to extend the spatial resolution of extinction measurements by using a technique called diffused back illumination (DBI). The light from a diode is diffused and targeted towards the flame. A camera on the other side of the spray records the extinction of the diffused light [46]. The principle remains the same, but it extends the measurement to a 2D projection through the measurement region.

Another such evolution of the technique is called forward illumination light extinction (FILE), where instead of illuminating the flame from the back, the light is sent toward the flame, reflected back through the flame and finally collected [47].

3.4 In-Cylinder Sampling

To complement the optical measurements of soot oxidation, in-cylinder gas samplings have been conducted in order to gather more information about the soot particle properties. Despite being an intrusive technique, gas sampling provides relevant information about physical and chemical properties of soot. A schematic of the setup used for the in-cylinder sampling can be found in Figure 3.4.

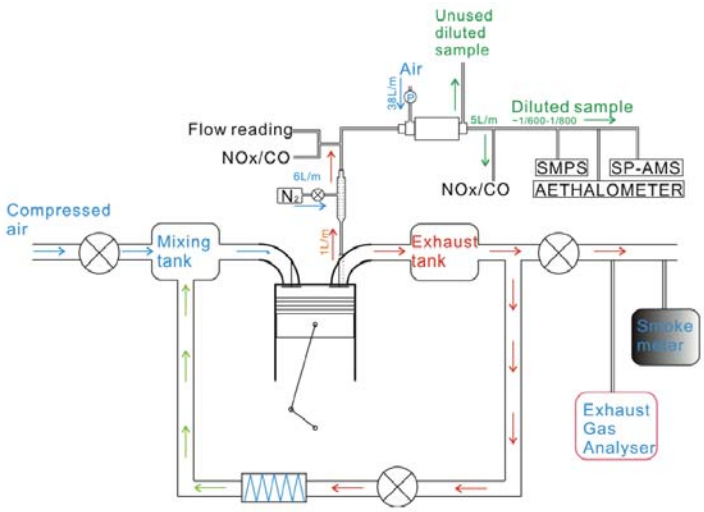

Figure 3.4 *Schematic of in-cylinder sampling setup.*

A solenoid unit controls the sampling valve [48] used in this study. During operation, the solenoid units actuates a hammer hitting the stem of the valve, creating a wave propagating towards the poppet valve provoking a short aperture. Depending on the voltage chosen on the electronic actuation device, the intensity of the hammer hit can be adjusted, varying the duration of the valve opening. The valve driver is controlled by a TTL signal from a computer program and triggered on crank angle basis. With these features the gas flow through the valve can be controlled in a wide range, with respect to sampling timing and sampling rate. In this study, the gas flow was kept constant at 1 liter per minute (at ambient atmospheric pressure and temperature) for each sampling point. This volume corresponds to approximately 0.05% of the total cylinder volume. With this flow rate, the minimum step-by-step resolution for the sampling timing can be less than 3.5 crank angle degrees at high in-cylinder pressures. The same 3-valve cylinderhead (Figure 3.3) as for the optical study was used, but the fast sampling valve replaced the optical insert as shown on Figure 3.5. Once sampled, the gases

are diluted with nitrogen (N_2) in order to prevent further oxidation of the particles. The subsequent dilution steps are used to reduce the amount of particles to a suitable level for the aerosol online gas analyzing system. This system is comprised an aethalometer, a soot particle aerosol mass spectrometer (SP-AMS) and a scanning mobility particle sizer (SMPS).

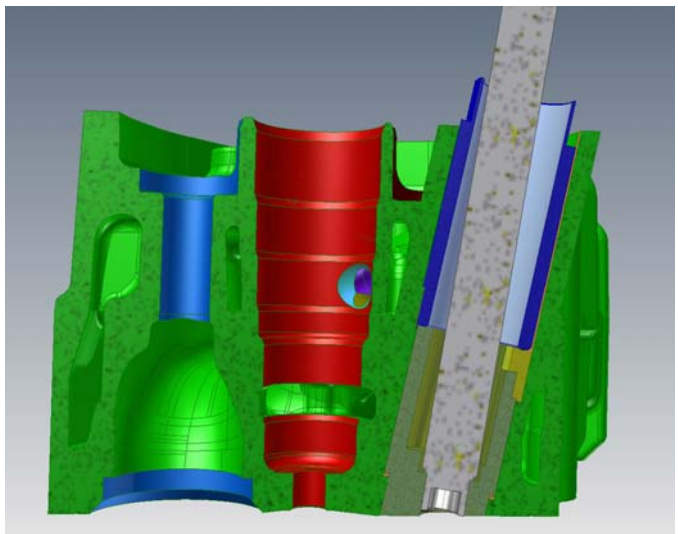

Figure 3.5 *3D cut of the 3 valve cylinderhead used for the sampling measurements. The sampling valve is located in the insert in grey. The red socket corresponds to the location of the injector.*

The aethalometer [49], which measures the Black Carbon, is based on the absorption of laser light by the probed particles. Seven different wavelengths are used, ranging from 370 nm to 950 nm. These allow determination of the optical properties of the soot particles. The BC concentration is obtained as the average of the measurements at the two highest wavelengths (880 nm and 950 nm) in order to reduce interferences from organics or polycyclic aromatic hydrocarbons that absorb in and near the ultraviolet region. The aethalometer also allowed the extraction of the Ångström exponent characterizing the wavelength dependence of the particle.

Particle chemical composition was investigated with a soot particle aerosol mass spectrometer [50] and was run in single or dual vaporizer mode. In the single vaporizer mode, particles are flash-vaporized upon impaction on a heated (600°C) tungsten surface. In the dual vaporizer mode, refractive black carbon containing particles are vaporized, in flight, using an intracavity Nd:YAG laser (1064 nm). The vapors are then ionized (70 eV electron ionization) and detected in a high resolution, time-of-flight mass spectrometer. The SP-AMS allows efficient sampling of particles in the diameter range ~70-500 nm.

A scanning mobility particle sizer was used to classify particles sizes based on geometric mean diameters (GMD) and number concentration. It should be pointed out that this refers to the size of the full soot aggregates rather than the size of the primary particle in the aggregates that are commonly measured with electron microscopy techniques. The SMPS voltage scan-up time was 120 seconds, which allowed averaging over at least three full size-scans at each measurement point. The configuration enables particle mobility diameter size classification in the range of 10 – 415 nm. The geometric mean diameter was calculated from the particle mobility size distributions assuming lognormal distributed data with a unimodal shape following the equation

$$GMD = exp\left[\frac{1}{N_t}\sum_{i=1}^{M}\left(N_i ln\left(D_{pi}\right)\right)\right] \tag{3.11}$$

3.5 Heat Release Analysis

The pressure inside the cylinder is measured continuously using a piezo-electric pressure transducer, a charge amplifier and an analog-digital converter. The charge amplifier gives a voltage proportional to the force on the sensor membrane.

The apparent rate of heat release is useful tool in order to monitor the combustion process and compare points of operation. A brief recap of the theory is given, based on [2].

The first law of thermodynamics dictates the energy balance in the combustion chamber of the engine as

$$\frac{dQ}{dt} = \frac{dU}{dt} + \frac{dW}{dt} + \sum_i m_i\, h_i \tag{3.12}$$

Where dQ/dt is the heat added to the system, dU/dt represents the change in internal energy, dW/dt is the work performed by the system, m and h are the mass and enthalpy of an element i entering the system.

The internal energy U can be expressed as

$$U = mC_vT \tag{3.13}$$

where m is the mass of the system, C_v is the specific heat constant at constant volume and T the temperature. Assuming that m is constant, the derivative of Eq. (3.13) is

$$\frac{dU}{dt} = mC_v \frac{dT}{dt} \tag{3.14}$$

Using the ideal gas law

$$pV = mRT \tag{3.15}$$

where V is the volume and R the specific gas constant. For m and R constant, the derivative of Eq. (3.15) gives

$$pdV + Vdp = mRdT \tag{3.16}$$

Inserting Eq. (3.16) into Eq. (3.14) gives

$$\frac{dU}{dt} = \frac{C_v}{R}\left(p\frac{dV}{dt} + V\frac{dp}{dt}\right) \tag{3.17}$$

The work can be expressed as

$$dW = pdV \tag{3.18}$$

Neglecting mass exchange and using Eq. (3.17) and Eq. (3.18) into Eq. (3.12) yields

$$\frac{dQ}{dt} = \frac{C_v}{R}\left(p\frac{dV}{dt} + V\frac{dp}{dt}\right) + p\frac{dV}{dt} \tag{3.19}$$

The specific gas constant can be expressed as

$$R = C_p - C_v \tag{3.20}$$

where C_p is the specific heat ratio at constant pressure. The ratio of specific heat is written as

$$\gamma = \frac{C_p}{C_v} \tag{3.21}$$

using Eq. (3.20) and Eq. (3.21) allow Eq. (3.19) to be rewritten and simplified using γ

$$\frac{dQ}{dt} = \frac{\gamma}{\gamma - 1} p\frac{dV}{dt} + \frac{1}{\gamma - 1} V\frac{dp}{dt} \tag{3.22}$$

Finally, using a crank angle time base, the apparent rate of heat release can be expressed as

$$\frac{dQ}{d\theta} = \frac{\gamma}{\gamma-1} p \frac{dV}{d\theta} + \frac{1}{\gamma-1} V \frac{dp}{d\theta} \tag{3.23}$$

In the work presented in this thesis, only the apparent rates of heat release were calculated. It was considered a sufficient approximation to illustrate the main characteristics of the combustion process. However, the author would like to point out that further corrections are possible and direct the reader to [2] for further information on how to calculate the losses by blow-by and heat losses to the walls.

The cumulative sum of the apparent rate of heat release can be calculated to extract the crank angle degree at which 50% of the heat has been released, CA50. This metric is important as it allows monitoring the combustion phasing in order to have comparable conditions during engine operation.

4 Results and Discussion

The results presented in this thesis are divided into four subchapters: the first assesses the validity of the laser extinction measurements, the following explains the reasons behind the choice of the metric to characterize the late cycle oxidation process, the third presents the impact of various studied parameters on the soot oxidation and how it correlates with exhaust soot levels. Finally, a subchapter is dedicated to a detailed study of oxygen availability due to its importance as a soot oxidizer.

4.1 LEM Validation

The laser extinction measurements were conducted in the 3-valve cylinderhead as presented in chapter 3.1. A representation of the laser path can be seen in Figure 3.3 and it can be seen that the laser path is located close to the edge of the bowl. In order for the laser extinction measurements to be relevant to the global combustion process, the assumption that the laser path studied is representative of the whole combustion chamber was made. Pictures of the combustion process occurring in the engine including the position of the laser are shown in Figure 4.1.

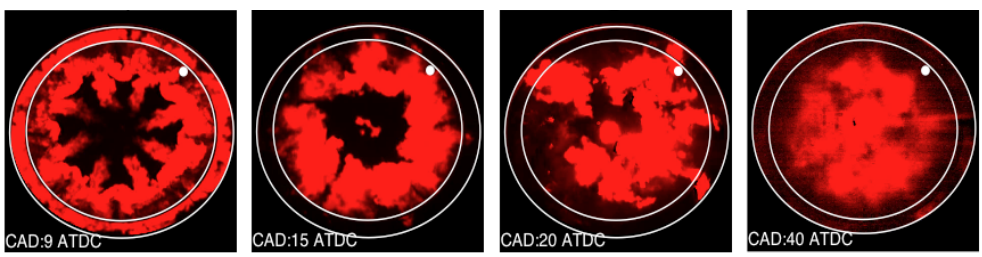

Figure 4.1 *Images of the soot natural luminosity at different CAD. The inner white circle represents the bowl wall, the outer one represents the periphery of the piston and the white dot represents the position of the laser beam. The shutter speed is adjusted and the intensity is digitally rescaled through custom scaling color maps.*

In this series of images, it can be seen that once the injection has ended, a few droplets of fuel burns with high intensity at the center of the chamber due to fuel

dribble while a ring-shaped cloud of soot forms due to the swirl motion of bulk gases in the cylinder and the burning fuel originating from the 8 sprays. From a qualitative perspective, the distribution of gases in the cylinder becomes quickly homogeneous and corroborates the assumption according to which the path of the laser is representative of the whole combustion chamber processes regarding soot.

A comparison between the signal from the laser extinction and the signal from soot natural luminosity was conducted in paper IV. Laser extinction and natural luminosity were recorded simultaneously. The signal from the laser extinction is restricted to the laser path while the natural luminosity is recorded from a larger region. The two signals are plotted on Figure 4.2 during a combustion cycle.

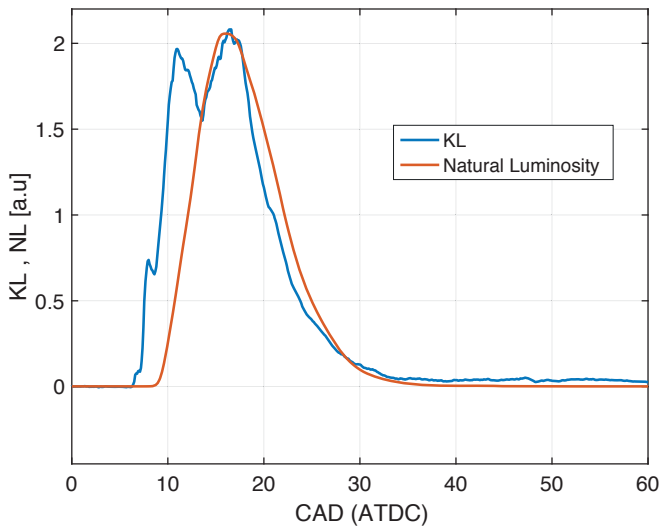

Figure 4.2 *signals of LEM(KL) and NL during a combustion cycle.*

There is good overlap of the two signals (R^2 = 98%, 13-40 CAD) further confirming that the laser path does actually represent the global soot processes in the cylinder in the late cycle. On a side note, the extinction signal rises earlier than the natural luminosity, likely due to perturbations also observed in a non-reactive case from liquid fuel droplets and other potential sources. It can also be noted that the signal from the extinction measurements do not fall down to zero as opposed to the natural luminosity signal. This is due to the fact that cold soot particles do not radiate any signal anymore, while the extinction measurements still detect the presence of soot particles in the late cycle. These two last notes emphasize further the relevance of the present extinction setup for studies in the late cycle as opposed to early soot formation processes where disturbances from other sources make the interpretation of the signal difficult.

The choice of wavelength for extinction measurement can be critical. The wavelength is usually chosen in the visible range for ease of alignment, but as long as possible as to avoid interferences from other species such as PAHs [43-45] as well as potential scattering from the particles. The aethalometer data from in-cylinder sampling measurements could allow a simple verification of the importance of choosing a longer wavelength for absorption measurements.

The aethalometer measures the absorption of the sampled particles at seven different wavelengths. This feature gives access to some particle optical properties such as the Ångström exponent. It is a physical quantity characterizing the wavelength dependence of a particle as well as optical properties such as size and other aerosol properties [51]. It is described following the equation:

$$\tau_\lambda = \tau_{\lambda_0} \left(\frac{\lambda}{\lambda_0}\right)^{-\alpha} \tag{4.1}$$

where α is the Ångström exponent corresponding to the sampled particles giving the optical thickness τ_λ at wavelength λ, compared to a reference wavelength of λ_0. Figure 4.3 shows the variation of the Ångström exponent with wavelength for a variation for inlet oxygen concentration at 50 CAD normalized at the highest wavelength available in the aethalometer (950 nm). The orange dashed line highlights a break between shorter wavelength and longer wavelength. It also corresponds to the aethalometer available wavelength (660 nm) closest to the one used during the extinction measurements (≈690 nm). The Ångström exponent corresponds to the slope of the black dashed lines. A slight change of slope can be observed between the shorter wavelengths and the longer ones. This means that the characteristics of the particles sampled are notably dependent on the wavelength.

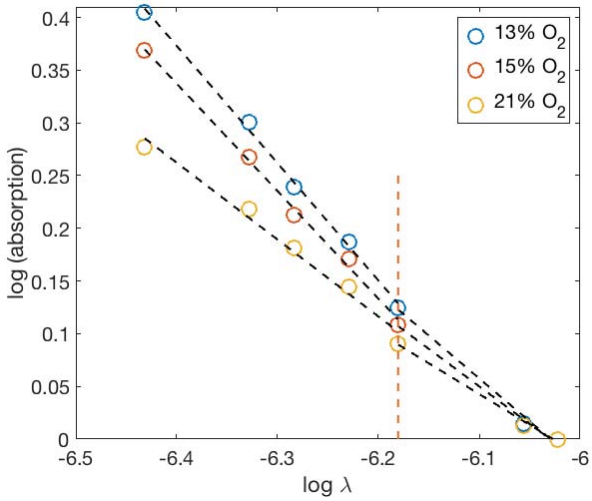

Figure 4.3 *Log of absorption in function of the logarithm of the wavelengths for 13, 15 and 21% inlet oxygen at 50 CAD. The dashed black lines show the trends of the data. A break at the log(660 nm) is shown as an orange dashed line. The Ångström exponent corresponds to the slope of the trends.*

Figure 4.4-left shows the evolution of the Ångström exponent during the cycle for shorter wavelength, corresponding to the slopes before the break as shown on Figure 4.3. The trend is similar for longer wavelength (Figure 4.4-right) however the amplitude of variation is much wider, particularly during the early cycle where a stronger concentration of PAH is expected.

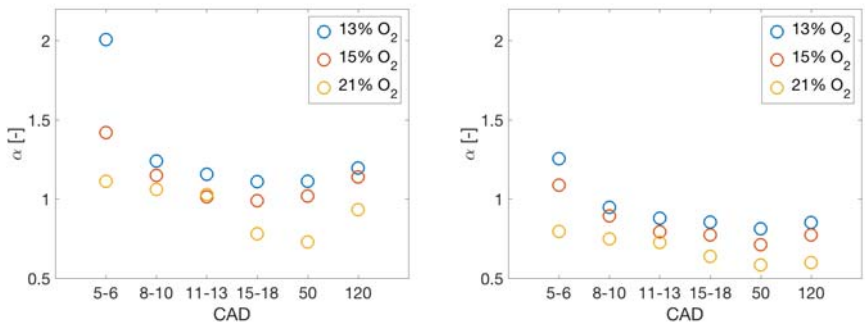

Figure 4.4 *variation of the Ångström exponent during the cycle for varying inlet oxygen concentration. The left diagram shows the evolutions of Ångström exponent for shorter wavelengths (370-660 nm), on the right diagram are shown the evolutions for longer wavelengths (660-950 nm).*

A summary of the maximum absolute variation of the Ångström exponent for each case can be found in Table 4.1. The measurement apparatus is more sensitive to

the variation of the optical properties of the particles probed at shorter wavelengths. Smaller variations are observed for longer wavelength, meaning that absorption-based measurement will be more consistent.

Table 4.1 *Recap of maximum absolute Ångström exponent variation during the cycle for various inlet oxygen concentrations and two sets of wavelengths.*

	13% O_2	15% O_2	21% O_2
λ = 370-660 nm	90%	43%	38%
λ = 660-950 nm	44%	38%	21%

The beam steering is a serious concern for extinction measurements. It originates from the steep variation of gradients of temperature in the combustion that will affect the refractive indices of the neighboring mediums. The collimated light can be steered out of collimation, sometimes out of the collecting sensors, and the loss of signal could result in an overestimation of the absorption by the particles.

A study by Musculus et al. [52] gives some simple guidelines in order to assess the quality of the measurement setup in regard to the beam steering and scattering. Figure 4.5. Shows the error induced by the beam steering in the evaluation of the optical thickness *KL* of the extinction measurements.

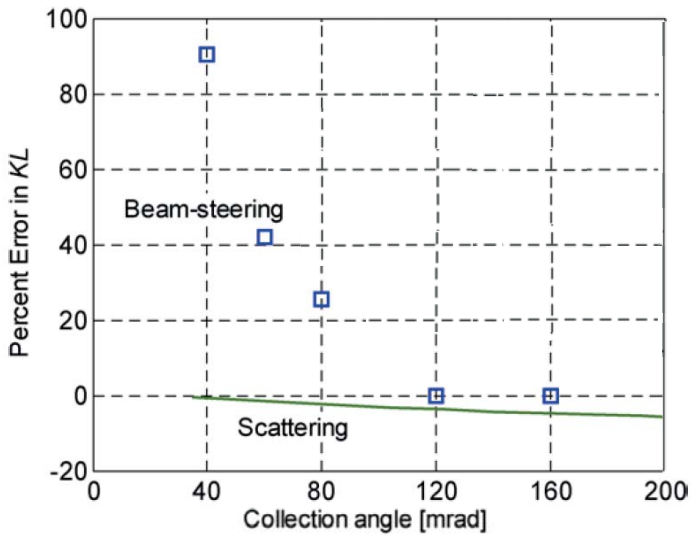

Figure 4.5 *Diagram showing the error induced in the estimation of KL due to beam steering and scattering [52].*

In the experiment presented in this thesis, the collection angle was close to 85 mrad, which means that error to beam steering was minimized to less than 20%. In addition to these preemptive measures, a study of the beam steering was conducted. The signal from the laser was sent onto a target and the spread of the signal was observed with a high-speed video camera. The dot of the laser was seen flickering and slightly increasing in size during the most intense parts of the combustion. However, it remained contained within the area corresponding to the edges of the light detector. Moreover, the beam steering is expected to be important during the early phases of the combustion (premixed phase) where the variations of temperature are the strongest. Since the current study focuses on the late cycle, the beam steering was admittedly neglected.

4.2 Characterizing the Late Cycle Oxidation

In order to characterize the soot oxidation, a robust metric was chosen that would allow comparison over a broad range of variation of parameters. When looking at the soot decay describing the late cycle soot oxidation, the shape of an exponential comes to mind. An example of such decay is shown in Figure 4.6.

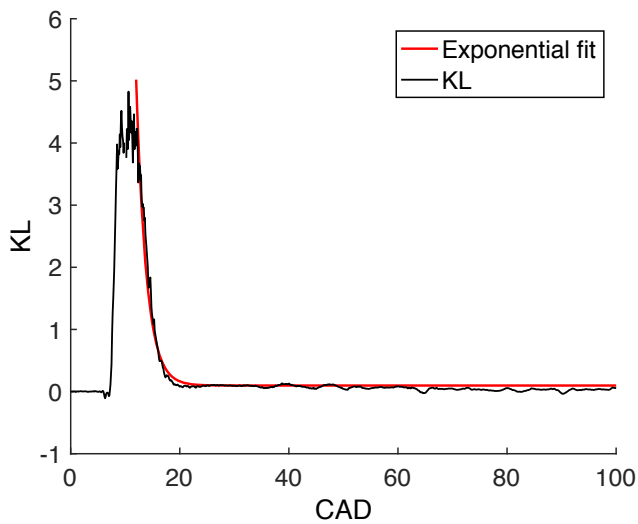

Figure 4.6 *Sample evolution of the optical thickness KL during the cycle. An exponential (in red) is fitted to the decay corresponding to the soot oxidation.*

By definition, the half-life $t_{1/2}$ of an exponential curve is given by

$$KL \propto e^{\frac{ln(2)t}{t_{1/2}}} \tag{4.2}$$

where *t* is the crank angle position, in CAD. For each exponential, the half-life can be extracted to describe the general behavior of the studied process. The advantage of choosing the half-life as metric is that it can describe the decay regardless of the starting point, meaning that the oxidation process could start from half the soot present in the cylinder and still describe the same exponential decay. Moreover, it is a parameter that proved to be robust across two different studies (on the same engine) including the variation of seven parameters. While the metric chosen for characterizing the oxidation process does not take ground from a physical perspective, it has the advantage of being universal enough to allow the comparison of all the parameters studied as well as removing the influence of the formation process.

4.3 Impact of Parameters on the Half-Life of Soot Oxidation

The effect on soot oxidation and exhaust PM concentration of the parameters presented in this subchapter were studied following a central composite design (CCD). The interest of using such method is to study both the importance of each parameter individually as well as potential interaction effects.

4.3.1 Temperature at TDC

Temperature is recognized as a strong factor affecting chemical reactions. In the case of soot processes, an increase in temperature is expected to increase oxidation rate faster than the formation rate [53]. A variation of the temperature of the bulk gases will not have a stark impact on the temperature of the flame as much as a varying the inlet oxygen concentration does. It is however expected to favor oxidation and possibly improve exhaust soot levels.

The effect of temperature at top dead center on the soot oxidation is shown on Figure 4.7 (left). A slight downward trend can be observed when the temperature at TDC was swept from 900 K to 1100 K, translating in a slight improvement of the soot oxidation rate. The values of the TDC temperature correspond to motored conditions.

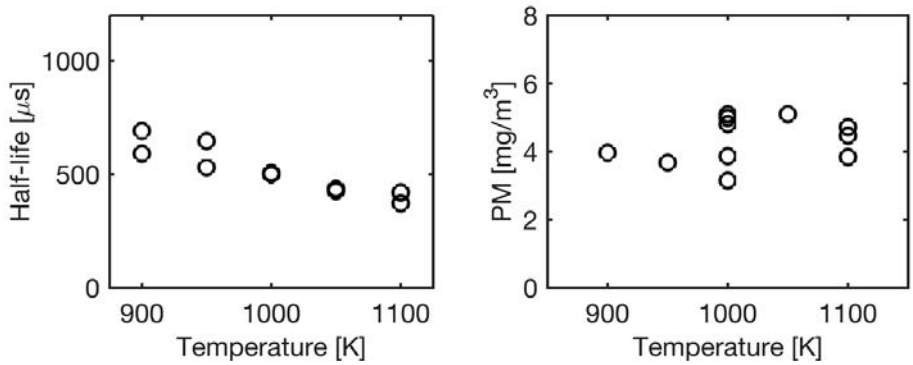

Figure 4.7 *Impact of a sweep of TDC gas temperature on the half-life of soot oxidation (left) and on the particulate matter (PM) exhausts concentration(right).*

This improvement of the soot oxidation rate does not seem to have an effect on the amount of PM in the exhaust as seen in Figure 4.7 (right). A likely explanation is that the soot formation rate is also affected and counterbalances the improved oxidation. While a strict answer cannot be given to explain the mechanism behind these observations, it can nonetheless be concluded that the temperature at TDC only has a limited impact on the soot oxidation.

4.3.2 Density at TDC

The gas density should positively affect the soot oxidation by increasing the number of oxidizer molecules per unit volume. In order to separate the density effect from that of temperature, it has been varied by changing the inlet pressure only. The density of gases at top dead center was swept from a 15.2 to 22.8 kg/m^3 and is shown in Figure 4.8 (left). The variation of density at TDC was done at motored conditions. When the density is increased, a strong reduction of the half-life of the oxidation is observed. So it can be concluded that density has a strong impact on the soot oxidation rate.

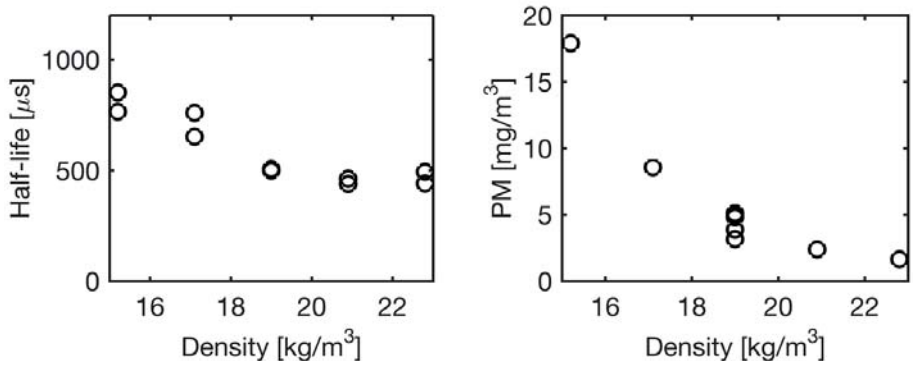

Figure 4.8 *Impact of a sweep of TDC gas temperature on the half-life of soot oxidation (left) and on the particulate matter exhausts concentration(right).*

This improvement of the soot oxidation rate results in an improvement of the exhaust PM concentrations as observed on Figure 4.8 (right). These observations confirm the hypothesis according to which gas density is an important factor on soot oxidation and emissions.

4.3.3 Injection Pressure

The late-cycle soot oxidation is a mixing-controlled process so increasing the turbulent kinetic energy in the bulk gases could enhance it. One way to do it is by increasing the injection pressure, which will create more energetic bulk-flow structures in the cylinder [54]. The influence of injection pressure on the soot oxidation is shown in Figure 4.9 (left). It should be noted that the same amount of fuel was injected for all cases by adjusting the duration of injection and monitoring the amount of heat released. Moreover, to minimize thermodynamic variation between cases, the CA50 was kept constant at 9 CAD ATDC. A steep reduction of the half-life can be observed at higher injection pressures, conveying the great importance of this parameter on the soot oxidation rate.

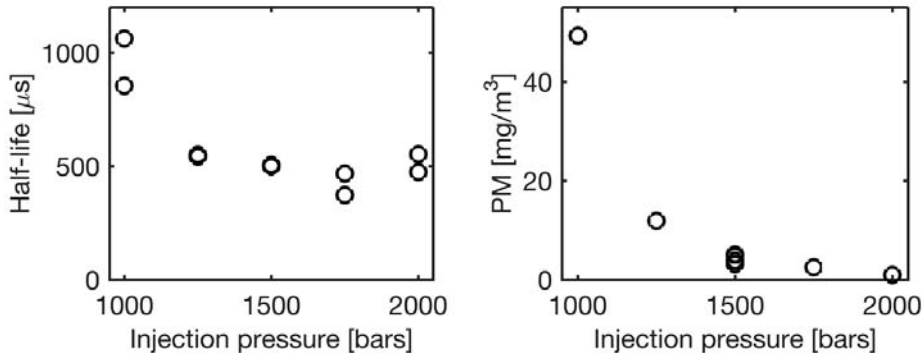

Figure 4.9 *Impact of a sweep of injection pressure on the half-life of soot oxidation (left) and on the particulate matter exhausts concentration (right).*

This strong impact of the injection pressure on the soot oxidation results in a strong reduction of exhaust PM concentration when injection pressure is increased in a mirrored behavior. Interestingly, these observations reveal the importance of the injection process for soot oxidation even long after the end of injection.

4.3.4 Engine Speed

Another way of improving the mixing-controlled oxidation process is by increasing the bulk gas turbulence. It can be achieved by increasing engine speed as the in-cylinder turbulence scales linearly with engine speed [2]. The effect of engine speed on soot oxidation is presented in Figure 4.10 (left). A slight upward trend can be observed which goes against the hypothesis initially formulated. The variation of the engine speed did not have any distinct impact on the rate of oxidation, at least in the range that could be studied in the engine.

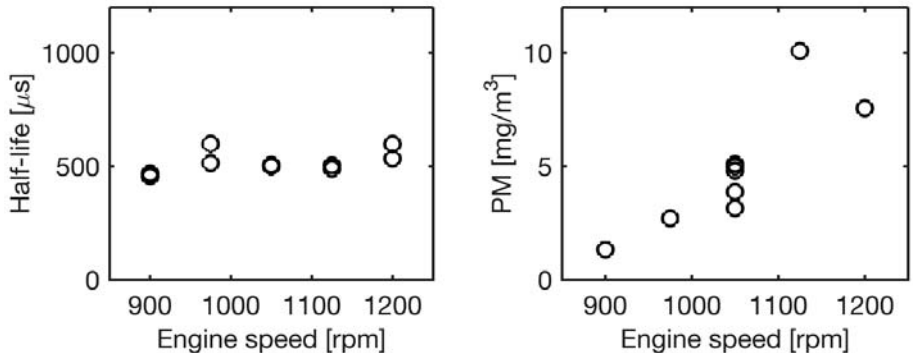

Figure 4.10 *Impact of a sweep of engine speed on the half-life of soot oxidation (left) and on the particulate matter exhausts concentration (right).*

Despite the counterintuitive result, the slight upward trend observed in the half-life of the soot oxidation rate is also observed in the exhaust PM levels as seen on Figure 4.10 (right). This could be explained by higher heat losses from the gases to the walls leading to lower temperatures as mentioned in a study by Payri et al. [55]. Moreover, the local turbulence levels may be more important than the global ones. An additional reason that could explain those results is that the effective time available for the soot oxidation reduces faster than the mixing accelerates the rate of oxidation since no major variation of the half-life is observed. In conclusion, the engine speed does not positively improve the oxidation of soot in the range of engine speed studied and actually has the opposite effect to the one originally expected.

4.3.5 Swirl Level

An additional way of improving the mixing-controlled process is by increasing the swirl. A higher swirl level will increase the fuel-air mixing, however, this effect can be mitigated by excessive spray interactions, which lead to particularly rich local equivalence ratio and therefore produce higher soot emissions [56]. The results from the variation of this parameter can be seen in Figure 4.11. The oxidation rate seems to deteriorate with higher swirl level. Despite an expected improvement of the oxidation rate with improve mixing of gases, the contrary is observed.

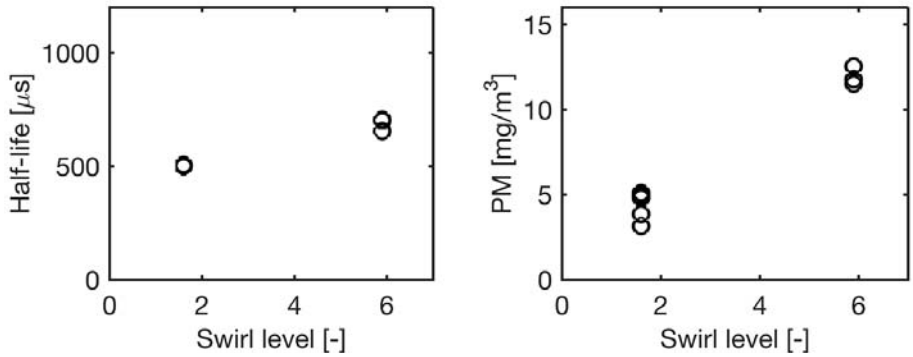

Figure 4.11 *Impact of a variation of swirl level on the half-life of soot oxidation (left) and on the particulate matter (PM) exhausts concentration (right).*

The deterioration of soot oxidation rate for higher swirl levels does however correlate with the levels of PM measured in the exhaust as seen in Figure 4.11 (right). It is possible that an intermediate level of swirl gives an improved oxidation rate and leads to lower PM concentration in the exhaust.

4.3.6 Injector Hole Size

An attempt to study the effect of injector hole size was also realized. The change of injector hole size induces drastic adjustment of the injection process. In the present case, when using the smaller-hole injector, the injected fuel amount was matched by verifying the cumulated heat released. The injection duration was increased from 720 μs to 1120 μs and as a result, the start of injection was advanced from 0 CAD ATDC to -6 CAD ATDC in order to maintain a constant CA50. The impact of such changes on the soot oxidation rate is shown in Figure 4.12(left). It shows that a shorter injection process with larger injector holes leads to a shorter soot oxidation.

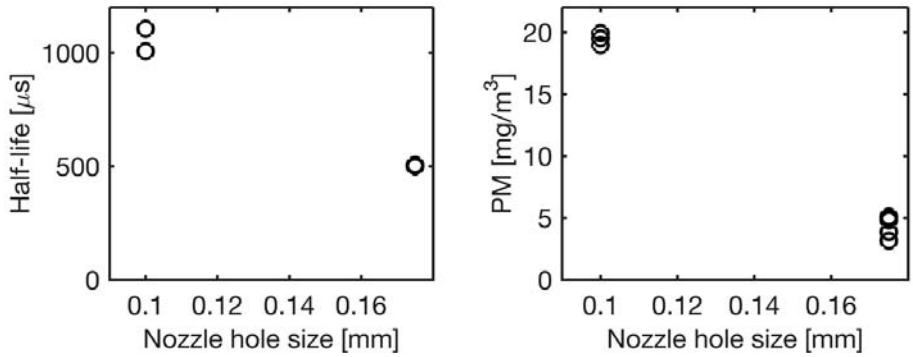

Figure 4.12 *Impact of a variation of injector hole size (0.1 – 0.175 mm) on the half-life of soot oxidation (left) and on the particulate matter exhausts concentration (right).*

The diagram in Figure 4.12 (right) shows the impact on emissions of PM and follows the trend observed with the oxidation rates. The data shows once more that an injection related parameter affects considerably the soot oxidation process and the exhaust levels. A larger hole will increase the fuel flow rate and the momentum flux. This will impart higher momentum to the gases and improve the mixing similarly to the injection pressure presented in the subchapter 4.3.3.

4.3.7 Correlation with Exhaust Soot Levels

The results contained in the previous subsections presenting the impact of the various parameters studied on the oxidation rate and the emission levels revealed similar trends. The dataset from these measurements is large enough to give a picture of the importance of the soot oxidation process compared to the soot formation process in regard to the emission levels.

It was mentioned earlier that the oxidation process was described following a single exponential (see equation 4.2). The PM contained in the cylinder can then be expressed as:

$$PM(t) = PM_0 e^{-\frac{\ln(2)\,t}{t_{½}}} \tag{4.3}$$

where $PM(t)$ is the amount of PM at a time t (for instance at exhaust valve opening), PM_0 is the amount of PM at the beginning of the oxidation dominated phase, and $t_{½}$ is the measured half-life of the oxidation process. Equation (4.3) can then be linearized by applying the natural logarithm on both sides and evaluated at the time of exhaust valve opening (EVO)

$$\ln(PM_{EVO}) = \ln(PM_0) - \frac{\ln(2)\, t_{EVO}}{t_{½}} \tag{4.4}$$

Here PM_{EVO} corresponds to the soot engine-out level. According to equation (3), plotting the engine-out levels of PM recorded versus the inverse of the half-life on a semi-logarithmic scale should display a linear relationship and assert the fact that the soot oxidation process governs the PM emission trends. This correlation is shown on Figure 4.13 with a relatively high coefficient of determination (R^2=66%).

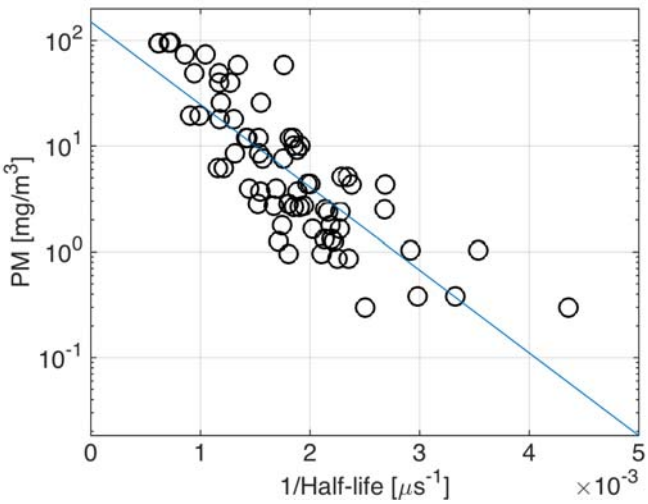

Figure 4.13 *Correlation between exhaust PM levels and oxidation half-lives on a semi logarithmic scale.*

If on the other hand, the PM measured in the exhaust were governed by the formation rate, their concentration would be proportional to the maximum amount measured in the cylinder. Such a correlation is shown in Figure 4.14 where the amount of soot formed corresponds to the value of *KL* at the start of the exponential fit, before the oxidation process dominates the global in-cylinder soot concentration behavior.

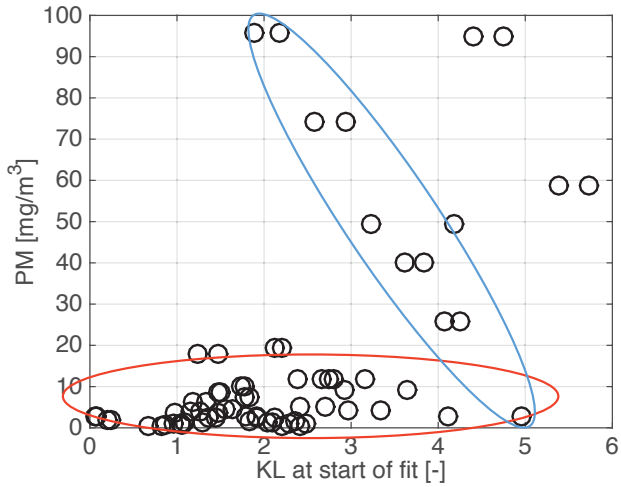

Figure 4.14 *Correlation between exhaust PM levels and KL at the start of fit of the soot oxidation exponential decays, illustrating amount of soot formed. The blue and red areas highlight two different trends.*

The red oval highlights points of operation where the PM emissions are low irrespective of the amount formed in the cylinder. The blue oval shows a trend where an increase of the soot formed in the cylinder results in lower emissions of PM, which is quite opposite to the expectations if soot formation were to govern soot emissions. In conclusion, it can be stated that soot formation cannot explain the trends in the exhaust, when in fact oxidation does so to a great extent.

4.4 Oxygen Concentration Impact

Dilution of intake oxygen with inert gases by means of EGR is a common strategy used in engines for reducing NO_x. It decreases the combustion temperature and thereby inhibits the formation of NO_x. On the other hand, EGR also tends to increase the soot emissions, a phenomenon known as the soot-NO_x trade-off. The phenomenon is due to lowered in-cylinder temperatures impeding both the NO_x formation and soot oxidation processes. Inlet oxygen concentration was identified as the most active parameter to affect the soot oxidation rate. This section is dedicated to present in detail the impact of oxygen concentration on the oxidation of soot and the mechanism behind its efficacy.

4.4.1 Exhaust Measurements

Reducing the inlet oxygen concentration reduces NO_x and increases soot emissions, up to a certain point where soot emissions reach a maximum. Beyond that point NO_x and soot both decrease simultaneously and the trade-off no longer exists. Akihama et al. [6] first described this phenomenon represented in Figure 4.15.

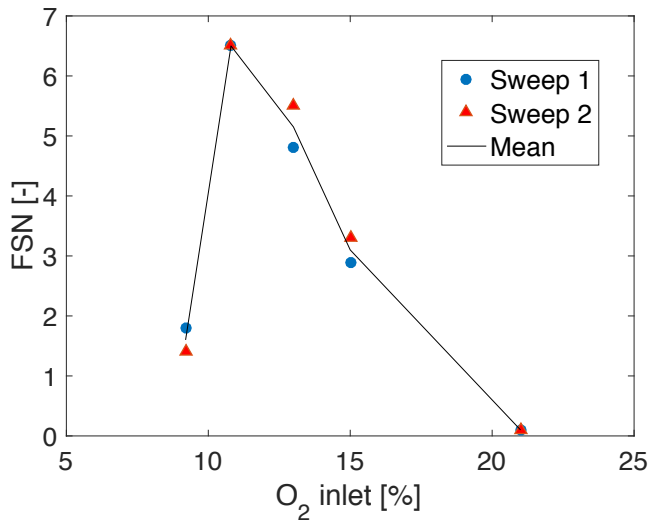

Figure 4.15 *Measurements of Filtered Smoke Number (FSN) for a sweep in intake O_2 concentration. Soot emissions increase with reduction of intake O_2, reach a maximum at 11% O_2 and then decrease again.*

Figure 4.16 shows a φ-T diagram. In this diagram the upper peninsula corresponds to the soot formation region and the lower right one corresponds to the NO_x formation region. The colored curves show the maximum flame temperature as function of the equivalence ratio φ, derived from homogeneous reactor simulations for varying intake oxygen concentrations. It is clearly seen that higher oxygen levels create conditions that are more prone to produce both soot and NO_x. When oxygen is reduced the maximum flame temperatures are reduced and eventually both the soot and NO_x regions are avoided. This explains the steep decrease in soot emissions observed at the lowest oxygen level in Figure 4.15, but not the increase when reducing the oxygen level from 21% to 11%.

A limitation of the φ-T diagram is that it only accounts for the soot formation rate, while soot emissions are the net result of both formation and oxidation of soot in the cylinder.

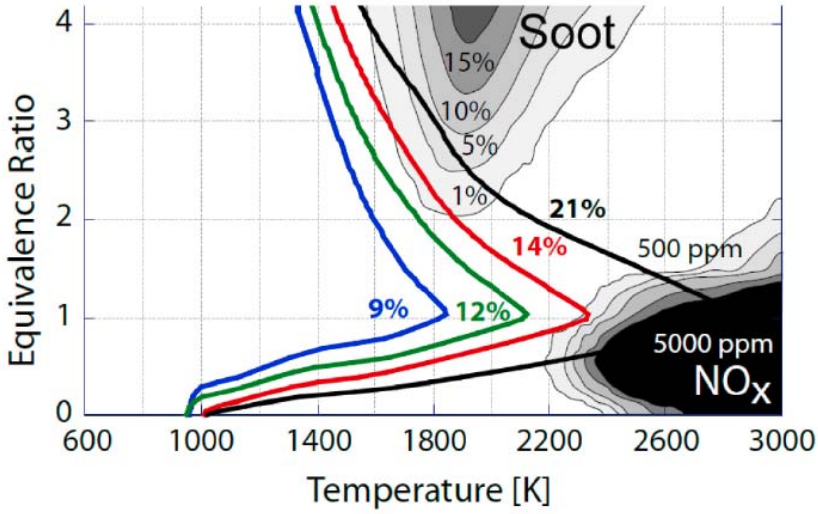

Figure 4.16 *Maximum flame temperatures from Chemkin simulations at varying intake O_2 mole fraction [57].*

4.4.2 Rate of Soot Oxidation

The impact of oxygen concentration on the soot oxidation was evaluated by extinction measurements. The optical thickness, which is directly proportional to the soot volume fraction, is shown in Figure 4.17. The height of the plateau prior to the decay gives some information about the amount of soot formed during the cycle. The slight increase observed at 15% inlet oxygen is potentially explained by saturation of the laser signal. Otherwise, the trends correspond well with what is expected from Figure 4.16. The amount of soot formed gradually decreases with a reduction of inlet oxygen, until almost no soot is formed at the 9% level.

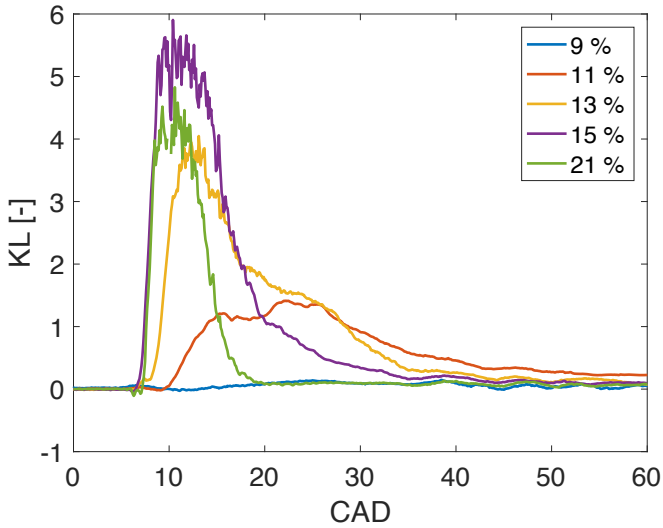

Figure 4.17 *KL as function of CAD in the interval of 0-60 CAD for inlet oxygen levels of 9 -21%.*

It can be seen that the decay after the peak, corresponding to the phase during which soot oxidation dominates over formation, becomes less steep with reduced inlet oxygen concentration. The rate of soot oxidation was evaluated by extracting the half-life of the decays and is presented in Figure 4.18.

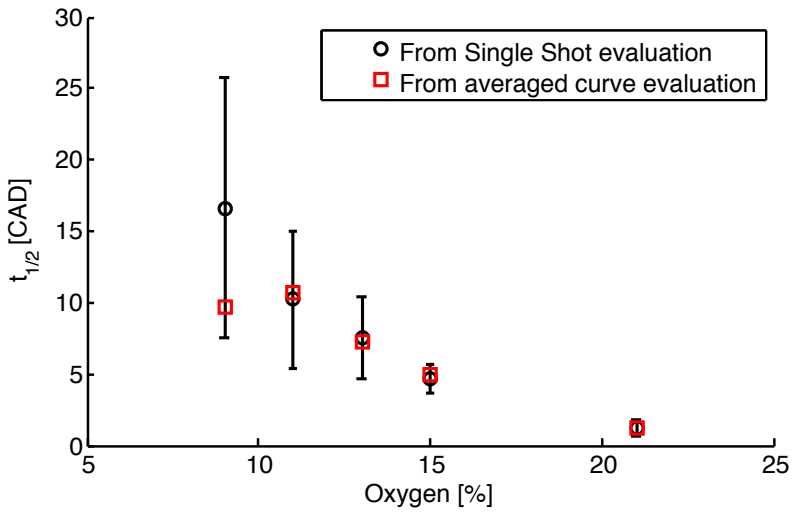

Figure 4.18 *The evaluated half-lives of the soot decay curve as function of inlet oxygen. Both from averaged and single cycle data.*

The half-life for the 9% oxygen concentration case shows poor precision due to the lack of soot formed leading to a weak signal as well as unstable combustion. For the other operating points, the half-life increases drastically with the reduction of oxygen availability, which explains the trends observed in the exhaust seen between 11% and 21% intake oxygen concentration in Figure 4.15.

4.4.3 Number and Size of Particles

The laser extinction measurements give a representation of the soot concentration in the cylinder, but do not yield access to information about the sizes and number of particles. These data could instead be by crank angle resolved in-cylinder sampling measurements in a metal engine. Due to technical difficulties linked to change of engine setup, the 9 and 11% oxygen concentration cases could not be reached so only the 13, 15 and 21% oxygen concentration cases are presented below. Figure 4.19 shows the evolution of the black carbon (BC) concentration measured with the aethalometer.

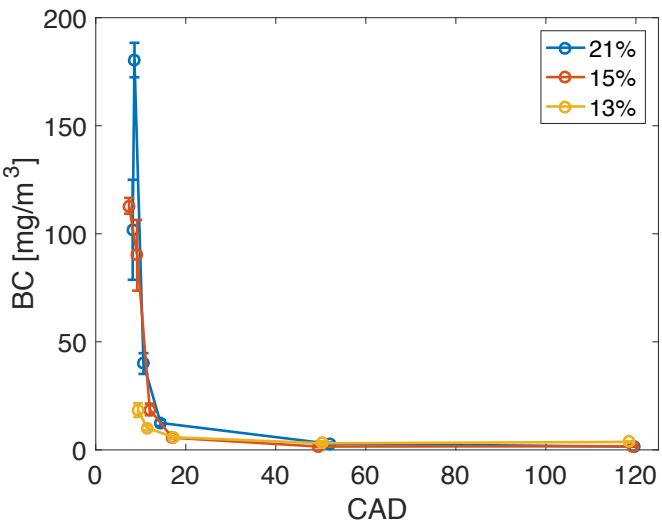

Figure 4.19 *In-cylinder soot mass concentration measured with the aethalometer.*

The concentration of soot is seen dropping during the oxidation-dominated phase as expected. It is also seen that the initial soot concentration decreases with decreasing oxygen concentration. Figure 4.20 shows that the late-cycle drop in BC is explained by both a reduction in the number of particles and their sizes.

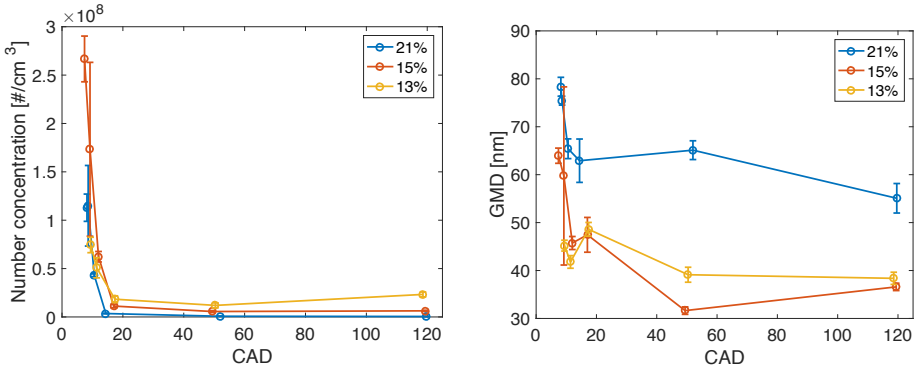

Figure 4.20 *In cylinder measurement of the soot particles by the size mobility particle spectrometer. Left: number concentration. Right: geometrical mean diameter.*

4.4.4 Chemical Properties of Soot Particles

Decreasing the flame temperature by EGR has been shown to result in soot particles that are more easily oxidized [58]. Soot particles that contain fullerene-like high curvature structures can have higher reactivity due to weaker C-C bonds [58,59], resulting in many times higher oxidation rates [58,60]. With the soot particle aerosol mass spectrometer, the fullerene signal was found to increase when decreasing the oxygen concentration (Figure 4.21). Increased fullerene-signals are considered as strong indications of high curvature (fullerenic) soot-nanostructures and may implicate that the soot produced using EGR is more reactive than without EGR. However, the results indicate that increased soot reactivity does not impact the soot oxidation rate significantly because of the more dominant effect of reduced temperatures and OH concentrations.

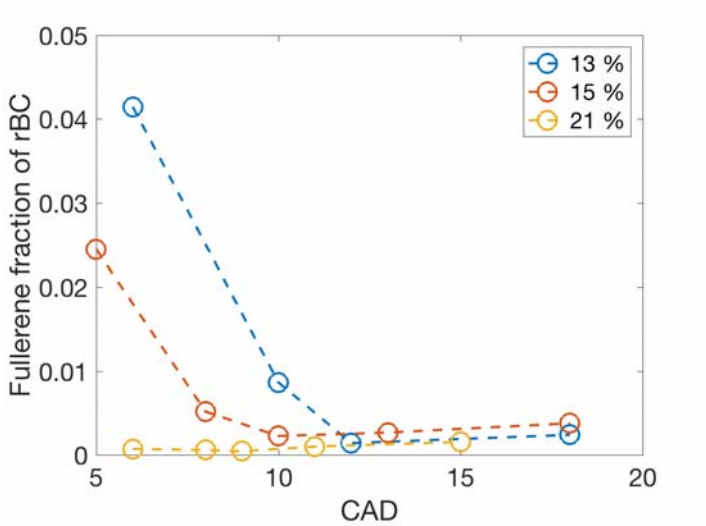

Figure 4.21 *Fraction of the refractive black carbon signal present as fullerene clusters during the cycle for a variation of inlet oxygen concentration.*

4.4.5 Influence of OH in the Flame

Oxygen and OH radicals are both important soot oxidizers [19]. According to Bartok and Sarofim [61], both OH and O_2 play a role under lean conditions while OH is likely to be dominating under fuel-rich and stoichiometric conditions.

Figure 4.22 reuses the data presented in Figure 4.16 and 4.18 for the 13, 15 and 21% oxygen cases zoomed in and normalized to highlight their similarities. The data presented in the two diagrams of Figure 4.22 originates from two engine setups and two different measurement techniques (laser extinction and sampling in combination with an aethalometer). Both the decays corresponding to the late cycle soot oxidation are seen slowing down as inlet oxygen concentration is reduced.

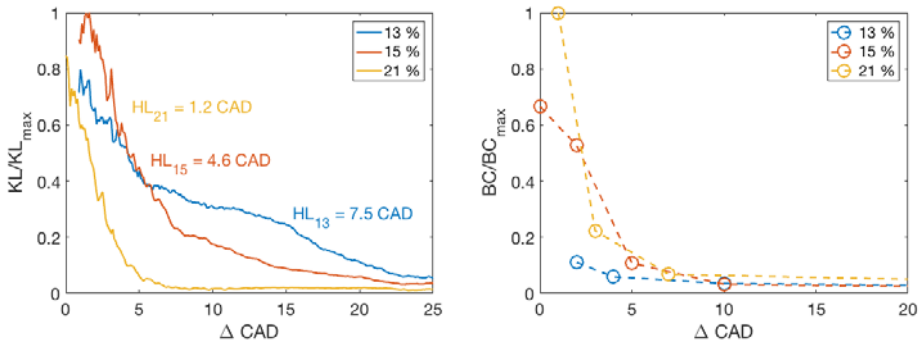

Figure 4.22 *Left: Evolution of KL (relative to the peak KL at 15% O_2) in the optical measurements shown from the start of decay. The half-life extracted from the exponential approximations are shown in CAD. Right: Evolution of black carbon from the in-cylinder sampling measurements shown from the start of decay.*

When decreasing the oxygen concentration from 21% to 13%, i.e. by a factor of less than two (-38%), the decay rates in Figure 4.22 (left) display a six-fold increase (translating to an 83% decrease of the oxidation rate). This indicates that the availability of oxygen in itself is not governing the oxidation rate.

Since the late-cycle soot oxidation is a mixing-controlled combustion process, it is expected to take place near stoichiometric conditions, and OH is thereby expected to be the main soot oxidizer under diesel conditions. About 10–20% of all OH collisions with soot are effective at gasifying a carbon atom [62,63]. Moreover, Guo et al. have shown that soot oxidation by OH has negligible activation energy and they point out that, for premixed and diffusion flames, optimized models indicate that soot oxidation by OH dominates over oxygen [63].

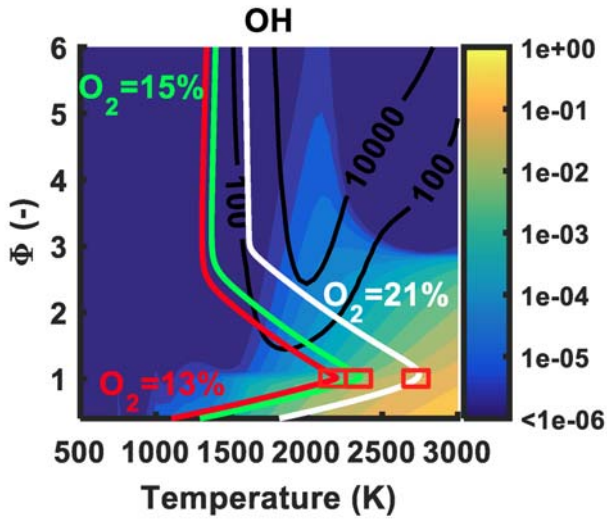

Figure 4.23 *Φ-T map of OH mass fraction constructed using a 0-D reactor with constant pressure, temperature and equivalence ratio. The three red squares highlight the maximum adiabatic flame temperature corresponding to the three cases (13, 15 and 21% O_2). The scale on the right represents the mass fraction of OH species.*

Figure 4.24 shows normalized number densities of OH extracted from Figure 4.23 (red squares), plotted against the soot oxidation half-lives displayed in Figure 4.22. Since the soot oxidation is expected to occur at stoichiometric conditions, the OH mass fractions are extracted at the maximum flame temperature. As expected, the half-life decreases with increasing OH concentration in the flame. Figure 4.24 also shows soot oxidation due to OH as calculated with Neoh's model [25]. It can be noted that the six-fold decrease in half-life previously mentioned is accompanied by a roughly six-fold increase in OH availability. As mentioned earlier, the activation energy of OH is negligible, so the temperature is not expected to impact the rate of oxidation by OH. The strong correspondence between OH concentration and reduction in soot oxidation rate supports the hypothesis that OH is the dominant soot oxidizer under diesel conditions.

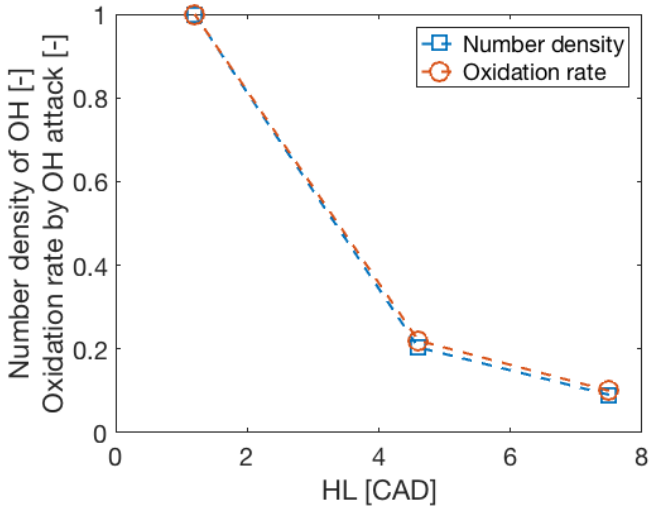

Figure 4.24 *Variation of the relative number density of OH (blue curve) and soot oxidation rate calculated with the Neoh et al. mechanism [25] (red curve) at the 3 cases studied, versus the variation of the oxidation half-life.*

5 Summary and Outlook

This final chapter summarizes the observations made in this thesis and highlights the contributions to the combustion engine research field. It also includes discussion on the limitations of the conclusions made as well as suggestions for potential investigations.

A common view on soot emissions is that a reduction of the soot formation will lead to a reduction of soot emissions. While this observation holds true for low temperature combustion concepts where the soot formation is often nearly or completely inhibited, this is not the case for conventional diesel combustion. Recent data indicate that, under most conditions encountered in current diesel engines, soot formation correlates only poorly with the resulting exhaust soot levels [7]. This observation finds further support in this thesis, which also highlights that the late-cycle oxidation of soot has a strong relationship to the level of PM emissions. In light of these results, the soot-NO_x trade-off has to be addressed by measures targeting soot oxidation rates and not the soot formation.

There are several interesting observation made in the study of the parameters that influence the soot oxidation rates. An increase of the density of the gases in the cylinder had a relatively strong and positive impact on the soot oxidation rates but, more interestingly, the injection pressure and the injector hole size were two of the parameters tested that affected the soot oxidation rate the most. These parameters are both linked to the injection process and the oxidation rates were measured after the end of injection, pointing out the importance of the injection process for the mixing, even in the late cycle. A simulation study using computational fluid dynamics (CFD) would be interesting to further investigate the impact of injection related parameters on the mixing process in the late cycle that leads to improved soot oxidation rates. The use of a segmented injection process with multiple pilot and post injection could potentially increase the mixing and oxidation rates even further.

The temperature of the gases in the combustion chamber had only a very limited impact on the soot oxidation. Two parameters were studied for their assumed effect of increasing the turbulent mixing, but were shown to have the opposite effect. While other phenomena like heat transfer could explain the reduction of oxidation rate at higher engine speeds, the results from an increased swirl level would need a more detailed study. An intermediate level of swirl could possibly

improve the oxidation rate while the higher swirl level studied in this thesis might have affected the mixing negatively. Also here, CFD simulations would be conducive to understanding how the global swirl ratio affects the local mixing in zones containing soot.

The oxygen was shown to be the most dominant parameter of this thesis for optimizing the soot oxidation rate. The detailed study of this parameter presented in Article III combines optical and sampling studies. The combination of those two techniques allowed interesting insights into the mechanisms behind its efficacy as well as strengthening the validity of the optical technique. Higher oxidation rates could be observed in the two different setups using two different techniques when using higher oxygen concentration. When reducing oxygen availability, the sampling data showed a slower maturation of the soot particles. This shift in the chemical properties of the soot particles would actually increase their reactivity and allow faster oxidation rates. This was however concerning a minority of the particles present in the cylinder. It was moreover widely overruled by the oxygen concentration's strong effect on the flame temperature. A higher oxygen concentration will lead to a higher flame temperature. This in turn will allow the production of more hydroxyl radicals, which are highly reactive soot oxidizers. The results of Article III successfully show that the reduction of oxidation rates observed with increased EGR rates correlated with the simulated OH concentrations in the flame rather than the simple reduction of oxygen concentration. This observation highlights once more the challenge to properly optimize the soot oxidation process while minimizing NO_x formation since both these species are formed at high temperature during the combustion.

Finally, it could be relevant to mention a few parameters that were not studied in the work presented in this thesis. For example, the oxygen content in the fuel was not studied. With the spread of biofuels, a study of the impact of oxygenated fuels on the soot oxidation process and the soot chemical properties would be of utmost interest. The optical configuration was technically limiting the study of soot oxidation at low loads and a narrow range of engine speed. It would be interesting to see if the observations made in this study are still applicable at higher loads and engine speed.

6 References

1. Cummins, L., ”Internal Fire”, Carnot Press, Oregon, US, 2000.
2. Heywood, J.B., “Internal Combustion Engine Fundamentals”, McGraw-Hill Book Co, New York, US, 1988.
3. Share of diesel in the European market from European Automobile Manufacturers Association, available at: http://www.acea.be/statistics/tag/category/share-of-diesel-in-new-passenger-cars (01/11/2016)
4. Fuel prices in Europe from The European Environment Agency http://www.eea.europa.eu/data-and-maps/indicators/fuel-prices-and-taxes/assessment-5 (01/11/2016)
5. Kamimoto, T. and Bae, M., “High Combustion Temperature for the Reduction of Particulate in Diesel Engines,” SAE Technical Paper 880423, 1988, doi:10.4271/880423.
6. Akihama, K., Takatori, Y., Inagaki, K., Sasaki, S. et al., “Mechanism of the Smokeless Rich Diesel Combustion by Reducing Temperature,” SAE Technical Paper 2001-01-0655, 2001, doi:10.4271/2001-01-0655.
7. Aronsson, U., Chartier, C., Andersson, Ö., Egnell, R. et al., “Analysis of the Correlation Between Engine-Out Particulates and Local Φ in the Lift-Off Region of a Heavy Duty Diesel Engine Using Raman Spectroscopy,” SAE Technical Paper 2009-01-1357, 2009, doi:10.4271/2009-01-1357.
8. Angrill, O., Geitlinger, H., Streibel, T., Suntz, R., and Bockhorn, H.,“Influence of Exhaust Gas Recirculation on Soot Formation in Diffusion Flames” Proceedings of the Combustion Institute, Volume 28, 2000/pp. 2643–2649.
9. Lack, D. A., Moosmüller, H., McMeeking, G. R., Chakrabarty, R. K., & Baumgardner, D., “Characterizing elemental, equivalent black, and refractory black carbon aerosol particles: a review of techniques, their limitations and uncertainties,” Analytical and Bioanalytical Chemistry, 406(1), 99–122,2014, http://doi.org/10.1007/s00216-013-7402-3

10. Salvi, S., Blomberg, A., Rudell, B., Kelly, F., Sandstrom, T., Holgate, S. T., Frew, A., “Acute inflammatory responses in the airways and peripheral blood after short-term exposure to diesel exhaust in healthy human volunteers,” American journal of respiratory and critical caremedicine 1999, 159, (3), 702-709.
11. Cancer, I. A. f. R. o., IARC: “Diesel engine exhaust carcinogenic”. Press release 2012, (213).
12. UNICEF “Clean the air for children” report, 2016, http://www.unicef.org/publications/index_92957.html (01/11/2016)
13. Intergovernmental panel on climate change (IPCC) fifth assessment report, 2013. http://www.climatechange2013.org (01/11/2016)
14. Aronsson, U., “Processes in Optical Diesel Engines, Emissions Formation and Heat Release”, Doctoral thesis, Lund University, 2011.
15. Van Basshuysen, R., Schäfer, F., “Internal Combustion Engine Handbook - Basics, Components, Systems, and Perspectives”. SAE International. (2004).
16. Dec, J.E., “A Conceptual Model of DI Diesel Combustion Based on Laser-Sheet Imaging,” SAE paper 970873, 1997.
17. Pickett, L., Siebers, D., and Idicheria, C., “Relationship Between Ignition Processes and the Lift-Off Length of Diesel Fuel Jets,” SAE Technical Paper 2005-01-3843, 2005, doi:10.4271/2005-01-3843.
18. Flynn, P., Durrett, R., Hunter, G., zur Loye, A. et al., “Diesel Combustion: An Integrated View Combining Laser Diagnostics, Chemical Kinetics, And Empirical Validation,” SAE Technical Paper 1999-01-0509, 1999, doi:10.4271/1999-01-0509.
19. Tree, D.R., Svensson, K.I., “Soot processes in compression ignition engines”, Progress in energy and Science 33 (2007) pp. 272-309.
20. Glassman, I., “Combustion”, San Diego: Academic Press; 1996.
21. Nagle, J. and Strickland-Constable, R.F., “Oxidation of carbon between 1000 and 2000 C” Proceedings of the fifth conference on carbon, vol. 1, pp. 265-325; 1962.
22. Park, C., and Appleton, J.P., “Shock-Tube Measurements of Soot Oxidation Rates,” Combustion and Flame, vol. 20, pp. 369-379; 1973
23. Fenimore, C.P. and Jones, G.W., “Coagulation of soot to smoke in hydrocarbon flames” Combustion and Flame, vol. 13, pp. 303-310; 1969.

24. Neoh, K.G., Howard, J.B., Sarofim, A.F., “Soot Oxidation in Flames”. Symp. (Int.) Combust. pp. 261–282; 1981.

25. Neoh, K.G., Howard, J.B., Sarofim, A.F., “Effect Of Oxidation On The Physical Structure of Soot”, Symp. (Int.) Combust. 20. pp.951–957;1985.

26. Dec, J. and Kelly-Zion, P., “The Effects of Injection Timing and Diluent Addition on Late-Combustion Soot Burnout in a DI Diesel Engine Based on Simultaneous 2-D Imaging of OH and Soot,” SAE Technical Paper 2000-01-0238, 2000, doi:10.4271/2000-01-0238.

27. Huestis, E., Erickson, P., and Musculus, M., “In-Cylinder and Exhaust Soot in Low-Temperature Combustion Using a Wide-Range of EGR in a Heavy-Duty Diesel Engine,” SAE Technical Paper 2007-01-4017, 2007, doi:10.4271/2007-01-4017.

28. Bowditch, F.W., “A New Tool for Combustion Research, A Quartz Piston Engine,” SAE paper 610002, 1961.

29. Aronsson, U., Solaka, H., Chartier, C., Andersson, Ö. et al., “Impact of Mechanical Deformation due to Pressure, Mass, and Thermal Forces on the In-Cylinder Volume Trace in Optical Engines of Bowditch Design,” SAE Technical Paper 2011-26-0082, 2011, doi:10.4271/2011-26-0082.

30. Mueller, C. and Martin, G., “Effects of Oxygenated Compounds on Combustion and Soot Evolution in a DI Diesel Engine: Broadband Natural Luminosity Imaging,” SAE Technical Paper 2002-01-1631, 2002, doi:10.4271/2002-01-1631.

31. Zhao H., Ladommatos N., “Optical diagnostics for soot and temperature measurement in diesel engines,” Progress in Energy and Combustion Science, vol. 24, no. 3, pp. 221-255, 1998, doi:10.1016/S0360-1285(97)00033-6.

32. Huestis, E., Erickson, P., and Musculus, M., “In-Cylinder and Exhaust Soot in Low-Temperature Combustion Using a Wide-Range of EGR in a Heavy-Duty Diesel Engine,” SAE Technical Paper 2007-01-4017, 2007, doi:10.4271/2007-01-4017.

33. Lopez, J., Martin, J., Garcia, A., Villalta, D. et al., “Characterization of In-Cylinder Soot Oxidation Using Two-Color Pyrometry in a Production Light-Duty Diesel Engine,” SAE Technical Paper 2016-01-0735, 2016, doi:10.4271/2016-01-0735.

34. Inagaki, K., Miura, S., Nakakita, K. and Watanabe, S., “Quantitative soot concentration measurement with the correction of attenuated signal

intensity using laser-induced incandescence", The Fourth International Symposium COMODIA 98 371-378,1998.

35. Talley, D.G., "Optical patternation method," US 6,734,965 B2, May 11, 2004.
36. Sjöholm, J., Wellander, R., Bladh, H., Richter, M. et al., "Challenges for In-Cylinder High-Speed Two-Dimensional Laser-Induced Incandescence Measurements of Soot," SAE Int. J. Engines 4(1):1607-1622, 2011, doi:10.4271/2011-01-1280.
37. Hentschel, W. and Richter, J., "Time-Resolved Analysis of Soot Formation and Oxidation in a Direct-Injection Diesel Engine for Different EGR-Rates by an Extinction Method," SAE Technical Paper 952517, 1995, doi:10.4271/952517.
38. Tree, D. and Dec, J., "Extinction Measurements of In-Cylinder Soot Deposition in a Heavy-Duty DI Diesel Engine," SAE Technical Paper 2001-01-1296, 2001, doi:10.4271/2001-01-1296.
39. Mancaruso, E., Merola, S., and Vaglieco, B., "Soot Concentration and Particle Size in a DI CR Diesel Engine by Broadband Scattering and Extinction Measurements," SAE Technical Paper 2005-24-013, 2005, doi:10.4271/2005-24-013.
40. Wellander, R., Berrocal, E., Kristensson, E., Richter, M., and Aldén, M., "Three-dimensional measurement of the local extinction coefficient in a dense spray," Measurement Science and Technology, 2011. 22(12): p. 125303.
41. Kristensson, E.,Berrocal, E., and Aldén, M., "Quantitative 3D imaging of scattering media using structured illumination and computed tomography". Optics Express, 2012. 20(13): pp.14437-14450.
42. Santoro, R.J., Semerjian, H.G., and Dobbins, R.A., "Soot particle measurements in diffusion flames," Combustion and Flame, 1983. 51: pp. 203-218.
43. Migliorini, F., Thomson,K. and Smallwood G., "Investigation of optical properties of aging soot" Applied Physics B, 2011. 104(2): 273-283.
44. Bejaoui, S., Mercier, X., Desgroux, P., and E. Therssen, "Laser induced fluorescence spectroscopy of aromatic species produced in atmospheric sooting flames using UV and visible excitation wavelengths," Combustion and Flame, 2014, http://dx.doi.org/10.1016/j.combustflame.2014.03.014.

45. Simonsson, J., Olofsson, N., Török, S. et al., “Wavelength dependence of extinction in sooting flat premixed flames in the visible and near-infrared regimes,” Appl. Phys. B (2015) 119: 657. doi:10.1007/s00340-015-6079-z

46. Manin, J., Pickett, L., and Skeen, S., “Two-Color Diffused Back-Illumination Imaging as a Diagnostic for Time-Resolved Soot Measurements in Reacting Sprays,” SAE Int. J. Engines 6(4):1908-1921, 2013, doi:10.4271/2013-01-2548.

47. Xu, Y., and Lee, C.F., “Forward-illumination light-extinction technique for soot measurement,” Appl. Opt. 45, pp. 2046-2057 (2006)

48. Fast Sampling Valve (FSV), VOLVO, patent nr. SE 9002548-7

49. Drinovec, L.; Močnik, G.; Zotter, P.; Prévôt, A.; Ruckstuhl, C.; Coz, E.; Rupakheti, M.; Sciare, J.; Müller, T.; Wiedensohler, A., “The "dual-spot" Aethalometer: an improved measurement of aerosol black carbon with real-time loading compensation”. Atmospheric Measurement Techniques 2015, 8, (5), pp. 1965-1979.

50. Onasch, T. B.; Trimborn, A.; Fortner, E. C.; Jayne, J. T.; Kok, G. L.; Williams, L. R.; Davidovits, P.; Worsnop, D. R., “Soot Particle Aerosol Mass Spectrometer: Development, Validation, and Initial Application,” Aerosol Science and Technology 2012, 46, (7), pp. 804-817.

51. Aerosol Ångström Exponent on GEODISC, NASA: http://disc.sci.gsfc.nasa.gov/data-holdings/PIP/aerosol_angstrom_exponent.shtml (01/11/2016)

52. Musculus, M.P.B., Pickett, L.M., “Diagnostic considerations for optical laser-extinction measurements of soot in high-pressure transient combustion environments,” Combustion and Flame 141 (2005) 371–391 doi:10.1016/j.combustflame.2005.01.013

53. Glassman, I., “Soot formation in combustion processes,” Proceedings of the 22nd international symposium on combustion. The Combustion Institute, 1988. p. 295–311.

54. Miles, P.C., “Turbulent Flow Structure in Direct-Injection, Swirl-Supported Diesel Engines,” in C. Arcoumanis, T. Kamimoto (eds.), Flow and Combustion in Reciprocating Engines, doi:10.1007/978-3-540-68901-04, Springer-Verlag: Berlin / Heidelberg, 2008.

55. Payri, F., Olmeda, P., Martin, J., and Carreño, R., “A New Tool to Perform Global Energy Balances in DI Diesel Engines,” SAE Int. J. Engines 7(1):43-59, 2014, doi:10.4271/2014-01-0665.

56. Kook, S., Bae, C., Miles, P., Choi, D. et al., “The Effect of Swirl Ratio and Fuel Injection Parameters on CO Emission and Fuel Conversion Efficiency for High-Dilution, Low-Temperature Combustion in an Automotive Diesel Engine,” SAE Technical Paper 2006-01-0197, 2006, doi:10.4271/2006-01-0197.

57. Aronsson, U., Chartier, C., Andersson, Ö., Johansson, B. et al., “Analysis of EGR Effects on the Soot Distribution in a Heavy Duty Diesel Engine using Time-Resolved Laser Induced Incandescence,” SAE Int. J. Engines 3(2):137-155, 2010, doi:10.4271/2010-01-2104.

58. Al-Qurashi K., Boehman A.L., “Impact of exhaust gas recirculation (EGR) on the oxidative reactivity of diesel engine soot,” Combustion and Flame, Volume 155, Issue 4, December 2008, Pages 675–695, http://dx.doi.org/10.1016/j.combustflame.2008.06.002

59. Vander Wal, R. L., & Tomasek, A. J. (2003). “Soot oxidation: dependence upon initial nanostructure”, Combustion and Flame, 134(1), 1-9. http://dx.doi.org/10.1016/S0010-2180(03)00084-1

60. Yehliu, K., Vander Wal, R. L., Armas, O., & Boehman, A. L. (2012). “Impact of fuel formulation on the nanostructure and reactivity of diesel soot,” Combustion and Flame, 159(12), 3597-3606, http://dx.doi.org/10.1016/j.combustflame.2012.07.004

61. Bartok, W., Sarofim, A.F., “Fossil Fuel Combustion: A Source Book,” New York. Wiley; 1991.

62. Haynes, B.S., Wagner, H.Gg., “Soot formation,” Progress in Energy and Combustion Science, 1981;7:229–273, http://dx.doi.org/10.1016/0360-1285(81)90001-0

63. Guo, H., Anderson, P.M., Sunderland, P.B., “Optimized rate expressions for soot oxidation by OH and O2,” In: Fuel 172 (2016), pp. 248-252. http://dx.doi.org/10.1016/j.fuel.2016.01.030

7 Summary of papers

7.1 Paper I

A Study of In-Cylinder Soot Oxidation by Laser Extinction Measurements During an EGR-Sweep in an Optical Diesel Engine

Gallo, Y., Simonsson, J., Lind, T., Bengtsson, P., Bladh H., and Andersson Ö.

SAE Technical Paper 2015-01-0800, 2015, doi:10.4271/2015-01-0800.

In this article, the impact of a reduction of oxygen on the soot oxidation is studied by mean of optical measurements. The measurements were carried on in a heavy-duty diesel engine with optical accesses. The extinction of a red laser vertically sent through the combustion chamber revealed the concentration of soot during the expansion. The rates of oxidation were evaluated by fitting an exponential to the decay rates of the soot concentration and the half-life of the decay were compared. The rates of soot oxidation showed that the oxidation of soot slowed down linearly with a reduction of oxygen concentration. Finally, it was shown that the rates of oxidation correlated with the soot levels measured in the exhaust.

Experiments were carried out together with Johan Simonsson. I analyzed the data with Johan Simonsson and wrote the paper together with Öivind Andersson.

7.2 Paper II

Parameters Influencing Soot Oxidation Rates in an Optical Diesel Engine

Gallo, Y., Li, Z., Richter, M., and Andersson, Ö.

SAE International Journal of Engines 9(4):2016, doi:10.4271/2016-01-2183.

In this second article, the observations made during the first article are extended to the study of a wide set of parameters expected to have an impact on the soot oxidation. The measurements were carried out in the same heavy-duty diesel engine. The same method to evaluate the soot oxidation rate as in the first article was used. The half-life were compared with the engine-out emissions and the importance of each parameter was evaluated through regression analysis. The results suggested that the injection pressure had the strongest effect on the late-cycle soot oxidation rate, while the temperature at TDC has the weakest effect of the parameters studied.

Experiments were carried out together with ZheMing Li. We also cooperated in the data evaluation and I wrote the paper together with Öivind Andersson.

7.3 Paper III

Investigation of Late-Cycle Soot Oxidation Using Laser Extinction and In-Cylinder Gas Sampling at Varying Inlet Oxygen Concentrations in Diesel Engines

Gallo, Y., Malmborg, V.B., Simonsson, J., Svensson, E., Shen, M., Bengtsson, P-E., Pagels, J., Tunér, M., Garcia, A., and Andersson, Ö.

Submitted to Fuel, 2016.

In this third article, the effect of oxygen concentration on the rates of soot oxidation presented in the first article is studied in further details. For this study, gas-sampling measurements confirmed the trends previously observed with the optical measurements. The oxygen availability affected the flame temperature and the concentration of OH available for soot oxidation. The analysis was completed with a simulation of OH availability and the results showed a higher correlation between soot oxidation rates and the availability of OH in the flame.

Experiments were carried out together with Vilhelm Malmborg and MengQin Shen. The simulation work was carried out together with Erik Svensson. I performed the data analysis and wrote the article together with Antonio Garcia and Öivind Andersson.

7.4 Paper IV

Comparison of Laser-Extinction and Natural Luminosity Measurements for Soot Probing in Diesel Optical Engines

Li, Z., **Gallo, Y.**, Richter, M., Lind, T., and Andersson, Ö.

SAE Technical Paper 2016-01-2159, 2016 doi:10.4271/2016-01-2159.

This forth article presents the comparison of laser extinction and natural luminosity through simultaneous measurements. The comparison highlights the differences between the two techniques and the superiority of the laser extinction for studies in the late cycle where soot are too cold to be recorded with natural luminosity. The natural luminosity recordings show that the path chosen for the laser extinction is representative to a larger region of the cylinder. Finally, a computational compensation for the laser intensity fluctuation and losses of signal by soot deposit on the optics is also presented.

Experiments were carried out together with ZheMing Li. We also cooperated in the data evaluation and ZheMing Li was the main responsible for the writing.

7.5 Paper V

Analysis of Soot Particles in the Cylinder of a Heavy Duty Diesel Engine with High EGR

Shen, M., Malmborg, V.B., **Gallo, Y.**, Waldheim, B., Nilsson, P., Eriksson, A., Pagels, J., Andersson, Ö., and Bengtsson, J.

SAE Technical Paper 2015-24-2448, 2015, doi:10.4271/2015-24-2448

In this fifth article, the points of operation recorded in the first article are reproduced in a full metal engine and the gases are sampled during the cylinder in order to observe the effect of EGR on the soot sizes and numbers. The sampling measurements show similar trends to the optical data in terms of concentration. A detailed evolution of the soot sizes and number is presented.

Experiments were carried out together with Ville Malmborg and MengQin Shen. I cooperated with Ville Malmborg for the data evaluation and MengQin Shen was the main responsible for writing the article.

7.6 Paper VI

Evolution of in-cylinder diesel soot and emission characteristics investigated with on-line aerosol mass spectrometry

Malmborg, V.B., Eriksson, A., Shen, M., Nilsson P., **Gallo, Y.**, Waldheim, B., Martinsson, J., Andersson, Ö., and Pagels, J.

Submitted to Journal of Environmental Science & Technology, 2016.

In this sixth article, the focus is on the chemical composition of the particles sampled following the same points of operation as in the first article. The results showed that a higher amount of PAH are subsisting longer in the cylinder at higher EGR rates, also leading to higher exhaust levels. Moreover, it was shown that a reduction of oxygen availability resulted in a slower maturation of soot, as displayed by the higher amount of fullerene-like structures probed.

Experiments were carried out together with Ville Malmborg and MengQin Shen. We also cooperated in the data evaluation and Ville Malmborg was the main responsible for writing the article.

Paper I

SAE INTERNATIONAL®

A Study of In-Cylinder Soot Oxidation by Laser Extinction Measurements During an EGR-Sweep in an Optical Diesel Engine

2015-01-0800
Published 04/14/2015

Yann Gallo, Johan Simonsson, Ted Lind, Per-Erik Bengtsson, Henrik Bladh, and Oivind Andersson
Lund University

CITATION: Gallo, Y., Simonsson, J., Lind, T., Bengtsson, P. et al., "A Study of In-Cylinder Soot Oxidation by Laser Extinction Measurements During an EGR-Sweep in an Optical Diesel Engine," SAE Technical Paper 2015-01-0800, 2015, doi:10.4271/2015-01-0800.

Abstract

Two competing in-cylinder processes, soot formation and soot oxidation, govern soot emissions from diesel engines. Previous studies have shown a lack of correlation between the soot formation rate and soot emissions. The current experiment focuses on the correlation between soot oxidation rates and soot emissions. Laser extinction is measured using a red (690nm) laser beam, which is sent vertically through the cylinder. This wavelength is long enough to minimize absorption interference from poly-aromatic hydrocarbons, while still in the visible regime. It is modulated at 72 kHz in order to produce 10 pulses per crank angle degree at an engine speed of 1200 rpm. The intake oxygen concentration is varied between 9% and 21%. The time resolved extinction measurements are used to estimate soot oxidation rates during expansion. High-speed video imaging is used in conjunction with the laser-extinction technique to indicate the location of the sooting regions, and to assess beam steering effects. The oxidation processes are described using single exponential decay fits and an attempt to correlate them with the late cycle rate of heat release was made.

Introduction

Diesel engines have undergone tremendous development during recent decades. They are favored for their high fuel efficiency but are also associated with high emissions of nitrous oxides (NO_x) and soot. One important focus of current diesel engine research is to understand the mechanisms behind these pollutants.

Exhaust gas recirculation (EGR) is a common method for reducing NO_x. It decreases the combustion temperature and thereby inhibits the formation of NO_x. On the other hand, EGR also tends to increase the soot emissions, a phenomenon known as the soot-NO_x trade-off. The phenomenon is due to lowered in-cylinder temperatures impeding both the NO_x formation and soot oxidation processes.

Decreasing intake O_2 by dilution with EGR thus tends to increase soot emissions, but beyond a certain point the soot emissions typically decrease drastically again. Figure 1 illustrates this effect with data collected under the conditions described in Table 2, which will be discussed later in the paper. In this case the soot emissions peak at 11% intake O_2. Below this point soot and NO_x decrease simultaneously and the trade-off no longer exists. The mechanism behind this phenomenon was first described by Akihama [1] and can be qualitatively understood using the now-classical φ-T diagram.

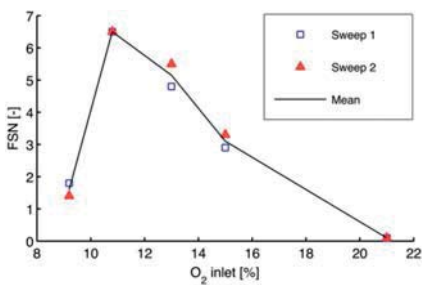

Figure 1. Measurements of Filtered Smoke Number (FSN) for a sweep in intake O_2 concentration. Soot emissions increase with reduction of intake O_2, reach a maximum at 11% O_2 and then decrease again.

Figure 2 shows a φ-T diagram (reproduced from [2] with permission). On this diagram the upper peninsula corresponds to the soot formation region and the lower right one corresponds to the NO_x formation region. The colored curves show the relationship between the maximum flame temperature and the equivalence ratio φ, derived from homogeneous reactor (Chemkin) simulations for varying intake O_2 concentrations. It is clearly seen that higher O_2 levels create conditions that are more prone to produce both soot and NO_x. When O_2 is reduced the maximum flame temperatures are reduced and eventually both the soot and NO_x regions are avoided. This explains

the steep decrease in soot emissions observed at the lowest oxygen level in Figure 1, but not the increase when reducing the O_2 level from 21% to 11%.

A limitation of the φ-T diagram is that it only accounts for the soot formation rate, while soot emissions are the net result of both formation and oxidation of soot in the cylinder. Previous studies indicate that, under conditions where substantial amounts of soot are formed, oxidation has a dominating influence on the soot emissions [3, 4]. Although the non-linear soot trend depicted in Figure 1 has been known for more than one decade [5, 6, 7, 8], only few direct experimental investigations of its underlying mechanisms are reported in the literature.

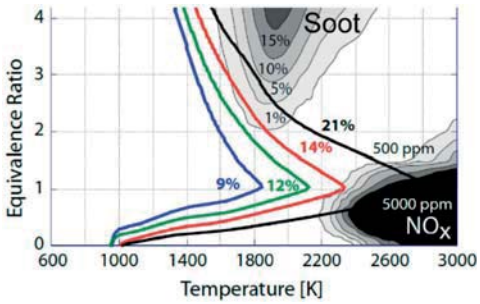

Figure 2. Maximum flame temperatures from Chemkin simulations at varying intake O2 mole fraction [2].

There are studies that investigate the emissions of soot during an intake O_2 sweep, but few in-cylinder studies. For example, Payri *et al.* measured the PM mass, size, and number density in the exhaust gases while varying intake O_2 between 9% and 13% in an early-injection low temperature combustion (LTC) mode. A peak in soot emissions was observed at 10% O_2 and, based on trends in ignition delay and estimated flame temperatures, they proposed that the peak was caused by a switch from poor soot oxidation to inhibited soot formation when the O_2 level was lowered [9]. There are also more fundamental studies in laboratory flames. For example, simultaneous imaging of various soot parameters in co-flowing diffusion flames, where EGR was simulated by adding CO_2 to the reactant flow, led to the conclusion that the increase in soot emissions is caused by lower oxidation rates when the temperature decreases [10]. While such studies expose fundamental processes, it is not straightforward to transfer the results to a realistic engine environment.

By contrast, Huestis *et al.* offered direct insights into the relevant underlying mechanisms by studying both the in-cylinder soot processes and the emissions, using two-color pyrometry in combination with exhaust soot measurements. The optical signal was collected from the whole cylinder cross-section and detected on three photo diodes with different bandpass filters. Decreasing the intake O_2 from 21% to 9% they saw that the late cycle soot oxidation rate decreased monotonically, but at the lowest O_2 levels the soot formation was essentially inhibited. The emissions followed the late cycle trends in in-cylinder soot mass [11].

While two-color pyrometry offers a useful qualitative tool for soot studies, it suffers from a number of uncertainties. One is due to the finite depth of field. Imaging the natural luminosity from underneath using a Bowditch optical configuration, most of the signal will originate from the soot that is closest to the optical piston. Depending on the optical density of the soot cloud, signal may or may not be detected in the interior of the flame. It is thereby difficult to know how representative the data are for the cylinder contents. Another uncertainty is associated with detecting signal on photo diodes (i.e. without spatial resolution). This results in superposition of several signals originating from regions with different temperatures and, again, the interpretation becomes difficult. Furthermore, the technique is incapable of detecting soot in the late cycle when the intensity of the thermal radiation decreases.

In the current study, in-cylinder soot oxidation rates are investigated using laser extinction measurements during a sweep in intake O_2 concentration. The laser extinction technique has the advantage of providing semi-quantitative soot concentration data in an extended region of the cylinder, while still being significantly less complex than most laser-based techniques used for soot measurement. With the setup used here the measurement volume covers the full vertical extent of the cylinder, which is an important feature when measuring during the expansion stroke. In contrast to the study by Huestis *et al.*, the measurement region only covers a fraction of the cylinder cross-section, but it will be shown by combustion imaging that the data are still representative for regions that contain soot during the late cycle. The current study thereby provides complementary information to the study in [11] and aims to present direct experimental evidence for the validity of two common hypotheses. The first is that the increase in soot when the intake O_2 is decreased (i.e. going from 21% to 11% O_2 in Figure 1) is due to deteriorating late cycle soot oxidation. The second is that the marked decrease at the lowest intake O_2 levels is due to drastically reduced soot formation. Another aim with this work is to investigate the validity of the approach proposed in [4], where the half-life of an exponential decay function fit to the late-cycle heat release is used as a proxy for the in-cylinder soot oxidation rate.

Laser Extinction Method

The laser extinction technique is a powerful tool for quantitative online measurements of soot and has successfully applied for several decades also in IC engines [12, 13, 14] and in spray vessels [15, 16, 17]. Extinction is a line-of-sight technique, where the initial and transmitted intensities, I_0 and I, are measured. Assuming that the in-cylinder soot is an optically thin medium, the Beer-Lambert law applies,

$$I = I_0 e^{-K_{ext} L}, \tag{1}$$

where K_{ext} is the extinction coefficient and L is the length of the absorbing medium, in this case the vertical extent of the combustion chamber. If the particle sizes are much smaller than the laser wavelength the scattering is assumed to be negligible, making $K_{ext} \approx K_{abs}$ [18]. With this assumption, the extinction coefficient can be given as function of the soot volume fraction, f_v according to:

$$K_{ext} = \frac{f_v 6\pi E(m)}{\lambda}, \quad (2)$$

where λ is the laser wavelength and $E(m)$ is the absorption function, see for example [19]. In this work we do not derive the soot volume fractions, but $K_{ext}L$-curves are shown instead. The reason for is that the $K_{ext}L$ values will remain constant if there is no net formation or oxidation of soot.

The laser wavelength, in this work 690 nm, is chosen to minimize possible absorption by polycyclic aromatic hydrocarbons (PAHs) as these might give additional extinction if they absorb at the laser wavelength. Recent results have shown that wavelengths longer than ~700 nm have negligible absorption of PAHs [19, 20, 21]. The use of 690 nm also gives a smaller scattering contribution to extinction compared to shorter wavelengths. Due to the size of typical soot particles from diesel engines, the assumption that the extinction coefficient is equal to the absorption coefficient might not be entirely safe, but this should not pose any problems as f_v is not calculated. $K_{ext}L$ should still be directly related to the amount of soot in the beam path.

Experimental Setup

Engine Specifications

The engine used for this study is a heavy-duty direct-injection diesel engine based on a Scania D12. It is operated as a single-cylinder engine, meaning that only one of the 6 cylinders of the engine is fired while the others are motored. A Scania XPI common rail fuel injection system capable of injection pressures up to 2500 bar is used, including a stock Scania injector with eight nozzle holes. The fuel used is Swedish diesel MK1. The engine, fuel system and fuel specifications are given in Table 1.

Table 1. Engine fuel system and specifications.

Engine base type	Scania D12 DI diesel
Bore	127 mm
Stroke	154 mm
Comp. Ratio	15.6
Swirl	2.18
Displacement	1.95 l
Injection system	XPI common rail
Nozzle flow number	207 pph
Number of holes	8
Firedeck angle	17 °
Hole diameter	0.175 mm
Fuel type	MK1 Diesel
Cetane number	51
Density	815 kg/m^3
Lower Heating Value	42.9 MJ/kg
Hydrogen/Carbon	1.85

The inlet air is conditioned in terms of pressure and temperature using a two-stage compressor and an inlet heater. A diesel furnace operated at stoichiometric conditions is used as a stable external source of EGR.

Table 2. Operating conditions. The SOI is adjusted from −4 CAD ATDC at 9% O_2 to −1 CAD ATDC for 21% O_2.

Operating conditions	
Speed	1200 rpm
Load	6 bar IMEPg
Pinj	2000
CA50	9 CAD ATDC
SOI	Adjusted to keep CA50 constant
DOI	650µs
Inlet P	1.8 bar
Inlet T	70°C
Fuel	MK1 Swedish Diesel
EGR rate	variable (9% to 21% O_2)
EGR source	Burner running at stoechiometry (fuel MK1)

The engine was operated at a speed of 1200 rpm and at low load (around 6 bar $IMEP_g$). The EGR was varied to obtain intake O_2 concentrations between 9% and 21%. The cylinder pressure was recorded through a 5mm long duct leading to the combustion chamber roof with a side-mounted Kistler 6125C transducer. For each point of operation the injection duration was kept constant. In order to maintain comparable in-cylinder conditions the start of injection was adjusted in order to keep the combustion phasing (CA50) at 9 crank angle degrees (CAD) after top dead center (ATDC). CA50 is the crank angle position where 50% of the total heat has been released. A summary of the engine operation conditions is given in Table 2.

Optical Design

The engine is modified according to a Bowditch design [22]. The piston extension has a full quartz piston top and a 45° mirror in a fixed position below it. In lieu of one of the exhaust valves an insert containing an angled window is inserted, providing optical access from the top of the cylinder. The angle of the window compensates for the angle of the optical access and makes it possible to obtain a vertical beam path through the cylinder. A cross-section of this optical access is given in Figure 3. The absence of one exhaust valve does not substantially affect the combustion process since the engine is running relatively slowly at 1200 rpm, allowing for effective gas scavenging.

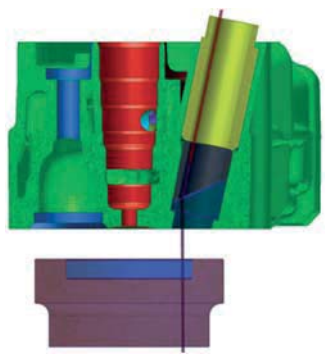

Figure 3. A cross-section of the optical design of the cylinder head and piston.

Measurement Apparatus

The laser-extinction setup is schematically shown in Figure 4. A CW laser diode operating at a wavelength of 690 nm (Hitachi, HL6738MG, 30 mW) was used as laser source for measuring the extinction by soot particles. The laser beam was collimated using an aspheric lens with focal length of 4.51 mm, directly mounted on the temperature-controlled laser diode mount (Thorlabs TCLDM9) where the laser diode is mounted. This created an approximately collimated laser beam with a beam width and height of 4 and 2 mm respectively. The laser mount was connected to controllers for diode case temperature (Thorlabs TED200) and driver current (Thorlabs LDC205C).

To obtain crank-angle resolved data an acousto-optic modulator (AOM) was used for intensity modulation of the laser beam. The engine's crank angle encoder sends a signal every 0.2 CAD and by using a Pulse Generator (Berkely Nucleonics model 575, 4 channels) producing two pulses for each trigger input, a resolution of 0.1 CAD can be approximately achieved. For an engine running at 1200 rpm this translates into a laser modulation frequency of 72 kHz. The entrance aperture of the AOM was 1.5 mm × 2 mm, which made a beam size reduction necessary. This was accomplished by using a telescope setup with one plano-convex lens (focal length 200 mm) and one plano-concave lens (focal length −40 mm). The laser beam was divided into two beams with a beam splitter prior to entering the engine and after the AOM. By using two photodiodes (Thorlabs PDA100A-EC), one measuring the attenuated signal and one a reference signal, the effect of laser intensity variation could be minimized. This is possible by measuring a calibration constant, making the reference beam proportional to the incident laser light intensity. The constant was measured during an engine cycle without injection in close proximity to the injection cycle where the soot measurement are taken, giving an individual calibration value for each 0.1 CAD (i.e. every laser pulse measured). It also ensures that variations in the transmission characteristics e.g. due to flame luminosity and window fouling during the engine cycle are taken into account. Nevertheless, to minimize the effects of background radiation, two filters were mounted on the photodiode measuring the transmitted laser beam; one short pass filter with cut-off wavelength 750 nm (Thorlabs FES0750) and one long pass-filter with cut-on wavelength of 650 nm (Thorlabs FEL0650). This created a relatively broad bandpass between 650 and 750 nm that did not fully suppress the background radiation. The remaining background contribution was removed during post processing, making use of the sequential background measurement points between the laser pulses.

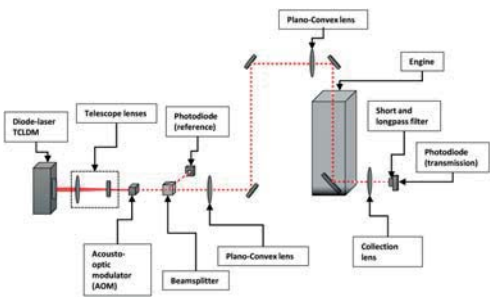

Figure 4. Optical setup for laser extinction measurements.

The laser beam was directed towards the top of the engine using Thorlabs ME1-P01 silver mirrors (>94% reflectance at 45° for 690nm). As the collimation of the laser beam was not perfect after the AOM, two plano-convex lenses (focal lengths 500 mm and 700 mm) were used to keep the laser at the preferred beam size of approximately 2 mm. A collection lens of 50 mm diameter with a focal length of 125 mm was positioned in front of the photodiode to minimize problems of beam steering that are likely to occur in turbulent environments like an engine [23]. The laser beam profile was recorded on a target located after the collecting lens at the photodiode position. During a combustion cycle, the beam profile increased slightly from an initial diameter of 1.2 mm up to 2 mm during the most intense part of the combustion (between 9 CAD and 20 CAD ATDC). The beam also showed a minor flickering with an amplitude of 1 mm around its position. Despite these beam steering effects, the whole laser beam was consistently maintained on the 10 mm diameter photodiode sensor surface. These fluctuations on the laser beam profile and position on the detector surface might induce some uncertainties as detailed in [23]. This could possibly explain some artifacts on the peak or plateau of the curves shown in Figure 7. However this study focuses on the oxidation of soot described by the decay rates seen later during the cycle where the beam steering is shown to have less effect [23] and therefore any influence of beam steering on the evaluated half lives, and hence the conclusions drawn in the paper, can be considered negligible.

The data was collected using a high-speed data acquisition (DAQ) card (National Instruments NI PCI 6132) capable of simultaneous measurements at a speed of 2.5 MS/s/ch. The DAQ-card recorded not only the two photodiodes, but also two signals indicating when the piston was at top dead center (TDC), enabling correlation between the laser pulses and CAD. The DAQ-card was triggered from the computer system controlling the injection system.

The natural combustion luminosity is recorded using a CMOS camera (Photron Fastcam SA-*Z*, 1024×1024 pixels) with a Nikon lens (50mm f/1.2). The images are used to provide information regarding the shape of the soot cloud and to justify the relevance of the region probed. At 1200 rpm, the 7.2 kHz frame rate gives one image per CAD, which are recorded from top dead center until 60 CAD ATDC. The camera settings are adjusted to compensate for the loss in signal due to the cooling of the flame and for lower flame temperature at lower oxygen concentration. The shutter speed was typically varied between 0.25μs for high intensity flames and 20μs for lower intensity flames.

Engine Measurements

During this study, the intake air was diluted with EGR to vary the concentration of O_2 in the intake while most other engine parameters were kept constant as described in Tables 1 and 2. This produced the characteristic soot curve seen in Figure 1, which was also observed by Akihama *et al.* [1]. The exhaust emission measurements were made in continuous operation with an aluminum piston top.

During the laser measurements, the engine was run in a skip-fired mode, meaning that fuel was injected once for every 20 engine cycles. This had several advantages. First, it gave the data acquisition system time to save and partially process the extinction data, giving quasi-instantaneous information about the quality of the undergoing

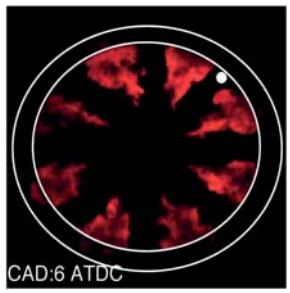

Figure 5. Combustion pattern at 6 CAD ATDC. Natural luminosity of soot was recorded. The white area represents the position of the laser during the measurements. The inner white circle represents the bowl wall; the outer one represents the periphery of the piston.

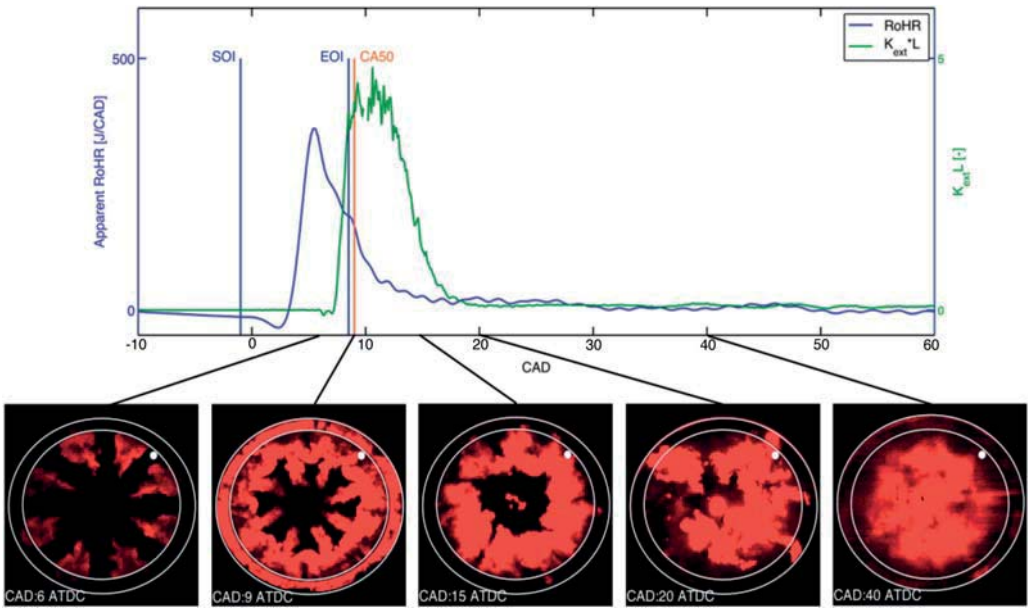

Figure 6. Images of natural luminosity of soot at different CAD related to the RoHR and the $K_{ext}L$ curve for 21% O_2. The shutter speed is 0.25 µs up until 15 CAD, 2.5 µs at 20 CAD and 20 µs at 40 CAD. The inner white circle represents the bowl wall, the outer one represents the periphery of the piston. The intensity is digitally rescaled through custom scaling color maps.

measurements. Second, the temperature of the optical parts was kept stable at a level close to that obtained with the aluminum piston (ensured by matching the heat release rates between the two engine configurations). Finally it limited the window fouling by limiting the number of fired cycles between each recorded cycle.

The laser beam is vertically aligned through the combustion chamber and the bottom of the quartz piston bowl as seen in Figures 3 and 4. The laser path is located between two sprays as seen in Figure 5. As the sooting regions of the jets enter the beam path several CAD after the start of injection, the measurements offer poor information about soot processes during the early combustion stages. This means that no conclusions can be drawn regarding the soot formation rates. Once the soot-containing regions have reached the beam path, however, the extinction signal will give information about the soot oxidation rates throughout the expansion stroke. This relies on the assumption that the burning gases spread along the perimeter of the bowl and attain a more or less homogeneous distribution in the azimuthal direction. It will be shown in the results section that this is indeed the case and, as a result, any vertical beam path along the bowl perimeter will provide representative information about the late-cycle soot history.

A previous study has showed that the late-cycle oxidation rate can be quantified by fitting an exponential decay function to the late-cycle heat release rate and extracting the half-life of the curve [4]. In the present study, the same approach is applied to both the extinction data and the heat release rate. The justification for the approach will be discussed at the end of the next section.

Results and Analysis

High-Speed Video Imaging

The natural luminosity images in Figure 6 are obtained by high-speed video imaging (HSV) and show the laser position in relation to the soot distribution. The images represent 6, 9, 15, 20, and 40 CAD ATDC and are displayed along with the rate of heat release and a $K_{ext}L$ curve for the 21% O_2 case. By 6 CAD ATDC, combustion has started and is localized at the extremities of the sprays. The rate of heat release (RoHR) rises rapidly, but the $K_{ext}L$ curve has not risen since the soot cloud has not yet entered the laser path. At 9 CAD ATDC the RoHR is beyond the premixed phase and the burning gas starts to form a ring around the periphery of the combustion chamber. The $K_{ext}L$ increases and reaches a plateau as the soot is transported into the laser path. At 15 CAD ATDC, the injection is over and the closing of the injector results in droplets at the center of the combustion chamber that burn slowly with high luminosity. The swirl mixes the soot region into a more homogeneous ring and the extinction signal is dropping as the soot oxidation begins to dominate over the soot formation. The RoHR is drastically slowing down due to the rapidly dissipating spray turbulence and, at 20 CAD ATDC, the soot cloud fills most of the combustion chamber. In terms of heat release, however, the combustion is essentially over. The $K_{ext}L$ curve has now dropped significantly. At 40 CAD, the soot cloud appears less intense due to rapid expansion cooling. It should be noted that the higher intensity at the center is not due to soot being transported from the bowl periphery towards the center, but due to the slow combustion of droplets that remain stagnant close to the injector.

From these images of the combustion it is seen that the position of the laser is relevant for studying the late-cycle soot oxidation as it is located in the soot cloud from the end of injection and throughout the expansion stroke.

Extinction Measurements

The results of the extinction measurements are presented in Figure 7, showing the ensemble averages of extinction curves from 29 cycles with injection. Increasing the number of measurement cycles was found to jeopardize the quality of the data due to excessive window fouling. It is important to keep in mind that though the extinction setup was automatically calibrated for each new cycle, thus taking window fouling into account, the quality of the data will worsen when the transmitted light intensity decreases too much. A rapid increase a few CAD after injection is evident for 21%, 15% and 13% O_2 with complete extinction being reached for the 21 % and 15 % cases. 11% O_2 produces a less rapid increase of the extinction with a later onset.

For 9% O_2, there is almost no extinction, but the peak extinction occurs approximately at the same location as for the case with 11% oxygen (~25 CAD ATDC). Another observation that can be made is that the extinction decreases at different rates. For all except the 9% case, which cannot clearly be observed, the rate of decrease is highest for 21% and drops until 11% O_2 is reached. At this operating point the extinction does not go back to zero until late in the cycle when the exhaust port is opened. At 9% O_2, soot formation is obviously very limited. Looking at the extinction levels just before exhaust port opening at 140 CAD ATDC, they qualitatively follow the emission results in Figure 1 very well.

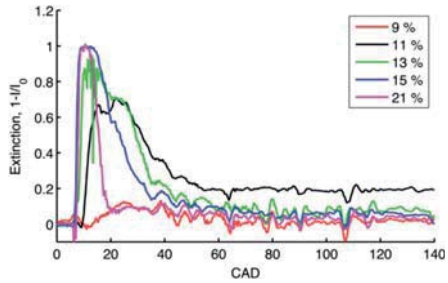

Figure 7. Extinction signal from 0 CAD ATDC to 140 CAD (exhaust valve opening) for inlet oxygen levels of 9 - 21 %.

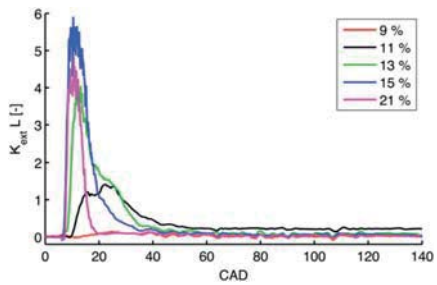

Figure 8. $K_{ext}L$ as function of CAD in the interval of 0-140 CAD (exhaust valve opening) for inlet oxygen levels of 9 - 21 %.

Using Eq. 1 together with the extinction data presented in Figure 7 it is possible to calculate the $K_{ext}L$-values. These are presented between 0 and 140 CAD in Figure 8 This interval is the where the most interesting observations occur, with a fast increase of soot, followed by decreases at different rates depending on the operating condition. It is also possible to see that the soot concentration peaks at different times for the different cases. The motivation for presenting the $K_{ext}L$ and not only K_{ext} is that $K_{ext}L$ is directly related to the amount of soot in the beam path. In other words, it remains constant if no net formation or oxidation takes place along the beam path, while K_{ext} will change when taking the piston position into account. In Figure 8 it appears as if the amount of soot is higher for the 15% case than the 21% case, but looking at the corresponding extinction curves in Figure 7 it is seen that both are saturated. For this reason, no conclusions can be drawn in the plateau region.

Assuming that the curves in Figure 8 follow an exponential decay after the peak, it would be possible to quantify the late-cycle soot oxidation rate by extracting the half-lives of the decay curves.

This has been done by fitting a linear equation to the logarithmic equivalent of the data in Figure 8. Depending on the inlet oxygen level used, different crank angle intervals were selected for the decay evaluation (see Table 3). The time intervals were selected based upon detailed analysis of the curve shapes. In a logarithmic representation, each case showed a linear region starting some tens of CAD after the peak, thus representing an onset of an exponential decay indicative of a single dominating mass loss mechanism such as oxidation as explained in the Discussion section. The linear region ends 40-50 CAD later as the laser extinction levels approaches the sensitivity

limit. The R^2-values are also presented in this table for the fits performed on the averaged curves presented in Figure 8. They show that in the fitted interval the data very nearly follows an exponential decay function, with R^2-values between 0.97 and 0.99 for the cases with O_2 levels of 11-21%. For the 9% O_2 case the fit is not very good due to higher noise levels in the data.

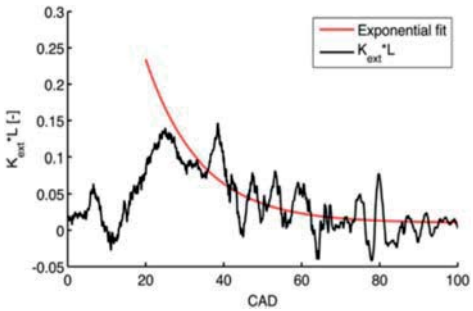

Figure 9a. Ensemble average over 29 $K_{ext}L$ curves for the 9%O2 case and exponential decay fit.

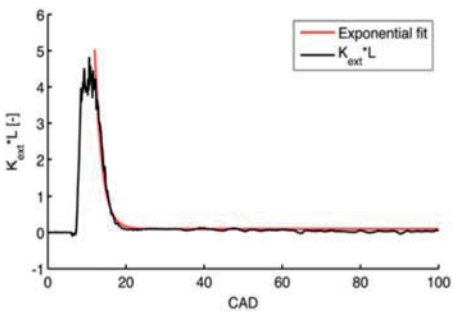

Figure 9b. Ensemble average over 29 $K_{ext}L$ curves for the 21% O2 case and exponential decay fit.

In Figures 9a and 9b two of the operating points are presented with corresponding fits to illustrate the difference between the best (21% O_2) and worst (9% O_2) fits. By definition, the half-life $t_{1/2}$ of an exponential curve is given by

$$K_{ext}L \propto e^{\frac{\ln(2)\,x_{CAD}}{t_{1/2}}}, \qquad (3)$$

where x_{CAD} is the crank angle position in CAD. This definition yields the values presented in Figure 10, where the half-lives have been evaluated from both individual cycles and from the ensemble-averaged data presented earlier (over 29 cycles). As expected, the half-life increases with decreasing oxygen content, but the standard deviation increases at the same time. The data for 9% O_2 is excessively noisy on a single cycle basis, causing the error bars to be quite large, and this is also why the half-life extracted from averaged curve does not match the average value of the single shot data. It can be observed in Figure 8 that with increased EGR level the $K_{ext}L$ value is decreasing from the point where the oxidation starts to be evaluated. It means that the pool of soot to oxidize is decreasing for higher EGR rates. At 9% O_2 virtually no soot is observed in the $K_{ext}L$ signal. The only likely explanation for this is a reduced soot formation, as shown in the φ-T diagram (Figure 2).

In summary, the results from the laser extinction measurements support both the hypotheses offered in the introduction: When the intake O_2 concentration is reduced the soot emissions increase due to deteriorating soot oxidation. However, when the O_2 concentration falls below 11% the soot formation is severely inhibited and the oxidation rate no longer limits the emission levels.

Table 3. Intervals used for the evaluation of the half-lives of the $K_{ext}L$-curves as well as R^2-values from the fittings of the averaged curves.

Oxygen level of inlet air	CAD interval ($K_{ext}L$-Fit)	R^2-values from averaged fit
9	25 – 50	0.3481
11	26 – 50	0.9698
13	15 – 50	0.9701
15	15 – 35	0.9773
21	12 – 20	0.9897

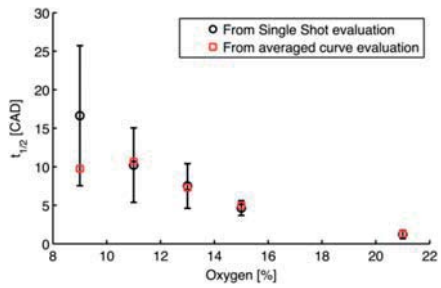

Figure 10. The evaluated half-lives of the soot decay curve as function of inlet oxygen. Both from averaged and single cycle data.

Heat Release Analysis

The apparent RoHR is presented for each operating point in Figure 11. All curves are characterized by a pronounced peak followed by the extended tail of the late-cycle mixing-controlled burn. The peak represents both spray-driven and premixed heat release, and the ratio between the two varies with the O_2 level.

The heat release occurring after the end of injection is of interest for the late-cycle soot oxidation. To quantify the oxidation rate, exponential decay functions were fit also to the RoHR curves. Due to the high RoHR during the initial peak, however, the decay rate will become biased if the fitting interval includes any premixed or spray driven heat release. Due to the long injections used in [4], the premixed phase was distinctly separated from the late-cycle mixing-controlled phase in that study. As a result, fitting an exponential function to the late-cycle heat release was straightforward. In the present study the injection duration is shorter, leading to blending between the premixed and mixing-controlled phases as seen in figure 11. It is not straightforward to discern any trends in the decay rates in Figure 11 but to investigate whether some effect of the O_2 concentration is present, half-lives were extracted from the curves.

A problem with the curves in Figure 11 is that the evaluated half-life is sensitive to the starting point of the fit. If the point is chosen too early, some of the premixed phase will be included when determining the decay rate and bias it toward a shorter half-life.

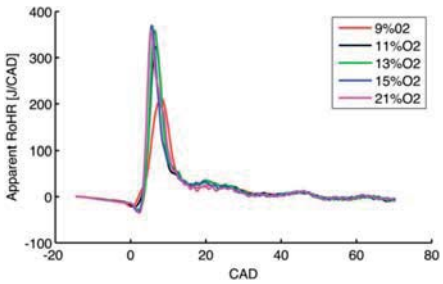

Figure 11. Average apparent RoHR between −15 and 70 CAD ATDC for 9, 11, 13, 15 and 21 %O_2 cases.

If the starting point is chosen too late, the fitting will not include enough information, as the curve will be too flat to represent the exponential decay accurately. It is therefore important to find a robust method for identifying the transition to the late-cycle mixing-controlled burn. Looking at Figure 12 it is seen that this transition is readily identified in the accumulated RoHR. The figure displays accumulated RoHR for a random collection of cycles operated with 11% O_2. A change of slope occurs at 10 CAD ATDC in all the curves, which is highlighted by a vertical green line. It was found that this breaking point occurred well after the end of injection at all operating conditions, and later in the cycle at lower O_2 concentrations. CA50 is marked with a red line in the diagram for reference. Due to the difficulty in identifying the change of combustion phase in the RoHR curves, it was decided that this visual criteria would be followed for all the cases. Half-lives were extracted using

$$RoHR \propto e^{\frac{\ln(2)\,x_{CAD}}{t_{½}}} \tag{4}$$

The results are given in Table 4 and shown in Figure 13. Just as for the extinction data in Figure 10, the half-lives of the mixing controlled RoHR increase as O_2 decreases. This means that that the late-cycle heat release becomes slower with decreasing intake O_2 levels.

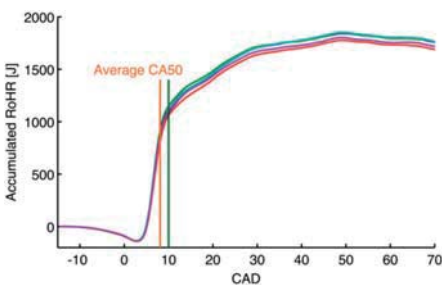

Figure 12. Accumulated RoHR for the 11% O_2 case. The red line indicates the CA50 position and the green line points out the change of slope corresponding to the transition from premixed to mixing-controlled RoHR.

This trend is observed regardless of criteria used for choosing the starting point of the exponential fit, albeit with varying slopes. It can be noted that the drop in half-life observed in the extinction data at 9% O_2 is observed in Figure 13 as well. This is due to the extended premixed burn pushing the start of the fitting interval later into the expansion stroke for that case. The RoHR thereby becomes slower and noisier for this case and the half-life obtained is probably less reliable as a result.

Table 4. Intervals used for the evaluation of the half-lives of the RoHR-curves as well as average R^2-values from the fittings of the single curves.

Oxygen level of inlet air	CAD interval (RoHR Fit)	R^2-values from averaged fit
9	11 – 70	0.8243
11	10 – 70	0.8674
13	9 – 70	0.8855
15	8 – 70	0.9083
21	7.5 – 70	0.9444

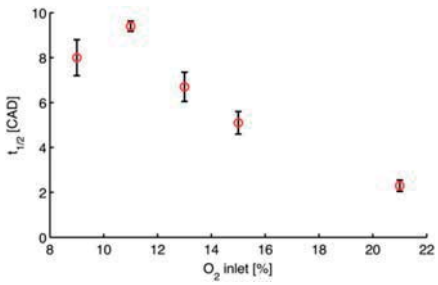

Figure 13. The evaluated half-lives of the late mixing-controlled RoHR exponential decay curve as function of inlet oxygen for average single cycle data.

Figure 14 shows the relationship between the half-lives obtained from the curves of $K_{ext}L$ and RoHR. Despite the indistinct shift from premixed to mixing-controlled burn in the RoHR, a strong correlation can be observed, confirming that the reduction of inlet O_2 will affect the late cycle oxidation process as probed by the two methods in a similar way. The implications of this observation are discussed in the next subsection. It should be noted that both evaluation methods probably yield unreliable half-lives for the 9% O_2 case, and it is likely a coincidence that this point follows the general trend in Figure 14 so well.

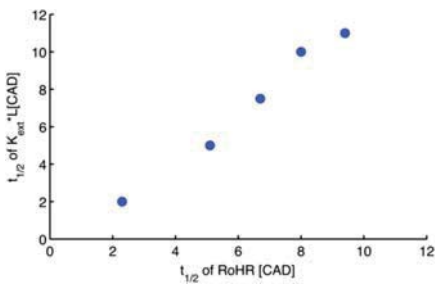

Figure 14. Correlation between RoHR and $K_{ext}L$ half-lives.

Discussion

As previously mentioned, an earlier study showed that the half-life of the late-cycle heat release is a good predictor of the soot emissions from a diesel engine [4]. Since it offers predictive capability as well as being quite readily obtained from heat release data, the half-life is interesting as a potential soot diagnostic. As the earlier study was not performed on an optical engine, the half-life could not be directly related to the in-cylinder soot processes. The data presented here, however, confirm that that the in-cylinder soot oxidation rate does correlate with the half-life of the late-cycle heat release.

It is relevant to ask whether the two half-lives stand in a direct relation to each other. Both measure the decay rate of an oxidation process in the cylinder, but even if the soot oxidation probably is exothermic, the RoHR will detect all reactions generating heat. Apart from soot, partially burned hydrocarbons and CO probably contribute a substantial share of the late cycle heat release. Furthermore, looking at the evaluation windows in Tables 3 and 4, it is seen that the window of the soot oxidation data is retarded in relation to that of the late-cycle heat release. These observations are likely to imply that the half-life obtained from the RoHR is not directly related to the soot oxidation rate. Still, the two half-lives are probably governed by the same in-cylinder processes.

Figure 15 shows a conceptual representation of the measured data and the process that they result from. The late-cycle mixing controlled combustion is governed by the availability of oxidizer and the mixing rate between oxidizer and oxidant (top bubbles). The oxidant is likely to consist of soot as well as other combustion intermediates. The rate of heat release thus gives information about the late-cycle oxidation of all these constituents, whereas the laser extinction measurements only probe the soot oxidation. The reason that the two methods produce results that correlate so well is not necessarily that the heat release gives direct information about the soot oxidation but, more likely, that the two sets of half-lives are determined by the efficiency of the same process - *i.e.* the mixing-controlled combustion.

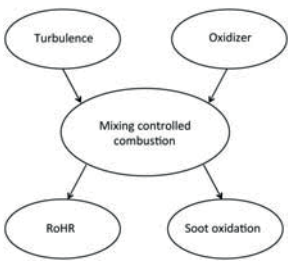

Figure 15. Conceptual representation of the common dependence of the RoHR and soot oxidation rate on the mixing-controlled combustion process.

Another relevant question is why the oxidation process should be expected to be described by a single exponential decay function in the first place. In general, the spray-induced turbulence tends to decay exponentially after the end of injection. Also the chemical oxidation of the soot should display an exponential dependence on time, at least if it can be approximately described as a first order chemical reaction. The rates of such reactions only depend on the concentration of one reactant and, since diesel engines are always operated with a surplus of air, the soot oxidation rate should be limited by the concentration of oxygen. If these two assumptions hold true, the soot oxidation rate should in fact be described by a double exponential decay function with two time constants. On the other hand, if the two time constants differ greatly from each other, the slower one will soon dominate and the curve will approach a single exponential function.

Regardless of these theoretical considerations, it is simple to find out whether a single exponential decay is an accurate representation by taking the logarithm of the data to see if they plot on a straight line. As previously mentioned, they do, and the high R^2-values of the fits further support this conclusion.

Conclusions

Laser extinction measurements were made in the cylinder of an optical heavy-duty diesel engine while sweeping the intake O_2 concentration. The late-cycle soot oxidation rates, as well as RoHR, were measured by fitting exponential decay functions to the data and extracting the half-lives. The conclusions can be summarized as follows:

- The engine-out emissions of soot show the typical rise when the intake O_2 decreases, followed by a steep decrease for very low O_2 concentrations.
- The laser extinction results confirm the hypothesis that the net oxidation rate decreases with decreasing intake O_2 levels, explaining the increase in soot emissions during the first part of the intake O_2 sweep.
- At the lowest intake O_2 levels, the extinction data show that soot formation is almost completely absent, explaining the marked drop in soot emissions at the end of the intake O_2 sweep.
- Exponential decay functions were fitted to the late cycle heat release rates. These decay rates show similar trends to those of the extinction data, indicating that heat release analysis can be used as a diagnostic tool for investigating the rate of in-cylinder soot oxidation. This would however be better suited for cases where the premixed phase of the combustion is distinctly separated from the control mixing-controlled one.

References

1. Akihama, K., Takatori, Y., Inagaki, K., Sasaki, S. et al., "Mechanism of the Smokeless Rich Diesel Combustion by Reducing Temperature," SAE Technical Paper 2001-01-0655, 2001, doi:10.4271/2001-01-0655.
2. Aronsson, U., Chartier, C., Andersson, Ö., Johansson, B. et al., "Analysis of EGR Effects on the Soot Distribution in a Heavy Duty Diesel Engine using Time-Resolved Laser Induced Incandescence," *SAE Int. J. Engines* 3(2):137-155, 2010, doi:10.4271/2010-01-2104.
3. Aronsson, U., Chartier, C., Andersson, Ö., Egnell, R. et al., "Analysis of the Correlation Between Engine-Out Particulates and Local Φ in the Lift-Off Region of a Heavy Duty Diesel Engine Using Raman Spectroscopy," *SAE Int. J. Fuels Lubr.* 2(1):645-660, 2009, doi:10.4271/2009-01-1357.

4. Lequien, G., Andersson, Ö., Tunestal, P., and Lewander, M., "A Correlation Analysis of the Roles of Soot Formation and Oxidation in a Heavy-Duty Diesel Engine," SAE Technical Paper 2013-01-2535, 2013, doi:10.4271/2013-01-2535.
5. Cheng, A. S., Upatnieks A., and Mueller C. J., "Investigation of Fuel Effects on Dilute, Mixing-Controlled Combustion in an Optical Direct-Injection Diesel Engine" Energy Fuels 21 (4), 1989-2002, 2007, doi:10.1021/ef0606456.
6. Noehre, C., Andersson, M., Johansson, B., and Hultqvist, A., "Characterization of Partially Premixed Combustion," SAE Technical Paper 2006-01-3412, 2006, doi:10.4271/2006-01-3412.
7. Ogawa, H., Miyamoto, N., Shimizu, H., and Kido, S., "Characteristics of Diesel Combustion in Low Oxygen Mixtures with Ultra-High EGR," SAE Technical Paper 2006-01-1147, 2006, doi:10.4271/2006-01-1147.
8. Colban, W., Miles, P., and Oh, S., "Effect of Intake Pressure on Performance and Emissions in an Automotive Diesel Engine Operating in Low Temperature Combustion Regimes," SAE Technical Paper 2007-01-4063, 2007, doi:10.4271/2007-01-4063.
9. Payri, F., Benajes, J., Novella, R., and Kolodziej, C., "Effect of Intake Oxygen Concentration on Particle Size Distribution Measurements from Diesel Low Temperature Combustion," *SAE Int. J. Engines* 4(1):1888-1902, 2011, doi:10.4271/2011-01-1355.
10. Angrill O., Geitlinger H., Streibel T., Suntz R. and Bockhorn H., "Influence of Exhaust Gas Recirculation on Soot Formation in Diffusion Flames" Proceedings of the Combustion Institute, Volume 28, 2000/pp. 2643-2649.
11. Huestis, E., Erickson, P., and Musculus, M., "In-Cylinder and Exhaust Soot in Low-Temperature Combustion Using a Wide-Range of EGR in a Heavy-Duty Diesel Engine," SAE Technical Paper 2007-01-4017, 2007, doi:10.4271/2007-01-4017.
12. Hentschel, W. and Richter, J., "Time-Resolved Analysis of Soot Formation and Oxidation in a Direct-Injection Diesel Engine for Different EGR-Rates by an Extinction Method," SAE Technical Paper 952517, 1995, doi:10.4271/952517.
13. Tree, D. and Dec, J., "Extinction Measurements of In-Cylinder Soot Deposition in a Heavy-Duty DI Diesel Engine," SAE Technical Paper 2001-01-1296, 2001, doi:10.4271/2001-01-1296.
14. Mancaruso, E., Merola, S., and Vaglieco, B., "Soot Concentration and Particle Size in a DI CR Diesel Engine by Broadband Scattering and Extinction Measurements," SAE Technical Paper 2005-24-013, 2005, doi:10.4271/2005-24-013.
15. Xu, Y. and Lee, C., "Investigation of Soot Formation in Diesel Combustion Using Forward Illumination Light Extinction (FILE) Technique," SAE Technical Paper 2004-01-1411, 2004, doi:10.4271/2004-01-1411.
16. Cenker, E., Bruneaux, G., Pickett, L., and Schulz, C., "Study of Soot Formation and Oxidation in the Engine Combustion Network (ECN), Spray A: Effects of Ambient Temperature and Oxygen Concentration," *SAE Int. J. Engines* 6(1):352-365, 2013, doi:10.4271/2013-01-0901.
17. Manin, J., Pickett, L., and Skeen, S., "Two-Color Diffused Back-Illumination Imaging as a Diagnostic for Time-Resolved Soot Measurements in Reacting Sprays," *SAE Int. J. Engines* 6(4):1908-1921, 2013, doi:10.4271/2013-01-2548.
18. Bohren, C.F and Huffman D.R., Absorption and scattering of light by small particles. 1998, New York, Wiley.
19. Migliorini F., Thomson K. and Smallwood G., "Investigation of optical properties of aging soot" Applied Physics B, 2011. 104(2): 273-283.
20. Bejaoui, S., Mercier, X., Desgroux, P., and Therssen E., "Laser induced fluorescence spectroscopy of aromatic species produced in atmospheric sooting flames using UV and visible excitation wavelengths", Combustion and Flame, 2014, http://dx.doi.org/10.1016/j.combustflame.2014.03.014.
21. Simonsson, J., Olofsson, N.-E., Török, S., Bengtsson, P.-E., and Bladh, H., "Wavelength dependence of extinction in sooting flat premixed flames in the visible and near infrared regime," Submitted to Applied Physics B, 2015
22. Bowditch, F., "A New Tool for Combustion Research A Quartz Piston Engine," SAE Technical Paper 610002, 1961, doi:10.4271/610002.
23. Musculus Mark P.B., Pickett Lyle M., "Diagnostic considerations for optical laser-extinction measurements of soot in high-pressure transient combustion environments," Combustion and Flame 141 (2005) 371-391 doi:10.1016/j.combustflame.2005.01.013

Contact information

Yann Gallo
Yann.gallo@energy.lth.se

Acknowledgements

The authors gratefully acknowledge the Swedish Energy Agency and KCFP (Project number 22485-3) for their financial support of this project as well as Carlos Micó Reche from the CMT-Motores Térmicos for his technical support.

ISSN 0148-7191

http://papers.sae.org/2015-01-0800

Paper II

2016-01-2183
Published 10/17/2016

doi:10.4271/2016-01-2183
saeeng.saejournals.org

Parameters Influencing Soot Oxidation Rates in an Optical Diesel Engine

Yann Gallo, Zheming Li, Mattias Richter, and Oivind Andersson
Lund University

ABSTRACT

Soot emissions from diesel engines are the net result of two competing processes: soot formation and soot oxidation. Previous studies have shown poor correlation between soot formation rates and the soot emissions. This article presents a systematic study of a number of parameters affecting soot oxidation rate and how it correlates with the soot emissions. An optical heavy-duty engine is used in conjunction with a laser extinction setup in order to collect time resolved data of the soot concentration in the cylinder during the expansion stroke. Laser extinction is measured using a red (685 nm) laser beam, which is sent vertically through the cylinder and modulated to produce 10 pulses per crank angle degree. Information is obtained about the amount of soot formed and the soot oxidation rate. The parameters studied are the motored density at top dead center (TDC), motored temperature at TDC, injection pressure, engine speed, swirl level and injector orifice diameter. A central composite design is employed to assess the importance of the parameters as well as identifying potential interaction effects. A single exponential decay function is fit to the extinction data to describe the oxidation process and the half-life of the decay is used as a measure of the oxidation rate. The half-lives are compared with engine out emissions and the importance of each parameter is studied using regression analysis. The results suggest that the injection pressure has the strongest effect on the late-cycle soot oxidation rate, while the temperature at TDC has the weakest effect of the parameters studied.

CITATION: Gallo, Y., Li, Z., Richter, M., and Andersson, O., "Parameters Influencing Soot Oxidation Rates in an Optical Diesel Engine," *SAE Int. J. Engines* 9(4):2016, doi:10.4271/2016-01-2183.

INTRODUCTION

Diesel engines are widely used in the transport sector due to their high efficiencies, but they suffer from significant emissions of nitrogen oxides (NO_x) and particulate matter (PM). The latter mostly consists of combustion-generated soot [1,2] and is connected with respiratory and cardiovascular diseases [3]. As soot particles are efficient light absorbers, they are also identified as major short-lived climate forcers (SLCF) and may also affect the climate by acting as condensation nuclei for cloud formation [4]. Despite a strong mitigation of PM emissions by diesel particulate filter reducing soot emissions from engines still represents an important challenge for the automotive industry.

PM and NOx are treated in tandem due to the fact that reducing emissions of one will often increase the emissions of the other [5,6,7]. In the cylinder, NO_x emissions can be reduced by lowering combustion temperatures [5,6]. PM emissions can be reduced by improving their oxidation during the combustion process. Previous studies have shown that reducing the formation of soot did not correlate with a reduction of soot emissions [8,9]. However, several studies have highlighted the importance of soot oxidation for the exhaust soot levels [10,11,12,13,14]. The late-cycle soot oxidation is expected to depend on a number of factors as described below.

Dilution with EGR strongly impacts the flame temperature [5,15]. The temperature has a strong effect on the soot oxidation, but also the reduced availability of oxidizers will inhibit the oxidation process. Gallo *et al.* showed that a reduction in intake oxygen concentration from 21 % to 9 % resulted in a gradually slower oxidation [10], which correlated well with a steady increase in soot emissions, at least until soot formation was severely inhibited by the reduced combustion temperature.

Temperature generally has a strong influence on chemical reaction rates. In the case of soot, the rate of soot oxidation will increase faster with temperature than the rate of formation [16,17]. In this study, the effect of the gas temperature at top dead center (TDC) is evaluated. It is expected to have a smaller impact on the flame temperature than the intake oxygen concentration, but could still affect the soot oxidation.

For a given oxygen concentration, the gas density should affect the soot oxidation by increasing the number of oxidizer molecules per unit volume. In order to separate the density effect from that of temperature, it is varied by changing the inlet pressure in this study.

Since the late-cycle soot oxidation is a mixing-controlled process it can be enhanced by increasing the turbulent kinetic energy in the bulk gases. This can be done by increasing the injection pressure, which will create more energetic bulk-flow structures in the cylinder [18]. It can also be achieved by increasing the engine speed, as the in-cylinder turbulence scales linearly with engine speed [5]. Yet another

way is to increase the swirl level [19,20]. A higher swirl level implies a fuel-air mixing improvement, nonetheless, this well-known effect can be mitigated by an excessive sprays interaction which leads to a particular rich equivalence ratio and therefore higher soot emissions [21,22].

In this study, in-cylinder soot oxidation rates are investigated using laser extinction measurements. The technique has been successfully used in a prior experiment where oxidation rates were studied during a sweep in intake oxygen concentration [10]. Here, the parameters discussed above are systematically varied using a central composite design (CCD) in order to identify their respective importance as well as potential interaction effects. The parameters are the motored gas density at TDC, the motored gas temperature at TDC, the injection pressure and the engine speed. The swirl and injector orifice diameter are also varied but are not included in the CCD. The objective is to identify the parameters that are most important for the soot oxidation rates and soot emissions. Fitting exponential decay functions to the extinction curves and extracting their half-lives gives a measure of the oxidation rates. These half-lives are then used to highlight how well oxidation rates correlate with exhaust soot levels.

LASER EXTINCTION TECHNIQUE

The laser extinction technique is a quantitative measurement technique for soot that has been applied successfully for several decades in IC engines [10, 23,24,25] as well as in spray vessels [26,27,28]. The intensity of a laser beam decreases as it passes through a region containing soot. The initial and transmitted intensities, I_0 and I, are measured and, assuming that the in-cylinder soot is an optically thin medium, the Beer-Lambert law applies:

$$I = I_0 e^{-KL}, \tag{1}$$

Here, K is the extinction coefficient and L is the length of the absorbing medium, in this case the vertical extent of the combustion chamber. Extinction is any process that prevents the initial intensity from reaching the detector, and is thus a combination of absorption and scattering of light out of the beam path. In the Rayleigh limit, where the particle sizes are much smaller than the laser wavelength, the scattering is assumed to be negligible and $K \approx K_{abs}$ [29]. Under this assumption, the extinction coefficient is a function of the soot volume fraction, f_v according to:

$$K = \frac{f_v 6\pi E(m)}{\lambda}, \tag{2}$$

where λ is the laser wavelength and $E(m)$ is the refractive index function, representing the imaginary part of $(m^2-1)/(m^2+2)$, in which m is the complex refractive index of the soot particles, see for example [30]. Throughout this paper, the soot concentration is presented as KL. This product is directly related to the average soot concentration through the cylinder, and is derived directly from the relative transmission measurement. Hence this product has a certain value for a specific soot concentration in the cylinder even during piston movement (assuming constant soot concentration along the diode-laser beam path). The decrease of KL under these assumptions can be related to net oxidation of the soot in the cylinder.

A diode-laser wavelength of 685 nm is chosen. This wavelength is in the visible spectral region (400-700 nm) facilitating alignment of the laser and detection system. The choice of a long wavelength in this region, close to 700 nm, is two-fold. Firstly, it minimizes influence from polycyclic aromatic hydrocarbons (PAHs), which are known to absorb radiation in both the ultraviolet and visible spectra regions [30,31,32]. Secondly, a longer wavelength also minimizes potential scattering contribution from the soot to the extinction measurements.

Due to the size of typical soot particles from diesel engines, the assumption that the extinction coefficient is equal to the absorption coefficient might not be entirely safe. However, given the uncertainties in the measurements and assumptions, potential scattering contribution will not influence the conclusions from this work.

EXPERIMENTAL SETUP

The engine used for this study is a heavy-duty direct-injection diesel engine based on a Scania D12 operated as a single-cylinder engine. A Scania XPI common-rail fuel injection system capable of injection pressures up to 2500 bars is used. Two injectors are used, including a stock injector with eight nozzle holes and a prototype injector with smaller holes. The fuel used is Swedish MK1 diesel. The base swirl level is 1.6 and a second swirl level of 5.9 is studied by adding flow plates to the inlet manifold which obstruct the 2 inlet ports, one fully and one partially. The engine, fuel system and fuel specifications are given in Table 1.

Table 1. Engine, fuel system and fuel specifications

Engine base type	Scania D12 DI diesel	
Bore	127 mm	
Stroke	154 mm	
Comp. Ratio	16	
Swirl	1.6	5.9
Displacement	1.95 l	
Injection system	XPI common rail	
Nozzle flow number	207 pph	70 pph
Number of holes	8	
Firedeck angle	17 °	16 °
Hole diameter	0.175 mm	0.1 mm
Fuel type	MK1 Diesel	
Cetane number	51	
Density	815 kg/m^3	
Lower Heating Value	42.9 MJ/kg	
Carbon/Hydrogen	0.53	

The inlet air is conditioned in terms of pressure and temperature using a two-stage compressor and an inlet heater. A diesel furnace operated at stoichiometric conditions is used as a stable external source of EGR. The exhaust soot levels are measured using a Pegasor particle sensor [33].

The cylinder pressure is recorded through a 5 mm long duct leading to the combustion chamber roof with a side-mounted Kistler 6125C transducer. For each point of operation the duration of injection is adjusted to match the accumulated heat released. In order to maintain comparable in-cylinder conditions the start of injection is adjusted in order to keep the combustion phasing constant. A more detailed overview of the operating conditions is developed in the Experimental design part and is summarized in table 2 and 3.

The engine has Bowditch-type optical access [34]. The piston extension has a full quartz piston top and a 45° mirror in a fixed position below it. An insert containing an angled window is used in lieu of one of the exhaust valves, providing optical access from the top of the cylinder. The angle of the window compensates for the angle of the optical access and makes it possible to obtain a vertical beam path through the cylinder. A cross-section of this optical access is given in Figure 1. The absence of one exhaust valve does not substantially affect the combustion process since the engine is running relatively slowly at a maximum of 1200 rpm, allowing for effective gas scavenging.

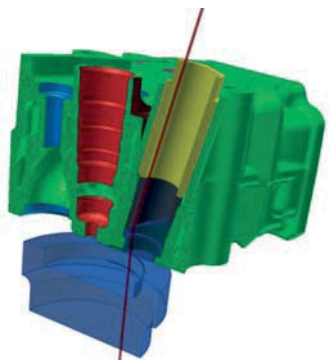

Figure 1. Cross section of the optical cylinder head and piston. In red is the location of the injector, the yellow and gray part is the optical insert replacing one exhaust valve.

The laser-extinction setup is schematically shown in Figure 2. The laser beam from a 50 mW continuous laser diode operating at 685 nm (Roithner LaserTechnik, QL68J6S-A/B/C) is collimated using an aspheric lens with focal length 4.51 mm, directly mounted on the temperature-controlled laser diode mount (Thorlabs TCLDM9). This provided an approximately collimated laser beam with a beam width and height of 4 and 2 mm, respectively. The laser mount is connected to controllers for diode case temperature (Thorlabs TED200) and driver current (Thorlabs LDC205C).

To obtain crank-angle resolved data the laser is intensity-modulated using an acousto-optic modulator (AOM) from AA Opto-Electronics (MT80 - A1.5), controlled using a driver from the same manufacturer (MODA80-1). The engine's crank angle encoder sends a signal every 0.2 CAD and by using a Pulse Generator (Berkeley Nucleonics model 575) producing two pulses for each trigger input, an approximate resolution of 0.1 CAD is achieved. For the engine running from 900 to 1200 rpm this translates into a laser modulation frequency of 54 to 72 kHz.

The laser beam is divided into two beams with a beam splitter prior to entering the engine and after the AOM. By using two photodiodes (Thorlabs PDA100A-EC), one measuring the attenuated signal and one a reference signal, the effect of laser intensity variation could be minimized. This is possible by measuring a calibration constant, making the reference beam intensity proportional to the incident laser light intensity. The constant is measured during an engine cycle without injection in close proximity to the injection cycle where the soot measurement is taken, giving an individual calibration value for each 0.1 CAD (i.e. every laser pulse measured). It also ensures that variations in the transmission characteristics e.g. due to flame luminosity and window fouling during the engine cycle are taken into account. Nevertheless, to minimize the effects of background radiation, three filters are mounted on the photodiode measuring the transmitted laser beam; one short pass filter with cut-off wavelength 700 nm (Thorlabs, FES0700) and two long pass-filter with cut-on wavelength of 650 nm (Thorlabs, FEL0650) and 665 nm (Schott, RG 665). This created a relatively narrow bandpass between 665 and 700 nm that did not fully suppress the background radiation. The remaining background contribution is removed during post processing, making use of the sequential background measurement points between the laser pulses. Further details about the setup as well as assessments of inaccuracy due to beam steering can be found in [10].

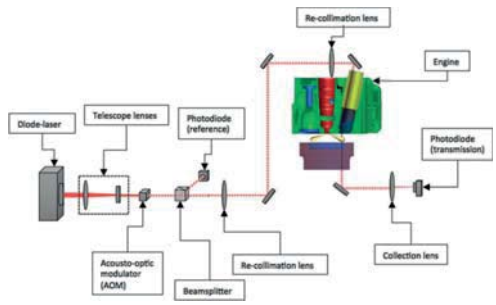

Figure 2. Optical setup for laser extinction measurements.

Figure 3 shows one image from a high-speed video taken during this experiment. In the image, NL is recorded. The white circle represents the piston bowl wall and the red dot roughly shows the laser location during the experiments.

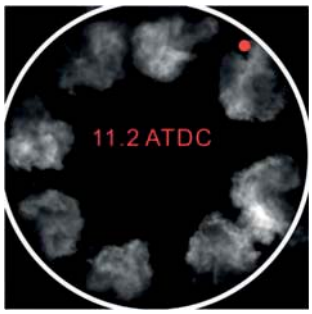

Figure 3. Natural luminosity image at 11.2 CAD ATDC was taken through the optical access. The white circle represents the piston bowl wall and the red dot is the position of laser.

Soot is first transported into the beam by the spray. It is then transported along the floor towards the center (out of path). Due to the centrifugal force and reverse squish flow it is then transported upwards outwards towards the squish region. Some of the parameters studied could affect the trends because of transport of PM out of the laser beam by affecting the radial fluid flows such as the injection pressure variation. Other parameters like temperature or density at TDC do not affect the radial flow. However, the trends observed are coherent to an oxidation process. And the clear correlation between oxidation rate and exhaust PM highlighted in this study further strengthen this assumption. Further discussions about the limitations of the technique can be found in [35].

EXPERIMENTAL DESIGN

To ensure the integrity of the optical parts, the engine is operated at a low load of 5 bars $IMEP_g$. The start of injection (SOI) is adjusted to keep the combustion phasing (CA50) constant for all points of operation at 9 CAD after top dead center (ATDC). CA50 is the crank angle position where 50% of the total heat has been released. Due to some limitations of the injection control system, The CA50 can vary around the target value. The start of injection (SOI) is carefully chosen to have the CA50 as close as possible to 9CAD ATDC. The duration of injection (DOI) is adjusted for each measurement in order to obtain the same cumulative heat release (CHR) of 1700 joules (J). In order to produce sufficient amounts of soot for the purposes of the experiment, the EGR is adjusted to obtain an intake O_2 concentration of 15 %. Swedish Diesel (MK1) is used for all measurements as well as in the furnace used as an external source of EGR. The standard swirl level of the engine is 1.6. One point of operation is measured with a swirl level of 5.9. The standard injector for this study has a nozzle of 0.175 mm. A measurement is also made with a smaller nozzle (0.1 mm). A summary of the general operating conditions can be found in the table 2.

Table 2. Summary of generic operating conditions. The values between parenthesis for swirl and injector nozzle correspond to extra measurements.

Operating conditions	
Load	5 bars IMEPg
CA50	9 CAD ATDC
SOI	Adjusted to keep CA50 @ 9 CAD ATDC
DOI	Adjusted to keep ARoHR @ 1700J
EGR rate	15% O_2
Fuel	MK1 Swedish Diesel
Swirl	1.6 (5.9)
Injector nozzle	0.175 mm (0.1mm)

The study of the most relevant parameters is conducted using a central composite design (CCD). The interest of such a design is that it supports fitting a quadratic model to the data while separating the effects of each parameter as well as identifying potential interactions between them [36]. This design of experiment revolves on the symmetrical variation of various parameters around a center point. In coded values "-1","0"and "+1" where "-1" represents the lower variation of the parameter, "+1" the higher variation and "0" is halfway through as reference base value. From this design of experiment, three sets of data are typically recorded. The first one is the set comprised of the corner points where all parameters are varied following their extreme values ("-1" and "+1"). The second set is the central point where all parameters are set to their base value ("0"). The third and final set is the axial points, where a single parameter is varied while the others are kept at their base value.

The engine speed is varied from 900 rpm up to 1200 rpm by steps of 75 rpm. The modulation frequency of the laser is adjusted accordingly in order to keep a temporal resolution of 0.1 CAD. The injection pressure is varied from 1000 bars up to 2000 bars by steps of 250 bars. Temperature and density at TDC represent the conditions of the gases without injection and combustion processes. The temperature at TDC is swept independently of density by adjusting inlet temperature and pressure. The values are obtained using the ideal gas law and adiabatic compression estimations. The inlet temperature is varied between 80°C and 160°C. Finally, the density at TDC is varied from 15.2 up to 22.8 kg/m^3 independently of the temperature by adjusting the inlet pressure following the same method of estimation as for temperature.

A summary of the CCD can be found in table 3. The CCD will allow a linear regression analysis. To be able to compare the effects of the factors the data are subjected to unit-variance scaling before fitting the regression model. This means that all factors are rescaled to have mean zero and range from -1 to 1. Thereby the actual unit of the factor does not affect the size of its coefficient in the model. Without unit-variance scaling, a given variation in injection pressure, for instance, would yield a different coefficient if the pressure were measured in Pa instead of bars.

Table 3. Recap of the CCD parameters

Central Composite Design					
Coded value	-1	-0,5	0	0,5	1
Speed [rpm]	900	975	1050	1125	1200
Pinj [bars]	1000	1250	1500	1750	2000
T @TDC [°C]	900	950	1000	1050	1100
ρ @TDC [kg/m^3]	15.2	17.1	19	20.9	22.8

Note that a CCD normally comprises measurements at three levels (with coded values of "-1", "0" and "1") but, here, intermediate measurements are recorded in order to better visualize the data in diagrams. The swirl ratio and nozzle size are studied but not included in the CCD, and will be presented separately.

RESULTS AND DISCUSSIONS

Exhaust Measurements

The concentrations of engine-out PM presented in figures 4a to 4f are recorded using the Pegasor instrument and following the conditions described in the Experimental Design part. Each circle in the diagrams correspond to a single measurement. The engine is operated following a similar protocol for each measurement point in order to improve accuracy. The engine is first motored until reaching a certain threshold temperature. Upon reaching this threshold temperature, the injection is activated and run continuously for 90 seconds and exhaust PM is recorded. The PM levels reach a plateau after a short period of 5 to 15 seconds and the last 30 seconds of each measurement are averaged in order to extract the PM values presented in Figure 4. When are showed the results of a single parameter sweep, only this parameter is varied, the other parameters from the CCD are kept at their base value.

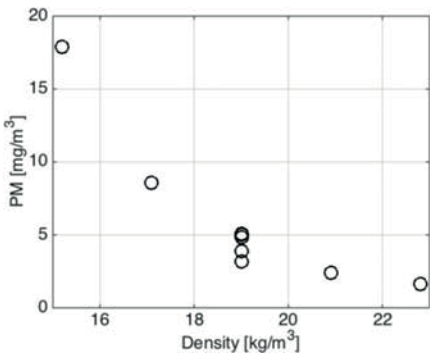

Figure 4 (a). Exhaust PM levels for a sweep of density at TDC.

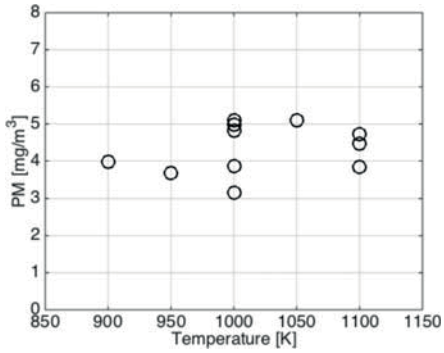

Figure 4 (b). Exhaust PM levels for a sweep of temperature at TDC.

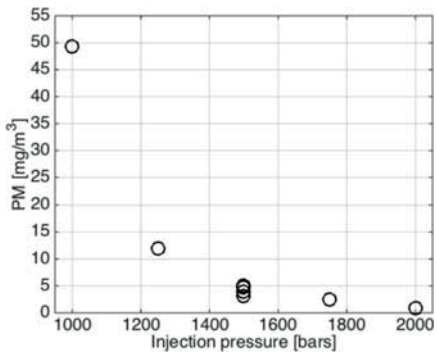

Figure 4 (c). Exhaust PM levels for a sweep of injection pressure.

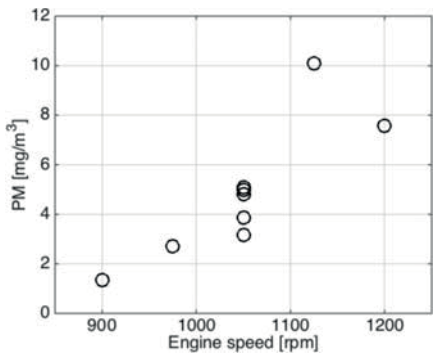

Figure 4 (d). Exhaust PM levels for a sweep of engine speed.

Figure 4. Measurements of PM concentration in the exhaust for a sweep of various parameters.

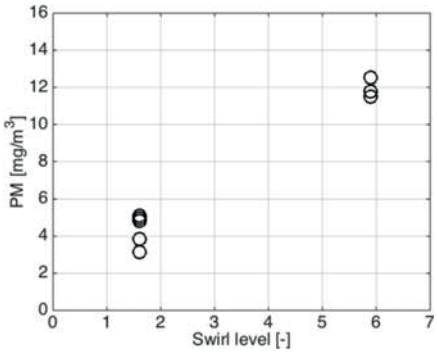

Figure 4 (e). Exhaust PM levels for a variation of swirl level.

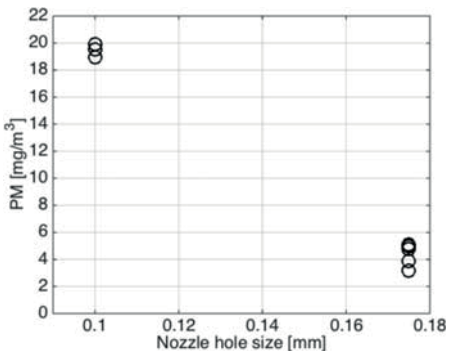

Figure 4 (f). Exhaust PM levels for a variation of nozzle size.

Figure 4 (cont). Measurements of PM concentration in the exhaust for a sweep of various parameters.

Figure 4a shows that the exhaust PM decreases non-linearly as the TDC density increases. When the TDC temperature is varied, however, Figure 4b reveals that the exhaust PM does not show any particular variation. When increasing the injection pressure from 1000 bars to 2000 bars, Figure 4c shows a steep non-linear decrease. This effect is similar to the impact of density at TDC presented in Figure 4a but even more pronounced.

Figure 4d presents the evolution of exhaust PM during a sweep of engine speed. As explained in the introduction, a higher engine speed should result in higher turbulence and improved mixing of soot and fresh gases during the combustion. However, the amount of exhaust soot measured shows a mild linear increase with engine speed. This could be due to reduced time for oxidation before the exhaust port opens at higher engine speeds.

Figure 4e shows the variation of exhaust PM for 2 swirl ratios. The lower level (1.6) corresponds to the base level of the CCD. The higher level of swirl (5.9) shows significantly higher exhaust soot concentration. A higher swirl level is expected to result in better late-cycle mixing but, in this case, it fails to translate into lower soot emissions. At higher swirl ratios, the flow structures formed can affect negatively the mixing, which could lead to trapping of partially-burned fuel within the bowl [22].

The effect of the injector orifice diameter is shown in Figure 4f. Smaller orifices affect the injection process drastically. In order to match the injected fuel amount (verified by matching the CHR) the injection duration is increased from 720 µs to 1120µs. As a result, the start of injection is advanced from 0 CAD ATDC to -6 CAD ATDC in order to maintain a constant CA50. The results in Figure 9 show that larger injector orifices reduce the soot emissions in this case.

The engine-out levels of soot presented in the Figure 4 highlight the parameters that most strongly affect the PM emissions. Increasing injection pressure and density at TDC strongly reduce soot emissions, while varying the temperature seems to have no impact. Counterintuitively, an increase in engine speed or swirl ratio increases the PM emissions. Finally, an injector with smaller holes increase the exhaust PM levels. All these parameters are expected to have a strong impact on the soot oxidation processes. The results from the laser extinction measurements presented in the following section will allow a look at the impact of those parameters on the oxidation process in the late cycle.

Extinction Measurements

The operating conditions are the same during the laser extinction measurements as during the exhaust PM measurements, except for running the engine in skip-firing mode. This means that fuel is injected every 14th cycle and motored during the remaining 13. This presents two main advantages. First, it provides time for the acquisition system to record and partially process the data for live evaluation of data quality. Secondly, it reduces the window fouling rate by limiting the number of fired cycles between each recorded one. Further discussions about the capabilities of the technique and its limitations can be found in [10]. Following a similar process as detailed in [10], 60 cycles are recorded for each point. In case of a high window fouling rate, the first 30 cycles recorded are kept and completed with a consecutive recording in order to obtain 60 exploitable cycles. A replicate set of measurements is recorded for each operating point in order to estimate the measurement error.

From the extinction measurements, an optical density *KL* is extracted which relates to the amount of soot found in the combustion chamber. A sample of these results can be found in Figure 5. In this figure, the result of *KL* is shown for a sweep of TDC density. The measurement region is located close to the bowl wall between two adjacent jets. The beginning of the *KL* curve presents a strong increase. This is due to movement of a sooting region in one of the jets into the path of the laser. Due to the swirling flow, the other jet will reach the measurement volume slightly later, giving rise to the second peak in the *KL* curve. As discussed in [10], after 15 to 20 CAD ATDC the soot is redistributed and can be considered homogeneous enough that the decay observed after the last peak of *KL* represents the evolution of soot during the late cycle. During this decay, the soot oxidation dominates over the soot formation.

As the sooting regions of the jet reach the laser path suddenly and with some delay, no quantitative conclusions can be drawn from the curves about the rate of soot formation. However, the height of the last peak of *KL* provides information about the amount of soot formed. A higher peak means a higher amount of soot in the cylinder prior to the late cycle oxidation phase. Regarding the oxidation, a steeper decay means a faster oxidation rate of the soot.

Two interesting observations can be made in Figure 5: the second peak increases with increasing TDC density, and the rate of decrease after the peak increases with density. This means that increasing density at TDC enhances both the soot formation and the soot oxidation. Figure 4a indicates that the increased oxidation strongly dominates over the increased formation.

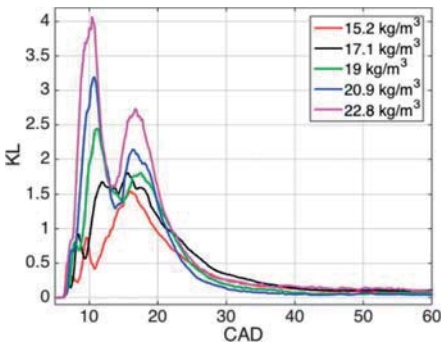

Figure 5. *KL* as function of CAD in the interval of 0-60 CAD for a sweep of density at TDC.

The oxidation rate can be characterized by fitting an exponential decay curve to the *KL* curve for each case [10]. The equation of the exponential fit is given by

$$KL \propto e^{-\frac{\ln(2)\,t}{t_{½}}}, \qquad (2)$$

where t is crank angle position in µs and $t_{½}$ is the corresponding half-life of the curve. As the half-life defines the rate of decay it is an inverse measure of the soot oxidation rate. The fitting starts 1 CAD into the part of the curve where oxidation dominates over formation, usually between 15 and 22 CAD ATDC. The end of fit is chosen at 150 CAD ATDC, just before EVO. The value of *KL* at the start of fit is used as a measure of the amount of soot formed. Due to the variation of engine speed for various operating conditions, the half-life extracted is converted to microseconds (µs) for universal comparison.

Regression Analysis

The half-lives for each point of the test matrix are extracted and subjected to a linear regression analysis. The result of the modeling can be seen in Figure 6, where the measured half-lives are plotted versus the predicted ones. All measurements are represented, including the corner points of the CCD. The model shows a relatively good coherence to the measurements with a R^2 of 88%. Thanks to the quality of the regression model, the importance of each parameter studied can be assessed and ranked. The interactions effect between parameters can also be highlighted.

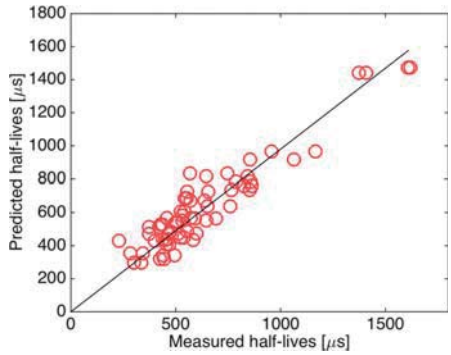

Figure 6. Visualization of the oxidation half-lives from measurements against the predicted ones from the linear regression model (R^2=88%).

Figures 7a to 7d present the half-lives measured for each sweep of an individual parameter while the others are kept at their base value as described in the table 3. The regression model associated with the relative parameter is also included in the plot for reference. It may seem that the model does not always embrace perfectly the data but it should be noted that the regression model is based on all measurements in the test matrix, not only those presented in the diagrams.

As already noted in Figure 4, looking at Figure 7a it can be seen that the half-life of *KL* becomes shorter for higher TDC density. This means that a higher density leads to an improved oxidation rate. This result also confirms the trend observed in engine out levels measured and shown in Figure 4a.

The half-lives for the TDC temperature sweep are presented in Figure 7b. A slight decrease of half-life of *KL* can be observed. This means that the TDC gas temperature has a limited impact on the oxidation rate. However, as shown in Figure 4b, it has no impact on the emission of PM. A possible explanation is that that temperature of the gases at TDC also increases the soot formation rate, and counterbalances the effect on the oxidation rate. The data from these experiments cannot allow a strict answer to this issue.

The half-lives for the injection pressure sweep are presented in Figure 7c. A steep decrease in half-life is observed at higher injection pressures. The decrease is more important below 1500 bars than above. From this plot, it can be concluded that the injection has a very strong impact on the oxidation rate even long after the end of injection. It is interesting to notice that this trend also mirrors that of engine out levels of PM shown in Figure 4c.

Figure 7d presents the variation of the half-life for a variation of engine speed. A weak increase of the half-life can be seen with an increase of the engine speed. Despite the increase in bulk turbulence

the soot oxidation actually seems to slow down. A potential reason for this could be higher heat losses from the gases to the walls leading to lower temperatures [37], and that local turbulence levels may be more important than global ones. However, the slight reduction in soot oxidation rate correlates with the engine out levels presented in Figure 4d.

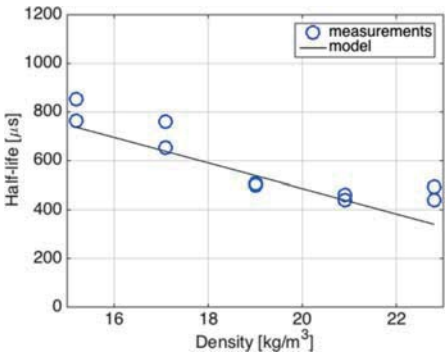

Figure 7 (a). Half-lives for a sweep of density at TDC

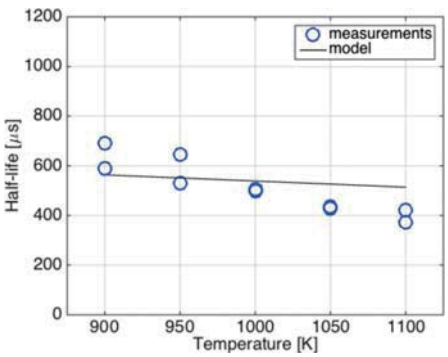

Figure 7 (b). Half-lives for a sweep of temperature at TDC

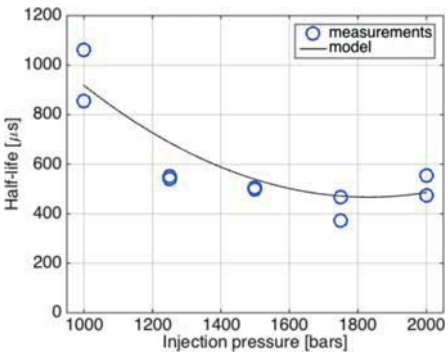

Figure 7 (c). Half-lives for a sweep of injection pressure

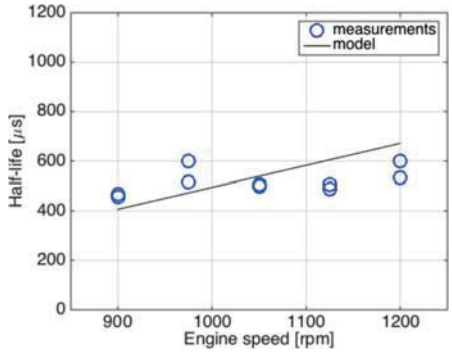

Figure 7 (d). Half-lives for a sweep of engine speed

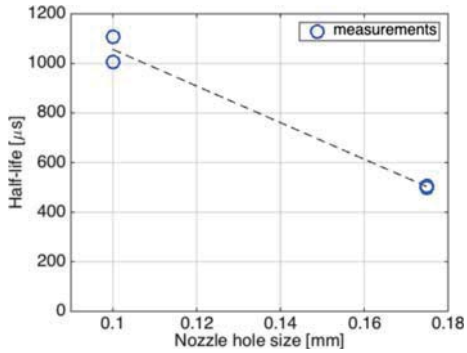

Figure 7 (e). Half-lives for a variation of nozzle size

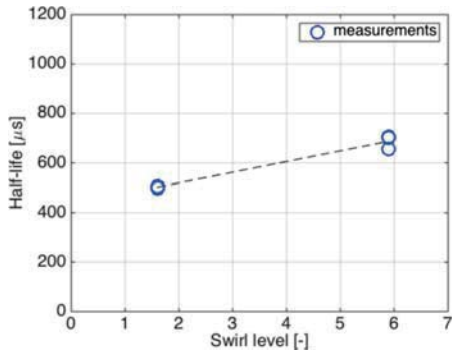

Figure 7 (f). Half-lives for a variation of swirl level

Figure 7. Visualization of oxidation half-life for variation of various parameters. Added on figures 7a, 7b, 7c and 7d are the prediction from the model associated with the relative parameter swept. On figures 7e and 7f only a linear fit of the average values is added.

Figure 7e and 7f present oxidation half-life results for variation of injector hole size and swirl level, respectively. As these parameters are only tested at two levels they are not included in the regression model and will be discussed separately.

In Figure 7e it can be seen that the half-life of the soot decay for a variation of injector hole size decreases strongly as the injector hole size is increased. As formerly mentioned, the injection duration is decreased to maintain the fuel quantity constant with the larger holes, and this leads to faster oxidation. It can be noted that this trend correlates with the exhaust PM as shown in Figure 4e. The comparison of half-lives for low and high swirl ratios is shown in Figure 7f, where the higher swirl seems to deteriorate the oxidation rate. The swirl level is likely too high and affects the mixing negatively as also seen in [22]. The reduced oxidation rate correlates with Figure 4f, however.

The relative importance of each studied factor is presented in a Pareto chart in Figure 8 and summarized in Table 4. By using a Pareto chart, the coefficients of the parameters are ranked from most important to least, including interaction effects while plotting the cumulative sum of the parameters. The 8 most important parameters identified and presented in the Pareto chart in Figure 8 accounts for 94% of the behavior of the model. The 6% remaining are parameters which coefficients are minor or not statistically relevant. It highlights that the injection pressure has the greatest impact on the oxidation rate followed closely by the TDC gas density. Increasing these parameters lead to enhanced oxidation rates. The engine speed is the third most important parameter identified, although an increase of this parameter yields an opposite effect on the oxidation rate by reducing it. The temperature seems to have the lowest impact of the 4 parameters studied in the regression analysis.

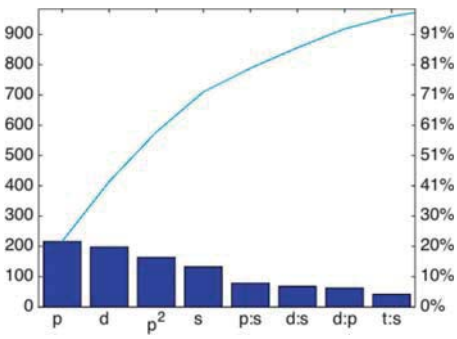

Figure 8. Pareto chart of the parameters varied. On the left y-axis is the duration of oxidation half-life according to the regression model. On the x-axis are ranked the most important parameters where "p" stands for injection pressure, "d" stands for density @TDC, p2 is the quadratic term for injection pressure. "s" is the engine speed, "t" is the temperature @TDC. A colon indicates an interaction effect. On the right y-axis is the cumulated importance of each parameter from most to least important as represented by the blue line.

Table 4. Coefficients from the regression analysis ranked by order of importance. The Swirl and injector hole size are listed apart for not being part of the CCD.

Parameter	Coefficient	Origin
InjectionP	-216.2	From regression analysis
Density	-198.1	
Injection P (quadratic)	163.3	
Engine speed	132.3	
InjectionP x engine speed	-78.5	
Density x engine speed	-67.8	
Density x injectionP	62.2	
Temperature x engine speed	41.3	
Temperature	-24.8	
Swirl	92.2	From linear fit
Injector hole size	-276.8	

The importance of swirl and injector hole size can be seen in table 4. The coefficients for these parameters come from a linear fit of the data shown in Figure 7e and 6f and are directly comparable to the coefficients obtained from the CCD design. Comparing to the 4 parameters from the regression model, the swirl level has an importance slightly inferior to that of the engine speed. Akin to it, increasing swirl level has a negative impact on the soot oxidation. The injection strategy imposed by various injector orifice diameters has the strongest impact of all. Within the factor ranges studied here, a larger-orifice injector apparently is the most effective choice for optimizing soot oxidation and reduces emissions.

It is interesting to note that the two most important parameters highlighted in table 4 are related to the injection process. A likely explanation for this is that it builds up bulk flow structures that survive long enough after the end of injection (EOI) and these are important for generating turbulences in the expansion stroke as described in [18].

Correlations

The oxidation rates presented in Figure 7 seem to follow similar trends as the amount of PM measured in the exhaust presented in Figure 4. The fact that the decay in soot concentration is described by a single exponential decay function suggests that the PM content in the cylinder can be described on the following form:

$$PM(t) = PM_0 e^{-\frac{\ln(2)\,t}{t_{½}}}, \quad (2)$$

where $PM(t)$ is the amount of PM at a time t (for instance at EVO), PM_0 is the amount of PM at the beginning of the oxidation dominated phase, and $t_{½}$ is the measured half-life of the oxidation process. Equation (2) can be linearized by taking the logarithm of both sides and evaluated at EVO:

$$\ln(PM_{EVO}) = \ln(PM_0) - \frac{\ln(2)\,t_{EVO}}{t_{½}}, \quad (3)$$

Here, PM_{EVO} corresponds to the engine-out emissions of soot. Plotting the soot emissions versus the inverse of the half-life in a semi-log diagram should thus display a linear relationship if the oxidation rate governed the trends in soot emissions. Such a plot is shown in Figure 9 and the correlation observed is relatively strong, confirming that the oxidation rate explains the major trends in the PM emissions at the operation points studied in this work.

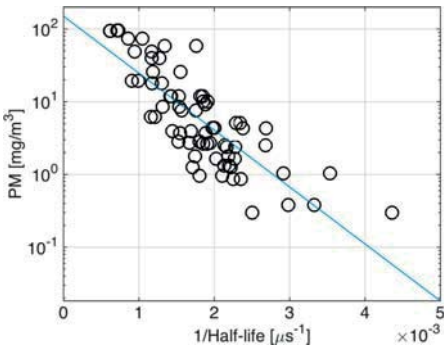

Figure 9. Correlation between exhaust PM levels and oxidation half-lives on a semi logarithmic scale. (R^2=66%)

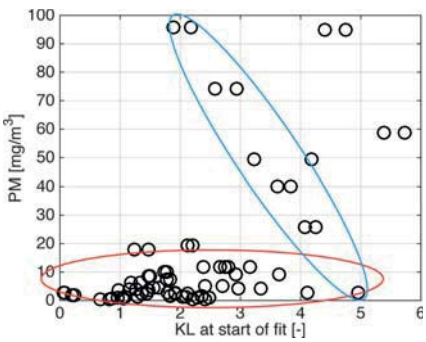

Figure 10. Correlation between exhaust PM levels and *KL* at the start of fit of the soot oxidation exponential decays, illustrating amount of soot formed. The blue and red areas highlight 2 different trends.

If, on the other hand, the soot formation were governing the soot emissions, the PM measured in the exhaust gases should be proportional to the maximum amount of soot measured in the cylinder. Figure 10 shows the correlation between the amount of soot formed (the peak *KL* value before oxidation becomes dominating) and the exhaust PM. The observations can roughly be categorized as belonging to one of two groups. The red oval indicates a group where the PM emissions are low regardless of the amount of soot formed. This suggests that the soot formation does not affect the emissions at all. The blue oval, on the other hand, indicates a group where the highest PM emissions are observed for the lowest amounts of soot formed, and vice versa. This is quite the opposite of what would be expected if the soot formation governed the emissions. In summary, the amount of soot formed does not explain the trends in soot emissions, whereas the soot oxidation does so to a large extent.

CONCLUSIONS

Laser extinction measurements were made in the cylinder of an optical heavy-duty diesel engine under variation of parameters expected to have an impact on the soot oxidation rate. The late-cycle soot oxidation rates were measured by fitting exponential decay functions to the data and extracting the half-lives. The conclusions can be summarized as follows:

- Increasing injection pressure and gas density at TDC strongly reduce the amount of PM emitted. Increasing the injector hole size allows for shorter injection duration and also strongly helps reducing PM emissions. Increasing engine speed and swirl slightly increase PM emissions, while the gas temperature at TDC has no impact.
- The study of soot oxidation rates suggests that an injector with larger holes leads to faster oxidation. Increasing the injection pressure strongly enhances the oxidation rate, as does increasing the TDC density. Increasing the swirl ratio from 1.6 to 5.9 reduces the oxidation rate as does increasing the engine speed. Finally, increasing the TDC temperature has a small impact on the oxidation rate.
- The fact that the injection pressure and the nozzle hole size are the two factors that have the strongest influence on the late-cycle oxidation rate suggests that the spray plays a key role in setting up flow structures that support the late-cycle mixing. It is interesting to note that the injection process has such a dominating role even well after the end of injection.
- The trends observed when varying swirl and engine speed are unexpected and indicate that global turbulence levels are not necessarily beneficial. Possibly, turbulence needs to be significantly increased at the specific locations where soot is oxidized to have an effect. The gas temperature at TDC showed very limited impact on the soot oxidation rate.
- PM in the exhaust gases showed a strong relationship with the oxidation rate at the operation points studied in this work, whereas soot formation proved to be a poor predictor of exhaust PM levels. This indicates that the soot oxidation rate governs the trends in PM emissions to a large extent, whereas the formation fails to do so.

REFERENCES

1. Maricq M. Matti, "Chemical characterization of particulate matter emissions from diesel engines: A review," Journal of Aerosol Science 38 (11): 1079 - 1118, 2007, doi:10.1016/j.jaerosci.2007.08.001.
2. Kittelson David B., "Engines and nanoparticles: A review," Journal of Aerosol Science 29 (5/6): 575-588, 1998, doi:10.1016/S0021-8502(97)10037-4.
3. Peng RD, Bell ML, Geyh AS, McDermott A, Zeger SL, Samet JM, and Dominici F. "Environmental Health Perspectives" 117 (6), 957-963 (2009)
4. UNEP/WMO, 2011. "Integrated Assessment of Black Carbon and Tropospheric Ozone." DEW/1351/NA
5. Heywood, J.B., Internal Combustion Engine Fundamentals, McGraw-Hill Book Co, New York, US, 1988.
6. Dec J.E., "Advanced compression-ignition engines-understanding the in-cylinder processes" Proceedings of the Combustion Institute Volume 32, Issue 2, 2009, Pages 2727-2742 doi:10.1016/j.proci.2008.08.008
7. Kamimoto, T. and Bae, M., "High Combustion Temperature for the Reduction of Particulate in Diesel Engines," SAE Technical Paper 880423, 1988, doi:10.4271/880423.
8. Aronsson, U., Chartier, C., Andersson, Ö., Egnell, R. et al., "Analysis of the Correlation Between Engine-Out Particulates and Local Φ in the Lift-Off Region of a Heavy Duty Diesel Engine Using Raman Spectroscopy," *SAE Int. J. Fuels Lubr.* 2(1):645-660, 2009, doi:10.4271/2009-01-1357.
9. Lequien, G., Andersson, Ö., Tunestal, P., and Lewander, M., "A Correlation Analysis of the Roles of Soot Formation and Oxidation in a Heavy-Duty Diesel Engine," SAE Technical Paper 2013-01-2535, 2013, doi:10.4271/2013-01-2535.
10. Gallo, Y., Simonsson, J., Lind, T., Bengtsson, P. et al., "A Study of In-Cylinder Soot Oxidation by Laser Extinction Measurements During an EGR-Sweep in an Optical Diesel Engine," SAE Technical Paper 2015-01-0800, 2015, doi:10.4271/2015-01-0800.
11. Huestis, E., Erickson, P., and Musculus, M., "In-Cylinder and Exhaust Soot in Low-Temperature Combustion Using a Wide-Range of EGR in a Heavy-Duty Diesel Engine," SAE Technical Paper 2007-01-4017, 2007, doi:10.4271/2007-01-4017.
12. Angrill O., Geitlinger H., Streibel T., Suntz R. and Bockhorn H., "Influence of Exhaust Gas Recirculation on Soot Formation in Diffusion Flames" Proceedings of the Combustion Institute, Volume 28, 2000/pp. 2643-2649.
13. Payri, F., Benajes, J., Novella, R., and Kolodziej, C., "Effect of Intake Oxygen Concentration on Particle Size Distribution Measurements from Diesel Low Temperature Combustion," *SAE Int. J. Engines* 4(1):1888-1902, 2011, doi:10.4271/2011-01-1355.
14. Lopez, J., Martin, J., Garcia, A., Villalta, D. et al., "Characterization of In-Cylinder Soot Oxidation Using Two-Color Pyrometry in a Production Light-Duty Diesel Engine," SAE Technical Paper 2016-01-0735, 2016, doi:10.4271/2016-01-0735.
15. Akihama, K., Takatori, Y., Inagaki, K., Sasaki, S. et al., "Mechanism of the Smokeless Rich Diesel Combustion by Reducing Temperature," SAE Technical Paper 2001-01-0655, 2001, doi:10.4271/2001-01-0655.
16. Tree D.R., Svensson K.I., "Soot processes in compression ignition engines" Progress in Energy and Combustion Science Volume 33, Issue 3, June 2007, Pages 272-309, doi:10.1016/j.pecs.2006.03.002
17. Glassman I. "Soot formation in combustion processes" Proceedings of the 22nd international symposium on combustion. The Combustion Institute, 1988. p. 295-311.
18. Miles, P.C. "Turbulent Flow Structure in Direct-Injection, Swirl-Supported Diesel Engines," in Arcoumanis C., Kamimoto T. (eds.), Flow and Combustion in Reciprocating Engines, DOI: 10.1007/978-3-540-68901-0 4, Springer-Verlag: Berlin / Heidelberg, 2008.
19. Miles, P.C., Bret H.R. and Reitz R.D., Squish-Swirl and Injection-Swirl Interaction in Direct Injection Diesel Engines, 6th International Conference on Engines for Automobile, Proceedings, ICE2003, Capri-Naples, Italy, 2003
20. Benajes Jesús, Martín Jaime, García Antonio, Villalta David, Warey Alok "In-cylinder soot radiation heat transfer in direct-injection diesel engines" Energy Conversion and Management, Volume 106, December 2015, Pages 414-427
21. De La Morena, J et.al "Influence of swirl ratio on combustion system performance of a 0.4l single cylinder Diesel engine" Thiesel Conference 2014 (Valencia, Spain)
22. Kook, S., Bae, C., Miles, P., Choi, D. et al., "The Effect of Swirl Ratio and Fuel Injection Parameters on CO Emission and Fuel Conversion Efficiency for High-Dilution, Low-Temperature Combustion in an Automotive Diesel Engine," SAE Technical Paper 2006-01-0197, 2006, doi:10.4271/2006-01-0197.
23. Hentschel, W. and Richter, J., "Time-Resolved Analysis of Soot Formation and Oxidation in a Direct-Injection Diesel Engine for Different EGR-Rates by an Extinction Method," SAE Technical Paper 952517, 1995, doi:10.4271/952517.
24. Tree, D. and Dec, J., "Extinction Measurements of In-Cylinder Soot Deposition in a Heavy-Duty DI Diesel Engine," SAE Technical Paper 2001-01-1296, 2001, doi:10.4271/2001-01-1296.
25. Mancaruso, E., Merola, S., and Vaglieco, B., "Soot Concentration and Particle Size in a DI CR Diesel Engine by Broadband Scattering and Extinction Measurements," SAE Technical Paper 2005-24-013, 2005, doi:10.4271/2005-24-013.
26. Xu, Y. and Lee, C., "Investigation of Soot Formation in Diesel Combustion Using Forward Illumination Light Extinction (FILE) Technique," SAE Technical Paper 2004-01-1411, 2004, doi:10.4271/2004-01-1411.
27. Cenker, E., Bruneaux, G., Pickett, L., and Schulz, C., "Study of Soot Formation and Oxidation in the Engine Combustion Network (ECN), Spray A: Effects of Ambient Temperature and Oxygen Concentration," *SAE Int. J. Engines* 6(1):352-365, 2013, doi:10.4271/2013-01-0901.
28. Manin, J., Pickett, L., and Skeen, S., "Two-Color Diffused Back-Illumination Imaging as a Diagnostic for Time-Resolved Soot Measurements in Reacting Sprays," *SAE Int. J. Engines* 6(4):1908-1921, 2013, doi:10.4271/2013-01-2548.
29. Bohren, C.F and Huffman D.R., Absorption and scattering of light by small particles. 1998, New York, Wiley.
30. Migliorini F., Thomson K. and Smallwood G., "Investigation of optical properties of aging soot" Applied Physics B, 2011. 104(2): 273-283.
31. Bejaoui, S., Mercier, X., Desgroux, P., and Therssen E., "Laser induced fluorescence spectroscopy of aromatic species produced in atmospheric sooting flames using UV and visible excitation wavelengths", Combustion and Flame, 2014, http://dx.doi.org/10.1016/j.combustflame.2014.03.014.
32. Simonsson, J., Olofsson, N.-E., Török, S., Bengtsson, P.-E., and Bladh, H., "Wavelength dependence of extinction in sooting flat premixed flames in the visible and near infrared regime," Submitted to Applied Physics B, 2015
33. Ntziachristos, L., Fragkiadoulakis, P., Samaras, Z., Janka, K. et al., "Exhaust Particle Sensor for OBD Application," SAE Technical Paper 2011-01-0626, 2011, doi:10.4271/2011-01-0626.
34. Bowditch, F., "A New Tool for Combustion Research A Quartz Piston Engine," SAE Technical Paper 610002, 1961, doi:10.4271/610002.
35. Li, Z., Gallo, Y., Lind, T., Andersson, O., et al. "Study of different optical soot measurements in a heavy-duty optical engine", SAE Technical Paper 2016-01-2159, 2016, doi:10.4271/2016-01-2159.
36. Andersson, Ö., "Experiment!: Planning, Implementing and Interpreting," Wiley, UK, 2012.
37. Payri, F., Olmeda, P., Martin, J., and Carreño, R., "A New Tool to Perform Global Energy Balances in DI Diesel Engines," SAE *Int. J. Engines* 7(1):43-59, 2014, doi:10.4271/2014-01-0665.

CONTACT INFORMATION

Corresponding author:

Yann.gallo@energy.lth.se

ACKNOWLEDGMENTS

This research was funded by the Swedish Energy Agency and the KCFP Engine Research Center at Lund University (project number 22485-3). The authors also gratefully acknowledge the technical support provided throughout the campaign by Martin Carlsson and Anders Olsson. Laboratory work and technical discussions were occasionally provided by Sanghoon Kook from the University of New South Wales in Sydney, Australia and Luigi Sequino from Istituto Motori of Naples, Italy.

Paper III

Investigation of Late-Cycle Soot Oxidation Using Laser Extinction and In-Cylinder Gas Sampling at Varying Inlet Oxygen Concentrations in Diesel Engines

Yann Gallo[a], Vilhelm B. Malmborg[b], Johan Simonsson[c], Erik Svensson[a], MengQin Shen[a], Per-Erik Bengtsson[c], Joakim Pagels[b], Martin Tunér[a], Antonio Garcia[d], Öivind Andersson[a]

[a] Division of Combustion Engines, Lund University, Sweden

[b] Division of Ergonomics and Aerosol Technology, Lund University, Sweden

[c] Division of Combustion Physics, Lund University, Sweden

[d] CMT Motores Térmicos, Universitat Politécnica de Valencia, Spain

Corresponding author

Yann Gallo

Lund University

Department of Energy Sciences – Combustion engines

Ole Römers väg 1

22363, Lund, Sweden

Yann.gallo@energy.lth.se

Abstract

This study focuses on the relative importance of O_2 and OH as oxidizers of soot during the late cycle in diesel engines, where the soot oxidation is characterized in an optically accessible engine using laser extinction measurements.. These are combined with in-cylinder gas sampling data from a single-cylinder engine fitted with a fast gas sampling valve. Both measurements confirm that the in-cylinder soot oxidation slows down when the inlet concentration of O_2 is reduced. A 38% decrease in intake O_2 concentration reduces the soot oxidation rate by 83%, a discrepancy indicating that O_2 in itself is not the main soot oxidizing species. Chemical kinetics simulations of OH concentrations in the oxidation zone and estimates of the OH-soot oxidation rate point towards OH being the dominant oxidizer.

Keywords

Soot oxidation, PM, OH, EGR, gas-sampling, laser extinction

Introduction

Diesel engines are favored by high efficiencies but are challenged by high emissions of nitrous oxides (NO_x) and particulate matter (PM), if not coupled with adequate exhaust aftertreatment technologies such as NO_x adsorbers and diesel particulate filters (DPF). Diluting the charge by Exhaust Gas Recirculation (EGR) is a widespread method for reducing the NO_x emissions by decreasing the combustion temperature. On the other hand, EGR generally increases PM emissions due to deteriorating in-cylinder soot oxidation rates [1,2]. Previous studies indicate that, under most conditions applicable to diesel engines, this oxidation has a dominating influence on the soot emission levels [2-5].

EGR reduces the intake oxygen concentration. This has a number of potential effects on the soot oxidation process. First, it will decrease the availability of oxygen during the late cycle, which could limit the oxidation rate. It also lowers the flame temperature, slowing the chemical kinetics of the oxidation process as well as decreasing the formation of hydroxyl radicals (OH) [6], which is believed to be the main oxidizing species [7-11]. A few experimental studies have studied the impact of EGR on the soot oxidation during diesel combustion in the cylinder. For example, Payri *et al*. measured the PM mass, size, and number density in the exhaust gases while varying intake O_2 between 9% and 13%. Though the study was concerning low temperature combustion (LTC) strategies, they could highlight the poor oxidation affecting the emissions before the inhibited formation dominated the emission trends at lower O_2 inlet concentration [12]. Using the same methodology to characterize the oxidation process, Gallo *et al*. [2] used the decay of the optical thickness (*KL*)

of the extinction signal whereas Lopez *et al*. [13] used the *KL* from two-color pyrometry measurements. Both studies reached the conclusion that a reduction of inlet O_2 leads to a slower soot oxidation rate. Also using two-color pyrometry, a study by Huestis *et al*. showed that decreasing the intake O_2 from 21% to 9% decreased the late cycle soot oxidation rates monotonically, and that the emissions followed the late cycle trends in in-cylinder soot mass [14]. While this last study pointed out the importance temperature on the oxidation process, none of these studies proposed an explanation for the mechanisms behind the reduction of oxidation rate observed at lower O_2 availabilities in the cylinder.

The purpose of this study is to cast light on the relative importance of O_2 and OH as soot oxidizers during the late cycle. It is based on data from optical measurements and in-cylinder gas sampling. The optical measurements are made using laser extinction in an optically accessible single-cylinder engine fitted with a Bowditch-type piston extender [15]. The gas sampling data are acquired from a single-cylinder engine without optical access, fitted with a fast gas sampling valve. The analysis is complemented with a simulation of OH availability in the flame using a zero-dimensional (0-D) reactor model.

Terminology

Different terms for soot are used in different communities. These include particulate matter (PM), soot, and black carbon (BC). PM is the generic term describing the particles contained in an aerosol. In the engine community, PM is defined as the constituents of the diluted exhaust gases that are adsorbed on a filter in a gravimetric test. In such a test, the exhausts are drawn through an efficient filter, which is weighed before and after the test. The difference in mass (due to both solid and liquid particles) is the PM mass. A soot particle is an agglomerate of roughly spherical primary particles consisting primarily of carbon. Soot is by far the

dominating constituent of PM. Black carbon is roughly equivalent to soot, i.e. light-absorbing carbonaceous particles originating from combustion sources. As it is measured optically, its name derives from its optical properties. BC is a term more commonly encountered in environmental contexts like aerosol physics, atmospheric chemistry or geophysical fields. As engine-out PM mostly consists of combustion-generated soot particles, it is an accepted approximation in the automotive and combustion engineering fields to use the terms PM, soot and BC more or less interchangeably.

Experimental facilities

Engine Setup

The engine used for the optical study is a heavy-duty direct-injection diesel engine based on a Scania D12, operated as a single-cylinder engine. A single-cylinder version of a Scania D13 is used for the in-cylinder gas sampling measurements. These engines are henceforth referred to as the optical and the all-metal engine. In order to produce as similar conditions as possible, both configurations employ the same cylinder head leading to identical swirl levels and the same injector for identical fuel flows. A Scania XPI common-rail fuel injection system capable of fuel pressures up to 2500 bar is used. The injector is a stock item with eight nozzle holes. The fuel used is Swedish MK1 diesel. Specifications of the engines, fuel system and fuel are given in Table 1.

Table 1. Engine and fuel specifications

Engine base type	Scania D12 DI diesel	Scania D13 DI diesel
Bore	127 mm	130 mm
Stroke	154 mm	160 mm
Comp. Ratio	15.6	16
Swirl	1.6	
Displacement	1.95 l	2.12 l
EGR	External	Internal
Injection system	XPI common rail	

Nozzle flow number	2174 cm^3/min
Number of holes	8
Firedeck angle	17 °
Hole diameter	0.175 mm
Fuel type	MK1 Diesel
Cetane number	51
Density	815 kg/m^3
Lower Heating Value	42.9 MJ/kg
Carbon-to-Hydrogen ratio	0.53

The two setups use different sources of EGR. On the optical engine, exhaust gases are produced using a diesel furnace operating at stoichiometric conditions. These are mixed with fresh air, heated and compressed to the desired inlet conditions in order to achieve a stable external source of "EGR". On the all-metal engine, exhaust gases are taken from the exhaust manifold and fed to the intake manifold, using flow and back-pressure valves to control the flow. The intake O_2 concentration is used to measure the EGR rate. In the optical engine, it is measured during engine operation without injection by a lambda sensor located in the exhaust. For the all-metal engine, the concentration of inlet O_2 is calculated as:

$$O_{2,in} = \frac{CO_{2,in}}{CO_{2,ex}}\left(O_{2,ex} - O_{2,amb}\right) + O_{2,amb} . \quad (1)$$

where $O_{2,ex}$ is the exhaust O_2 concentration measured by a lambda sensor, $O_{2,amb}$ is the ambient O_2 concentration set at 20.95%. $CO_{2,in}$ and $CO_{2,ex}$ are the CO_2 concentrations of inlet and exhaust both measured using an infrared detector in an AVL AMA i60 emission system.

Another difference between the setups is the shape of the piston bowl. In the D12 engine, the bottom of the bowl is flat in order to facilitate the optical access, while the D13 engine has a slightly conical bowl bottom. As shown in Figure 1, both configurations had open combustion chambers. These differences could cause variations in the in-cylinder flow that could affect

the late-cycle mixing process. This may lead to different soot oxidation rates and, thus, different average soot emissions from the two engines. It should be noted, however, that the experiment consists in a variation in the intake oxygen concentration. This variation is the same in both engines and affects chemical aspects of the soot oxidation rather than the flow. For this reason, the trends in soot oxidation rates that result from the intake O_2 variation are expected to be the same in both engines.

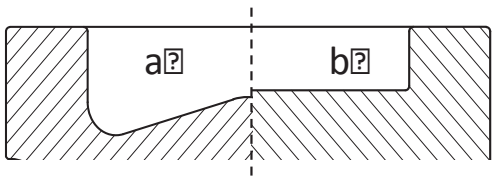

Figure 1. Profile of the metal piston used in the D13 engine (a) and of the quartz piston used in the D12 engine (b).

Operating conditions

The engines are operated at a speed of 1200 rpm and a load of 6 bar $IMEP_g$. The EGR rate is varied in order to obtain various inlet O_2 concentrations (13%, 15% and 21%). The cylinder pressure is monitored using a side-mounted Kistler 6125C transducer coupled to a Kistler 5011B10 charge amplifier. A crank angle encoder giving 1800 pulses per revolution is used, resulting in one pulse per 0.2 CAD. The injection pressure is kept constant as well as the duration of injection (650 µs). The start of injection is adjusted in order to maintain CA50 at approximately 9 CAD ATDC. A summary of the operating conditions is given in Table 2.

Table 2. Engines operating conditions

Operating conditions		
Engine	Scania D12 DI diesel	Scania D13 DI diesel
Speed	1200 rpm	

Load	6 bar $IMEP_g$	
P_{inj}	2000	
CA50	8 CAD ATDC	
SOI	Adjusted to keep CA50 constant	
DOI	650µs	
Inlet P	1.8 bar	1.65 bar
Inlet T	70°C	
Fuel	MK1 Swedish Diesel	
EGR rate	Variable (13%, 15% and 21% O_2)	

In order to compensate for the difference in compression ratio, the top dead center (TDC) conditions in temperature and density are matched between the engines. This is realized by applying adiabatic compression calculations, leading to the use of a substantially lower inlet pressure on the all-metal engine. A sample motored pressure trace at 15% inlet O_2 from the optical engine is compared with a motored one from the all-metal engine without EGR in Figure 2a. The apparent heat release rate (AHRR) from a case with combustion at 15% O_2 is shown in Figure 2b for the two engines. The differences in thermodynamic conditions at TDC and during combustion are minor, justifying the validity of the comparison between setups.

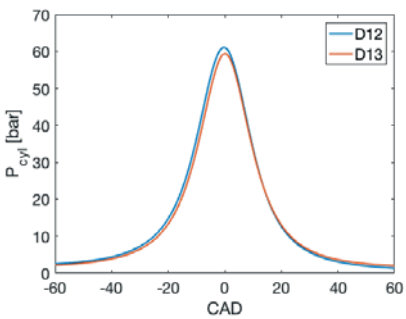

Figure 2a. Sample motored trace for the 15% [O_2] case. The D13 trace (all-metal engine) is recorded without EGR.

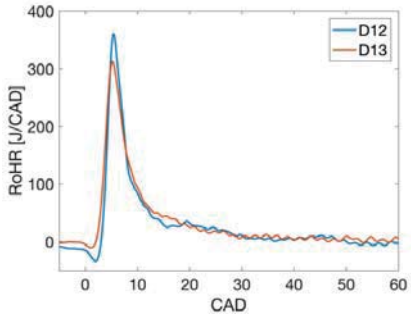

Figure 2b. Sample AHRR for the 15% [O_2] case.

Soot measurement techniques

Laser extinction method

The laser extinction technique is a quantitative measurement technique for soot that has been applied successfully in combustion engines for several decades [2,3, 16-18] as well as in spray vessels [19-21]. The intensity of a laser beam decreases as it passes an absorbing medium, *e.g.* containing soot. The initial and transmitted intensities, I_0 and I, are measured and, assuming that the in-cylinder combustion medium is optically thin, the Beer-Lambert law applies:

$$I = I_0 e^{-KL}. \quad (2)$$

Here, K is the extinction coefficient and L is the length of the absorbing medium, in this case the vertical extent of the combustion chamber. Extinction is any process that decreases the initial laser intensity, and is thus a combination of absorption and scattering of light out of the beam path. For particles with sizes much smaller than the laser wavelength, the scattering is negligible in comparison with the absorption (i.e. the Rayleigh approximation), and K is then equal to the absorption coefficient [22]. Under this assumption, K can be related to the soot volume fraction, f_v, as

$$K = \frac{f_v 6\pi E(m)}{\lambda}. \quad (3)$$

where λ is the laser wavelength. *E(m)* is the refractive index function, representing the imaginary part of $(m^2\text{-}1)/(m^2\text{+}2)$, where *m* is the complex refractive index of the soot particles, see *e.g.* [23]. In the present work the laser wavelength 685 nm was used, which is rather long in order to better fulfill the Rayleigh scattering approximation and avoidance of PAH absorption, as well as to facilitate laser beam alignment using a visible laser wavelength. Throughout this paper, the product *KL* is used as a measure of the soot in the cylinder, and it is directly related to the amount of soot in the beam path and obtained directly from the relative transmission measurement. This product *KL* thus remains constant if the soot content in the beam path remains constant, even if the piston moves, under assumptions of negligible beam steering and non-varying optical properties of the soot. Assuming that no net transport of soot occurs out of the beam path (i.e. that transport out of the beam path is balanced by transport into it), a decrease in *KL* after the end of injection (EOI) can thereby be attributed to net oxidation of the soot in the cylinder. This is a fair assumption when measuring close to the bowl periphery in a swirl-supported combustion system, since the soot quickly becomes evenly distributed in the azimuthal direction after the end of injection, and since the swirling flow sets up a quasi-steady flow through the beam path. To obtain a high temporal resolution, the photodiode laser beam is modulated at a frequency of 72 kHz using an acousto-optic modulator (AOM), giving 10 laser pulses per CAD at an engine speed of 1200 rpm.

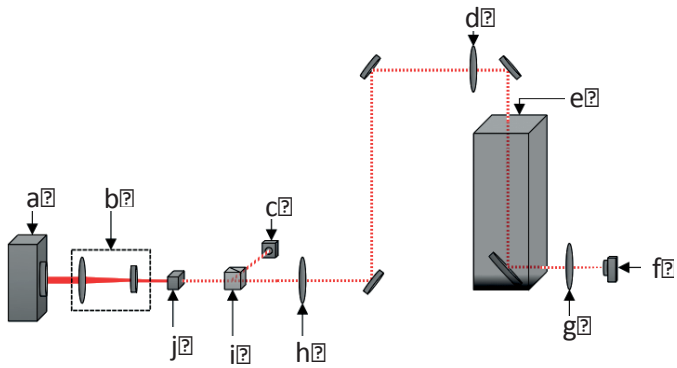

Figure 3. The parts of the laser extinction setup. Diode laser (a), telescope lenses (b), photodiode for the reference signal (c), re-collimation lens (d), schematic of engine (e), photodiode (f), collection lens (g), re-collimation lens (h), cubic beam splitter (i), and AOM (j).

A schematic representation of the setup is shown in Figure 3. The Bowditch piston extension has a full quartz piston top and a 45° mirror in a fixed position below it. An insert containing an angled window is used in place of one of the exhaust valves, providing optical access from the top of the cylinder. The angle of the window compensates for the angle of the insert and makes it possible to obtain a vertical beam path through the cylinder. A cross-section of this optical access is given in Figure 4. The absence of one exhaust valve does not substantially affect the combustion process since the engine is running at a relatively low speed of 1200 rpm, allowing for effective gas scavenging. A more detailed presentation of the setup and method of measurement can be found in [2].

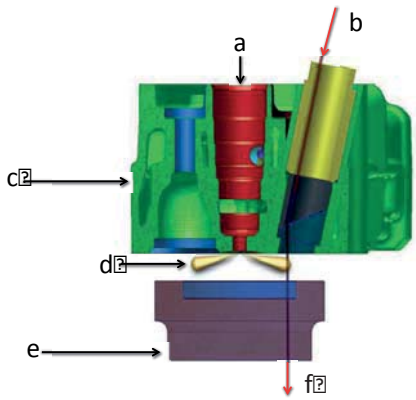

Figure 4. Section through the cylinder head used in the extinction setup. Injector location (a), laser entrance (b), cylinderhead (c), burning sprays (d), optical piston (e), and laser exit (f).

In-cylinder gas sampling

In-cylinder gas sampling was performed on the all-metal engine, fitted with the same cylinder head as used in the optical measurements. In the all-metal engine, the quartz window in the insert (yellow detail in Figure 4) was replaced with a fast-acting gas-sampling valve [24]. During operation a solenoid hammer actuates the valve by hitting the top of the valve stem. The hammer is controlled by the valve driver, itself driven by a TTL (Transistor-Transistor Logic) signal from a computer program and triggered on crank angle basis. With these features the gas flow through the valve can be controlled in a wide range, with respect to sampling timing, sampling rate and sampling duration. In this study, the undiluted gas flow rate sampled from the cylinder was kept constant at 1 liter per minute (at ambient atmospheric pressure and temperature) for each sampling point. This volume corresponds to approximately 0.05% of the total cylinder volume. For the sampling settings used to achieve this flow rate, the minimum step-by-step sampling resolution, i.e. the duration between the valve opening and closing, can be less than 3.5 crank angle degrees CAD at high in-cylinder pressures [25].

Figure 5 presents the dilution and gas analyzing system. The gases are diluted with nitrogen (N_2) during the first step (D1) in order to prevent further oxidation of the particles. The following steps (D2 and D3) reduce the amount of particles to a level suitable for the aethalometer (Model AE33, Magee Scientific), used to measure the BC concentration.

The aethalometer is based on measurement of the extinction of particles deposited on a filter substrate. Seven different wavelengths are used, ranging from 370 nm to 950 nm. These allow determination of the optical properties of the soot particles. In this study, the BC concentration is obtained as the average of the measurements at the two highest wavelengths (880 nm and 950 nm) in order to reduce interferences from organics or polycyclic aromatic hydrocarbons (PAHs) that absorb in and near the ultraviolet region [24].

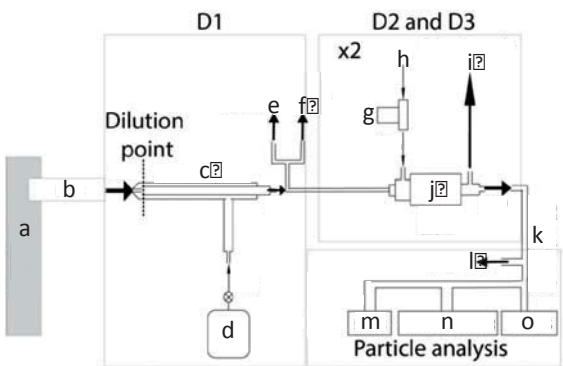

Figure 5. Diagram of dilution and gas analyzing system [24]. D1, D2 and D3 are dilution steps. Engine (a), fast sampling valve (b), dilution probe (c), N_2 bottle (d), NO_x measurement (e), flow reading (f), pressure regulator (g), air (h), diluted sample (i, not used), ejector diluter (j), diluted sample (k), NO_x measurement (l), SMPS (m, not used in this article), aethalometer (n), and SP-AMS (o, not used in this study).

The two techniques used in this study present fundamental differences. The extinction measurements are non-intrusive and 1-D along the beam path. On the other hand, the sampling measurements are intrusive and probe in a 3-D region located close to the sampling valve inlet. The data from the two different techniques will be analyzed and compared.

Simulation tools

The availability of OH in the flame is evaluated using a *Φ-T* map, a concept first introduced by Kamimoto et al [27]. The *Φ-T* map of OH mass fraction is constructed using a 0-D reactor, from LOGEsoft [28], with constant pressure, temperature and equivalence ratio. The MK1 Diesel was modeled by a surrogate fuel with 70 percent *n*-heptane together with 30 percent toluene. Lars Seidel's chemical mechanism for *n*-heptane could then be applied in the simulations [29]. The addition of toluene is used to mimic the sooting behavior of diesel, which *n*-heptane alone cannot. Such surrogate for diesel fuel has been commonly used in diesel combustion studies [30,31] and ascertained in [32]. The map consists of a grid of nodes at different *Φ* and *T* conditions (the pressure is constant for all nodes). One simulation is performed at every node and the *Φ-T* map shows the OH yield after 2 milliseconds.

Dependency of the soot oxidation rate on O_2 and OH availability

Gallo et al. observed a constant degradation of the soot oxidation rate with reduced intake O_2 level, leading to increased soot emissions [2]. This was accompanied with an increase in the engine-out emissions of soot. Figure 6a shows the optical thickness, *KL*, in the cylinder for three intake O_2 levels. As previously mentioned, *KL* is proportional to the soot amount in the beam path. The curves show a marked late-cycle decay due to soot oxidation. Figure 6b shows aethalometer data from the all-metal engine. The curves represent the content of BC in

samples drawn from the cylinder at different crank angle positions during the cycle. In both these figures it can be seen that the 21% O_2 data set represents the steepest decay and the 13% O_2 case the slowest. The two measurement setups independently show that a global effect of the reduction in inlet O_2 concentration is a reduction in the rate of soot oxidation.

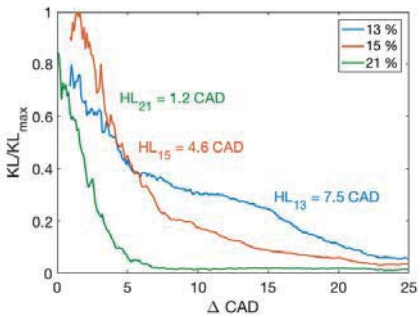

Figure 6a. Evolution of KL (relative to the peak KL at 15% O_2) in the optical measurements shown from the start of decay. The half-life extracted from the exponential approximation is shown in CAD.

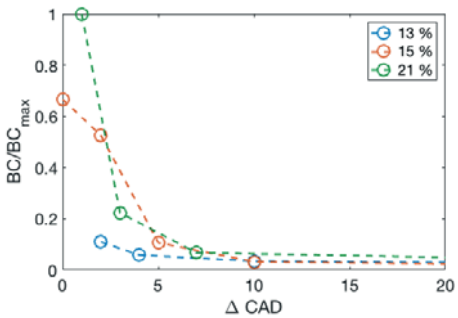

Figure 6b. Evolution of BC from the in-cylinder sampling measurements shown from the start of decay.

There are several potential ways to quantify these soot oxidation rates. One method is to fit an exponential decay function to the extinction curves and extracting the half-life (HL) [2,3].

Although the 13% O_2-case in Figure 6a is not perfectly described by an exponential, the half-lives extracted from the curves still give a useful estimate of the overall oxidation rates. When decreasing the inlet O_2 concentration from 21% to 13%, *i.e*. by a factor of less than two (-38%), the oxidation half-lives in Figure 6a display a six-fold increase (translating to an 83% decrease of the oxidation rate). This indicates that the availability of O_2 in itself is not governing the oxidation rate. A linear dependence of the oxidation rate on the intake O_2 concentration is not expected, however, as the O_2 concentration affects other aspects of the oxidation chemistry by affecting the flame temperature. This will be discussed below.

O_2 and OH are both important soot oxidizers [9]. According to Bartok and Sarofim [7], both OH and O_2 play a role under lean conditions while OH is likely to be dominating under fuel-rich and stoichiometric conditions [7]. Since the late-cycle soot oxidation is a mixing-controlled combustion process, it is expected to take place near stoichiometric conditions, and OH is thereby expected to be the main soot oxidizer under diesel conditions. About 10–20% of all OH collisions with soot are effective at gasifying a carbon atom [8,11]. Moreover, Guo et al. have shown that soot oxidation by OH has negligible activation energy and they point out that, for premixed and diffusion flames, optimized models indicate that soot oxidation by OH dominates over O_2 [11].

While dilution with EGR affects the availability of O_2, it has an even greater impact on the flame temperature. The flame temperature, in turn, has a strong effect on the availability of OH. Figure 7 represents Φ-T maps obtained using the 0-D reactor model. The colored iso-fields represent the OH concentration and the white, green and red curves represent the adiabatic flame temperatures at the different O_2 concentrations using an initial temperature of

900 K. The maximum adiabatic flame temperature is 2744 K at 21% O_2, and drops to 2196 K for the 15% O_2 case.

Figure 8 shows normalized number densities of OH extracted from Figure 7, plotted against the soot oxidation half-lives displayed in Figure 6a. Since the soot oxidation is expected to occur at stoichiometric conditions, the OH mass fractions are extracted at the maximum flame temperature. As expected, the oxidation rate increases with the OH concentration in the flame. It can be noted that the six-fold decrease in half-life previously mentioned is accompanied by a roughly six-fold increase in OH availability.

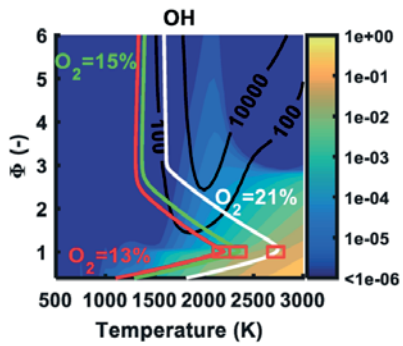

Figure 7. Φ-T map of OH mass fraction constructed using a 0-D reactor with constant pressure, temperature and equivalence ratio. The three red squares highlight the maximum adiabatic flame temperature corresponding to the three cases (13, 15 and 21% O_2). The scale on the right represents the mass fraction of OH species.

Besides the availability of OH, the local temperature could be expected to affect the soot oxidation rate. In Seidel's mechanism, however, the activation energy for OH-soot reactions is zero, yielding a dependence on OH concentration and the soot area-to-volume ratio, but not on temperature. This is motivated by OH being a very reactive species. The current study

provides no data on soot morphology but, assuming that the area-to-volume ratio remains constant, the temperature dependence of the OH-soot reactions can be estimated using the model of Neoh et al. [33]

$$\omega_{OH} = \gamma_{OH} \frac{3 n_{OH}}{N_A} \left(\frac{8RT}{\pi M_{OH}} \right)^{1/2}. \quad (4)$$

Here, ω_{OH} is the soot oxidation rate, n_{OH} and M_{OH} are the number density and the molar mass of OH, R is the general gas constant and N_A is Avogadro's number. γ_{OH} is the collisional frequency between OH and the soot surface and is assigned a value of 0.13 by Neoh *et al*. [33]. Inserting the OH concentrations and the peak adiabatic flame temperatures from the simulations into this model yields the oxidation rates presented in Figure 8 alongside the OH number density. Both the number densities and the rates are normalized to facilitate comparison. Although the temperature drops by 25%, the estimated oxidation rate drops at the same rate as the OH concentration. This supports both the assumption that the OH-soot reactions do not have a strong temperature dependence and rather follow the OH availability, as well as the claim that OH is the dominant soot oxidizer.

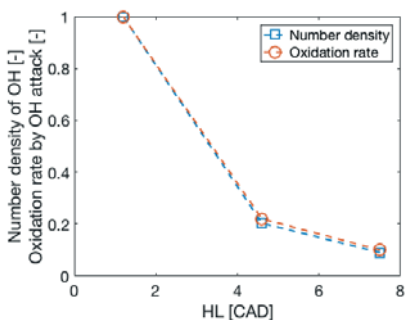

Figure 8. Variation of the relative number density of OH (blue curve) and soot oxidation rate according to Neoh et al. [32] (red curve) at the 3 cases studied, versus the variation of the oxidation half-life.

Conclusions

The in-cylinder soot oxidation slows down when the inlet concentration of O_2 is reduced. This observation has been confirmed through measurements using two techniques on two different engine setups. Decreasing the intake O_2 concentration by 38% reduces the soot oxidation rate by 83%. The non-linear impact of O_2 on the soot oxidation indicates that O_2 availability is not limiting the soot oxidizing process in itself.

The reduction of inlet O_2 concentration has a strong impact on the adiabatic flame temperature. It is hypothesized that the temperature affects the soot oxidation rate mainly through its effect on the mass fraction of OH during combustion. When the maximum flame temperature drops from 2700 K to 2400 K, the OH concentration drops roughly six times. This corresponds well to the drop in the oxidation rate. Both the chemical mechanism used for the OH simulations and the soot oxidation model by Neoh *et al*. state that the temperature dependence of soot oxidation due to OH is negligible, due to the high reactivity of OH radicals. In combination, these findings indicate that OH is the dominant oxidizer under diesel conditions.

Acknowledgement

The authors gratefully acknowledge the Swedish Energy Agency, the Competence Center for Combustion Processes KCFP (Project number 22485-3), and the competence center METALUND funded by FORTE for financially supporting this research.

References

1. Akihama, K., Takatori, Y., Inagaki, K., Sasaki, S. et al., "Mechanism of the Smokeless Rich Diesel Combustion by Reducing Temperature," SAE Technical Paper 2001-01-0655, 2001, doi:10.4271/2001-01-0655.
2. Gallo, Y., Simonsson, J., Lind, T., Bengtsson, P. et al., "A Study of In-Cylinder Soot Oxidation by Laser Extinction Measurements During an EGR-Sweep in an Optical Diesel Engine," SAE Technical Paper 2015-01-0800, 2015, doi:10.4271/2015-01-0800.
3. Gallo, Y., Li, Z., Richter, M., Andersson, Ö., " Parameters influencing soot oxidation rates in an optical diesel engine," SAE Technical Paper 2016-01-2183, 2016, doi:10.4271/2016-01-2183.
4. Aronsson, U., Chartier, C., Andersson, Ö., Egnell, R. et al., "Analysis of the Correlation Between Engine-Out Particulates and Local Φ in the Lift-Off Region of a Heavy Duty Diesel Engine Using Raman Spectroscopy," SAE Technical Paper 2009-01-1357, 2009, doi:10.4271/2009-01-1357.
5. Lequien, G., Andersson, Ö., Tunestal, P., and Lewander, M., "A Correlation Analysis of the Roles of Soot Formation and Oxidation in a Heavy-Duty Diesel Engine," SAE Technical Paper 2013-01-2535, 2013, doi:10.4271/2013-01-2535.
6. Dec, J. and Kelly-Zion, P., "The Effects of Injection Timing and Diluent Addition on Late-Combustion Soot Burnout in a DI Diesel Engine Based on Simultaneous 2-D Imaging of OH and Soot," SAE Technical Paper 2000-01-0238, 2000, doi:10.4271/2000-01-0238
7. Bartok, W., Sarofim, A.F., “Fossil Fuel Combustion: A Source Book “ New York. Wiley; 1991.

8. Haynes, B.S., Wagner, H.Gg., “Soot formation”, Progress in Energy and Combustion Science, 1981;7:229–273, http://dx.doi.org/10.1016/0360-1285(81)90001-0
9. Tree D.R., Svensson K.I., “Soot processes in compression ignition engines” Progress in Energy and Combustion Science Volume 33, Issue 3, June 2007, Pages 272–309, doi:10.1016/j.pecs.2006.03.002
10. Hayashida, K., Nagaoka, S., Ishitani, H., “Growth and oxidation of graphitic crystallites in soot particles within a laminar diffusion flame”. In: Fuel 128 (2014), pp. 148-154. http://dx.doi.org/10.1016/j.fuel.2014.03.008
11. Guo, H., Anderson, P.M., Sunderland, P.B., “Optimized rate expressions for soot oxidation by OH and O2”. In: Fuel 172 (2016), pp. 248-252. http://dx.doi.org/10.1016/j.fuel.2016.01.030
12. Payri, F., Benajes, J., Novella, R., and Kolodziej, C., "Effect of Intake Oxygen Concentration on Particle Size Distribution Measurements from Diesel Low Temperature Combustion," SAE Int. J. Engines 4(1):1888-1902, 2011, doi:10.4271/2011-01-1355
13. Lopez, J., Martin, J., Garcia, A., Villalta, D. et al., "Characterization of In-Cylinder Soot Oxidation Using Two-Color Pyrometry in a Production Light-Duty Diesel Engine," SAE Technical Paper 2016-01-0735, 2016, doi:10.4271/2016-01-0735.
14. Huestis, E., Erickson, P., and Musculus, M., "In-Cylinder and Exhaust Soot in Low-Temperature Combustion Using a Wide-Range of EGR in a Heavy-Duty Diesel Engine," SAE Technical Paper 2007-01-4017, 2007, doi:10.4271/2007-01-4017.
15. Bowditch, F., "A New Tool for Combustion Research A Quartz Piston Engine," SAE Technical Paper 610002, 1961, doi:10.4271/610002.

16. Hentschel, W. and Richter, J., "Time-Resolved Analysis of Soot Formation and Oxidation in a Direct-Injection Diesel Engine for Different EGR-Rates by an Extinction Method," SAE Technical Paper 952517, 1995, doi:10.4271/952517.
17. Tree, D. and Dec, J., "Extinction Measurements of In-Cylinder Soot Deposition in a Heavy-Duty DI Diesel Engine," SAE Technical Paper 2001-01-1296, 2001, doi:10.4271/2001-01-1296.
18. Mancaruso, E., Merola, S., and Vaglieco, B., "Soot Concentration and Particle Size in a DI CR Diesel Engine by Broadband Scattering and Extinction Measurements," SAE Technical Paper 2005-24-013, 2005, doi:10.4271/2005-24-013.
19. Xu, Y. and Lee, C., "Investigation of Soot Formation in Diesel Combustion Using Forward Illumination Light Extinction (FILE) Technique," SAE Technical Paper 2004-01-1411, 2004, doi:10.4271/2004-01-1411.
20. Cenker, E., Bruneaux, G., Pickett, L., and Schulz, C., "Study of Soot Formation and Oxidation in the Engine Combustion Network (ECN), Spray A: Effects of Ambient Temperature and Oxygen Concentration," *SAE Int. J. Engines* 6(1):352-365, 2013, doi:10.4271/2013-01-0901.
21. Manin, J., Pickett, L., and Skeen, S., "Two-Color Diffused Back-Illumination Imaging as a Diagnostic for Time-Resolved Soot Measurements in Reacting Sprays," *SAE Int. J. Engines* 6(4):1908-1921, 2013, doi:10.4271/2013-01-2548.
22. Bohren, C.F and D.R. Huffman, “Absorption and scattering of light by small particles”. 1998, New York, Wiley.
23. F. Migliorini, K. Thomson and G. Smallwood, “Investigation of optical properties of aging soot” Applied Physics B, 2011. 104(2): 273-283.

24. Shen, M., Malmborg, V., Gallo, Y., Waldheim, B. et al., "Analysis of Soot Particles in the Cylinder of a Heavy Duty Diesel Engine with High EGR," SAE Technical Paper 2015-24-2448, 2015, doi:10.4271/2015-24-2448.
25. Malmborg, V.B., Eriksson, A.C., Shen M., Nilsson, P. et al., "Evolution of in-cylinder diesel soot and emission characteristics investigated with on-line aerosol mass spectrometry", Under review in Environmental Science & Technology.
26. Onasch, T.B., Trimborn, A., Fortner, E.C., Jayne, J.T., et al., "Soot Particle Aerosol Mass Spectrometer: Development, Validation, and Initial Application", Aerosol Science and Technology, 2012, http://dx.doi.org/10.1080/02786826.2012.663948
27. Kamimoto, T. and Bae, M., "High Combustion Temperature for the Reduction of Particulate in Diesel Engines," SAE Technical Paper 880423, 1988, doi:10.4271/880423
28. LOGE AB. LOGEsoft. http://loge.se/Products/products.html. [accessed 04.09.2016].
29. Lars Seidel et al. "Comprehensive kinetic modeling and experimental study of a fuel-rich, premixed n-heptane flame". In: Combustion and Flame 162.5 (2015), pp. 2045 – 2058. http://dx.doi.org/10.1016/j.combustflame.2015
30. Wang, X., Song, C., Lu G., Song, J., et al., "Evolution of in-cylinder polycyclic aromatic hydrocarbons in a diesel engine fueled with n-heptane and n-heptane/toluene". In: Fuel 158 (2015), pp. 322-329. http://dx.doi.org/10.1016/j.fuel.2015.05.053
31. Machrafi, H., Cavadias, S., Gilbert, P., "An experimental and numerical analysis of the HCCI auto-ignition process of primary reference fuels, toluene reference fuels and diesel fuel in an engine, varying the engine parameters". In: Fuel 89 (2008), pp. 1007-1016. http://dx.doi.org/10.1016/j.fuproc.2008.03.007

32. Chen, W., Shuai, S., Wang, J., “A soot formation embedded reduced reaction mechanism for diesel surrogate fuel”. In: Fuel 88 (2009), pp. 1927-1936. http://dx.doi.org/10.1016/j.fuel.2009.03.039

33. Neoh, K.G., Howard, J.B., Sarofim A.F. (1974) Effect of oxidation on the physical structure of soot. Proc. Comb. Inst. 20:951

Paper IV

SAE INTERNATIONAL

Comparison of Laser-Extinction and Natural Luminosity Measurements for Soot Probing in Diesel Optical Engines

2016-01-2159
Published 10/17/2016

Zheming Li, Yann Gallo, Ted Lind, Oivind Andersson, Marcus Alden, and Mattias Richter
Lund University

CITATION: Li, Z., Gallo, Y., Lind, T., Andersson, O. et al., "Comparison of Laser-Extinction and Natural Luminosity Measurements for Soot Probing in Diesel Optical Engines," SAE Technical Paper 2016-01-2159, 2016, doi:10.4271/2016-01-2159.

Abstract

Soot emissions from diesel internal combustion engines are strictly regulated nowadays. Laser extinction measurement (LEM) and natural luminosity (NL) of sooty flames are commonly applied to study soot. LEM measures soot along the laser beam path and it can probe soot regardless of temperature. NL integrates the whole field of view and relies on soot temperature. In this work, a comparison of simultaneously recorded LEM and NL data has been performed in a heavy-duty optical engine. A 685 nm laser beam is used for LEM. The laser was modulated at 63 kHz, which facilitated subtraction of the background NL signal from the raw LEM data. By Beer-Lambert's law, *KL* factor can be calculated and used as a metric to describe soot measurements. A compensation of transmitted laser intensity fluctuation and soot deposits on optical windows has been performed in this work. The data compensation successfully reduced the transmitted laser intensity fluctuation and made it possible to study in-cylinder low temperature soot residual. The *KL* curves were compared with NL curve in this work. In the late cycle the *KL* curve can successfully show the low temperature soot which is not detected by NL. The *KL* curve is found to rise about 2 CAD ahead of the corresponding NL curve due to liquid fuel spray disturbance. In this case, LEM is not a suitable method to calculate *KL* for analyzing the early soot formation if there are liquid phase fuel droplets crossing the probing laser beam.

Introduction

The engine out soot emission is considered as the net result of formation and oxidation of soot in cylinder. It has been shown in previous studies that soot formation does not correlate well with soot emissions[1, 2]. Thus understanding the soot oxidation process is necessary to help to reduce soot emissions.

There are different approaches to measure in-cylinder soot. Both spatially and temporally resolved soot detecting techniques have been developed and applied in IC engines. Planar Laser-induced Incandescence (PLII) is a commonly used 2D imaging technique of probing soot [3, 4, 5, 6]. This technique requires a high laser power and suitable energy profile across the laser sheet to reach the signal 'plateau' where the signal is independent of laser fluence[7]. In-cylinder sampling[8, 9, 10, 11] is another soot measurement.

For certain cases, it is not always necessary to use the complex techniques. Some relatively simple techniques such as Laser-extinction measurements (LEM) and natural luminosity (NL) measurements can give sufficient information. They can provide temporal resolved data and have been commonly used in high pressure vessels[12, 13, 14] as well as in IC engines[13, 15, 16, 17, 18, 19]. With this temporally resolved soot data, the combined outcome of soot formation and oxidation can be studied.

LEM is a line-of-sight measurement. Sending a laser through the interested medium, the laser intensities before (I_0) and after (I) are measured. The transmittance of the soot cloud can be related to its optical density using Beer-Lambert's law, the *KL* factor can be calculated from equation (1)

$$e^{-KL} = \frac{I}{I_0} \tag{1}$$

Here, K is the mean extinction coefficient along the beam path and L is the length of the absorbing medium. K consists of two parts: scattering and absorption. If the particle sizes are much smaller than the laser wavelength the scattering is assumed to be negligible. It has been commonly accepted to assume that extinction by soot is dominated by absorption rather than scattering[13]. In this optical engine case, L varies with time and cannot be measured easily. KL is related to optical density of soot [13] and in this work it will be used as a metric to describe soot measurements.

In optical engines, soot deposits are always a problem for data collection. The soot deposits on optical parts would also cause a loss in transmitted laser intensity and could thus falsely be interpreted as an increased amount of soot. Window cleaning by an additional laser was applied in previous studies [13, 19], but some minor residue still accumulated during most runs. A subtraction of soot deposits on the

window has also been done in those works. The advantage of using an additional high power laser for window cleaning is that the window will be cleaner before thoroughly cleaning between each two test runs, which refers to longer available data sequences collection in each test run. However, the soot deposits subtraction only calibrates the *KL* value for the next cycle to zero before combustion, the *KL* bias due to soot deposits during the combustion cycle is still not corrected. Adding an additional high power laser also makes the relatively 'simple' technique more complex. In this work, a correction to compensate soot deposition will be performed by software calibration instead of hardware cleaning which also corrects for the soot deposit accumulation process during the cycle.

The broadband thermal radiation from hot soot particles is the dominant source of luminosity during the combustion of traditional hydrocarbon diesel fuel after the premixed burn [20]. A general expression of NL signal is given by Mueller et.al[21]. Part of that expression is the Planck's law for blackbody radiation in equation (2),

$$B_\lambda(\lambda,T) = \frac{2hc^2}{\lambda^5}\frac{1}{e^{\frac{hc}{\lambda k_B T}}-1} \quad (2)$$

Where k_B is the Boltzmann constant, h is the Planck constant and c is the speed of light in the medium. The spectral radiance of a body, B_λ, describes the amount of energy it gives off as radiation of different wavelength. Equation (2) shows B_λ as a function of λ and T. It can be noted that in a given wavelength, the soot NL is linked to soot volume but is also highly sensitive to temperature. NL is also a line-of-sight technique, in the sense that the measured quantity is integrated along the whole field of view.

Both LEM and NL have been widely used for soot detection. LEM measures soot along the laser beam path regardless of temperature, while NL shows the information from hot radiating soot within the field of view and is sensitive to soot temperature.

In present study, simultaneous LEM and NL data are recorded. A compensation of soot deposit and laser intensity fluctuation in LEM data is described in detail. The LEM data correction used in present work has significantly reduced the signal attenuation in late cycle. Other sources which might affect LEM data e.g. laser scattering, is discussed in the results section. A comparison between these two methods will also be discussed in this work.

Experimental Setup

The engine is modified according to a Bowditch design. The piston extension has a full quartz piston top and a 45° mirror in a fixed position below it. In lieu of one of the exhaust valves an insert containing an angled window is inserted, providing optical access from the top of the cylinder. The angle of the window compensates for the angle of the optical access and makes it possible to obtain a vertical beam path through the cylinder. A cross-section of this optical access is given in Figure 1. The absence of one exhaust valve does not substantially affect the combustion process since the engine is running relatively slowly at a maximum of 1200 rpm, allowing for effective gas scavenging.

The engine used for this study is a heavy-duty direct-injection diesel engine based on a Scania D12 and operated as a single-cylinder engine. A Scania XPI common rail fuel injection system capable of injection pressures up to 2500 bar is used. The engine, fuel system and fuel specifications are given in Table 1.

Table 1. Engine parameters

Engine base type	Scania D12 DI diesel
Bore	127 mm
Stroke	154 mm
Comp. Ratio	16
Swirl	1.6
Displacement	1.95 l
Injection system	XPI common rail
Nozzle flow number	207 pph
Number of holes	8
Firedeck angle	17 °
Hole diameter	0.175 mm
Fuel type	MK1 Diesel
Cetane number	51
Density	815 kg/m3
Lower Heating Value	42.9 MJ/kg
Carbon/Hydrogen	0.53

The laser-extinction setup is schematically shown in Figure 1. A continuous wavelength laser diode operating at a wavelength of 685 nm (Roithner LaserTechnik, QL68J6S, 50 mW) was used as laser source for measuring the extinction by soot particles. The laser beam was collimated using an aspheric lens with focal length of 4.51 mm, directly mounted on the temperature-controlled laser diode mount (Thorlabs TCLDM9). This created an approximately collimated laser beam with a beam width and height of 4 and 2 mm respectively. The laser mount was connected to controllers for diode case temperature (Thorlabs TED200) and driver current (Thorlabs LDC205C).

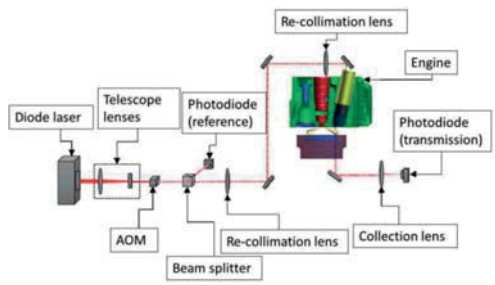

Figure 1. Sketch of experimental setup

To subtract background interferences an acousto-optic modulator (AOM) was used for intensity modulation of the laser beam. The AOM (MT80 - A1.5, AA Opto-Electronic) was controlled using an AOM driver (MODA80-1, AA Opto-Electronic). A resolution of 0.1 CAD can be approximately achieved. For the engine running at 1050 rpm this translates into a laser modulation frequency of 63 kHz. The

laser beam was divided into two beams with a beam splitter prior to entering the engine and after the AOM. By using two photodiodes (Thorlabs PDA100A-EC), one measuring the extinction signal and one a reference signal, the effect of laser intensity variation could be minimized. The laser beam from this diode laser was not exactly collimated. It becomes a bit divergent when it transmitted further away from the diode, so two re-collimation lenses were placed before the insert tube entrance.

Laser beam steering artifacts have been considered before design of this experiment. A 50 mm diameter spherical lens was applied to collect the extinction laser, it is large enough to capture the entire extinction beam and the whole beam also hits the sensitive part of the sensor even with beam steering. Since the signal collected is a sum of both laser intensity and natural luminosity, when the photodiode (transmission) was right mounted in the focal point, the signal from photodiode was saturated during combustion. So it was placed slightly closer to the collection lens than focal length to avoid signal saturation. To minimize the effects of background radiation, three filters were mounted on the photodiode measuring the transmitted laser beam: one short pass filter with cut-off wavelength 700 nm (Thorlabs, FES0700) and two long pass-filter with cut-on wavelength of 650 nm (Thorlabs, FEL0650) and 665nm (Schott, RG 665). This created a relatively narrow bandpass between 665 and 700 nm that did not fully suppress the background radiation.

Table 2. Operating condition

Operating condition	
Load	5 bar IMEPg
CA50	9 CAD ATDC
SOI	0 CAD
DOI	860 µs
EGR rate	15% O_2
Engine speed	1050 rpm
Injection pressure	1500 bars

In this paper all the data shown is from the same operating condition in the Table 2. The engine was operated in skip-fire mode, one fired cycle in every 14 cycles.

Data processing

Figure 2 shows one image from a high speed video taken during this experiment. In the image, NL is recorded. The white circle represents the piston bowl wall and the red dot roughly shows the laser location during the experiments.

Figure 3. shows the raw data collected from photodiode (transmission). The laser pulses can be identified from this raw data. The modulation amplitude was calculated from each pulse. Both the transmitted laser intensity for each laser pulse and background NL can be obtained by the mean top and bottom values from the raw data as shown in Figure 3.

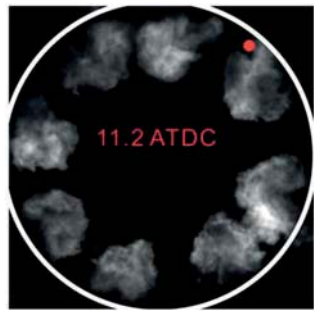

Figure 2. Natural luminosity image at 11.2 CAD ATDC was taken through the optical access. The white circle represents piston bowl wall and the red dot is the position of laser.

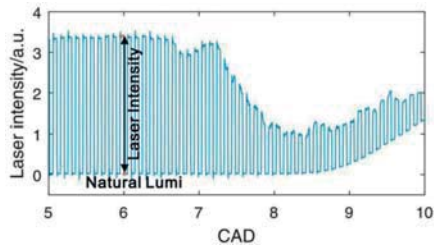

Figure 3. Raw data from photodiode (transmitting)

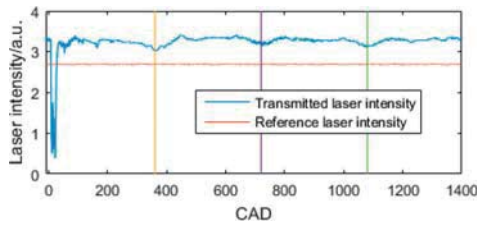

Figure 4. Collected 2 cycles transmitted laser intensity and reference laser intensity

Figure 4 shows the original transmitted and reference laser intensity. During this experiment, for each run two sequential engine cycles' data was recorded, one fired followed by one motored cycle. It can be seen that in the motored cycle (720-1440 CAD ATDC), the laser intensity still varies. Since the laser is pulsed, the input laser power did vary a bit from pulse to pulse, however comparing to the input laser power fluctuation (reference laser intensity), the transmitted laser power fluctuation is larger. The input laser power fluctuation will be canceled out when calculate the *KL* factor. In one data collection sequence, data from 60 test runs were recorded. However, due to window fouling only the data from the first 50 runs were used in the present work. The correlation coefficient *R* has been calculated between each motored cycle transmitted laser intensity and the second motored cycle as expressed in equation (3). Where *N* is the cycle number, *I* is the transmitter laser intensity, *n* is sample size. When *R* is close to +1, it means the two data sets have a strong positive linear correlation [22]. The result has been plotted in Figure

5. It shows that all 50 runs have strong linear correlation. This also means that the transmitted laser intensity fluctuation is repeatable and consistent during 50 runs collection sequence.

$$R(I_N, I_2) = \frac{1}{n-1}\sum_{i=1}^{n}\left(\frac{I_{N_i}-\mu_{I_N}}{\sigma_{I_N}}\right)\left(\frac{I_{2_i}-\mu_{2_i}}{\sigma_{I_2}}\right) \quad (3)$$

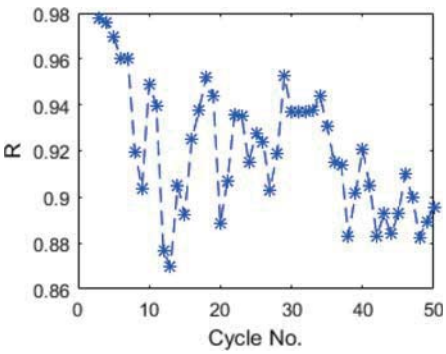

Figure 5. The correlation coefficient from different cycles

The data correction for transmitted laser intensity is in two steps.

Step 1, The soot cloud transmissivity is calculated for each cycle. It is defined as the ratio of the transmitted intensity during a fired cycle to that for a motored cycle[13] as the following equation:

$$\tau = \frac{(I_{LaserOn}-I_{LaserOff})_{Fired}}{(I_{LaserOn}-I_{LaserOff})_{Motored}} \quad (4)$$

In equation (4), τ is the transmissivity and I is the transmitted intensity. In this work, the motored cycle data was collected after the fired cycle, the mean laser intensity from -10 CAD ATDC to 5 CAD ATDC was calculated for both motored and fired cycle, so transmissivity in this work is defined as equation (5)

$$\tau = \frac{\left(Avg(I_{Laser}(-10\ CAD{:}5\ CAD))\right)_{Motored}}{(Avg(I_{Laser}(-10\ CAD{:}5\ CAD)))_{Fired}} \quad (5)$$

In an early study[19], it shown that the homogeneity of soot deposition would affect the transmitted intensity attenuation. However, in this work the laser beam size is relatively small compared to the piston bowl size so the effect of non-uniform soot deposition in laser beam cross area is negligible. Although soot deposits on the optical window from each fired cycle was not cleaned in this work, the soot deposit accumulation does not change transmitted intensity attenuation much. Which can be seen by the good agreement in Figure 5. So the transmitted laser intensity fluctuation is a result of the gas flow disturbance and laser beam steering artifacts. Since the intensity fluctuation trend is consistent in one data collection sequence, it is possible to compensate for this. In each test run, the data from the motored cycle is used as 'background' for beam steering subtraction of the fired cycle in the same run. A transmitted laser intensity fluctuation factor is calculated by equation (6)

$$\gamma = \frac{(I_{LaserOn}-I_{LaserOff})_{Transmitted,Motored}}{(I_{LaserOn}-I_{LaserOff})_{Reference,Motored}} \quad (6)$$

Here, the transmitted laser intensity fluctuation factor γ is defined as the ratio between transmitted laser intensity and reference laser intensity from the motored cycle. This factor has been calculated for every laser pulse and applied to compensate the transmitted laser intensity fluctuation in the corresponding fired cycle. This transmissivity τ in equation (5) is used to calibrate the transmitted laser intensity for the next fired cycle. In additional, transmitted laser intensity fluctuation compensation for each laser pulse has been done in this work for all data in the first step.

The motored cycle data does not match all the deviations found in the fired cycle, i.e. the small bump in Figure 4 could be seen on the fired cycle curve around 160 CAD but not in the motored cycle. This difference is possibly due to the temperature and pressure difference, especially during gas exchange and it cannot be removed by the motored cycle γ.

Step 2, in Figure 6, an averaged *KL* curve over 50 runs as a function of CAD has been plotted. Due to the swirl motion and non-uniform distribution of soot clouds from individual spray plumes inside the combustion chamber, two main peaks can be clearly observed in *KL* curve. In addition, it should be noted that the *KL* curve is slightly higher than zero after combustion than before combustion even after gas exchanging. The same trend can also be seen in the single run result.

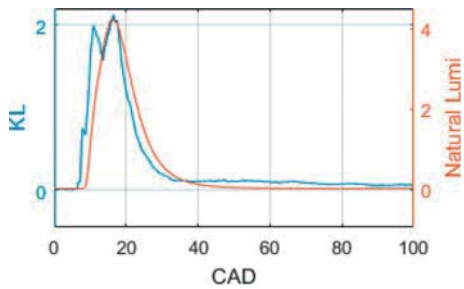

Figure 6. *KL* curve as a function of CAD

The *KL* nonzero phenomenon has been reported by previous study[13]. They claimed the source of this residual attenuation is soot deposits on the in-cylinder surfaces of the windows[19]. This soot deposit should not be considered as effective data for in-cylinder soot analysis and this should thus be compensated for.

In the present work, a soot deposit compensation is done based on the followings procedures. Soot deposits on optical windows is non-uniform, theoretically each point on the optical piston should have its own specialized soot formation or window fowling factor as a function of time and this factor is not constant for every point, the local soot volume around the laser projection spot should be known for this compensation. LEM measures soot only through the beam path thus *KL* factor could be used to relate to local window fouling factor. However, the *KL* value in the early phase does not really measure soot only which will be discussed in the Results and Discussion section later. Although when high temperature

combustion occurs the *KL* relates to local soot, soot deposition is accumulated during combustion, if the data in the beginning is wrong the error data will affect the results in all following points. In this compensation process, it is approximated that the soot deposition is proportional to the average soot volume in a larger region, which relates to NL intensity.

$$\frac{I_{Cor}(t)}{I_{Ori}(t)} = 1 - \frac{\int_{0\ CAD}^{t\ CAD} I_{NL}dx}{\int_{0\ CAD}^{180\ CAD} I_{NL}dx}(1-\tau) \quad (6)$$

In equation (4), the averaged laser transmissivity before and after combustion is calculated. The corresponding mean laser intensity from the following motored cycle was compared to the reference and soot deposits compensation has been made on the ratio between them. Since window fouling is an accumulative process, i.e. it doesn't occur instantly, the *KL* curve is slightly higher after combustion than before combustion due to soot window fouling. In equation (6) the integral describes how much percentage of soot has already attached on the window by t CAD. Which inversely refers to the ratio of transmitted laser intensity. Knowing the original transmitted laser intensity and NL data, the corrected laser intensity can be achieved from equation (6). The transmitting laser intensity from each cycle has been compensated by the same method in this work

In Figure 7 the transmitted laser intensity curves from a single cycle are plotted, the laser intensity curve from a motored cycle (720-1080 CAD) is overlaid with the corresponding fired cycle curve. In the late cycle, a similar trend of the motored cycle transmitted laser intensity curve (light blue curve) and the original data (red curve) can be observed.

Comparing the corrected curve (blue) to the original curve (red) in Figure 7, in the later phase (200-350 CAD) the decreasing trend at the end of the red curve is not seen on the blue curve. However, since the motored cycle data was used for transmitted laser intensity fluctuation compensation, the gas flow motion and temperature gradient is not the exactly same as a fired cycle. So after this compensation, the blue curve is still not a constant flat curve in the plateau after combustion.

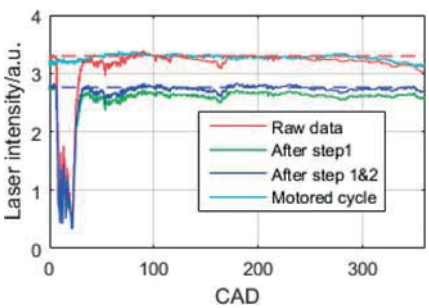

Figure 7. Transmitted laser signal compensation process

Results and Discussions

The *KL* was calculated once again base on the corrected transmitting laser intensity data. The average over 50 runs of corrected *KL* and original *KL* have been plotted as a function of CAD in Figure 8. The averaged NL from the same raw data is plotted. In order to compare all four curves, they have been normalized in Figure 8, the mean value before combustion (-10 to 5 CAD) is set to zero and the peak value near 16 CAD is set to 1.

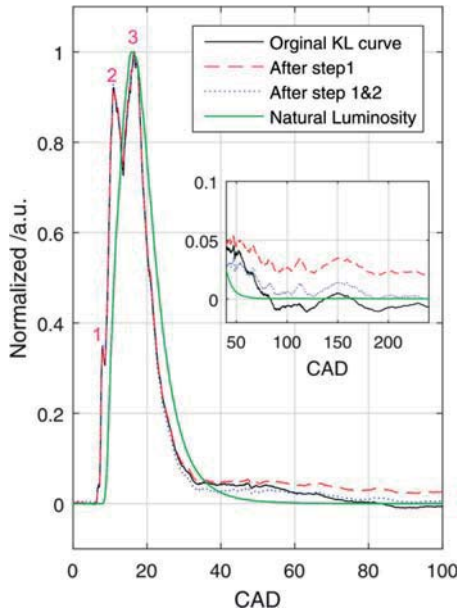

Figure 8. Normalized *KL* data and NL data.

Firstly, in Figure 8, the *KL* curve calculated from raw transmitted laser intensity is plotted as the original *KL* curve in black solid line. It can be seen that the original *KL* curve is even below zero after 82 CAD. This cannot be true, since there is soot deposit on the window and it is found the average transmitted laser intensity after fired cycle is lower than before combustion. All the results after 80 CAD is not clear whether due to transmitted laser intensity fluctuation or real low temperature soot concentration change. The *KL* value calculated from transmitted laser intensity after step 1 is plotted as red dashed line. After step 1, transmitted laser intensity fluctuation has been compensated, no negative value is observed on this *KL* curve.

After step2, the soot deposits on optical windows have been removed. From the enlarged plot in Figure 8, all *KL* curves are not constant at zero but the corrected *KL* curve after step 2 is closer to zero than the other two *KL* curves in general. The impact from soot deposits has been reduced on the corrected *KL* curve after step 2. However there is still a variation on the corrected *KL* curve. It is difficult to tell if the data variation in the enlarged plot is due to real soot non-uniform flowing in the cylinder or noise from signal collection. So in very late cycle (after 100 CAD), the detected low temperature soot level is too low to be analyzed even after all corrections. However, looking at the

corrected *KL* curve after step 2, a slowly decreasing can be seen in the enlarged view from 50 to 80 CAD. This decreasing trend is difficult to be identified from the original curve or to clarify whether this is a real trend of the data or from the data attenuation. This late cycle decreasing trend shows that there is still a slow soot oxidizing process during this late cycle.

Before Peak 1

Comparing the *KL* curves with the NL curve, it can be seen that the *KL* curves start to increase in ahead of the NL curve. Since the photodiode only collects the signal from 665 nm to 700 nm, in this wavelength region, the background luminosity is mostly high temperature soot luminosity[20]. So the LEM detects something before NL curve rising.

A test with the same fuel injection strategy in the engine was performed under non-reacting conditions. The *KL* factor from this test is plotted in Figure 9. It is found that something is detected by the LEM even without high temperature combustion. It is quite consistent and the rising timing (6.7 CAD) is very close to the rising timing (6.4 CAD) of the *KL* curves in Figure 8. This is suspected to the disturbance by liquid fuel spray from two perspectives.

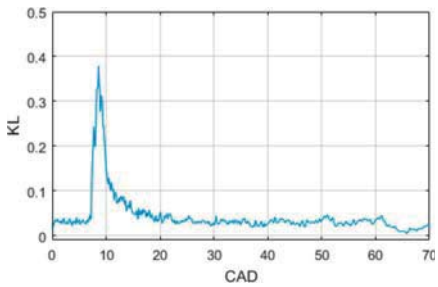

Figure 9. *KL* curve in the no combustion case.

First is the refractive index variation or beam steering. During the liquid fuel propagation process, a temperature and density gradient will be generated by this evaporating fuel spay[13]. When this spray cloud front crosses the laser beam path, the refractive index would be affected. Beam steering affect has been studied in an early work [13] that the beam steering fluctuation by spray cloud front should be minimized when the collection angle is reasonable large. In this work the size of collecting photodiode active area is 10*10 mm. Although the collecting photodiode is not placed on the focal point , it is close to the focal point and the photodiode active area is 12.5 times of the beam cross area. The collection angle is sufficiently large. In summary, the beam steering fluctuation by the spray cloud front should not significantly affect the results in this setup.

Secondly, the extinction coefficient $K \approx K_{abs}$ only applies when the particle sizes are much smaller than the laser wavelength. In optical engines, there are many factors affecting the fuel droplet size, in an early work it is found for diesel fuel sprays, the droplet size is in the range of μm[23]. The fuel spray droplet size is not smaller than the laser wavelength like the soot particles. The scattering light from liquid sprays should not be neglected. Therefore, laser scattering technique is actually commonly used for probing liquid fuel sprays.

In another work about diesel spray impinging study[24] in reacting environment, with 1000 bars injection pressure (1500 bars in this work), 1.0 ms ASOI (corresponds to 6.3 CAD in this work), 0.133 mm injector diameter (0.175 mm in this work), at 40 mm impinging case (the radius of piston bowl is 41 mm in this work) there is still liquid phase fuel droplets near the wall. Although the parameters are not exactly the same as our setup, considering the plot at Figure 9, liquid phase fuel crossing the laser beam is reasonable explanation for the early rising of *KL* curve. In this case, the scattering coefficient K_{scat} should not be neglected. The extinction coefficient *K* cannot be assumed to roughly equal to absorbing coefficient K_{abs}.

Although the *KL* scattering is found in the injection but no high temperature reaction case, the key parameters in this case e.g. temperature, pressure and so on, are not comparable to the fired cases. The motored scattering *KL* could not be used to calibrate the fired cases *KL*. For above reasons, it should be noted that the LEM is not a proper method to calculate *KL* for analyzing the early soot formation in this case. Thus LEM data should not be used as a reference for soot deposits compensation during data processing previously.

The liquid fuel spray disturbance is one of the explanations for this early *KL* rising. There could be some other unknown affects also contributing to this.

13 to 40 CAD

In order to compare peak 3 of *KL* curve to NL curve before NL curve crossing *KL* curves, the correlation coefficients between both corrected and original *KL* data to NL data have been calculated from 13 CAD to 40 CAD respectively. The R value is 0.9904 between corrected *KL* and NL, while it is 0.9817 between the original *KL* and NL. The results show a great agreement between the LEM and NL in this region. This confirms that the NL mainly comes from the soot incandescence[20]. A high speed video was taken at the same engine condition through the optical piston. It can be seen that during this period the homogeneity in the whole combustion chamber is relatively good. Although the LEM measures soot only through the laser beam path and NL contains information in a larger region, from 13 to 40 CAD the NL curve has strong correlation coefficient to *KL* curve.

After Peak 3

Looking at the curves after peak 2, all four curves seem to follow a similar trend. However, the NL curve crosses the *KL* curves close to 40 CAD and drops all the way to zero at around 70 CAD. Obviously, from the calibrated *KL* curve after step1 it is confident to say that there is low temperature soot detected by LEM in the later cycle since it is above zero but not by NL. As mentioned previously, the LEM can detect soot regardless of temperature while NL is from the high temperature soot radiation. In the later phase of combustion, the cylinder temperature drops. According to Planck radiation curve, the signal intensity of soot radiation in the 665-700 nm range is too low to be detected when the soot temperature is lower than ~800 K. However, this low temperature soot is detected by LEM. This detected soot consists of soot deposits on optical windows and free flowing in-cylinder soot residual.

Conclusions

In present work, an attempt of signal correction for LEM data is applied. The LEM data correction significantly reduced *KL* fluctuation from 50 to 120 CAD. The LEM data correction helps to subtract the soot deposit on optical windows from the total low temperature soot at late cycle.

A comparison of NL and LEM results is performed. The conclusions are summarized as follows:

1. *KL* curve was found to rise more than 2 CAD earlier than the corresponding NL curve.
2. Diesel fuel spray in liquid phase has a significant effect on LEM results before start of ignition due to liquid spray scattering in present study.
3. LEM is not a suitable method to calculate *KL* for analyzing the early soot formation if there are liquid phase fuel droplets crossing the probing laser beam.
4. Although LEM and NL data contains soot information from different volume. The correlation coefficient between NL and *KL* curves are larger than 0.98 from 13 to 40 CAD.
5. LEM detects soot at temperature below 800 K where NL from soot is below our detectable limits.

References

1. Aronsson, U., Chartier, C., Andersson, Ö., Egnell, R., et al., "Analysis of the Correlation Between Engine-Out Particulates and Local Φ in the Lift-Off Region of a Heavy Duty Diesel Engine Using Raman Spectroscopy," *SAE Int. J. Fuels Lubr.*, 2009. 2(1): p. 645-660 doi: 10.4271/2009-01-1357.
2. Lequien, G., Andersson, Ö., Tunestal, P., and Lewander, M., "A Correlation Analysis of the Roles of Soot Formation and Oxidation in a Heavy-Duty Diesel Engine," SAE International 2013-01-2535, 2013, doi: 10.4271/2013-01-2535.
3. Lind, T., Li, Z., Micó, C., Olofsson, N. et al., "Simultaneous PLIF Imaging of OH and PLII Imaging of Soot for Studying the Late-Cycle Soot Oxidation in an Optical Heavy-Duty Diesel Engine," *SAE Int. J. Engines* 9(2):849-858, 2016, doi:10.4271/2016-01-0723.
4. Sjöholm, J., Wellander, R., Bladh, H., Richter, M. et al., "Challenges for In-Cylinder High-Speed Two-Dimensional Laser-Induced Incandescence Measurements of Soot," *SAE Int. J. Engines* 4(1):1607-1622, 2011, doi:10.4271/2011-01-1280.
5. O'Connor, J. and Musculus, M., "In-Cylinder Mechanisms of Soot Reduction by Close-Coupled Post-Injections as Revealed by Imaging of Soot Luminosity and Planar Laser-Induced Soot Incandescence in a Heavy-Duty Diesel Engine," *SAE Int. J. Engines* 7(2):673-693, 2014, doi:10.4271/2014-01-1255.
6. Lilik, G., Mueller, C., Dumitrescu, C., and Gehrke, C., "The Visualization of Soot Late in the Diesel Combustion Process by Laser Induced Incandescence with a Vertical Laser Sheet," *SAE Int. J. Engines* 8(2):716-734, 2015, doi:10.4271/2015-01-0801.
7. Bartok W, S.A., *Fossil Fuel Combustion*. 1991, New York: Wiley.
8. Shen, M., Malmborg, V., Gallo, Y., Waldheim, B. et al., "Analysis of Soot Particles in the Cylinder of a Heavy Duty Diesel Engine with High EGR," SAE Technical Paper 2015-24-2448, 2015, doi:10.4271/2015-24-2448.
9. Bertoli, C., Del Giacomo, N., and Beatrice, C., "Diesel Combustion Improvements by the Use of Oxygenated Synthetic Fuels," SAE Technical Paper 972972, 1997, doi:10.4271/972972.
10. Li, Z., Song, C., Song, J., Lv, G., et al., "Evolution of the nanostructure, fractal dimension and size of in-cylinder soot during diesel combustion process," *Combustion and Flame*, 2011. 158(8): p. 1624-1630 doi: http://dx.doi.org/10.1016/j.combustflame.2010.12.006.
11. Song, C., Zhao, Z., Lv, G., Song, J., et al., "Carbonyl compound emissions from a heavy-duty diesel engine fueled with diesel fuel and ethanol-diesel blend," *Chemosphere*, 2010. 79(11): p. 1033-1039 doi: http://dx.doi.org/10.1016/j.chemosphere.2010.03.061.
12. Ohmstede, G. and Hentschel, W., "Time-Resolved Infrared Spectroscopy: Evaluation of Temperature for Various EGR Rates in a DI-Diesel Engine," SAE Technical Paper 952516, 1995, doi:10.4271/952516.
13. Musculus, M.P.B. and Pickett, L.M., "Diagnostic considerations for optical laser-extinction measurements of soot in high-pressure transient combustion environments," *Combustion and Flame*, 2005. 141(4): p. 371-391 doi: http://dx.doi.org/10.1016/j.combustflame.2005.01.013.
14. Siebers, D. and Higgins, B., "Flame Lift-Off on Direct-Injection Diesel Sprays Under Quiescent Conditions," SAE Technical Paper 2001-01-0530, 2001, doi:10.4271/2001-01-0530.
15. Xu, Y. and Lee, C., "Investigation of Soot Formation in Diesel Combustion Using Forward Illumination Light Extinction (FILE) Technique," SAE Technical Paper 2004-01-1411, 2004, doi:10.4271/2004-01-1411.
16. Cenker, E., Bruneaux, G., Pickett, L., and Schulz, C., "Study of Soot Formation and Oxidation in the Engine Combustion Network (ECN), Spray A: Effects of Ambient Temperature and Oxygen Concentration," *SAE Int. J. Engines* 6(1):352-365, 2013, doi:10.4271/2013-01-0901.
17. Manin, J., Pickett, L., and Skeen, S., "Two-Color Diffused Back-Illumination Imaging as a Diagnostic for Time-Resolved Soot Measurements in Reacting Sprays," *SAE Int. J. Engines* 6(4):1908-1921, 2013, doi:10.4271/2013-01-2548.
18. Gallo, Y., Simonsson, J., Lind, T., Bengtsson, P. et al., "A Study of In-Cylinder Soot Oxidation by Laser Extinction Measurements During an EGR-Sweep in an Optical Diesel Engine," SAE Technical Paper 2015-01-0800, 2015, doi:10.4271/2015-01-0800.
19. Musculus, M., Dec, J., and Tree, D., "Effects of Fuel Parameters and Diffusion Flame Lift-Off on Soot Formation in a Heavy-Duty DI Diesel Engine," SAE Technical Paper 2002-01-0889, 2002, doi:10.4271/2002-01-0889.
20. Dec, J. and Espey, C., "Chemiluminescence Imaging of Autoignition in a DI Diesel Engine," SAE Technical Paper 982685, 1998, doi:10.4271/982685.

21. Mueller, C. and Martin, G., "Effects of Oxygenated Compounds on Combustion and Soot Evolution in a DI Diesel Engine:Broadband Natural Luminosity Imaging," SAE Technical Paper 2002-01-1631, 2002, doi:10.4271/2002-01-1631.
22. Andersson, Ö., *Experiment!: Planning, Implementing and interpreting*. 2012: John Wiley & Sons, Ltd.
23. Blaisot, J.B. and Yon, J., "Droplet size and morphology characterization for dense sprays by image processing: application to the Diesel spray," *Experiments in Fluids*, 2005. 39(6): p. 977-994 doi: 10.1007/s00348-005-0026-4.
24. Li, K., Dong, P., Matsuo, T., Shi, B. et al., "Characteristics of Diesel Spray Flame under Flat Wall Impinging Condition --LAS, OH* Chemiluminescence and Two Color Pyrometry Results," SAE Technical Paper 2014-01-2636, 2014, doi:10.4271/2014-01-2636.

Contact Information

zheming.li@forbrf.lth.se

Acknowledgments

The financial support from Competence Center Combustion Processes (KCFP) and the China Scholarship Council (CSC) are gratefully acknowledged.

Definitions/Abbreviations

PLII - Planer Laser induced incandescence

LEM - Laser-extinction measurements

NL - Natural luminosity

CAD - Crank angle degree

TDC - Top dead center

ATDC - After top dead center

The Engineering Meetings Board has approved this paper for publication. It has successfully completed SAE's peer review process under the supervision of the session organizer. The process requires a minimum of three (3) reviews by industry experts.

ISSN 0148-7191

http://papers.sae.org/2016-01-2159

Paper V

SAE INTERNATIONAL

Analysis of Soot Particles in the Cylinder of a Heavy Duty Diesel Engine with High EGR

2015-24-2448
Published 09/06/2015

Mengqin Shen
Combustion Engines, Lund University

Vilhelm Malmborg
Ergonomics & Aerosol Tech., Lund Univ.

Yann Gallo
Combustion Engines, Lund University

Bjorn B. O. Waldheim
Scania CV AB

Patrik Nilsson, Axel Eriksson, and Joakim Pagels
Ergonomics & Aerosol Tech., Lund Univ.

Oivind Andersson and Bengt Johansson
Combustion Engines, Lund University

CITATION: Shen, M., Malmborg, V., Gallo, Y., Waldheim, B. et al., "Analysis of Soot Particles in the Cylinder of a Heavy Duty Diesel Engine with High EGR," SAE Technical Paper 2015-24-2448, 2015, doi:10.4271/2015-24-2448.

Abstract

When applying high amount of EGR (exhaust gas recirculation) in Partially Premixed Combustion (PPC) using diesel fuel, an increase in soot emission is observed as a penalty. To better understand how EGR affects soot particles in the cylinder, a fast gas sampling technique was used to draw gas samples directly out of the combustion chamber in a Scania D13 heavy duty diesel engine. The samples were characterized on-line using a scanning mobility particle sizer for soot size distributions and an aethalometer for black carbon (soot) mass concentrations. Three EGR rates, 0%, 56% and 64% were applied in the study. It was found that EGR reduces both the soot formation rate and the soot oxidation rate, due to lower flame temperature and a lower availability of oxidizing agents. With higher EGR rates, the peak soot mass concentration decreased. However, the oxidation rate was reduced even more. This led to increased soot mass concentrations with increasing EGR in late expansion and in the exhaust. During the combustion cycle, both particle number concentrations and particle mean diameters initially increased, followed by a decrease after the peak in soot mass. Generally, increasing EGR reduced the in-cylinder particle mean diameter but increased particle number concentrations. Therefore, increased particle number concentrations were the main reason for increased soot mass emissions with increasing EGR.

Introduction

Direct injection compression ignition (CI) diesel engines show higher efficiency over spark ignition (SI) engines. However, stricter emission standards also demands continued reduction in engine-out emissions especially for nitrogen oxide (NO_x) and particulate matter (PM). Soot is a major component of PM. To reduce engine-out emissions and reach future emission regulations, advanced technologies including those focusing on improving in-cylinder combustion process have been investigated.

Partially Premixed Combustion (PPC) provides the potential of significant reduction of NOx and soot for diesel engines [1, 2, 3]. One possible way to achieve PPC is utilizing early injection strategies and exhaust gas recirculation (EGR). It has been demonstrated that EGR is an effective technology allowing significant NOx emission reductions from most types of diesel engines [4]. Due to the inert diluents, EGR reduces the total amount of oxygen available in the charge, and thus the flame temperature. This generally results in increased engine-out soot emissions, which was also found in previous PPC work [5, 6].

It has been shown [7] that the soot mass concentration measured in the exhaust is the result of competing processes to form and oxidize soot, i.e., the net difference between these processes. Studies with optical diagnostics in a heavy duty engine indicated that, under conditions

where substantial amounts of soot are formed with higher rates of EGR, oxidation has a dominating influence on the soot emissions [8,9]. A lot of research has focused on sampling of exhaust emissions regarding soot mass and particle properties. The results demonstrated that increasing EGR reduces particle size but increases particle number concentration in exhaust gas [10,11]. Boehman et al. [12] also investigated the impact of EGR on the nanostructure and oxidative reactivity of diesel soot in the exhaust. The results showed that EGR exerts a strong influence on the physical properties of exhaust soot which can lead to enhanced oxidation rate and different burning modes. Their further study has demonstrated that the thermal effect of EGR is the most important factor governing the soot reactivity [13]. In comparison, however, less work describing the effect of EGR on in-cylinder soot has been carried out. It is not well known how the soot properties vary during combustion in the cylinder.

In this study we investigated the soot formation and oxidation processes in the cylinder during combustion when adding EGR. It was accomplished using a fast sampling valve which was used to draw gas samples from the cylinder at well-defined crank angles. The sampled gas was analyzed regarding the black carbon mass and particle number concentration, as well as soot particle size distributions. Black Carbon (BC) mass was measured with an aethalometer, and the particle size distribution and particle number concentration were measured by a Scanning Mobility Particle Sizer (SMPS). The aim was to trace the soot emission penalty with high amount of EGR in exhaust back to the soot particle's history during combustion and expansion in the cylinder. To highlight the effect of EGR on particle emissions, conventional diesel combustion with 0% EGR was investigated in comparison with 56% and 64% EGR cases.

Experimental Setup

Test Engine Setup

The experimental engine is based on a Scania D13 heavy duty engine modified to operate with only one of six cylinders. Figure 1 shows the test bench and Table 1 gives the engine specifications. The engine was equipped with a production XPI common rail injection system. The injector used was a production one with the nozzle specification shown in Table 2.

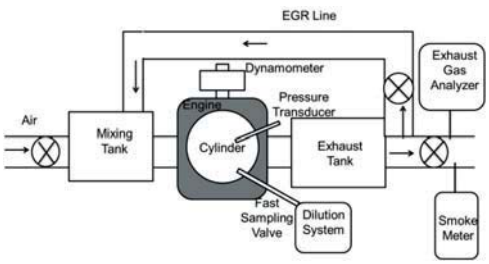

Figure 1. Schematic diagram of experimental setup

Table 1. Geometrical properties of the Scania D13.

Displacement Volume [cm3]	2124
Stroke [mm]	160
Bore [mm]	130
Connecting Rod [mm]	255
Compression Ratio [-]	15:1
Swirl Ratio [-]	2.1
IVC [CAD ATDC]	-141
EVO [CAD ATDC]	137

Table 2. XPI injection specifications.

Spray Angle [deg]	148
Orifices [-]	8
Orifices Diameter [mm]	0.179

The EGR ratio used in this paper is defined as the ratio of carbon dioxide in the intake gas and exhaust gas, as expressed by Equation 1.

$$EGR = \frac{CO_{2_{Inlet}}}{CO_{2_{Exhaust}}} \quad (1)$$

Soot emissions in exhaust gas were measured with an AVL415S smoke meter, with a measurement range from 0 to 10.0 FSN. HC, CO, exhaust CO_2, NO_X and intake CO_2 emissions were measured with a Horiba measurement system (MEXA-9100EGR). Each analyzer was calibrated with an appropriate calibration gas before every set of measurements.

Fast Gas Sampling Technique and Dilution System

Fast Sampling Valve

The sampling valve is actuated by a solenoid unit as can be seen in Figure 2. This electronic unit allows the control of the hammer which in turn can hit the needle, making the start time of sampling and sampling flow rate controllable. The electronic actuation device is controlled by a voltage signal through a computer program and triggered by the crank angle signal. With these features the gas flow through the valve can be controlled in a wide range, with respect to sampling timing, sampling rate, etc. In this study, the gas flow was kept constant at 1 lpm (liter per minute) (at ambient atmospheric pressure and temperature) for each sampling point. This volume corresponds to approximately 0.05% of the total gas in the cylinder. With this desired flow rate, the minimum step-by-step resolution for the sampling timing can be 1 CAD at 1200 rpm engine speed.

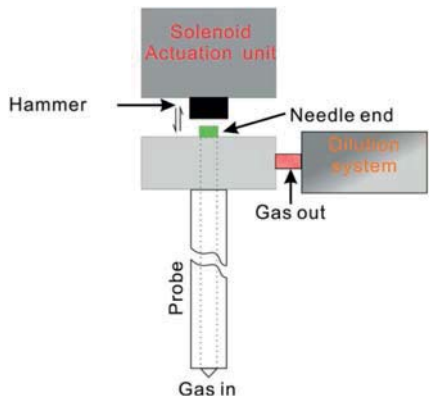

Figure 2. Fast sampling valve operating unit

Figure 3 displays the valve voltage signal to control the solenoid actuation device, cylinder pressure signal and heat release data in a motoring case. In this test, sampling time was decided to be the minimum valve voltage timing. As can be seen, the sampling gas flow doesn't affect pressure trace much as it takes about 0.05% of the total gas in the cylinder at a sampling flow of 1 liter/min. This indicates that the sampling has negligible effect on the combustion process in the cylinder. Despite of sampling locally, compared to the study in optical engine [14] or studies where the total gas from the cylinder in the engine was sampled [15], similar trends in term of soot mass variations are found in this study.

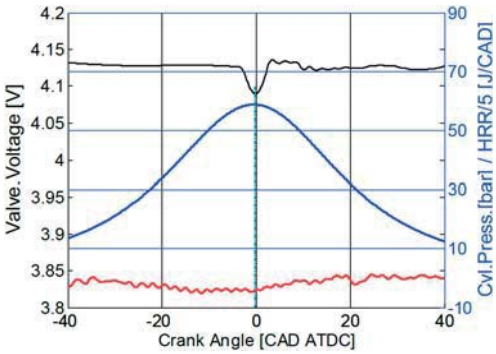

Figure 3. In-cylinder pressure, heat release rate and valve control voltage for motoring case

The sampling valve tip was mounted directly into the cylinder head, replacing one of the exhaust ports, as shown in Figure 4 below. The gas samples were taken between two injection jets in the cylinder. With an anticlockwise swirl, the below spray close to the probe will come to the sampling system first.

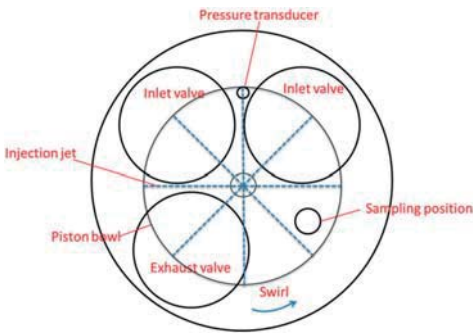

Figure 4. Gas sampling location (top view)

Dilution System

The sampled in-cylinder gas was diluted in three steps marked D1, D2 and D3 in Figure 5. In the first step of the dilution (D1) the extracted gas was diluted with N_2 to a ratio of approximately 1:6. The dilution probe was in direct connection with the fast sampling valve (FSV). The first dilution ensures a significant decrease of particle coagulation and condensation rates as early as possible in the sampling line. Furthermore, diluting the sample with N_2 in D1 reduces the risk of oxidizing the particles post-extraction. The second (D2) and third (D3) dilution steps comprise two ejector diluters where the aerosol flow was diluted nominally 1:100 with air, stripped of particles and vapors using HEPA and activated carbon filters.

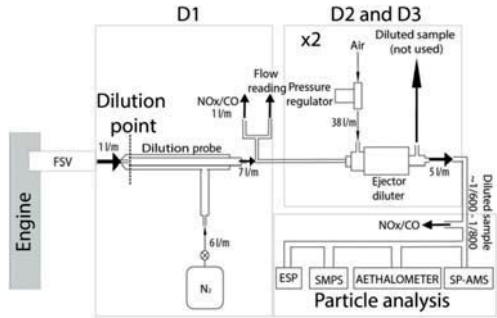

Figure 5. Dilution system (only SMPS and aethalometer results were analyzed in this paper)

Dilution Error Estimate

The dilution ratio in D1 was measured using two mass flow meters, one measuring the N_2 flow and one to assure that the extracted in-cylinder gas volume corresponded to 1 lpm at atmospheric pressure. The N_2 flow was logged during the experiment. The deviation in N_2 flow during one measurement point is less than 1% of the flow and the induced error is considered negligible.

To measure the dilution ratio over the two ejector diluters (D2 and D3), the NO_X concentration was monitored before and after the two dilution points. Before every set of measurements, one reference point at high NOx concentration would be run to make sure the dilution ratio could be calculated. The average dilution over the two ejector diluters for the timing of the different EGR ratios is shown in Figure 6.The standard deviation represented by the error bars is less than 10% of the total dilution ratio. The average dilution factor at each level of EGR was used to account for dilution.

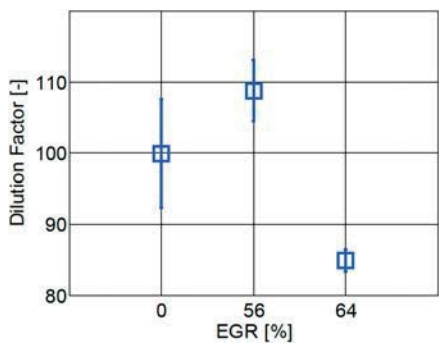

Figure 6. Dilution over the ejectors (NOX measurement)

Measurement Techniques

In-cylinder soot (Black Carbon) mass concentrations was measured with an aethalometer. Particle number weighted size distributions were determined with a Scanning Particle Mobility Sizer (SMPS).

Optical BC Quantification

To quantify the soot or BC mass, a filter based seven-wavelength optical technique was used (Aethalometer, model AE33, Magee Scientific) [16]. The instrument was operated at an aerosol flow rate of 2 lpm and with 1 minute averaged time resolution. The seven laser diodes operate at wavelengths between 370 - 950 nm. To quantify the total BC mass concentration, the average mass absorption of the two longest wavelengths at 880 nm and 950 nm were used (equation 2). This ensures that BC mass is determined without significant influence from constituents which are strong absorbers only in the near-UV to UV spectrum, such as PAHs.

$$BC = \frac{BC_{\lambda=950nm} + BC_{\lambda=880nm}}{2} \quad (2)$$

Particle Mobility Size Distributions

An SMPS consisting of an electrostatic classifier (model 3071; TSI inc.), a DMA model 3081 and a condensation particle counter (CPC, model 3010; TSI inc.) was used to classify particles sizes based on equivalent mobility diameters and number concentration. It should be pointed out that this refers to the size of the full soot aggregates rather than the size of the primary particle in the aggregates that are commonly measured with electron microscopy techniques. The sheath air flow rate of the DMA was controlled at 6.0 lpm using a needle valve and a pump in a closed loop. The CPC model 3010 includes a critical orifice which connected to vacuum gives an aerosol flow rate fixed at 1.0 lpm through both the DMA and CPC. The SMPS voltage scan-up time was 120 seconds and the retrace of the voltage was given 15 seconds. This allowed us to average over at least three full size scans at each measurement point. The configuration enables particle mobility diameter size classification in the range of 10 - 415 nm. The geometric mean diameter (GMD) was calculated from the particle mobility size distributions assuming lognormal distributed data with a unimodal shape following equation 3 [17], where N_t is the total particle number, i is the size bin, M the total number of size bins in the SMPS, N_i is the particle number in the size bin i and D_{pi} is the midpoint diameter of the size bin.

$$\mathrm{GMD} = \exp\left[\frac{1}{N_t}\sum_{i=1}^{M}\left(N_i \ln\left(D_{pi}\right)\right)\right] \quad (3)$$

Experiment Strategies and Operation Conditions

The fuel used in this experiment was Swedish diesel MK1 with the specifications shown in Table 3. Table 4 summarized the engine operating conditions in the current test. During the measurement, engine speed was kept at 1200 rpm and the common rail pressure was set to 2000 bar. Intake temperature and intake pressure were 337 K and 1.65 bar respectively while EGR was changed from 0 up to 64%. Start of injection (SOI) timing varied to keep CA50 constant.

Table 3. Main properties and specifications of the fuel.

CN	H/C	O/C	LHV [MJ/kg]	A/Fs
54	1.83	0	43.15	14.49

Table 4. Engine running conditions.

	IMEPg [bar]	CA50 [CAD ATDC]	CoV [%]	SOI [CAD ATDC]	EGR [%]	O_2 in [%]	λ [-]
1	5.5	7.9	2.1	-1.5	0	21	3.82
2	5.5	7.5	2.3	-3.5	56	15	1.86
3	5.5	7.3	2.2	-4.5	64	13	1.56

To get a result independent on the influence of cyclic variations in the combustion process, each sampling point was taken over 10 minutes or approximately 6000 fired cycles. Variations in soot particle concentration and composition are therefore smoothed and are less affected by cycle-to-cycle variations than from e.g. total cylinder-gas extraction measurements. Before every set of measurements, one reference point (high NOx concentration point: 0% EGR, valve opening at 120 CAD ATDC) would be run to make sure of no leakage in the dilution system. Soot sampling in motoring cycles was done before the measurement and after the measurement was finished as a reference background level.

Results and Discussions

Engine Performance and Emissions

The Heat Release Rate (HRR) for different EGR cases were calculated and shown in Figure 7. In this plot, the HRR data are averaged over 500 cycles. The ignition delay (duration between start of injection and start of combustion) is prolonged with the increase of EGR. In the non-EGR case, combustion started before injection ended. The mixing-controlled combustion occurred after premixed combustion and lasted to the early stage of the expansion stroke. The premixed burn spike is distinctly separated from the mixing controlled-combustion phase. With increasing EGR, premixed burn increases and peak HRR during mixing-controlled combustion decreases. As a result the combustion duration is reduced. With 64% EGR, there is not a very clear distinction between premixed and mixing-controlled combustion and only one peak in HRR shows.

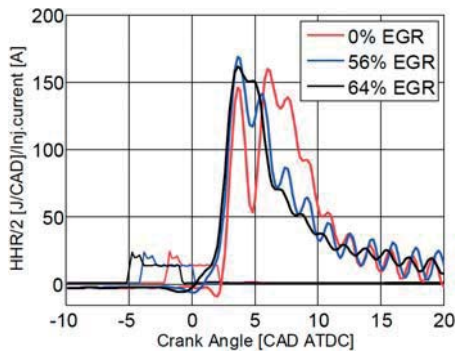

Figure 7. Heat release rate for the three EGR rates.

The gross specific CO, HC, NOx and soot emissions for the three EGR levels are plotted in Figure 8. In the conventional diesel combustion case, very low CO, HC and soot emissions but extremely high NO_X can be found. The EGR containing CO_2 replaces a portion of the incoming ambient air and dilutes the air. Substances in EGR with higher specific heat capacity can bear the heat from combustion,

which leads to lowered combustion temperature. Thereby, an increasing EGR rate at a constant intake pressure, leads to decreases in NO_X emissions, while CO and soot emissions increase. The strong trend in NO_X with respect to EGR indicates a strong variation in adiabatic flame temperature as NO_X formation is dependent on the flame temperature in near-stoichiometric zones. HC emissions are maintained low with variations in EGR (0.11, 0.05,0.05g/kWh for 0%, 56% and 64% EGR respectively). This could be due to temperatures being sufficient to oxidize the partially burnt fuel into CO, even if the last step oxidization to CO_2 is not completed. The HC formation then mainly comes from injector dribble which is generally too rich to burn.

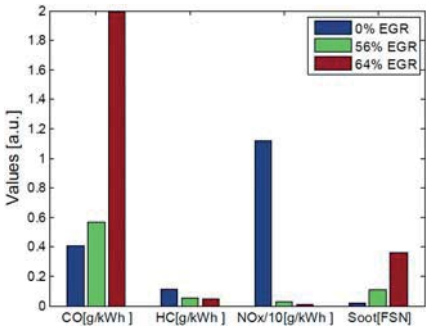

Figure 8. Gross specific CO, HC, NOx and soot emissions for the three EGR rates

In-Cylinder Soot Formation and Oxidation

The history of in-cylinder soot, shown as the Black Carbon (BC) mass concentration, and NO_X during combustion and expansion in the no EGR case are given in Figure 9. Almost no soot can be measured before injection. The relatively high level of NO_X before injection comes from the residual gas as only one exhaust valve was used and gas exchange could become poor. During combustion, soot is formed very rapidly resulting in a sharp increase of the measured black carbon concentration until reaching a maximum at 8 CAD ATDC, slightly after CA50. In this phase, soot formation dominates [18]. After the initial peak of soot mass, there is fast soot oxidation. Then the soot oxidation rate slows down as the temperature decreases during the expansion stroke. During the soot oxidation process, nearly all of the formed soot is oxidized with the in-cylinder gas. NO_X remains essentially constant during the slow soot oxidation phase, providing evidence that the sampled gas is representative of the cylinder content during this phase.

Figure 10 shows the history of the in-cylinder soot concentration together with HRR during combustion using the three EGR rates. The in-cylinder soot curves show a characteristic shape for the three cases. As can be seen, only a small amount of soot was detected through the valve in premixed burn. Then in the diffusion combustion part, the soot concentration increase rapidly to the peak value in a short period of time near 9 CAD ATDC. Then in the late combustion phase, soot is mainly oxidized. An increase in EGR leads to a reduction in peak soot concentration.

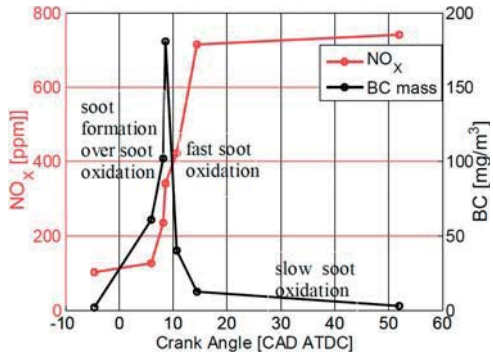

Figure 9. In-cylinder soot (Black Carbon) and NOx concentration during combustion and expansion (0% EGR).

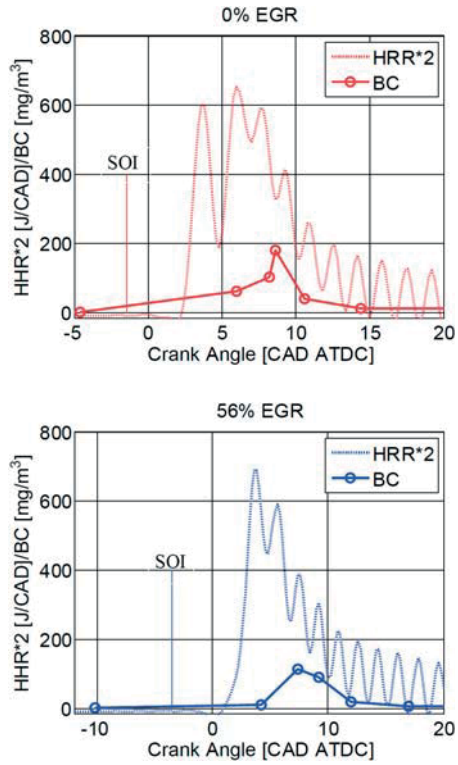

Figure 10. In-cylinder soot mass and HRR for three EGR rates.

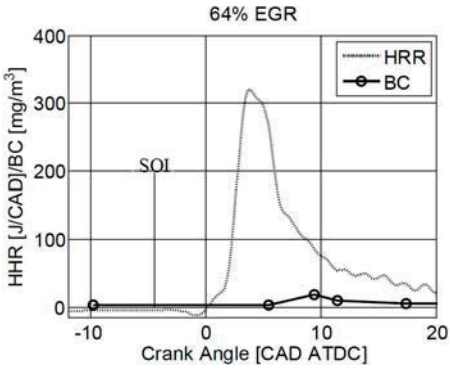

Figure 10. (cont.) In-cylinder soot mass and HRR for three EGR rates.

Figure 11 depicts soot mass concentration including the measured variability (+— 1std) during combustion and expansion for all three EGR levels. It is again clear that EGR reduces peak soot mass during combustion. Increasing EGR to 56%, the peak soot concentration decreases from 180 mg/m^3 to about 110 mg/m^3. Adding more EGR, the peak soot is reduced furthermore, down to about 20 mg/m^3. Nearly constant levels are reached at about 50 CAD ATDC and are maintained until the late expansion stage around 120 CAD ATDC.

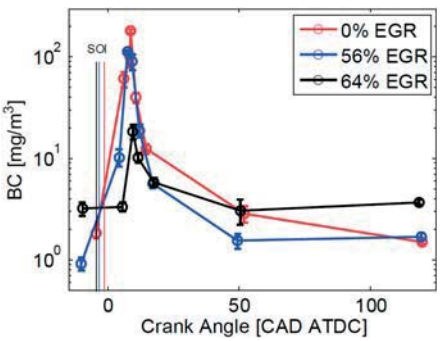

Figure 11. In-cylinder soot mass concentration under three EGR rates (plotted in normal scale and logarithmic scale respectively).

The in-cylinder total soot mass concentration is the net result of soot formation and soot oxidation. When applying EGR, the gas temperature is reduced due to the dilution effect of the EGR and results in a reduction of the soot formation rate. This leads to a decrease in total soot concentration. For soot oxidation, the OH radical is considered as a major oxidant [19]. Soot oxidation can be promoted if soot and OH can be mixed by diffusion at a temperature high enough for oxidation to take place. Simulation work in a light duty diesel engine [20] observed that a thin, locally-concentrated OH layer surrounded the soot mass cloud for lower EGR cases on the rising part of soot emission bump. This observation suggests that, the fast oxidation rate with 0% EGR case is due to enough OH and high gas temperature while the relatively lower oxidation in 56% and 64% EGR cases is because of lower OH formation and/or reduced mixing as well as lower gas temperature. Less efficient oxidation explains the increased late cycle soot mass with increasing EGR. The increase in CO in Figure 8 also indicates that soot is oxidation limited because of lower flame temperature at high EGR.

For the total particle number concentration, shown in Figure 12, similar trends were found as in the soot mass concentration curves. The increase before the peak indicates increasing particle formation/ inception and the decrease after the peak indicates that particle number concentration is reduced by oxidation and coagulation. The higher, the applied EGR rate, the higher particle number density remains after combustion (around 18 CAD ATDC to 120 CAD ATDC) as well as before injection. The 56% EGR case shows the highest peak value and most pronounced initial reduction, while the 64% EGR case has the lowest peak value.

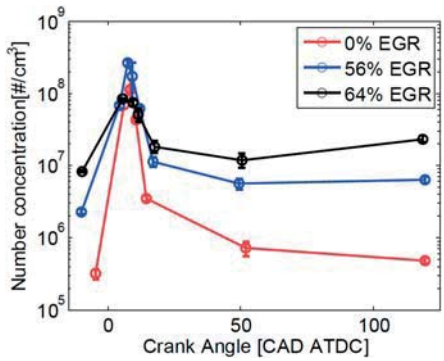

Figure 12. Particle number concentration.

As can be seen, EGR increases both soot mass concentration and soot number density in late expansion. The peak values in terms of soot mass are found for the non-EGR case while the peak soot number density appears in the 56% EGR case. To explain the different trends, the particle size distribution at different crank angle timing during combustion and expansion is presented in Figure 13 and a summary of the geometric mean diameters (GMD) of the soot aggregates is given in Figure 14. Individual particle size distributions at each crank angle in the three EGR cases are plotted in Figure 15 in Appendix.

For the non-EGR case (Figure 13a), in the soot formation phase (from SOC to 8.6 CAD ATDC), particle size distribution shifts toward larger diameter as fuel burns more because of the agglomeration and surface growth processes that occur in the cylinder [21,22]. The maximum number of particles increases which indicates a high inception rate. During the soot oxidation phase (around 10.6-52 CAD ATDC), the number concentration of particles larger than 80 nm is reduced first and the GMD shifts towards smaller diameters.

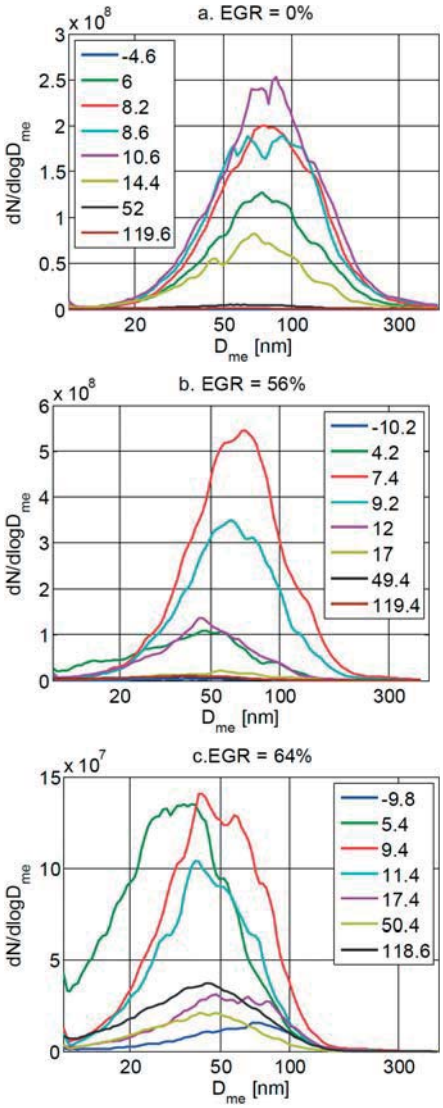

Figure 13. Particle size distribution at different crank angles.

When adding 56 % EGR, the maximum number distribution peak (GMD) shift from around 40 nm to around 65 nm during soot formation (from SOC to 7.4 CAD ATDC), then during soot oxidation until the late expansion phase, the size distribution is displaced towards smaller particles again. Similarly, the total particle number concentration first increases and then drops. By contrast, compared to non-EGR, although the peak soot mass concentration is lower than for non-EGR, the corresponding maximum number of particles is observed to be higher. The smaller size of the soot agglomerates when adding EGR is the main reason for this. Increasing EGR to 64%, a similar trend can be found in terms of the shift in size distribution. The GMD shifted towards even smaller particles, between 30 nm and 40 nm (Figure 13.c), which leads to even lower soot mass concentrations. Compared to 0% EGR, a general trend observed when EGR is added is a narrowing of the particle size distributions and smaller geometric standard deviation (GSD). This trend is observed at almost all the measured crank angle positions (measured GSD intervals: 0% EGR [1.71-2.24], 56% EGR [1.63-1.85], 64% EGR [1.63-1.78]).

Increasing EGR thus leads to a significant decrease in the diameter of the agglomerates (GMD), as shown in Figure 14. From around 9 CAD ATDC to 18 CAD ATDC, particles size reduces significantly due to soot formation zones mixing with the oxidizer surrounded [20]. Very little change in particle diameter at 64% EGR case suggests slow soot oxidation rate due to a lack of oxidizers and lower flame temperatures. In early expansion (from about 18 CAD ATDC till 50 CAD), the soot aggregate size keeps is almost constant in the non-EGR case while it is reduced in both cases with EGR.

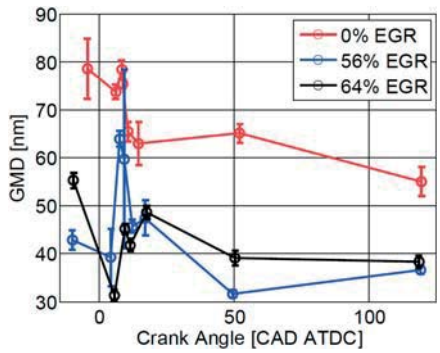

Figure 14. Geometric mean particle mobility diameter.

During the expansion stroke, the soot aggregate sizes stay almost constant for the non-EGR case and thus the decreased soot mass concentration with increasing CAD Figure 11 is due to a reduction in the number of particles in Figure 12). With higher EGR rates, the reduction in soot mass is attributed to the decrease in both particle size and number density. In late expansion (approximately 120 CAD ATDC), more particles but with smaller mean diameter are found with higher EGR rates, which agrees with previous findings in exhaust gas [10, 11]. Thereby, higher particle number density is the main contributor to the increase in engine-out soot mass emissions with increasing EGR.

Summary and Conclusions

A fast gas sampling technique was used to draw gas samples directly out of the combustion chamber in a Scania D13 heavy-duty diesel engine, as a function of crank angle from before fuel injection until the late expansion phase. Three EGR rates were utilized to investigate their effect on soot particle characteristics in the cylinder. The samples were analyzed with respect to soot mass concentration, soot particle number density and particle size distribution.

The major conclusions include:

- An enhanced pre-mixing of fuel and air at higher EGR rates results in more premixed burn and reduced gas temperature during combustion. Soot can be detected during premixed combustion. The soot mass concentration increases rapidly later in the beginning of the diffusion combustion.
- With absence of EGR, the highest peak soot mass concentration is formed. However, nearly all of the soot is oxidized with the in-cylinder gas during the ongoing combustion and expansion. EGR tends to reduce both soot formation rate and soot oxidation rate due to lower flame temperature and less oxidizer. Despite of lower peak soot mass, a much stronger decrease in soot oxidation leads to increased soot emissions when adding EGR.
- The number concentration of soot aggregates show similar trends as the soot mass concentration as a function of the combustion cycle. However the highest number concentration peak is found at low EGR in contrast to the soot mass trends (no EGR).
- The total soot mass and particle number and size measurements show similar trends during combustion. With higher EGR, the particle mean diameter decreases and particle number increases during the expansion stroke. Therefore, when adding EGR, increased soot emissions is attributed to higher particle number despite of smaller particle size.
- The consistency between observations derived with the fast gas sampling valve together with aerosol particle instruments and other existing techniques to quantify in-cylinder soot found in literature gives confidence with respect to the reliability of the measurements. Although the technique requires further assessment, the fast gas sampling valve may provide a valuable tool in future in-cylinder soot studies and e.g. serve to enhance the interpretation of laser extinction measurements which have much higher time resolution but do not capture all features of the aerosol present in the cylinder.

References

1. Noehre, C., Andersson, M., Johansson, B., and Hultqvist, A., “Characterization of Partially Premixed Combustion,” SAE Technical Paper 2006-01-3412, 2006, doi:10.4271/2006-01-3412.
2. Manente, V., Zander, C., Johansson, B., and Tunestal, P., et al., “An Advanced Internal Combustion Engine Concept for Low Emissions and High Efficiency from Idle to Max Load Using Gasoline Partially Premixed Combustion,” SAE Technical Paper 2010-01-2198, 2010, doi:10.4271/2010-01-2198.
3. Manente, V., Tunestal, P., Johansson, B., and Cannella, W., “Effects of Ethanol and Different Type of Gasoline Fuels on Partially Premixed Combustion from Low to High Load,” SAE Technical Paper 2010-01-0871, 2010, doi:10.4271/2010-01-0871.
4. Diesel net, http://www.dieselnet.com/tech/engine_egr.php.
5. Lewander, M., Johansson, B., and Tunestal, P., “Investigation and Comparison of Multi Cylinder Partially Premixed Combustion Characteristics for Diesel and Gasoline Fuels,” SAE Technical Paper 2011-01-1811, 2011, doi:10.4271/2011-01-1811.
6. Shen, M., Tuner, M., Johansson, B., and Cannella, W., “Effects of EGR and Intake Pressure on PPC of Conventional Diesel, Gasoline and Ethanol in a Heavy Duty Diesel Engine,” SAE Technical Paper 2013-01-2702, 2013, doi:10.4271/2013-01-2702.
7. Balthasar, Detailed soot modelling in laminar and turbulent reacting flows. Doctorial thesis. Lund University 2000.
8. Aronsson, U., Chartier, C., Andersson, Ö., Egnell, R. et al., “Analysis of the Correlation Between Engine-Out Particulates and Local Φ in the Lift-Off Region of a Heavy Duty Diesel Engine Using Raman Spectroscopy”, *SAE Int. J. Fuels Lubr.* 2(1):645-660, 2009, doi:10.4271/2009-01-1357.
9. Lequien, G., Andersson, Ö., Tunestal, P., and Lewander, M., “A Correlation Analysis of the Roles of Soot Formation and Oxidation in a Heavy-Duty Diesel Engine,” SAE Technical Paper 2013-01-2535, 2013, doi:10.4271/2013-01-2535.
10. Jung, Y., Qi, D., and Bae, C., “Assessment of Soot Particles in an Exhaust Gas for Low Temperature Diesel Combustion with High EGR in a Heavy Duty Compression Ignition Engine,” SAE Technical Paper 2013-01-2572, 2013, doi:10.4271/2013-01-2572.
11. Iwata, H., Konstandopoulos, A., Nakamura, K., Ogyu, K. et al., “Experimental Study of Physical and Chemical Properties of Soot under Several EGR Conditions,” SAE Technical Paper 2014-01-1593, 2014, doi:10.4271/2014-01-1593.
12. Khalid, A., Ansre L,B., “Impact of exhaust gas recirculation (EGR) on the oxidative reactivity of diesel engine soot”, *Combustion and Flame* 158 (2008) 675-695,2008.
13. Khalid, A., Angela D.L., and Ansre L,B., “The deconvolution of the thermal, dilution, and chemical effects of exhaust gas recirculation (EGR) on the reactivity of engine and flame soot”, *Combustion and Flame* 158 (2011) 1696-1704,2011.
14. Idicheria, C. and Pickett, L., “Soot Formation in Diesel Combustion under High-EGR Conditions,” SAE Technical Paper 2005-01-3834, 2005, doi:10.4271/2005-01-3834.
15. Li, Z., Song, C., Song, J. et al., “Evolution of the nanostructure, fractal dimension and size of in-cylinder soot during diesel combustion process”, *Combustion and Flame* 158 (2011) 1624-1630,2011.
16. Drinovec, L., Mocnik, G., Zotter, P., Prévôt, A. S. H., Ruckstuhl, C., Coz, E., Rupakheti, M., Scaire, J., Müller, T., Wiedensohler, A. and Hansen, A. D. A. (2014). Atmospheric Measurement Techniques Discussions. 7, 10179-10220.
17. Seinfeld, J. H., & Pandis, S. N., “Atmospheric chemistry and physics: from air pollution to climate change”, Wiley, cop. 2006.
18. Eismark, J., Balthasar, M., Karlsson, A., Benham, T. et al., “Role of Late Soot Oxidation for Low Emission Combustion in a Diffusion-controlled, High-EGR, Heavy Duty Diesel Engine,” SAE Technical Paper 2009-01-2813, 2009, doi:10.4271/2009-01-2813.
19. Aronsson, U., Chartier, C., Andersson, Ö., Johansson, B. et al., “Analysis of EGR Effects on the Soot Distribution in a Heavy Duty Diesel Engine using Time-Resolved Laser Induced Incandescence”, *SAE Int. J. Engines* 3(2):137-155, 2010, doi:10.4271/2010-01-2104.

20. Tao, F., Liu, Y., RempelEwert, B., Foster, D. et al., “Modeling the Effects of EGR and Injection Pressure on Soot Formation in a High-Speed Direct-Injection (HSDI) Diesel Engine Using a Multi-Step Phenomenological Soot Model,” SAE Technical Paper 2005-01-0121, 2005, doi:10.4271/2005-01-0121.
21. Lighty et al. “Soot oxidation. Combustion generated fine carbonaceous particule”, Proceedings of an International Workshop held in Villa Orlandi, Anacapri, may 13-16,2007
22. Heywood, J. B. (1988). *Internal Combustion Engine Fundamentals*. Mc Graw- Hill, NewYork. http://www.Dieselnet.com/standards/eu/ld.html.
23. Tree, D. R., and Svesson, K. I., “Soot Processes in Compression Ignition Engines”, *Prog. Energy Combust. Sci.* 33:272-309,2007

Contact Information

Mengqin Shen
Lund University
Department of Energy Sciences
Mengqin.Shen@energy.lth.se

Acknowledgments

The author would like to acknowledge the Competence Center for the Combustion Processes, KCFP, and the Swedish Energy Agency (Project number 10738150289) for the financial support. JP, VM and PN were supported by the competence center METALUND funded by FORTE.

Abbreviations

NO_x - nitrogen oxides i.e. NO, NO2
PM - particulate matter
EGR - exhaust gas recirculation
BC - black carbon
IVC - intake valve opening
EVO - exhaust valve closing
SMPS - scanning mobility particle sizer
FSN - filter smoke number
UHC - unburned hydrocarbons
CO - carbon monoxide
CO2 - carbon dioxide
CAD - crank angle degree
CA50 - crank angle at 50% completion of heat release
SOI - start of injection
HRR - heat release rate
SOC - start of combustion

APPENDIX

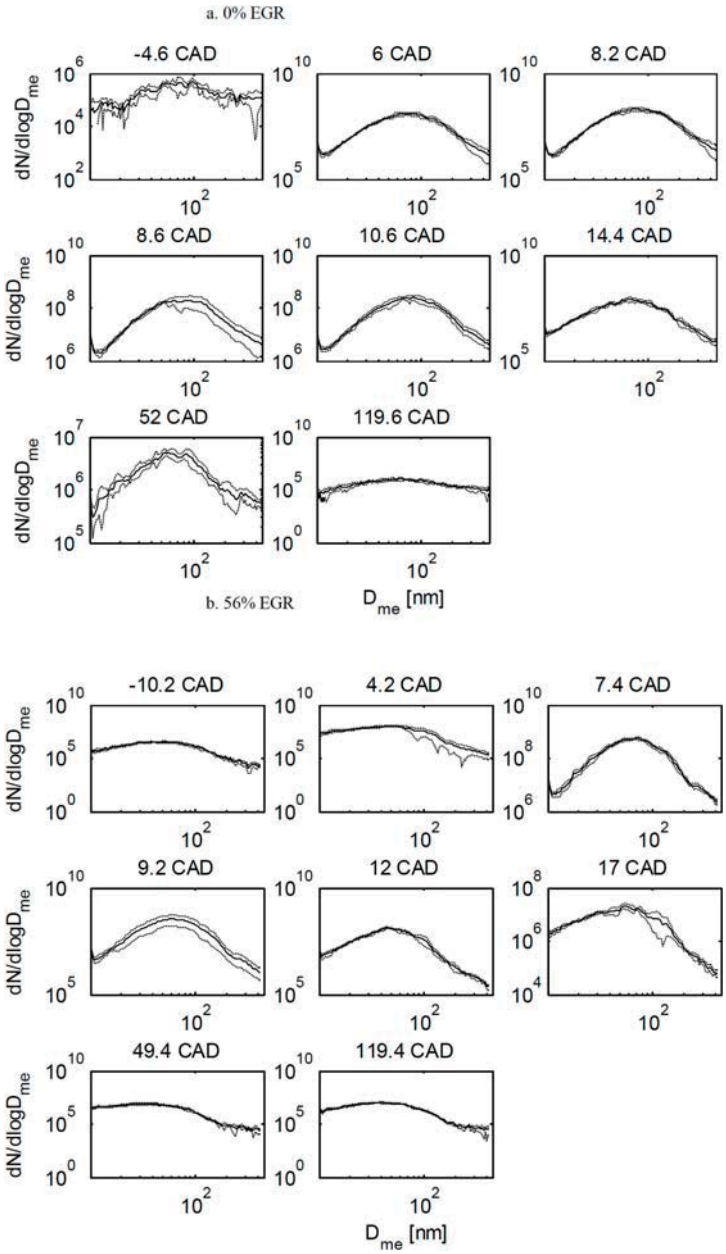

Figure 15. Particle size distribution at each individual crank angle.

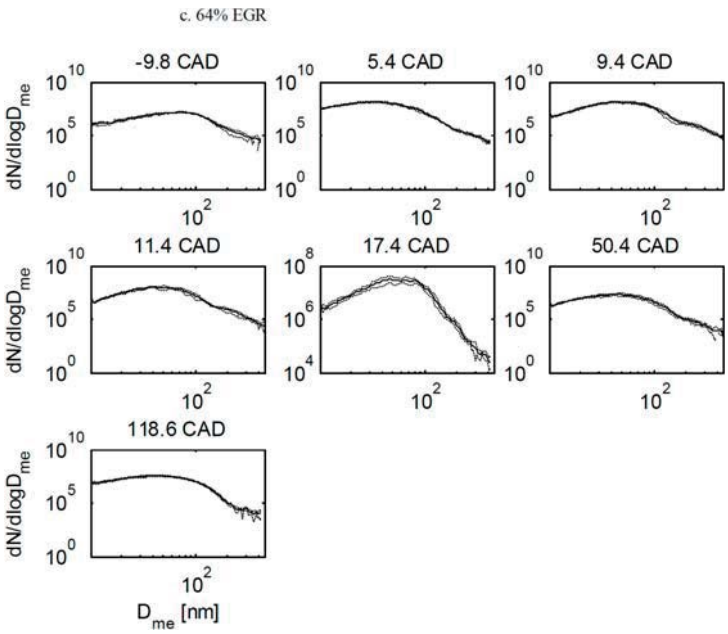

Figure 15. (cont.) Particle size distribution at each individual crank angle.

The Engineering Meetings Board has approved this paper for publication. It has successfully completed SAE's peer review process under the supervision of the session organizer. The process requires a minimum of three (3) reviews by industry experts.

ISSN 0148-7191

http://papers.sae.org/2015-24-2448

Paper VI

Evolution of in-cylinder diesel engine soot and emission characteristics investigated with on-line aerosol mass spectrometry

V. B. Malmborg[*1], *A.C. Eriksson*[1,2], *M. Shen*[3], *P. Nilsson*[1], *Y. Gallo*[3], *B. Waldheim*[4], *J. Martinsson*[2], *Ö. Andersson*[3], *J. Pagels*[1]

[1]Division of Ergonomics and Aerosol Technology, Lund University, Box 118, SE-22100, Lund, Sweden

[2]Division of Nuclear Physics, Lund University, Box 118, SE-22100, Lund, Sweden

[3]Division of Combustion Engines, Lund University, P.O. Box 118, SE-221 00, Lund, Sweden

[4]Fluid and Combustion Simulations, Engine Development, Scania CV AB, Sweden

ABSTRACT It is important to directly link health and climate-relevant soot (black carbon) emission characteristics to specific combustion conditions in the design of diesel engines with low environmental impact. The in-cylinder evolution of soot properties over the combustion cycle and as a function of exhaust gas recirculation (EGR) was investigated in a modern heavy-duty diesel engine. A novel combination of a fast gas-sampling valve and a soot particle aerosol mass spectrometer (SP-AMS) enabled on-line measurements of the in-cylinder soot chemistry**.** The results show that introducing EGR reduces soot formation rates. However, the late cycle soot oxidation rate (soot removal) is reduced even more, and the net effect is increased soot emissions. Increased EGR results in an accumulation of polycyclic aromatic hydrocarbons (PAHs) during combustion, and leads to increased PAH emissions. We report mass spectral and optical signatures which include a class of fullerene-like carbon clusters that we hypothesize to represent less graphitized, C_5-containing fullerenic (high tortuosity or curved) soot nanostructures arising from decreased combustion temperatures and increased premixing of air and fuel with EGR. Altered soot properties are of key importance when designing emission control strategies such as diesel particulate filters. Oxygen-rich biodiesel fuels and novel engine concepts may promote premixing in diesel engines and, in particular, lead to increased emissions of diesel soot with fullerenic nanostructures. The impact of this on climate and health is unclear.

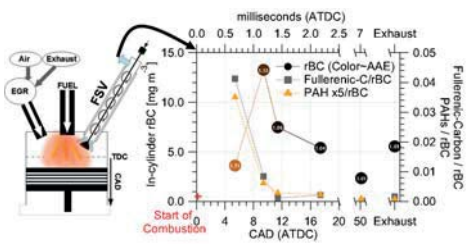

INTRODUCTION

Diesel engines are a major source of air pollution as they emit large amounts of fine particulate matter and nitrogen oxides (NO_x) to the atmosphere. Diesel exhaust and soot particles can cause acute inflammatory response in airways and peripheral blood[1], decreased lung function[1], asthmatic symptoms[2] and are classified as carcinogenic[3]. Soot emissions (often referred to as black carbon; BC) also contribute to global warming through short lived climate forcing[4]. Consequently, reducing diesel engine NO_x and soot emissions is an essential measures to improve air quality and reduce the anthropogenic climate impact. For these reasons stringent diesel engine emission regulations of fine particulates and NO_x have been introduced, for example, in the European Union and the United States.

Modern diesel engines commonly apply exhaust gas recirculation (EGR) to reduce NO_x emissions. With EGR, a fraction of the engine inlet air is replaces by exhaust gases. This reduces the oxygen concentration and combustion temperature and consequently the rate at which NO_x forms[5]. However, soot emissions increase rapidly with the decreasing inlet oxygen (O_2) concentration[6, 7].

Soot emissions from diesel engines are determined by two competing in-cylinder processes, namely soot formation and soot oxidation[8]. The soot formation rate is determined by the availability of acetylene, the formation of polycyclic aromatic hydrocarbons (PAHs) and the inception of soot particles[9], all of which are processes that depend strongly on temperature and local mixing of fuel and air. Soot oxidation (removal) depends strongly on the availability of hydroxyl radicals, O_2 and the temperature. The soot reactivity towards oxidation also depends strongly on soot nanostructure[10, 11] and surface oxygen content[11]. The soot reactivity is of key

53 importance when designing and optimizing Diesel Particulate Filters (DPFs), the most important
54 and efficient soot particle emission mitigation technique in modern diesel vehicles.

55 To increase our understanding of the processes governing soot emissions, studying in-cylinder
56 soot properties can provide fundamental information on the relationship between combustion
57 conditions and soot properties. These properties include particle size, chemical composition (e.g.,
58 elemental carbon and organic components, including PAHs), microstructure (e.g., primary and
59 aggregate sizes) and nanostructure (e.g., fringe length, tortuosity and separation distance). A
60 recently emerging topic is the identification of high curvature (high tortuosity) soot
61 nanostructures found in biodiesel emissions[12] and in laboratory studies of partially premixed
62 flames[13]. These properties may influence soot formation and oxidation rates, as well as soot
63 reactivity and thus the design and efficiency of DPFs. Moreover, combining in-cylinder particle
64 characterization and exhaust characterization can improve our knowledge of the relationship
65 between combustion conditions and the eventual toxicity of emitted soot particles, which in a
66 complex way depends on soot size, surface area and reactivity, surface coating material (e.g.,
67 PAHs) and metal content[14].

68 A number of techniques for studying in-cylinder particle concentrations and properties have
69 been established. Engines modified to allow optical access[15] have enabled non-invasive highly
70 time-resolved studies of in-cylinder gases (oxidants, PAHs, etc.) using laser induced
71 fluorescence[16, 17] and studies of soot concentration using laser induced incandescence[18, 19] and
72 laser extinction[20]. Recently, TEM grids were mounted inside a cylinder allowing detailed studies
73 of particle nanostructure using high resolution transmission electron microscopy[21] (HR-TEM). A
74 total cylinder sampling system[22] can be used for rapid (1 ms) extraction of the full cylinder
75 volume from a single combustion cycle and to study soot properties using an array of off-line

techniques including HR-TEM and Raman microscopy[23, 24]. Off-line techniques involve particle sampling, handling and often also chemical processing that could possibly lead to unintended changes in particle properties. On-line aerosol measurement techniques are commonly used in ambient measurements to characterize particle properties directly in the aerosol phase. On-line aerosol measurement techniques are commonly used in ambient measurements to characterize particle properties directly in the aerosol phase, for example to investigate the transformation of climate-relevant soot properties upon aging in the atmosphere[25]. The direct radiative forcing of BC can be described by knowledge of soot morphology and coating thickness[26], for which on-line characterization is essential.

Fast sampling valves[27-29] (FSVs) are in-cylinder gas extraction techniques that enable particle characterization using on-line aerosol instruments. FSVs repeatedly extract a small volume of in-cylinder gases at a well-defined position in the combustion process. The repeated extraction produces a semi-continuous flow of in-cylinder gases, and because of the small volume sampled in each extraction, the FSV has a negligible impact on combustion[29]. Additionally, the aerosol extracted is averaged over a large number of fired cycles which decreases the sensitivity to cycle-to-cycle variations compared to other in-cylinder particle extraction techniques.

The soot particle aerosol mass spectrometer (SP-AMS) was recently developed[30] to enable on-line chemical analysis of soot particles. The SP-AMS enables chemical analysis of the soot core by overlapping a focused Nd-YAG laser beam (λ=1064nm) with a beam of particles, permitting decoupled vaporization and electron ionization (70 eV) and thus detection of highly refractory species such as elemental carbon and heteroatoms (e.g., oxygen in the solid carbon core) in a high resolution time-of-flight (HR-ToF) mass spectrometer. The SP-AMS also allows the composition of non-refractory material (e.g., organic material coating the soot core) to be

characterized by vaporizing particles on a heated porous-tungsten vaporizer at 600°C[31]. Probing in-cylinder particles with the SP-AMS can therefore provide more detailed on-line information on the composition of the refractory soot core and of condensed non-refractory material on soot particles than present laser diagnostic techniques, and without the potential artifacts associated with off-line particle analysis.

We combined an FSV[29] and the SP-AMS to directly and continuously probe the evolution of in-cylinder particle composition and concentration as combustion progresses in a modern heavy duty diesel engine. We specifically address the implementation of lowered combustion temperatures and increased premixing using EGR, and its effect on soot characteristics during combustion.

Our results show that in-cylinder soot processes exhibit two distinct phases: a soot formation dominated phase and a soot oxidation dominated phase. These soot phases are well described in the literature[24, 32, 33], which indicates that we have probed representative in-cylinder conditions. We found that EGR decreases both soot oxidation and soot formation rates which resulted in increased soot and PAH emissions. Finally, at high EGR we identify fullerene-like carbon cluster signals in the SP-AMS data. These large carbon clusters are hypothesized to represent high tortuosity (curved) soot nanostructures, linking combustion with EGR to increased C_5 chemistry also found in select premixed flames[13].

METHOD

Engine Operation.

A heavy duty Scania D13 engine was operated at low load (5.5 bar IMEPg) and 1200 rpm. The common rail fuel injection pressure was set to 2000 bar, the air intake temperature and pressure

were set to 337 K and 1.65 bar respectively. The fuel used was Swedish diesel MK1 with ultra-low sulphur content, a cetane number of 56.8, an aromatic content of 4.4 vol.% and an alkane content of 95.6 vol.%. A synthetic lubrication oil (Powerway GE 40, Statoil) was used. Engine conditions were altered by running the engine at no EGR (0%), 56% and 64% EGR. These three EGR levels correspond to engine inlet air O_2 concentrations of 21%, 15% and 13%, respectively. When introducing EGR, the start of fuel injection (SOI) was initiated earlier in order for CA50 (the crank angle position where 50% of the heat has been released) to remain approximately constant (~7.5 CAD ATDC). Regulated gas phase emissions were monitored for the three EGR concentrations of 21%, 15% and 13% inlet O_2, and were (in g/kWh): hydrocarbons (HC) 0.113, 0.054, 0.046; carbon monoxide (CO) 0.41, 0.57, 1.99; nitrogen oxides (NO_x) 11.2, 0.27, 0.08, respectively. For a complete description of the engine and the operating conditions, the reader is referred to Shen et al.[29].

Aerosol Sampling and Dilution.

To extract in-cylinder particles, a fast sampling valve[29] (FSV) was mounted on the cylinder head by replacing one of the exhaust ports. The FSV encompasses a water-cooled cylinder with an inner stem and a solenoid hammer mounted on top of the inner stem which opens the valve when actuated. The sampling location of the FSV was fixed throughout the measurement and located between two adjacent fuel jets. The working principles of the FSV have previously been described[29], however the key features are presented in the supporting information (SI). When the valve opens, gases flow from high pressure inside the cylinder towards atmospheric pressure in the sampling line. The reported sampling positions represent the opening of the FSV. NO_x forms during combustion and NO_x concentrations in the extracted in-cylinder gas was used to confirm that representative sampling could be obtained. The NO_x concentrations increased rapidly during

the combustion and reached a plateau concentration in the late combustion cycle (Figure S1) consistent with the exhaust NO_x concentration (within a 30% range error). The sampling resolution of the FSV (i.e. the duration that the valve is open) was estimated to approximately 0.5-1 ms (4-6 CAD) at high in-cylinder pressures (>50 bars), and less than 2 ms (14 CAD) at low in-cylinder pressures during the late cycle (see SI). As shown in SI, particle losses during extraction with the FSV were estimated to less than 30% for particles with mobility diameters between 10-250 nm, the main range of diesel exhaust particles.

After exiting the FSV, the extracted aerosol was diluted in three stages with a nominal dilution factor of 700 times and transported to the instruments. The dilution ratio varied by less than 20% throughout all the measurements, confirmed by NO_x measurements before and after the dilution[29]. A schematic representation of the dilution system is given in Figure S2. Exhaust particles were sampled with one stage of the dilution system at 21% inlet O_2 concentration and two stages in series at 15% and 13% inlet O_2 concentration. The measured in-cylinder refractory black carbon (rBC) concentrations, accounting for SP-AMS collection efficiency as described below, spanned over two orders of magnitude (dilution adjusted concentrations: 2-170 mg m^{-3}). In the exhaust, the concentrations were even lower (down to 0.14 ±0.01 mg m^{-3} for 21% O2). These lower concentrations are in part due to late-cycle oxidation. In a few cases the engine was operated in motored mode (without combustion) which showed concentrations of about 1 mg m^{-3}. This indicates possible resuspension of previously deposited particles in the FSV (see SI, Figure S8) that together with high dilution ratios (~700) in the late-cycle FSV measurements caused increased uncertainty in measurements for a few cases, primarily late cycle points at 21% inlet O_2.

Aerosol Characterization.

Particle chemical composition was investigated with a soot-particle aerosol mass spectrometer[30] (Aerodyne Inc. Billerica, MA, USA). The SP-AMS was run in single or dual vaporizer mode. In the single vaporizer mode, particles are flash vaporized upon impaction on a heated (600°C) tungsten surface. In the dual vaporizer mode, particles containing rBC are vaporized using an intracavity Nd:YAG laser (1064 nm). The vapors are then ionized (70 eV electron ionization) and detected in a HR-ToF mass spectrometer. The SP-AMS allows efficient sampling of particles in the diameter range ~70-500 nm[34, 35] (vacuum aerodynamic diameter). The SP-AMS was calibrated using the standard procedure with aerosolized ammonium nitrate particles for single vaporizer mode and Regal Black particles (Cabot Inc., Boston, MA, USA) for calibration of rBC in dual vaporizer mode. The apparent relative ionization efficiency of rBC relative to ammonium nitrate, RIE_{app}, was 0.47. The SP-AMS set-up and calibration is further detailed in SI.

The equivalent BC mass concentration and absorption angstrom exponent (AAE) were analyzed using an aethalometer[36] (model AE33, Magee Scientific). A scanning mobility particle sizer (SMPS, classifier model 3071, CPC 3010, TSI Inc.) was used to measure the particle mobility size distribution. The in-cylinder diesel soot concentration was measured simultaneously using the SP-AMS and the aethalometer. The rBC mass concentration correlated well with the total BC mass measured with the aethalometer (R^2=0.99) with an rBC to BC ratio of 0.18 (Figure S9). This difference between the two instruments is likely caused by lower SP-AMS collection efficiency[37] for diesel soot compared to the calibrant (Regal Black) and differences between optical detection (aethalometer) and chemical detection (SP-AMS). Reported rBC concentrations have been scaled to the BC concentrations using the factor 0.18.

To quantify the contribution of particle phase in-cylinder PAHs to the total organic aerosol (OA), molecular masses corresponding to nine parent peaks of common PAH isomers between MW 202 and MW 300 ($C_{16}H_{10}$, and $C_{24}H_{12}$) were included. Smaller PAHs (with 2-3 rings, MW <202) were not included in the analysis due to their high vapor pressure and lack of AMS analysis of pure lab standards. We accounted for the relative abundance of the parent peaks in the mass spectra (~0.25) found in previous laboratory calibrations for 7 PAH isomers[38].

RESULTS AND DISCUSSION

In-Cylinder Soot Formation and Oxidation.

The engine was operated at three levels of EGR corresponding to 21% (no EGR), 15% and 13% inlet O_2 concentrations. At each level of EGR, the FSV was used to extract in-cylinder gas and particles at a number of positions during the combustion cycle. The reported in-cylinder concentrations have been converted to standard temperature and pressure (STP) and are reported in mg m^{-3}. The positions in the combustion cycle were chosen so that the soot formation dominated phase (increasing rBC concentration), the soot peak and the soot oxidation dominated phase (decreasing rBC concentration) were distinguishable.

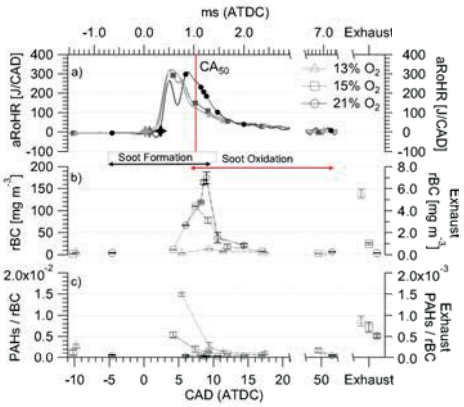

Figure 1: (a) In-cylinder heat release rates. Stars represent the start of combustion. The following symbols represent the aerosol sampling positions: triangles, 13% inlet O_2; squares, 15% inlet O_2; circles, 21% inlet O_2. The CA50 was kept constant when changing EGR and is illustrated by the vertical red line. (b) SP-AMS rBC (soot) mass concentration. (c) The relative concentration of PAHs to rBC as a function of the combustion cycle. The position in the combustion cycle when particles were sampled with the FSV is shown in milliseconds (ms, top) and crank angle degrees (CAD, bottom) after the top dead center (ATDC, located at t=0). Three levels of EGR are shown corresponding to 21%, 15% and 13% O_2 inlet O_2 concentrations. Exhaust emission values are shown on the right axis. Black and red arrows show the soot formation dominated phase and soot oxidation dominated phase respectively. Error bars represent standard errors of the mean.

The apparent rate of heat release (aRoHR) derived from the in-cylinder pressure data is presented in Figure 1a. The start of injection (SOI) occurred earlier when EGR was applied and the start of combustion (SOC) was delayed, which increased the time allowed for premixing of air and fuel by 0.8 CAD when the inlet O_2 concentration was changed from 21% to 13%. The aRoHR is characterized by two well defined peaks at 21% inlet O_2 concentration. The two peaks

222 indicate premixed or partially premixed combustion (first peak) and spray driven combustion
223 (second peak) which transition into diffusion controlled combustion when the fuel injection
224 stops. As a result of lowered temperatures and slower kinetics when EGR is introduced, the two
225 peaks are poorly defined at 15% inlet O_2 concentration and only one peak is observed at 13%
226 inlet O_2 concentration.

227 Due to the high in-cylinder temperatures, the in-cylinder soot mass will principally be
228 determined by the concentration of refractory black carbon (rBC). The in-cylinder rBC
229 concentrations measured with the SP-AMS is presented in Figure 1b. The rBC concentration
230 increases rapidly after SOC ("soot formation phase"), it reaches a maximum shortly after CA50
231 ("soot peak"), it then decreases rapidly ("soot oxidation phase"). The soot peak concentration
232 decreases strongly with increasing EGR which shows that soot formation rates are reduced by
233 lower inlet O_2 concentrations. Most of the soot formation and oxidation observed in Figure 1b
234 occurs within approximately 2 ms (14 CAD).

235 Exhaust rBC concentrations increased with increasing EGR: 0.14 (±0.01) mg m^{-3} at 21% inlet
236 O_2 concentration; 1.03 (±0.09) mg m^{-3} at 15% inlet O_2 concentration; 5.67 (±0.40) mg m^{-3} at 13%
237 inlet O_2 concentration. This shows that soot oxidation rates are significantly reduced by EGR and
238 that soot oxidation is the dominant in-cylinder process that governs soot emissions from the
239 engine. Lower soot oxidation rates with decreasing inlet O_2 concentrations have previously been
240 shown to be the cause of increased soot exhaust emissions with increasing EGR[33, 39].

241 In-cylinder soot particle size distributions from the current measurements have been reported
242 previously[29]. The exhaust soot size distributions for the three levels of EGR had the following
243 geometrical mean mobility diameters (GMD) and standard deviations: 54.8±0.3 nm, 1.69±0.01 at

21% inlet O_2 concentration; 46.9±1.4 nm, 1.78±0.02 at 15% inlet O_2 concentration; 70.3±3.4 nm, 1.64±0.01 at 13% inlet O_2 concentration.

Figure 1c shows the ratio of particle phase PAHs (4-6 ring PAHs, MW 202-300) relative to the rBC concentration. At 21% inlet O_2 concentration, the PAH to rBC ratio is low throughout the combustion cycle. At 13% and 15% inlet O_2 concentration we observed elevated ratios during the soot formation dominated phase that decreased as the combustion proceeded. These observations are consistent with large PAHs (in the size range from Pyrene (MW 202) to Coronene (MW 300) being involved in the formation and growth of soot particles. It shows that lowered flame temperatures with EGR reduces the soot formation rates, allowing the concentration of larger PAHs to accumulate. The particle phase PAH emissions in the exhaust (MW 202-300) increased with EGR and were 0.1 μg m^{-3} at 21% inlet O_2 concentration; 0.7 μg m^{-3} at 15% inlet O_2 concentration; and 4.8 μg m^{-3} at 13% inlet O_2 concentration. Thus a fraction of the PAHs that accumulates during combustion with EGR survives, and the process leads to increased emissions.

The observed soot trends presented in Figure 1b resemble the results of in-cylinder soot measurements found in the literature and illustrate a general consistency between in-cylinder soot trends obtained by our combination of the FSV with on-line aerosol instruments, and results acquired using non-invasive optical techniques such as laser extinction[33] and the total cylinder sampling technique[24, 32].

Aerosol Mass Spectra of Soot in the Formation and Oxidation Dominated Phases

Figure 2 shows aerosol mass spectra of particles sampled from the soot formation dominated and oxidation dominated phases at 13% inlet O_2 (high EGR). The sizes of carbon clusters resulting from IR laser vaporization followed by electron ionization (70 eV) of the soot cores are

shown in Figures 2a, b. Carbon clusters were grouped into low-carbons (C_1^+-C_5^+), mid-carbons (C_6^+-C_{29}^+) and fullerenic-carbons (C_{30}^+-C_{58}^+). During both soot formation and oxidation, rBC was dominated by C_1^+-C_3^+ ion fragments. Signals from larger mid- and fullerenic-carbon clusters were pronounced in the soot formation phase and low in the oxidation phase (Figure 2b).

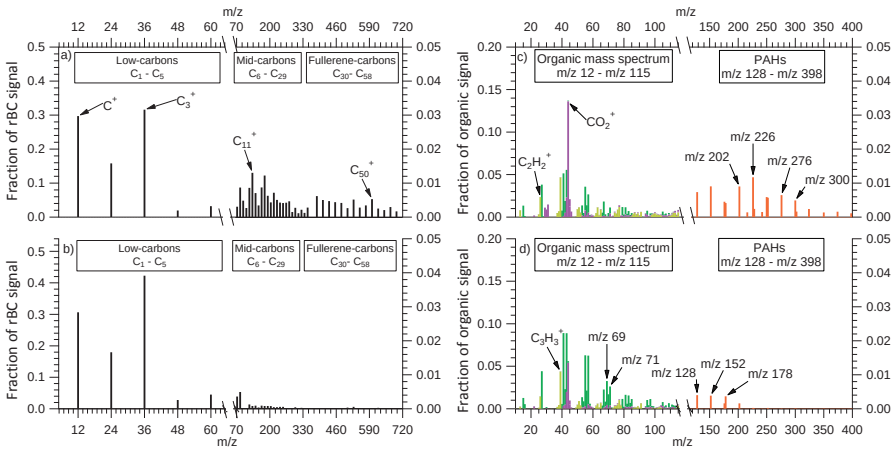

Figure 2: Refractory carbon cluster ion distributions and non-refractory organic ion fragments at 13% inlet O_2 concentration during intense soot formation (a and c) at 5 CAD (ATDC) and after intense soot oxidation (b and d) at 18 CAD (ATDC). Carbon clusters are divided into low-carbon clusters (C_1^+-C_5^+, left axis), mid-carbon clusters (C_6^+-C_{29}^+, right axis) and fullerenic-carbon clusters with even carbon numbers (C_{30}^+-C_{58}^+, right axis). Organic ion fragments: aliphatic fragments ($C_xH_{y>x}^{+\cdot}$ green), unsaturated and aromatic fragments ($C_xH_{y\leq x}^+$, light green), oxidized organic fragments ($C_xH_yO_z^+$, magenta) are shown on the left axis, and PAHs (orange) are shown on the right axis.

Low volatility organic species condense onto the soot particles and form OA primarily when gases cool during extraction with the FSV and in the subsequent piping. The OA observed can be

considered as the low volatility in-cylinder vapor species that will ultimately condense and form a soot coating in the engine exhaust. Aerosol mass spectra with the laser turned off (Figures 2c, d) were used to identify organic ion fragments (m/z 10-115) and the main PAHs (parent peaks: m/z 128-400). The organic mass spectra show strong contributions from the hydrocarbon peaks $C_3H_5^+$ (m/z 41), $C_3H_7^+$ (m/z 43), $C_4H_7^+$ (m/z 55), and $C_4H_9^+$ (m/z 57). High signal intensity is also found at m/z 67, 69, 71 and m/z 81, 83, and 85. The origin of these hydrocarbon fragments are related to straight-chain alkanes (*n*-alkanes), branched alkanes ($C_nH_{2n+1}^+$) and cycloalkanes ($C_nH_{2n-1}^+$ and $C_nH_{2n-3}^+$) and they commonly dominate diesel exhaust OA[40-42]. Ratios larger than 1 of the signal intensities at m/z 69 and 71, and at m/z 83 and 85 are likely only for an OA containing more than 95% lubrication oil[40, 43]. These ratios are shown in Figure S10. OA was dominated by unburnt lubrication oil throughout the combustion cycle.

Other strong non-refractory components include CO_2^+ and other oxidized fragments in the $C_xH_yO_z^+$ family, as well as $C_2H_2^+$, $C_3H_3^+$, $C_5H_3^+$. The latter fragments are mainly of unsaturated aliphatic or aromatic origin and were assigned their own class in this study, denoted $C_xH_{y\leq x}^+$. The contribution of these two classes to OA decreased from the soot formation to the soot oxidation phase, with the mass spectra in the soot oxidation dominated phase being more similar to diesel exhaust OA signatures in the literature[40].

Figures 2c, d show that PAHs are significantly more abundant in particles during soot formation. The larger PAHs decreased substantially in the soot oxidation phase. Wang et al.[32] found that the naphthalene concentration accounted for 26-84% of the total PAH mass throughout the combustion cycle, thus the signal that we detect with the AMS in the particle phase for the volatile PAHs (2-3 rings) may be only a fraction of their total concentrations. The reason we observed a signal from Naphthalene, given its high vapor pressure, may be due to

strong adsorption to the soot core surfaces and to a small extent fragmentation of larger PAHs during electron ionization.

Evolution of In-Cylinder Soot Characteristics

Figure 3 shows the evolution of soot properties between the soot formation and soot oxidation dominated phases at 21%, 15% and 13% inlet O_2 concentrations using the subgroups of rBC and OA described above. An intense transition of soot properties takes place between the soot formation phase and soot oxidation phase at 15% and 13% inlet O_2 concentration, but much smaller differences were observed at 21% O_2. In the refractory mass spectra of the soot cores, a transition in the composition of rBC was observed at 15% and 13% inlet O_2 concentrations. The mass spectra had relatively high fractions of mid- and fullerenic-carbons during the soot formation phase, and were completely dominated by low-carbons in the soot oxidation phase. During the soot formation phase, non-refractory mass spectra of low volatility organics at 15% and 13% inlet O_2 concentrations were, in addition to aliphatic fragments ($C_xH_{y>x}^+$), composed of substantial fractions of aromatic and unsaturated fragments ($C_xH_{y\leq x}^+$), oxidized organics fragments ($C_xH_yO_z^+$), and PAHs.

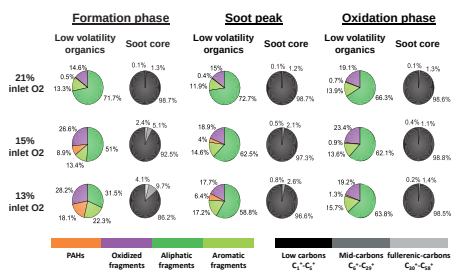

Figure 3: Soot chemical compositions during soot formation, soot peak and soot oxidation phases for 21%, 15% and 13% inlet O_2 concentrations. Left columns: grouped ion fragments originating

from low volatility organics. Right columns: refractory carbon clusters from the soot core. Refractory soot core carbon clusters: low-carbons C_1^+-C_5^+ (black), mid-carbons C_6^+-C_{29}^+ (dark grey) and fullerenic-carbon C_{30}^+-C_{58}^+ (light grey). Non-refractory low volatility organics: aliphatic fragments ($C_xH_{y>x}^+$, green), unsaturated and aromatic fragments ($C_xH_{y\leq x}^+$, light green), oxidized organics fragments ($C_xH_yO_z^+$, magenta) and PAHs (orange).

Figure 4 (a-f) shows a more detailed analysis of the in-cylinder soot evolution and comparison with the exhaust for: (a) fullerenic-carbons, (b) refractory CO_2^+, (c) oxidized non-refractory organic fragments ($C_xH_yO_z^+$), (d) PAHs (m/z = 202-300) and (e) the wavelength dependency of light absorption (AAE, 370-950 nm). Normalized rBC concentrations in Figure 4f are shown for reference to the evolution of in-cylinder soot mass.

The fullerenic-carbon mass fraction ($C_{30\text{-}58}^+$) shown in Figure 4a accounts for several percent of rBC in the soot formation dominated phase at 15% and 13% inlet O_2 concentration. The $C_{30\text{-}58}^+$ fraction decreases gradually as the combustion proceeds. At 21% inlet O_2 concentration, fullerenic-carbon represents a negligible fraction of rBC. As shown in SI, fullerenic-carbon signals from the exhaust soot at 21% inlet O_2 concentration were only slightly higher than the non-refractory organic background signal obtained with the laser turned off. At 13% inlet O_2 concentration, the signals from fullerenic-carbon clusters in the exhaust were clearly higher than the organic background (Figure S12), although they were very low compared to the total signal from all refractory carbon clusters.

Recently, SP-AMS mass spectra of refractory carbon clusters from 12 different soot and manufactured carbon black sources were characterized[44]. Fullerene signals were not observed in mass spectra from graphitic (mature) soot, nor in amorphous carbon but they were detectable in

biomass burning, ethylene flame soot and Nano-C fullerene black, for example[44]. The authors concluded that fullerene signals in the SP-AMS may arise from carbon nanostructures that can form fullerenes upon heating[44].

It was recently shown[13] that partial premixing of oxygen in benzene (and ethylene) flames introduced high curvature C_5-containing, fullerenic nanostructures in the soot formed. The C_5 production was suggested to proceed through partial benzene oxidation yielding the phenoxy radical followed by CO loss to produce C_5. EGR, when used in diesel engines as in this study, allows a higher degree of premixing of O_2 in the soot formation zone similar to the model flame systems discussed above. Thus, we hypothesize that the fullerenic-carbon signals correlate with high curvature, C_5-containing fullerenic-soot nanostructures[45]. EGR has also been shown to affect exhaust soot properties resulting in a more reactive soot with a higher disorder of the soot nanostructure[46], consistent with fullerenic-carbon signals in mass spectra of exhaust soot only being present during combustion with EGR. In previous SP-AMS studies of diesel exhaust, fullerenic-carbon signals were commonly not observed[44, 47]. The evolution of soot nanostructures during the diesel combustion cycle has previously been investigated using HR-TEM[23] where it was found that the soot rapidly became more graphitic as the combustion proceeded, and that after 50 CAD the gradual increase in graphitic structure was small. Following the discussion of Onasch et al.[44], we interpret the decay in fullerenic-carbon signal at 15% and 13% inlet O_2 concentration as a gradual ordering of the soot nanostructure, analogous to the results of Li et al.[23]. The low signal from fullerenic-carbon clusters in the late combustion cycle and exhaust is consistent with graphitic soot and reduced content of fullerenic nanostructures.

The importance of the soot nanostructure for reactivity and oxidation rates has been well documented[10, 48]. Shorter graphene layer planes increase the reactive carbon layer edge sites and

fullerenic nanostructures have weaker C-C bonds due to the curvature of the molecules which increases the accessibility for oxidation by O_2 and OH[48]. We therefore hypothesize that soot associated with the fullerenic-carbon signals in the SP-AMS is oxidized (removed) more rapidly than soot that does not produce a fullerenic-carbon signal. This could explain the lower signals from soot extracted late in the combustion cycle and in the exhaust.

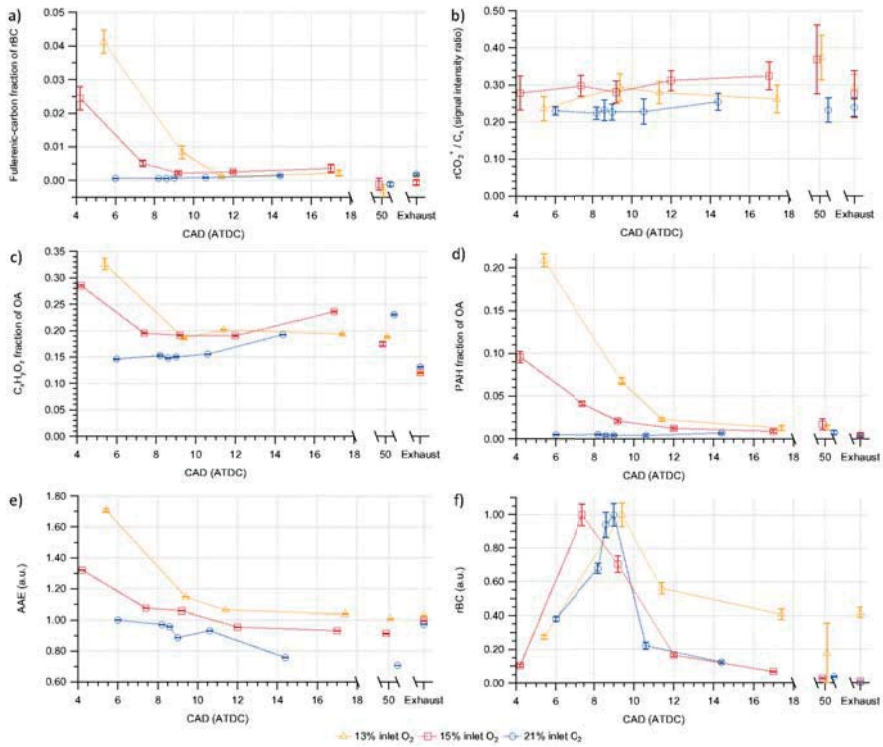

Figure 4: Evolution of soot properties during the combustion cycle and at 21%, 15% and 13% inlet O_2 concentrations. (a) Fullerenic-carbon fraction of rBC. (b) rCO_2^+ normalized to the total refractory C_x^+ (i.e., carbon cluster, signal intensity). (c) Oxidized organic ($C_xH_yO_z^+$) fraction of total OA concentration. (d) PAH fraction of total OA concentration. (e) Variations in AAE with

the combustion cycle. (f) rBC normalized to their respective peak in-cylinder concentration. Error bars represent standard errors of the mean.

In addition to rBC, the refractory part of the mass spectrum included considerable signal intensity from CO_2^+ ions. The refractory CO_2^+ (rCO_2^+) intensity to that of the refractory C_x^+ signal intensity varied only weakly over the combustion cycle (Figure 4b), with slightly higher ratios when EGR was applied to the engine. We also observed refractory $C_3O_2^+$ ions. The signal from $rC_3O_2^+$ ions was approximately ten times lower than the ion signal from rCO_2^+. However, and more importantly, the $rC_3O_2^+$ and rCO_2^+ signals show trends in the combustion cycle that are similar to those of the X-ray photoelectron spectroscopy analyses of oxygenated surface functional groups reported in the literature[24]. We hypothesize that these refractory oxygen-containing ion fragments observed in the SP-AMS mass spectra arise as a result of partial oxidation of soot cores, and that the ions originate from oxygenated functional groups in the soot core carbon nanostructure and on the soot core surface as suggested previously in laboratory[49] as well as ambient[50] measurements. We are not yet at a stage to fully quantify the rCO_x^+ signal, however, as the apparent RIE of rCO_x^+ in the SP-AMS appears to be much higher than that for rBC and closer to that of non-refractory organic aerosol[49]. In previous SP-AMS studies, the highest peak in the rCO_x^+ class is CO^+. Unfortunately, we could not report this peak due to strong interferences from the gas phase N_2 signal at m/z 28.

When EGR is applied, the fraction of non-refractory oxidized organic fragments ($C_xH_yO_z^+$) to the total OA decays from an initially high fraction (~30%) down to ~15% as the combustion proceeds (Figure 4c). This may be a result of the higher availability of O_2 during the early combustion cycle due to the increased premixing with EGR. However, because this decay is

403 correlated with the decay in the fullerenic-carbon signal, it could be associated with decreased
404 reactivity of the soot surfaces as the combustion proceeds. With no EGR, the initial contribution
405 from oxidized organics to the total OA is low and instead, a gradual increase is observed as the
406 combustion proceeds. This results in a small increase of the oxidized organic fraction of OA in
407 the exhaust at 21% inlet O_2 concentration relative to 15% and 13% inlet O_2 concentration. These
408 observations indicate that the mechanism responsible for the higher fraction of non-refractory
409 oxidized organics in the exhaust at 21% inlet O_2 concentration compared to the EGR cases could
410 be the higher availability of O_2 during the late cycle. A small fraction of the signal originating
411 from surface oxides as described above for rCO_x^+ may be volatile enough to be vaporized at 600
412 °C. This may explain the part of the signal in the non-refractory spectra that varies only weakly
413 with CAD.
414 Figure 4d shows the quantified mass fraction of all selected PAHs to the total OA mass. At
415 21% inlet O_2 concentration, PAHs made up only a small fraction of the total in-cylinder OA.
416 With EGR, PAHs made up a considerable fraction of OA in the soot formation dominated phase.
417 The PAH fraction of OA was 18.1% at 13% inlet O_2 concentration and 8.9% at 15% inlet O_2
418 concentration in the soot formation phase. In the soot oxidation phase and exhaust, the PAH
419 fraction of OA was low at all three EGR levels but increased with EGR.
420 The in-cylinder PAH fraction of OA was strongly correlated with the fullerenic-carbon
421 fraction of rBC (r=0.91), which suggests that these derive from similar in-cylinder combustion
422 processes. Soot formation is linked to the formation of moderately sized PAHs[9]. Considering
423 only the growth of PAHs and soot particles, we propose that the low concentration of PAHs
424 (MW 202-300) at 21% inlet O_2 concentration in the soot formation phase is a result of faster
425 particle inception and surface reactions rates (i.e., much more rapid soot formation) than PAH

formation rates. On the other hand, we propose that at 15% and 13% inlet O_2 concentration, the elevated PAH concentrations are direct results of lower combustion temperatures, which allows the PAH concentration to accumulate due to slower particle inception and reactions with soot surfaces. A previous in-cylinder PAH diagnostics study using laser induced fluorescence shows that the PAH residence time in the flame-jet before the onset of soot formation increases drastically with increasing EGR, from tens of microseconds with no EGR to milliseconds with high EGR (12.7% O_2)[16]. Extending the argumentation to include soot properties, these results suggest that when introducing EGR, longer residence times of PAHs and soot precursors coupled with lower flame temperatures are also important for the formation of fullerenic nanostructures.

Finally, we observed variations in the optical properties of the in-cylinder soot (Figure 4e) by analyzing the Absorption Ångström Exponent (AAE), a measure of the absorption wavelength dependency of the particles. The AAE is highest in the early stages of combustion and progressively becomes smaller as the combustion proceeds. Remarkable transitions in AAE are observed when reducing the inlet O_2 concentration. In the soot formation dominated phase the AAE was 1.7 at 13% inlet O_2 concentration, 1.3 at 15% inlet O_2 concentration, and 1.0 at 21% inlet O_2 concentration. In the soot oxidation dominated phase, AAE was 1.1, 1.0 and close to 0.8 at 13%, 15% and 21% inlet O_2 concentrations, respectively. The order was similar in the exhaust but the differences were smaller. At 21% inlet O_2 concentration in the late combustion cycle, the concentrations were very low and the AAE measurement was most likely affected by the previously mentioned background particles that were released from the sampling valve without combustion in the motored mode. These background particles had a larger size in the SMPS and appear to be associated with a lower AAE than the particles in the exhaust.

We conclude that the low AAE found in diesel exhaust soot is due to a gradual decrease in AAE as the combustion proceeds. The variations in AAE as the combustion proceeds resemble the trends associated with increasing graphitization of the soot. Correlating the observed in-cylinder soot AAE with SP-AMS data, we conclude that the overall OA to BC ratio of the in-cylinder diesel soot shows a low correlation (r=0.08) with the observed changes in AAE (OA originates mostly from lubrication oil). However, when grouped into their respective OA families, the fraction of OA belonging to aliphatic ($C_xH_{y>x}^+$) fragments was inversely correlated (r=-0.82) with AAE, while the PAH fraction (r=0.93), unsaturated and aromatic ($C_xH_{y\leq x}^+$) fraction (r=0.84), and oxidized organic ($C_xH_yO_z^+$) fraction (r=0.68) were positively correlated with AAE. In addition to non-refractory components, a strong correlation between AAE and the fullerenic-carbon fraction (r=0.91) and mid-carbon fraction of rBC (r=0.90) was observed.

It has previously been shown that variations in AAE can be related to nanostructural differences, with reported values of AAE≈2 for fullerene soot[51] and AAE≈2 for spark discharge soot with high curvature nanostructure[52]. Since fullerenic-carbons were exclusively observed during IR laser vaporization with the SP-AMS, this group of species correlating with AAE also suggests that intrinsic properties of the soot core can cause the variations in AAE, in addition to variations caused by UV-absorbing organics such as PAHs.

Implications

Evidence of fullerenic soot signatures in SP-AMS mass spectra from ambient air was recently reported[53]. This stresses the importance of understanding the mechanisms behind the formation of fullerenic soot and associated organics such as PAHs. In addition, it merits further studies on

the removal efficiency and transformation of fullerenic soot in DPFs, as well as on the toxicological responses, atmospheric transformation and climate relevance of such emissions.

Previous studies on EGR highlight an increased reactivity towards oxidation in exhaust soot[54, 55]. The presence of fullerenic carbon clusters in our SP-AMS mass spectra implies that EGR leads to the formation of high tortuosity (high curvature) soot nanostructures. To elucidate the formation mechanisms of fullerenic soot in diesel engines, studies on soot formation using well-defined premixed flames[13] and shock tubes[56] may thus prove highly relevant. We found that the fullerene signals are reduced as combustion proceeds in the cylinder. Future studies should evaluate if this is due to preferential removal by oxidation of these structures or to a gradual conversion towards more graphitized soot nanostructures.

The results have important implications for emission control systems in modern vehicles. The oxidation reactivity of soot is a key input parameter when designing DPFs which effectively reduce BC emissions[57]. It is well known that soot nanostructure affects the oxidation reactivity. Diesel oxidation catalysts will reduce the PAH concentration. However, DPFs can increase the emissions of select nitro-PAHs[58, 59]. The influence of EGR on soot nanostructure and concentrations of PAHs merits further studies on how exhaust after-treatment can impact the final emitted aerosol properties. We also found altered optical properties of diesel soot with high fullerenic-carbon signals. If these can be definitively linked to fullerenic nanostructures, it will affect the direct radiative forcing and the accuracy of BC source apportionment based on AAE for such emissions.

The blending of increasing fractions of oxygen containing FAME (fatty acid methyl esters) biodiesel into fossil diesel is currently encouraged to mitigate CO_2 emissions. FAME is associated with reduced particle emissions compared to fossil diesel[60] but was recently found to

493 be associated with increased fractions of high tortuosity nanostructures[12] and increased in-vitro
494 toxicity[61]. Formation of high tortuosity fullerenic soot nanostructures has been linked to
495 premixing of fuel and oxygen in the soot formation zone[13]. EGR results in increased premixing
496 of fuel and air, while biodiesel provides oxygen from the fuel. If diesel soot reactivity increases
497 with EGR and biodiesel, it may be possible to increase the efficiency of soot removal in DPFs.
498 We propose that future research include in-cylinder sampling with the FSV and sampling at
499 different stages in the exhaust after treatment system, combined with the SP-AMS and the mass-
500 spectrometric signatures developed here. Such studies may involve novel engine concepts (e.g.,
501 low temperature combustion) and biodiesel fuels, and has potential to provide novel information
502 of in-cylinder chemistry that can aid the design of combustion systems which ultimately
503 influence emissions, climate effects and particle toxicity.
504

505 ASSOCIATED CONTENT

506 **Supporting Information**.

507 NO_x vs CAD; Dilution system and experimental set-up; The fast gas-sampling valve (FSV);
508 SP-AMS set-up, calibration and data analysis; SMPS mass weighted size distributions in late
509 cycle and exhaust; rC_x^+ and BC correlation; Adjusting for gas phase CO_2 and CHO; Origin of the
510 organic aerosol: lube oil vs diesel; Refractory fullerenic-carbon signal vs non-refractory
511 background signal

512 AUTHOR INFORMATION

513 **Corresponding Author**

*Address: Ergonomics & Aerosol Technology, Lund University, Box 118, 22100 Lund, Sweden; Phone: +46 462220892; E-mail: vilhelm.malmborg@design.lth.se

Notes

The authors declare no competing financial interest.

ACKNOWLEDGMENT

This research was financed by Metalund, the FORTE Centre for Medicine and Technology for Working Life and Society, GenDies at the Competence Center for the Combustion Processes, Lund University and the Swedish Energy Agency (Project number 10738150289), and The Swedish Research Council VR project nr. 2013-5021. The authors acknowledge Volvo AB for providing the FSV hardware, Scania CV AB for providing the engine and Jan Eismark (Volvo AB), Timothy Benham (Chalmers University of Technology) and Mats Bengtsson (Lund University) for their technical support, Tim Onasch for discussions on the SP-AMS data, and Bengt Johansson for his contribution to the experimental procedure.

REFERENCES

1. Salvi, S.; Blomberg, A.; Rudell, B.; Kelly, F.; Sandstrom, T.; Holgate, S. T.; Frew, A., Acute inflammatory responses in the airways and peripheral blood after short-term exposure to diesel exhaust in healthy human volunteers. *American journal of respiratory and critical care medicine* **1999,** *159*, (3), 702-709.
2. Riedl, M.; Diaz-Sanchez, D., Biology of diesel exhaust effects on respiratory function. *Journal of Allergy and Clinical Immunology* **2005,** *115*, (2), 221-228.
3. Cancer, I. A. f. R. o., IARC: Diesel engine exhaust carcinogenic. *Press release* **2012**, (213).
4. Stocker, T. F., *Climate change 2013: the physical science basis: Working Group I contribution to the Fifth assessment report of the Intergovernmental Panel on Climate Change*. Cambridge University Press: 2014.
5. Mitchell, D. L.; Pinson, J. A.; Litzinger, T. A. *The effects of simulated EGR via intake air dilution on combustion in an optically accessible DI diesel engine*; 0148-7191; SAE Technical Paper: 1993.
6. Aronsson, U.; Chartier, C.; Andersson, Ö.; Johansson, B.; Sjöholm, J.; Wellander, R.; Richter, M.; Alden, M.; Miles, P. C. *Analysis of EGR effects on the soot distribution in a heavy duty diesel engine using time-resolved laser induced incandescence*; SAE Technical Paper: 2010.
7. Akihama, K.; Takatori, Y.; Inagaki, K.; Sasaki, S.; Dean, A. M. *Mechanism of the smokeless rich diesel combustion by reducing temperature*; 0148-7191; SAE technical paper: 2001.
8. Tree, D. R.; Svensson, K. I., Soot processes in compression ignition engines. *Progress in Energy and Combustion Science* **2007,** *33*, (3), 272-309.
9. Wang, H., Formation of nascent soot and other condensed-phase materials in flames. *Proceedings of the Combustion Institute* **2011,** *33*, (1), 41-67.
10. Yehliu, K.; Vander Wal, R. L.; Armas, O.; Boehman, A. L., Impact of fuel formulation on the nanostructure and reactivity of diesel soot. *Combustion and Flame* **2012,** *159*, (12), 3597-3606.
11. Song, J.; Alam, M.; BOEHMAN∗, A. L., Impact of alternative fuels on soot properties and DPF regeneration. *Combustion Science and Technology* **2007,** *179*, (9), 1991-2037.
12. Savic, N.; Rahman, M.; Miljevic, B.; Saathoff, H.; Naumann, K.; Leisner, T.; Riches, J.; Gupta, B.; Motta, N.; Ristovski, Z., Influence of biodiesel fuel composition on the morphology and microstructure of particles emitted from diesel engines. *Carbon* **2016,** *104*, 179-189.
13. Huang, C.-H.; Vander Wal, R. L., Partial premixing effects upon soot nanostructure. *Combustion and Flame* **2016,** *168*, 403-408.
14. Ristovski, Z. D.; Miljevic, B.; Surawski, N. C.; Morawska, L.; Fong, K. M.; Goh, F.; Yang, I. A., Respiratory health effects of diesel particulate matter. *Respirology* **2012,** *17*, (2), 201-212.
15. Bowditch, F. W. *A new tool for combustion research a quartz piston engine*; 0148-7191; SAE Technical Paper: 1961.
16. Bobba, M. K.; Musculus, M. P. B., Laser diagnostics of soot precursors in a heavy-duty diesel engine at low-temperature combustion conditions. *Combustion and Flame* **2012,** *159*, (2), 832-843.

17. Leermakers, C. A. J.; Musculus, M. P. B., In-cylinder soot precursor growth in a low-temperature combustion diesel engine: Laser-induced fluorescence of polycyclic aromatic hydrocarbons. *Proceedings of the Combustion Institute* **2015,** *35*, (3), 3079-3086.
18. Dec, J. E. *Soot distribution in a DI diesel engine using 2-D imaging of laser-induced incandescence, elastic scattering, and flame luminosity*; 0148-7191; SAE Technical Paper: 1992.
19. Dec, J. E.; Kelly-Zion, P. L. *The effects of injection timing and diluent addition on late-combustion soot burnout in a DI diesel engine based on simultaneous 2-D imaging of OH and soot*; 0148-7191; SAE Technical Paper: 2000.
20. Zhao, H.; Ladommatos, N., Optical diagnostics for soot and temperature measurement in diesel engines. *Progress in Energy and Combustion Science* **1998,** *24*, (3), 221-255.
21. Zhang, R.; Kook, S., Influence of fuel injection timing and pressure on in-flame soot particles in an automotive-size diesel engine. *Environ Sci Technol* **2014,** *48*, (14), 8243-50.
22. Pipho, M. J.; Ambs, J. L.; Kittlelson, D. In *In-cylinder measurements of particulate formation in an indirect injection diesel engine*, 1986; Univ. of Minnesota 0009 1986 conf-860263: 1986.
23. Li, Z.; Song, C.; Song, J.; Lv, G.; Dong, S.; Zhao, Z., Evolution of the nanostructure, fractal dimension and size of in-cylinder soot during diesel combustion process. *Combustion and Flame* **2011,** *158*, (8), 1624-1630.
24. Wang, L.; Song, C.; Song, J.; Lv, G.; Pang, H.; Zhang, W., Aliphatic C–H and oxygenated surface functional groups of diesel in-cylinder soot: Characterizations and impact on soot oxidation behavior. *Proceedings of the Combustion Institute* **2013,** *34*, (2), 3099-3106.
25. Zhang, R.; Khalizov, A. F.; Pagels, J.; Zhang, D.; Xue, H.; McMurry, P. H., Variability in morphology, hygroscopicity, and optical properties of soot aerosols during atmospheric processing. *Proceedings of the National Academy of Sciences* **2008,** *105*, (30), 10291-10296.
26. Peng, J.; Hu, M.; Guo, S.; Du, Z.; Zheng, J.; Shang, D.; Zamora, M. L.; Zeng, L.; Shao, M.; Wu, Y.-S., Markedly enhanced absorption and direct radiative forcing of black carbon under polluted urban environments. *Proceedings of the National Academy of Sciences* **2016,** *113*, (16), 4266-4271.
27. Bertoli, C.; Del Giacomo, N.; Beatrice, C. *Evaluation of combustion behavior and pollutants emission of advanced fuel formulations by single cylinder engine experiments*; 0148-7191; SAE Technical Paper: 1998.
28. Karagiorgis, S.; Collings, N.; Glover, K.; Coghlan, N.; Petridis, A., Residual gas fraction measurement and estimation on a homogeneous charge compression ignition engine utilizing the negative valve overlap strategy. *SAE Technical Paper* **2006,** *2*, 006-01.
29. Shen, M.; Malmborg, V.; Gallo, Y.; Waldheim, B. B. O.; Nilsson, P.; Eriksson, A.; Pagels, J.; Andersson, O.; Johansson, B., Analysis of Soot Particles in the Cylinder of a Heavy Duty Diesel Engine with High EGR. *SAE Technical Paper* **2015**, 2015-24-2448.
30. Onasch, T. B.; Trimborn, A.; Fortner, E. C.; Jayne, J. T.; Kok, G. L.; Williams, L. R.; Davidovits, P.; Worsnop, D. R., Soot Particle Aerosol Mass Spectrometer: Development, Validation, and Initial Application. *Aerosol Science and Technology* **2012,** *46*, (7), 804-817.
31. DeCarlo, P. F.; Kimmel, J. R.; Trimborn, A.; Northway, M. J.; Jayne, J. T.; Aiken, A. C.; Gonin, M.; Fuhrer, K.; Horvath, T.; Docherty, K. S., Field-deployable, high-resolution, time-of-flight aerosol mass spectrometer. *Analytical chemistry* **2006,** *78*, (24), 8281-8289.
32. Wang, X.; Song, C.; Lv, G.; Song, J.; Li, H.; Li, B., Evolution of in-cylinder polycyclic aromatic hydrocarbons in a diesel engine fueled with n-heptane and n-heptane/toluene. *Fuel* **2015,** *158*, 322-329.

33. Gallo, Y.; Simonsson, J.; Lind, T.; Bengtsson, P.-E.; Bladh, H.; Andersson, O. *A Study of In-Cylinder Soot Oxidation by Laser Extinction Measurements During an EGR-Sweep in an Optical Diesel Engine*; 0148-7191; SAE Technical Paper: 2015.
34. Liu, P. S.; Deng, R.; Smith, K. A.; Williams, L. R.; Jayne, J. T.; Canagaratna, M. R.; Moore, K.; Onasch, T. B.; Worsnop, D. R.; Deshler, T., Transmission efficiency of an aerodynamic focusing lens system: Comparison of model calculations and laboratory measurements for the Aerodyne Aerosol Mass Spectrometer. *Aerosol Science and Technology* **2007,** *41*, (8), 721-733.
35. Jayne, J. T.; Leard, D. C.; Zhang, X.; Davidovits, P.; Smith, K. A.; Kolb, C. E.; Worsnop, D. R., Development of an aerosol mass spectrometer for size and composition analysis of submicron particles. *Aerosol Science & Technology* **2000,** *33*, (1-2), 49-70.
36. Drinovec, L.; Močnik, G.; Zotter, P.; Prévôt, A.; Ruckstuhl, C.; Coz, E.; Rupakheti, M.; Sciare, J.; Müller, T.; Wiedensohler, A., The" dual-spot" Aethalometer: an improved measurement of aerosol black carbon with real-time loading compensation. *Atmospheric Measurement Techniques* **2015,** *8*, (5), 1965-1979.
37. Willis, M. D.; Lee, A. K. Y.; Onasch, T. B.; Fortner, E. C.; Williams, L. R.; Lambe, A. T.; Worsnop, D. R.; Abbatt, J. P. D., Collection efficiency of the Soot-Particle Aerosol Mass Spectrometer (SP-AMS) for internally mixed particulate black carbon. *Atmospheric Measurement Techniques Discussions* **2014,** *7*, (5), 5223-5249.
38. Herring, C. L.; Faiola, C. L.; Massoli, P.; Sueper, D.; Erickson, M. H.; McDonald, J. D.; Simpson, C. D.; Yost, M. G.; Jobson, B. T.; VanReken, T. M., New Methodology for Quantifying Polycyclic Aromatic Hydrocarbons (PAHs) Using High-Resolution Aerosol Mass Spectrometry. *Aerosol Science and Technology* **2015,** *49*, (11), 1131-1148.
39. Huestis, E.; Erickson, P. A.; Musculus, M. P. *In-cylinder and exhaust soot in low-temperature combustion using a wide-range of EGR in a heavy-duty diesel engine*; 0148-7191; SAE Technical Paper: 2007.
40. Canagaratna, M. R.; Jayne, J. T.; Ghertner, D. A.; Herndon, S.; Shi, Q.; Jimenez, J. L.; Silva, P. J.; Williams, P.; Lanni, T.; Drewnick, F., Chase studies of particulate emissions from in-use New York City vehicles. *Aerosol Science and Technology* **2004,** *38*, (6), 555-573.
41. Tobias, H. J.; Beving, D. E.; Ziemann, P. J.; Sakurai, H.; Zuk, M.; McMurry, P. H.; Zarling, D.; Waytulonis, R.; Kittelson, D. B., Chemical analysis of diesel engine nanoparticles using a nano-DMA/thermal desorption particle beam mass spectrometer. *Environmental Science & Technology* **2001,** *35*, (11), 2233-2243.
42. Massoli, P.; Fortner, E. C.; Canagaratna, M. R.; Williams, L. R.; Zhang, Q.; Sun, Y.; Schwab, J. J.; Trimborn, A.; Onasch, T. B.; Demerjian, K. L., Pollution gradients and chemical characterization of particulate matter from vehicular traffic near major roadways: Results from the 2009 Queens College Air Quality Study in NYC. *Aerosol Science and Technology* **2012,** *46*, (11), 1201-1218.
43. Sakurai, H.; Tobias, H. J.; Park, K.; Zarling, D.; Docherty, K. S.; Kittelson, D. B.; McMurry, P. H.; Ziemann, P. J., On-line measurements of diesel nanoparticle composition and volatility. *Atmospheric Environment* **2003,** *37*, (9), 1199-1210.
44. Onasch, T. B.; Fortner, E. C.; Trimborn, A. M.; Lambe, A. T.; Tiwari, A. J.; Marr, L. C.; Corbin, J. C.; Mensah, A. A.; Williams, L. R.; Davidovits, P.; Worsnop, D. R., Investigations of SP-AMS Carbon Ion Distributions as a Function of Refractory Black Carbon Particle Type. *Aerosol Science and Technology* **2015,** *49*, (6), 409-422.

45. Goel, A.; Hebgen, P.; Vander Sande, J. B.; Howard, J. B., Combustion synthesis of fullerenes and fullerenic nanostructures. *Carbon* **2002,** *40*, (2), 177-182.
46. Xu, Z.; Li, X.; Guan, C.; Huang, Z., Effects of injection timing on exhaust particle size and nanostructure on a diesel engine at different loads. *Journal of Aerosol Science* **2014,** *76*, 28-38.
47. Dallmann, T.; Onasch, T.; Kirchstetter, T.; Worton, D.; Fortner, E.; Herndon, S.; Wood, E.; Franklin, J.; Worsnop, D.; Goldstein, A., Characterization of particulate matter emissions from on-road gasoline and diesel vehicles using a soot particle aerosol mass spectrometer. *Atmospheric Chemistry and Physics* **2014,** *14*, (14), 7585-7599.
48. Vander Wal, R. L.; Tomasek, A. J., Soot oxidation: dependence upon initial nanostructure. *Combustion and Flame* **2003,** *134*, (1), 1-9.
49. Corbin, J. C.; Sierau, B.; Gysel, M.; Laborde, M.; Keller, A.; Kim, J.; Petzold, A.; Onasch, T. B.; Lohmann, U.; Mensah, A. A., Mass spectrometry of refractory black carbon particles from six sources: carbon-cluster and oxygenated ions. *Atmospheric Chemistry and Physics* **2014,** *14*, (5), 2591-2603.
50. Massoli, P.; Onasch, T. B.; Cappa, C. D.; Nuamaan, I.; Hakala, J.; Hayden, K.; Li, S. M.; Sueper, D. T.; Bates, T. S.; Quinn, P. K., Characterization of black carbon-containing particles from soot particle aerosol mass spectrometer measurements on the R/V Atlantis during CalNex 2010. *Journal of Geophysical Research: Atmospheres* **2015,** *120*, (6), 2575-2593.
51. McMeeking, G.; Fortner, E.; Onasch, T.; Taylor, J.; Flynn, M.; Coe, H.; Kreidenweis, S., Impacts of nonrefractory material on light absorption by aerosols emitted from biomass burning. *Journal of Geophysical Research: Atmospheres* **2014,** *119*, (21), 12,272–12,286.
52. Schnaiter, M.; Horvath, H.; Möhler, O.; Naumann, K. H.; Saathoff, H.; Schöck, O. W., UV-VIS-NIR spectral optical properties of soot and soot-containing aerosols. *Journal of Aerosol Science* **2003,** *34*, (10), 1421-1444.
53. Wang, J.; Onasch, T. B.; Ge, X.; Collier, S.; Zhang, Q.; Sun, Y.; Yu, H.; Chen, M.; Prévôt, A. S.; Worsnop, D. R., Observation of Fullerene Soot in Eastern China. *Environmental Science & Technology Letters* **2016,** *3*, (4), 121-126.
54. Li, X.; Xu, Z.; Guan, C.; Huang, Z., Oxidative Reactivity of Particles Emitted from a Diesel Engine Operating at Light Load with EGR. *Aerosol Science and Technology* **2015,** *49*, (1), 1-10.
55. Al-Qurashi, K.; Boehman, A. L., Impact of exhaust gas recirculation (EGR) on the oxidative reactivity of diesel engine soot. *Combustion and Flame* **2008,** *155*, (4), 675-695.
56. Qiu, C.; Khalizov, A. F.; Hogan, B.; Petersen, E. L.; Zhang, R., High Sensitivity of Diesel Soot Morphological and Optical Properties to Combustion Temperature in a Shock Tube. *Environmental science & technology* **2014,** *48*, (11), 6444-6452.
57. Liu, Z. G.; Berg, D. R.; Swor, T. A.; Schauer, J. J., Comparative analysis on the effects of diesel particulate filter and selective catalytic reduction systems on a wide spectrum of chemical species emissions. *Environmental science & technology* **2008,** *42*, (16), 6080-6085.
58. Liu, Z. G.; Wall, J. C.; Ottinger, N. A.; McGuffin, D., Mitigation of PAH and Nitro-PAH Emissions from Nonroad Diesel Engines. *Environmental science & technology* **2015,** *49*, (6), 3662-3671.
59. Heeb, N. V.; Schmid, P.; Kohler, M.; Gujer, E.; Zennegg, M.; Wenger, D.; Wichser, A.; Ulrich, A.; Gfeller, U.; Honegger, P., Secondary effects of catalytic diesel particulate filters: conversion of PAHs versus formation of nitro-PAHs. *Environmental science & technology* **2008,** *42*, (10), 3773-3779.

60. Lapuerta, M.; Armas, O.; Rodriguez-Fernandez, J., Effect of biodiesel fuels on diesel engine emissions. *Progress in energy and combustion science* **2008,** *34*, (2), 198-223.
61. Hedayat, F.; Stevanovic, S.; Milic, A.; Miljevic, B.; Nabi, M. N.; Zare, A.; Bottle, S.; Brown, R. J.; Ristovski, Z. D., Influence of oxygen content of the certain types of biodiesels on particulate oxidative potential. *Science of the Total Environment* **2016,** *545*, 381-388.

ISRN LUTMDN/TMHP-16/1124-SE
ISSN 0282-1990
ISBN 978-91-7753-054-1 (PRINT)
ISBN 978-91-7753-054-1 (PDF)

Printed by Tryckeriet i E-huset, Lund 2016